INFORMATION TO USERS

The most advanced technology has been used to photograph and reproduce this manuscript from the microfilm master. UMI films the text directly from the original or copy submitted. Thus, some thesis and dissertation copies are in typewriter face, while others may be from any type of computer printer.

The quality of this reproduction is dependent upon the quality of the copy submitted. Broken or indistinct print, colored or poor quality illustrations and photographs, print bleedthrough, substandard margins, and improper alignment can adversely affect reproduction.

In the unlikely event that the author did not send UMI a complete manuscript and there are missing pages, these will be noted. Also, if unauthorized copyright material had to be removed, a note will indicate the deletion.

Oversize materials (e.g., maps, drawings, charts) are reproduced by sectioning the original, beginning at the upper left-hand corner and continuing from left to right in equal sections with small overlaps. Each original is also photographed in one exposure and is included in reduced form at the back of the book. These are also available as one exposure on a standard 35mm slide or as a 17" x 23" black and white photographic print for an additional charge.

Photographs included in the original manuscript have been reproduced xerographically in this copy. Higher quality 6" x 9" black and white photographic prints are available for any photographs or illustrations appearing in this copy for an additional charge. Contact UMI directly to order.

U·M·I

University Microfilms International
A Bell & Howell Information Company
300 North Zeeb Road, Ann Arbor, MI 48106-1346 USA
313/761-4700 800/521-0600

Order Number 9000287

Dielectric thermal analysis of polymeric matrices

Nass, Kirk Alan, Ph.D.

University of Washington, 1989

U·M·I
300 N. Zeeb Rd.
Ann Arbor, MI 48106

Dielectric Thermal Analysis

of

Polymeric Matrices

by

Kirk A. Nass

A dissertation submitted in partial fulfillment
of the requirements for the degree of

Doctor of Philosophy

University of Washington

1989

Approved by 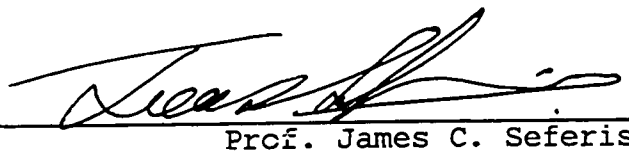

Prof. James C. Seferis
(Chairperson of the Supervisory Committee)

Program Authorized
to Offer Degree Chemical Engineering

Date March 16, 1989

University of Washington

Abstract

Dielectric Thermal Analysis of Polymeric Matrices

by Kirk A. Nass

Chairperson of the Supervisory Committee:
Professor James C. Seferis
Department of Chemical Engineering

While the commercial application of polymeric composite materials is increasing, methods of processing composites are becoming more complex and cost prohibitive. Several in situ monitoring techniques have been proposed to permit the development of "smart" processes, which would reduce processing time and cost per part. One proposed technique, dielectric spectroscopy, monitors changes in the electrical properties of polymers during processing. While dielectric instrumentation has become quite sophisticated and commercially available, the relationships between the dielectric properties and the changing chemical and physical states of polymers during processing have not been quantified. This study seeks to elucidate these relationships by considering dielectric spectroscopy as a thermal analysis technique for polymer characterization. The behaviors of both ionic and dipolar species in polymers were considered. Classical thermoanalytical expressions were developed for determining the activation energies of

Doctoral Dissertation

In presenting this dissertation in partial fulfillment of the requirements for the Doctoral degree at the University of Washington, I agree that the Library shall make its copies freely available for inspection. I further agree that extensive copying of this dissertation is allowable only for scholarly purposes, consistent with "fair use" as prescribed in the U.S. Copyright Law. Further consent is given to the Polymeric Composites Laboratory to reproduce and use this work at the discretion of its director. Requests for copying or reproduction of this dissertation may be referred to University Microfilms, 300 North Zeeb Road, Ann Arbor, Michigan 48106, to whom the author has granted "the right to reproduce and sell (a) copies of the manuscript in microform and/or (b) printed copies of the manuscript made from microform."

Signature Kirk A. Dass

Date March 16, 1989

dielectric transition and polymerization from the dielectric properties. Models which combine the contributions of ionic conductivity and dipolar relaxation were developed for relating the extent of reaction to the dielectric properties of thermosetting polymers during both isothermal and nonisothermal reaction. Ionic conduction was described using the Keinle-Race expression; the isofrequency dielectric response was described in terms of the dipolar relaxation time, using the Lane-Seferis-Bachmann equation. Using the principles of kinetic viscoelasticity, the relaxation time was considered as a function of the extent of reaction and an entanglement parameter. An expression relating the entanglement parameter to the parameters in the WLF equation was derived. Methods for removing polarization effects from dielectric cure data were also derived. The developed dielectric data analysis methods were tested using a model epoxy/amine resin for high performance polymeric composites, TGDDM cured with 25 phr DDS hardener. Differential scanning calorimetry (DSC) studies of the model resin were performed for comparison and integration into the dielectric models. The success of this approach demonstrates the usefulness of dielectric thermal analysis techniques and provides further basis for the development of quantitative dielectric techniques for polymeric composite process monitoring.

TABLE OF CONTENTS

LIST OF TABLES

LIST OF FIGURES

ACKNOWLEDGEMENTS

Probably the most important lesson to be learned in graduate school is that you are nothing by yourself and, at the same time, you have nothing but yourself. With regards to the former, I am lucky to have been surrounded by people who have tried, by example, to teach me to be a professional scientist and engineer, to respect other opinions, and to be a good friend. With regards to the latter, I hope that I have learned.

Prof. James C. Seferis, my research advisor, provided many opportunities for which I am extremely grateful. Although always demanding (and occasionally unreasonable), he listened, advised, and counseled thoughtfully. I am most thankful, however, that at the most difficult times during the research, he gave the best direction by giving me the freedom to solve problems without pressure.

The sponsoring institutions of the Polymeric Composites Laboratory continue to make it a success through their financial and technical support. Several Laboratory sponsors were involved in this research throughout its course: Owens-Corning Fiberglas Corporation, Army Research Office, National Science Foundation (through a Presidential

Young Investigator Award to Prof. J.C. Seferis), Lockheed Missiles and Space Co., and IBM. Equipment support provided by Tetrahedron Associates and DuPont Instruments was especially appreciated.

Dr. Michael Bachmann, formerly of Owens-Corning Fiberglas and presently at ICI Americas, provided invaluable technical input. The contributions of Mr. Vincent Noto of Tetrahedron Associates were also appreciated. I sincerely thank Professors Bruce Finlayson, Bradley Holt, and Ilhan Aksay of the University of Washington and Dr. R. Bruce Prime of IBM for giving of their time to serve as members of my Supervisory Committee. I also thank the faculty of the Chemical Engineering Department for helping me to grow professionally.

The staff of the PCL were constant sources of technical and emotional support. Professors Jan-Anders Manson and Eamor Woo provided both calm answers to panicked questions and friendship. Sunny Yuh and Tai Matsuda kept the Lab afloat and made a difference to me by taking the time to listen, to care, to advise, and to laugh. Nate Brown, Garry Duschl, and Louise Peterson kept things from literally falling apart. The Chemical Engineering Department staff, especially Joyce Chandler, Bonnie MacDonald, Linda Wilkins,

and Devota Madrano, made overcoming administrative obstacles enjoyable.

The students of the PCL are an amazing group. Eric Stark and Kaveh Pournoor were instrumental in my survival during the first years of graduate school. Steve Dillman provided springboards for technical discussions which aided in my understanding of the project. Christy Loechelt was an invaluable resource not only for answering thermal analysis questions, but also for helping me through the trauma of writing. Glenna Shields always lent a shoulder to cry on. Without Corey MacMillan, I never would have run a successful dielectric experiment and the Lab would never have had an operating computer.

My friends in Seattle and in Illinois continue to believe in me. Elsa Schirmer has always been a true friend. Cindy (Neu) Steimle taught me that it was OK to be smart; Richard Rapoza taught me that it was OK to be gay and smart. I can't thank them or any of my friends enough.

My family have always supported me, even though they didn't necessarily understand why I wanted to go to college or graduate school. I can only begin to express the love and appreciation I have for them. Susan Nass, my mother, taught me to be independent; David Nass, my father, did the

same, but in a different way. Lisa and Mark Nass, my sister and brother, put up with me. Cecile Bessette, my great aunt (and to whom this dissertation is dedicated), has always expected the best for me and from me.

Finally, the contributions of my own family have been the most significant of all. My partner and best friend, Michael Gillespie, and my children, Shelley and Drew Gillespie, have loved me unconditionally and have been continual sources of joy and inspiration in my life. Although the next phase of our lives is full of uncertainty, I know we'll make it together.

TO CECE

LOVE KIRK

(I made it myself.)

CHAPTER 1

INTRODUCTION

Polymers have emerged as an important class of materials, producing a wide range of lightweight nonstructural products with higher strength to weight ratios than possible with metals. Plastic piping, flooring, thermal and electric insulation, bottles, and films are excellent examples of such products. Polymeric composites, formed by incorporating reinforcing fibers into polymer matrices, have expanded polymer applications to include structural parts in automobiles and in both commercial and military aircraft [1,2].

To a large extent, application of polymeric materials is determined by their properties, which are functions of chemical composition, microstructure, macrostructure, and processing history. Polymer strength is enhanced by modifying molecular structure, crosslinking molecules, increasing crystalline content, or changing crystalline morphology. By these means, new polymers may be developed and existing polymers may be modified to suit specific applications. However, these possibilities cannot become realized until the complex and elusive interrelationships between the processing, structure, and properties of

polymeric materials are fully understood [3-5].

The cost of production has recently become another important factor in the use of polymers and polymeric composites. Their usage is promoted by reductions in material costs; for example, the average price of carbon fibers has decreased more than 85% in the past 20 years, from $200 to $25 per pound [6]. However, processing the inexpensive starting materials is expensive. Currently, the cost of producing quality polymeric composite parts for aerospace applications is 50% greater than for metals, precluding extensive substitution of composites for metals on most aircraft [6,7].

A significant portion of the production cost is due to the extensive post-production quality control and inspection required to offset the high rate of poor quality parts typically produced by standard processing techniques. Voids, improper fiber distribution, and poor consolidation of constitutive laminate plies are common. Industrial processing cycles are typically chosen by trial and error, simply because information is scarce regarding the physical and chemical changes occurring during the transformation of polymer and reinforcement into a composite material. Such information may not exist for newly formulated systems [2].

Ideally, flawless composite parts can be produced if the property, structure, and processing relationships are

known [8]. Batch variations in the starting materials could be offset by properly adjusting the processing parameters during production. This "smart" processing would reduce processing time, increase production rate, decrease energy requirements, and substantially reduce production costs per part [8].

"Smart" processing, however, requires methods for determining the physical and chemical state of the material in real time. A variety of techniques are therefore being investigated and developed to nondestructively monitor polymers and composites in situ during processing. Several of these techniques have been employed industrially, but with limited success. According to Robert N. Neff Jr., chief of the Nonmetals and Composites Group at Wright Patterson Air Force Base, "One problem is that the sophistication of nondestructive testing techniques often can exceed our ability to interpret what is found." [3]

Dielectric spectroscopy is one such nondestructive technique which has reached a high level of instrumental sophistication. Dielectric monitoring has been employed, although unsuccessfully, to control industrial polymeric composite processing. Successful implementation may eventually occur, but only by first studying the relationships between the processing, the chemical and physical state, and the dielectric properties of polymers

and polymeric composite materials.

This work approaches dielectric spectroscopy as a technique for analyzing polymers during processing, rather than as a technique specifically suited for closed-loop process control. In this manner, the monitored signals and the state of the polymer during processing may be related. Approaches are developed for analyzing polymeric matrices under a variety of processing conditions, with specific emphasis on analyzing thermosetting matrices during reaction.

1.1 Methods of Polymer Analysis

A variety of techniques have been employed to analyze the properties of polymers and composites. Spectroscopic, thermal, sonic, photoacoustic, and electrical property measurements have been developed. While differing in the types of polymer behavior detected, each method is essentially noninvasive and nondestructive. Several of the methods have been adapted for monitoring the development of polymer properties during either real or simulated processing conditions [18,19,28,29].

1.1.1 Spectroscopic Techniques

The intensities and locations of peaks in spectra of thermosetting polymers have been correlated to physical and

chemical changes during reaction in thermosets. Infrared spectra obtained during the cure of several epoxy systems have been used to determine kinetic reaction parameters [9-11]. Although clearly indicating property changes during processing, suitable methods for directly obtaining infrared spectra in situ have not been developed.

Viscosity changes have been detected by the emission of weak visible chemiluminescence [12], but fluorescence methods have been studied in more detail. The viscosity of nonfluorescent polymers is tracked by monitoring the behavior of incorporated fluorescent dyes. The fluorescence intensity of incorporated dyes increased with viscosity during polymerization of polyesters, epoxies, and polyimides [13,14].

Nitroxide spin probes have also been added to epoxies during cure and monitored by electron spin resonance spectroscopy (ESR) [15]. The intensities and splitting characteristics of the ESR spectra of the probes changed as viscosity increased with reaction. Incorporating probes of various molecular size provided viscosity information during different stages of cure.

Some polymers produce fluorescence spectra which may be measured experimentally. Several epoxy/amine resin systems have been monitored during cure using fluorescence methods [16,17]. As in the incorporated dye studies, viscosity

changes due to reaction were detected. The molecular sources of the fluorescence were not identified.

The results of one fluorescence study were extended through the development of a fluorescence "optrode" cure sensor (FOCS), in order to monitor composite laminates in situ during processing [18,19]. Laser light is directed by optical fibers onto the surface of the polymer. The emitted fluorescence is relayed via the optical fiber to a photodetector. The fluorescence spectra obtained throughout processing are examined qualitatively. The FOCS technique appears promising, but quantitative treatment of the data in terms of viscosity or extent of reaction has not yet been performed.

1.1.2 Thermal Analysis Techniques

The complexity of their molecular structure makes spectroscopic analysis of many polymers extremely difficult. Alternate analyses which examine thermal properties have become increasingly accepted as methods for polymer characterization [20]. By providing not only qualitative, but quantitative information regarding polymer physical behavior and chemistry, thermal analysis techniques are especially suited for investigating the interrelationships between processing, structure, and polymer properties.

Each technique measures a different aspects of kinetic

and thermodynamic phenomena as a functions of time and temperature. Differential scanning calorimetry (DSC) detects changes in heat capacity; light-sensitive materials may be analyzed by differential photocalorimetry (DPC). Thermogravimetry (TGA) measures changes in weight and thermomechanical analysis (TMA) detects dimensional changes. Dynamic mechanical analysis (DMA) measures the viscoelastic and mechanical response of materials to an oscillating force field.

More detailed analysis of polymers is provided by combining thermal analysis techniques with standard analytical chemistry techniques, such as TGA/mass spectrometry [21,22] and TGA/Fourier transform infrared spectroscopy [23]. Detailed descriptions of these and other thermal analytical techniques appear elsewhere [20]. Although the wealth of thermal analysis data and discussion is much too large to be presented here, the usefulness and versatility of these techniques for polymer characterization are apparent.

1.1.3 Sonic Techniques

In addition to dynamic mechanical analysis, other methods of measuring the mechanical properties of polymers and composites have been devised. Ultrasonic wave propagation has proven to be the most practical of these

methods for measuring the response of polymers during processing. In addition, sonic techniques have the potential for probing polymer microstructure (acoustic microscopy) and for direct measurement of physical properties such as modulus and fracture toughness.

Changes in the velocity and attenuation of longitudinal and shear sonic wave pulses in curing thermosetting polymers were shown to be related to polymerization and crosslinking [24]. Subsequently, ultrasonic studies of neat epoxy systems have been performed and used to determine kinetic parameters for the curing reactions [25-27]. Epoxy/carbon fiber composites have also been monitored ultrasonically during cure [28]. In another study, an acoustic waveguide incorporated into neat epoxy and epoxy/carbon fiber composite specimens measured the mechanical properties both during and after cure [29].

1.1.4 Photoacoustic Techniques

Under controlled conditions, materials emit vibrational (acoustic) energy when exposed to an excitation light source. This behavior is categorized as "the photoacoustic effect." The acoustic emissions of thermosetting polymers are functions of reaction, forming the basis of a new polymer analysis technique, photoacoustic monitoring [30].

The sample is placed in an acoustically isolated

chamber filled with an inert gas. As light from an intensity modulated source impinges on the sample. only those wavelengths which correspond to vibrational quantum transitions in the material are absorbed. The release of vibrational energy increases the sample temperature, causing pressure fluctuations in the gas. These fluctuations are detected as sound waves by a microphone, which records their attenuations and frequencies.

One technique for interpreting photoacoustic data is through the calculation of thermal properties. Changes in the photoacoustically-measured thermal diffusivity of reacting polymers have been used to track polymerization [30]. The thermal diffusivity, which incorporates both heat capacity and thermal conductivity, is independent of viscosity and was therefore compared directly to the extent of reaction during polymerization.

Molecular information may be obtained through more sophisticated analysis of photoacoustic data [31]. The microphone signal may be processed using Fourier transform techniques to discern the intensities and frequencies of the individual vibrations which contribute to the observed pressure fluctuations. The deconvoluted signal is an infrared spectrum of the polymer, made quantitative by using a carbon black reference. The spectra thus obtained may be analyzed by standard techniques to determine chemical

information and the extent of reaction.

By detecting material vibrations rather than radiation absorption, quantitative infrared spectra can be obtained for optically opaque materials, e.g. carbon fiber composites. However, the incident radiation penetrates only 100 μm into the sample [31], so only surface properties are measured for thick specimens. Also, only isothermal experiments are possible with current photoacoustic instrumentation.

1.2 Electrical Techniques for Analyzing Polymers

Initial electrical experiments with polymers merely determined their insulation properties [32], but improvements in instrumentation have led to the application of electrical techniques for investigating polymer physical behavior [33]. Electrical experiments are easy to instrument and simple to perform. Subsequently, a great deal of research has been performed to measure the electrical properties of both reacting and nonreacting polymers.

1.2.1 Direct Current Methods

Direct current (DC) methods were the first electrical techniques used to monitor polymers during reaction. Studies which measured the DC resistivity of polymerizing

alkyd resins were first published in 1934 by Keinle and Race [34]. In their experiments, the resins were observed to become more resistive during polymerization; the resistivity was directly proportional to the degree of polymerization. This observation provided the basis for using DC resistivity data to determine the kinetic parameters of the polymerization of many thermosetting polymers [9,10,35-40]. Monitoring the DC conductivity during industrial processing was proposed in a technique termed "ion graphing" [41], but was not developed further.

1.2.2 Alternating Current Methods: Dielectric Spectroscopy

The majority of electrical monitoring research has focused on using alternating current (AC), or dielectric, methods of measuring polymer properties. AC experiments, while difficult to instrument, are less susceptible to extraneous sources of noise than DC experiments. Dielectric spectroscopy has been used to measure the properties of a wide variety of nonreacting polymers. Adhesives [42], polyethylene [43], natural rubber elastomers [44], rubber-toughened epoxies [45], cured epoxy/amine resins [46], and cured epoxy/fiberglass composites exposed to moisture [47] and solvents [48] have been recently studied using dielectric techniques.

The results of early AC dielectric experiments using

reacting polymers suggested the application of dielectric spectroscopy to monitor polymerization under real processing conditions [49]. Published case studies of industrial dielectric cure monitoring quickly followed [50]. Experiments with commercial epoxy/graphite fiber prepreg demonstrated that outgassing, void formation, and viscosity influence dielectric behavior during cure [51]. Additional studies demonstrated that DC conductivity and AC phase lag are related to viscosity during cure [52-54].

Since these early experiments, dielectric measurements have been taken during the processing of both thermosetting and thermoplastic polymers. Studies focusing on the processing behavior of photopolymers [55], adhesives [56], polyimides [57], polyesters [58], polyetheretherketone [59], polyester/glass fiber prepreg [60], and polyaromatic cyanate esters [61] have been published. A substantial amount of dielectric research has been performed with epoxy/amine resins [62-70].

Unlike many of the other polymer analysis techniques, dielectric spectroscopy has been commercially developed for industrial application. Interdigitated microchip electrodes were first constructed by Senturia et al. for monitoring polymerization via "microdielectrometry" [64]. The sensors may be placed directly on the surface of the polymer or composite during processing. Kranbuehl et al. developed a

nearly identical microsensor for use in "dynamic dielectric analysis" [68], or "frequency dependent electromagnetic analysis" [69]. Microwave dielectric techniques have also been proposed to not only analyze thermoset cure [71], but also to provide microwave heating of laminates as an alternative processing method [72].

1.3 Dielectric Properties of Polymers

Applying alternating current to a dielectric material, such as a nonreacting polymer, produces a response which is a function of both frequency and temperature. The dielectric properties of materials undergoing physical or chemical changes, such as reacting or crystallizing polymers, are also time dependent. Understanding these behaviors provides the basis of dielectric thermal analysis techniques. The first step in developing this understanding is the identification of the sources of dielectric signals in polymers.

1.3.1 Definitions

Dielectric spectroscopy is analogous to dynamic mechanical analysis, which measures the response of materials to an oscillating force field [73]. In dielectric experiments a sinusoidal electric field is applied, whereas in dynamic mechanical experiments a sinusoidal stress or

strain is applied. The electric field may be expressed in complex form, E^*, in terms of its amplitude, E_o; angular frequency, w; and time, t:

$$E^* = E_o \exp (iwt) \tag{1.1}$$

The angular frequency is related to the applied frequency, f, by:

$$w = 2\pi f \tag{1.2}$$

The resulting complex electric displacement, D^*, lags the electric field by the phase angle δ:

$$D^* = D_o \exp [i(wt - \delta)] \tag{1.3}$$

The complex dielectric constant, ε^*, is defined as the proportionality constant between the applied electric field and the electric displacement:

$$D^* = \varepsilon^* E^* \tag{1.4}$$

The dielectric constant may be expressed in terms of its real and imaginary components:

$$\varepsilon^* = \varepsilon' - i\varepsilon'' \tag{1.5}$$

In physical terms, the value of ε' is related to the amount of electric energy stored in the material and hence ε' is termed the "storage component." The value of ε'', the "loss component" of ε^*, is proportional to the amount of electric energy dissipated by the material. These components are related to the phase lag δ by:

$$\tan \delta = \varepsilon''/\varepsilon' \qquad (1.6)$$

Tan δ is also termed the "dissipation."

The storage and loss components may be experimentally measured by placing the material between parallel plate electrodes. ε' is related to the measured capacitance, C (farads):

$$\varepsilon' = \frac{Cd}{Ae_o} \qquad (1.7)$$

In this equation, A is the electrode area in cm^2, d is the spacing between the electrodes in cm, and e_o is the permittivity of free space, 8.854×10^{-14} farads/cm. The phase angle δ, and hence tan δ, are determined by comparing the phase behaviors of the applied AC voltage and the resulting AC current. ε'' values are calculated from the measurements of ε' and tan δ and Equation 1.6. When

dielectric experiments are performed using interdigitated electrodes, voltage/current data are converted to ε' and ε'' data using previously generated calibration tables.

The apparent conductivity of the material, σ, can be determined from ε'' data and the frequency, w, using:

$$\sigma = \varepsilon'' w \varepsilon_o \tag{1.8}$$

The conductivity is expressed in units of ohm-cm^{-1}. When substantial sources of DC, i.e. frequency independent, conduction are present, curves of the apparent conductivity measured at several frequencies collapse to a single curve. AC contributions to the apparent conductivity appear as deviations of individual frequency curves from the convergent curve.

1.3.2 Sources of Dielectric Signals in Polymers

The dielectric properties of materials result from the interactions between electrical charge carriers in the material and the alternating electric field. These interactions are diagrammed in Figure 1.1. At the audio and radio frequencies commonly employed in dielectric experiments, the dielectric response arises from ions and permanent dipoles in the material. Ions in polymers can result from unreacted monomer, catalyst, moisture, thermal

ionization, or impurities [33,74]. Most polymers contain polar moities such as carbonyl, epoxide, amine, or halogen substituted groups [75]. Polymers which are not inherently dipolar, such as polyethylene, exhibit dielectric behavior due to small quantities of dipolar impurities [75].

The behaviors of both ions and dipoles are affected in an electric field. Ions are attracted to the electrode of opposite polarity. Migration of the ions towards the electrodes is charge conduction, which dissipates electrical energy and influences the values of tan δ and ε''. Ions which accumulate at the electrodes cause inhomogeneities in the electric field strength in the material. This space-charge polarization increases the capacitance and the value of ε'.

Dipoles in an electric field experience a torque and orient in the direction of the field [75]. However, the dipoles may be prevented from orienting in synchronization with an alternating field by steric interactions. The time scale of the orientation is characterized as the dipolar relaxation time. If the period of the field oscillation and the relaxation time are equal, a resonance condition is produced and the material exhibits high dielectric loss. Consequently, the dielectric properties may be expressed as a function of the dipolar relaxation time and frequency.

The behaviors of ions and dipoles in polymers are

significantly influenced by physical and chemical changes, such as those occurring during reaction and crystallization. The typical dielectric responses of thermosets during isothermal cure are presented in Figure 1.2. During the initial stages of cure, the resin is typically a low viscosity liquid, ions migrate easily in response to the field, and electrode polarization develops. As reaction proceeds, the viscosity increases dramatically, restricting ionic movement, and the DC conductivity of the resin decreases. Dipolar relaxation is also hampered by the growing polymer network, resulting in changes in both ε' and ε''. Thermoplastic polymers below the melting point cannot exhibit ionic conductivity. Dipolar relaxation is affected by crystalline orientation and amount [75], so changes in ε' and ε'' are expected to occur during thermoplastic processing.

1.3.3 Difficulties in Measuring the Dielectric Properties of Polymers

Dielectric spectroscopy can provide a wealth of information about the chemistry and physics of polymers under processing conditions. However, several sources of interference affect the experimentally observed dielectric response. While some sources can be minimized, inherent problems do exist in applying dielectric techniques for

analyzing polymers and polymeric composites.

Water is a ubiquitous problem in measuring the dielectric properties of polymers. Being highly polar, the presence of less than 1 wt% water in polymers has a large effect on the dielectric properties [48]. Removing the water from polymers by heating above 100°C may not be practical if reaction or other events occur at lower temperatures. In addition, water is easily absorbed by many polymers and may affect thermoset cure kinetics [76]. Desiccating specimens and reducing exposure to moisture help to reduce the influence of water on the observed dielectric properties.

Conducting species, such as carbon fibers in polymeric composites, cause particular problems in performing dielectric measurements. Care must be taken to prevent shorting the electrodes, which would invalidate the measurement. Parallel plate electrodes may be insulated with barrier films, however, the dielectric properties of the film can mask the response of the sample [77].

Interdigitated electrodes cannot be used to measure the properties of carbon fiber composites directly because direct contact with the specimen is required. Shorting is circumvented, however, by placing the electrodes along the outside edge of the composites and measuring the dielectric properties of the excess resin which bleeds out [68].

However, the behavior of the bled resin may not represent the properties of the entire laminate.

While experimental problems exist in measuring the dielectric properties of carbon fiber composites, expressions have been developed to relate the dielectric properties of composite materials to those of their constituents. These expressions provide a possible means for extracting the neat polymer dielectric properties from carbon fiber composite dielectric data.

One approach described the general transport properties of composites with respect to upper- and lower-bound (series and parallel) property mixing rules [78]. While not directly applicable to continuous carbon fiber composites, this method worked well for particulate-filled polymers. Another, more rigorous approach accounted for the electrical field variations caused by interfacial polarization in composite materials [79]. Several mixture formulae were presented, but none are immediately useful for continuous fiber systems. However, both of these studies do begin to address the issue of composite dielectric data analysis.

1.4 Describing the Dielectric Properties During Reaction

In attempts to apply dielectric spectroscopy to monitor and control polymer processing, several approaches have been taken to relate dielectric data to viscosity and extent of

reaction data during thermoset cure. These models relate either the conduction of ionic impurities or the relaxation of the dipolar portions of the polymer molecules to cure, ignoring that these processes occur simultaneously. To date, the developed models have been applied only to isothermal cure. Relationships between dielectric properties and structure for thermoplastic processing have not been proposed.

1.4.1 Ionic Conductivity Models

The analogy between ionic conductivity and viscosity during reaction has been used by several researchers to describe the dielectric behavior of reacting systems. One approach described conductivity and viscosity by identical mathematical treatments. Another employed more fundamental formalism by comparing the diffusion limitations of conductive and viscous transport.

1.4.1.1 WLF Approach

A description of ionic conductivity during reaction has been developed by Senturia et al. [80] by applying the Williams-Landel-Ferry (WLF) equation [81], which describes the time/temperature superposition of the viscoelastic properties of polymers above the glass transition temperature:

$$\log(a_T) = - \frac{C_1(T - T_g)}{C_2 + (T - T_g)} \qquad (1.9)$$

In this equation, a_T represents the ratio of a viscoelastic property at a temperature, T, to the value at the glass transition temperature, T_g. C_1 and C_2 are constants specific to each polymer. Universal values of 17.44 and 51.6 were initially proposed for C_1 and C_2, respectively [81]. The WLF equation is applicable in the range $T_g \leq T \leq T_g + 100°C$.

Equation 1.9 was extended by first describing the temperature dependence of the ionic conductivity of nonreacting systems. Reaction effects were incorporated by defining several of the parameters in Equation 1.9 as functions of T_g. The value of the glass transition temperature was then related to the extent of reaction.

To account for the temperature behavior of ionic conductivity, $\sigma(T)$, the shift factor was defined as [80]:

$$\log (a_T) = \log \frac{\sigma(T)}{\sigma(T_g)} \qquad (1.10)$$

Experimental evidence suggested that $\log (\sigma(T_g))$ and C_2 were linear functions of T_g. After substituting and rearranging,

the WLF equation, Equation 1.9, was expressed as:

$$\log(\sigma(T)) = (C_5 + C_6 T_g) - \frac{C_1(T - T_g)}{C_3 + C_4 T_g + (T - T_g)} \quad (1.11)$$

The constants C_3, C_4, C_5, and C_6 were believed to have unique values for each polymer system and were determined by performing nonlinear regression on conductivity and T_g data.

The glass transition temperature was then related to the extent of reaction, α, using the DiBenedetto equation [82]:

$$\frac{T_g - T_{go}}{T_{go}} = \frac{(E_x/E_m - F_x/F_m)\alpha}{1 - (1 - F_x/F_m)\alpha} \quad (1.12)$$

T_{go} is the glass transition temperature of unreacted polymer, E_x/E_m represents the ratio of lattice energies for fully crosslinked polymer and monomer, and F_x/F_m is the ratio of segmental mobilities. Combining Equations 1.11 and 1.12 produced the final relationship for modelling ionic conductivity and reaction.

The success of this modelling approach is difficult to assess since satisfactory comparisons of model results and experimental data have not been published. However, the WLF approach has been used to study the curing behavior of

several epoxy/amine resins [83-87]. While considerable effort has been placed in determining the parameters used in the modelling scheme, very little is known about their physical significance.

1.4.1.2 Free Volume Approach

Diffusion-limited kinetics were combined with free volume models by Sanford and McCullough to describe the temperature and molecular weight dependences of conductivity and viscosity during isothermal reaction [88]. Their modelling strategy produced a direct relationship between conductivity and viscosity during reaction. This method compared favorably to the results of initial experiments on an epoxy/amine resin.

The basis for the free volume approach to modelling both conductivity and viscosity was an expression proposed by Macedo and Litovitz for the temperature dependence of diffusivity, D (cm^2/sec) [89]:

$$D = D_o \exp(-E_D/RT) \exp(-b_D/f) \qquad (1.13)$$

D_o is the diffusivity pre-exponential, E_D is the activation energy for diffusion, b_D is a constant, and f is the fractional free volume, which is a function of temperature and T_g. The glass transition temperature was related to

reaction by the DiBenedetto equation, Equation 1.12. Equation 1.13 was applied to describe viscosity by incorporating an empirical molecular weight dependence, M raised to the power n:

$$\eta = \eta_o M^n \exp(-E_\eta/RT) \exp(-b_\eta/f) \qquad (1.14)$$

In this equation, η_o is the viscosity pre-exponential and E_η is the activation energy for viscous transport. As in Equation 1.13, b_η is a constant and f is the fractional free volume.

The results of this model were compared to viscosity data of an epoxy/amine system during isothermal cure. The parameter values used in the calculations were compiled from various literature sources, rather than through regression techniques. The model successfully described the viscosity of the resin, but only at elevated temperatures.

When applied to conductivity, Equation 1.13 was expressed as:

$$\sigma = \sigma_o M^n \exp(-E_\sigma/RT) \exp(-b_\sigma/f) \qquad (1.15)$$

Experiments suggested that conductivity varies with the inverse square of the molecular weight, i.e. n = -2.

Literature parameter values were used in Equation 1.15 to produce model responses. Agreement between data and the model was good, but only at the higher cure temperatures.

An expression which directly related viscosity and conductivity was obtained by combining Equations 1.14 and 1.15. The resulting equation was of the form:

$$\eta = A \exp[(-E_\eta-(E_\sigma/2))/RT]\ \sigma^{-n/2} \qquad (1.16)$$

The success of this approach was demonstrated, but only for two cure temperatures. The results thus far, however, validate the free volume description. The results of low temperature experiments require additional investigation of the modelling approach.

Using conductivity measurements alone to predict (and possibly control) conversion, glass transition temperature, and viscosity, as proposed in these models, is inherently dangerous. The measured conductivity results from ionic impurities in the resin, which are subject to batch variation. Differences of even small amounts of ionic impurities have a large effect on the conductivity of the polymer. In one study, resin conductivity was found to decrease by an order of magnitude upon purification [90].

1.4.2 Dipolar Relaxation and ε' Models

The relaxation of dipolar segments of the polymer molecules during processing provides another means for modelling dielectric property changes. Dipolar relaxation is not easily identifiable in the dielectric data, unlike ionic conductivity. Little treatment of reaction effects on relaxation behavior has been presented in the literature, though a few attempts to model these effects have been made.

1.4.2.1 WLF Approach

In addition to ionic conductivity, the WLF approach to modelling viscoelastic properties has been applied to dipolar relaxation. Lane and Khattak related relaxation time, τ, to temperature by [91]:

$$\log \frac{\tau(T)}{\tau(T_g)} = - \frac{C_1(T - T_g)}{C_2 + (T - T_g)} \qquad (1.17)$$

In their treatment, the glass transition temperature during reaction, $T_g(\alpha)$, varied between the values of unreacted and completely reacted polymer, T_{go} and $T_{g\infty}$, using a rule of mixtures proposed by Bueche [92]:

$$\frac{1}{T_g(\alpha)} = \frac{1 - \alpha}{T_{go}} + \frac{\alpha}{T_{g\infty}} \qquad (1.18)$$

Combining Equations 1.17 and 1.18 permitted the relaxation time to be directly related to reaction.

Experimental determinations of τ during isothermal reaction of an epoxy/amine resin were compared to values calculated using the WLF approach and an empirical equation. The empirical equation expressed relaxation time by [91]:

$$\ln (\tau/\tau_o) = K\alpha \qquad (1.19)$$

Agreement between the data and the WLF approach was poor, the empirical model performed better. Caution must be used in evaluating these models though, since the amount and range of experimental data were limited. The value of relaxation time is difficult to determine during the initial stages of cure since the dielectric properties are dictated entirely by ionic conductivity [91].

1.4.2.2 Frölich Approach

A more direct modelling approach, taken by Sheppard and Senturia, related the values of ε' at low and high frequency to the number and strength of dipoles in the polymer [93]. As dipoles are produced and consumed by reaction, the limiting values of ε' change. In nonreacting systems, the low frequency limit of ε', ε_r, and the high frequency limit, ε_u, were related by the Frölich equation to the number of

dipoles present, N_i, and their dipole moments, μ_i, [73]:

$$\frac{(\varepsilon_r - \varepsilon_u)(2\varepsilon_r + \varepsilon_u)}{\varepsilon_r(\varepsilon_u + 2)^2} = \frac{\Sigma\, N_i \mu_i^2}{9\varepsilon_o kT} \qquad (1.20)$$

This equation was modified for application to reacting polymers by using a kinetic model to account for the number of dipoles and an empirical temperature correction, T_{int}:

$$\frac{(\varepsilon_r-\varepsilon_u)(2\varepsilon_r+\varepsilon_u)}{\varepsilon_r(\varepsilon_u+2)^2} = \frac{\Sigma\, N_i(\alpha)\mu_i^2}{9\varepsilon_o kT}\left[\frac{1}{T} - \frac{1}{T_{int}(\alpha)}\right] \qquad (1.21)$$

In experiments with curing epoxy/amine systems, three dipolar species were considered: epoxide, primary amine, and secondary/tertiary amine. An empirical autocatalytic rate equation was used to calculate the numbers of epoxide and primary amine groups reacted and secondary and tertiary amine groups produced. Good agreement between the model and data was evident at several isothermal temperatures.

This model, although successfully representing the cure data presented, requires dielectric data to be obtained over a wide frequency range in order to accurately extrapolate values of ε_r and ε_u. Determination of values of ε' during early reaction is difficult at low frequencies when

space-charge polarization effects are present. Also, the inclusion of the temperature correction factor in Equation 1.21 makes this analysis suspect.

1.5 Defining the Scope of the Research

The development of dielectric spectroscopy as a technique for analyzing polymers and polymeric composites under processing conditions is the focus of this work. The approach taken in this development is to utilize both the ionic and dipolar dielectric responses to extract kinetic and thermodynamic information. The relationships derived for dielectric data analysis are compared to the results of standard thermal analysis techniques using a model thermosetting polymer that has potential application as a matrix in high performance composites.

Chapter 2 contains a description of the experimental aspects of the study. The chemistry and properties of the model epoxy/amine thermosetting resin are first introduced. The different instruments employed and analysis schemes are also described. Dielectric data obtained during both isothermal and nonisothermal cure of the model system are presented and qualitatively interpreted by comparison to calorimetry data.

Quantitative thermal analysis via dielectric spectroscopy is developed through the description of kinetic

and thermodynamic parameters in terms of the dielectric properties in Chapter 3. Specifically, expressions for the activation energies of dielectric transitions and chemical reaction are derived. The equations are checked by comparing the parameters calculated from the dielectric data for the model system to those obtained by standard thermal analysis techniques.

The dielectric response of thermosetting resins during isothermal cure is addressed in more detail in Chapter 4. The effects of reaction on both ionic conductivity and dipolar relaxation are determined and a modelling approach combining the two phenomena is developed. A method for determining the contribution of electrode polarization to the observed values of ε' is also described. The parameters are determined from the dielectric data during isothermal cure of the model system in a wide range of temperatures. The implications of the parameter values are also discussed.

Expressions describing the dielectric properties of thermosets during cure under nonisothermal conditions are developed in Chapter 5. Ionic conductivity effects, electrode polarization, and dipolar relaxation are again included. The approach taken in Chapter 4 was applied to nonisothermal cure based on qualitative similarities between the dielectric cure properties noted in Chapter 2. The isothermal relaxation equations are extended by

incorporating the temperature dependence of the relaxation time and by making several assumptions. The nonisothermal model parameters are determined for the model system and compared to the isothermal parameters.

This work provides a significant step in applying dielectric thermal analysis to both thermosetting and thermoplastic high performance matrices for composites. The significance of the research and additional areas of concentration for future investigation are summarized in Chapter 6. The success of this study permits dielectric spectroscopy to be applied to polymer property characterization in general and perhaps to closed-loop control of polymer composite processing.

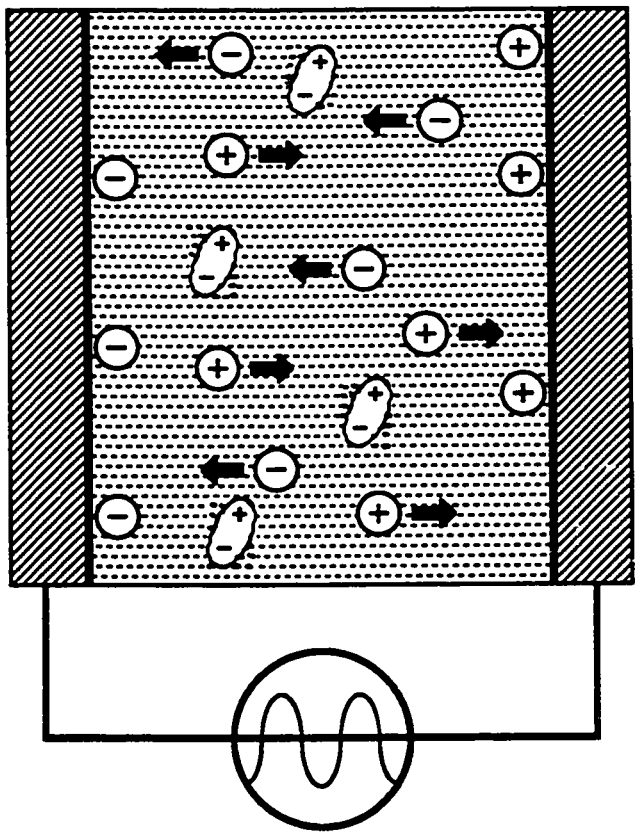

Figure 1.1 - Behavior of ions and dipoles in an electric field.

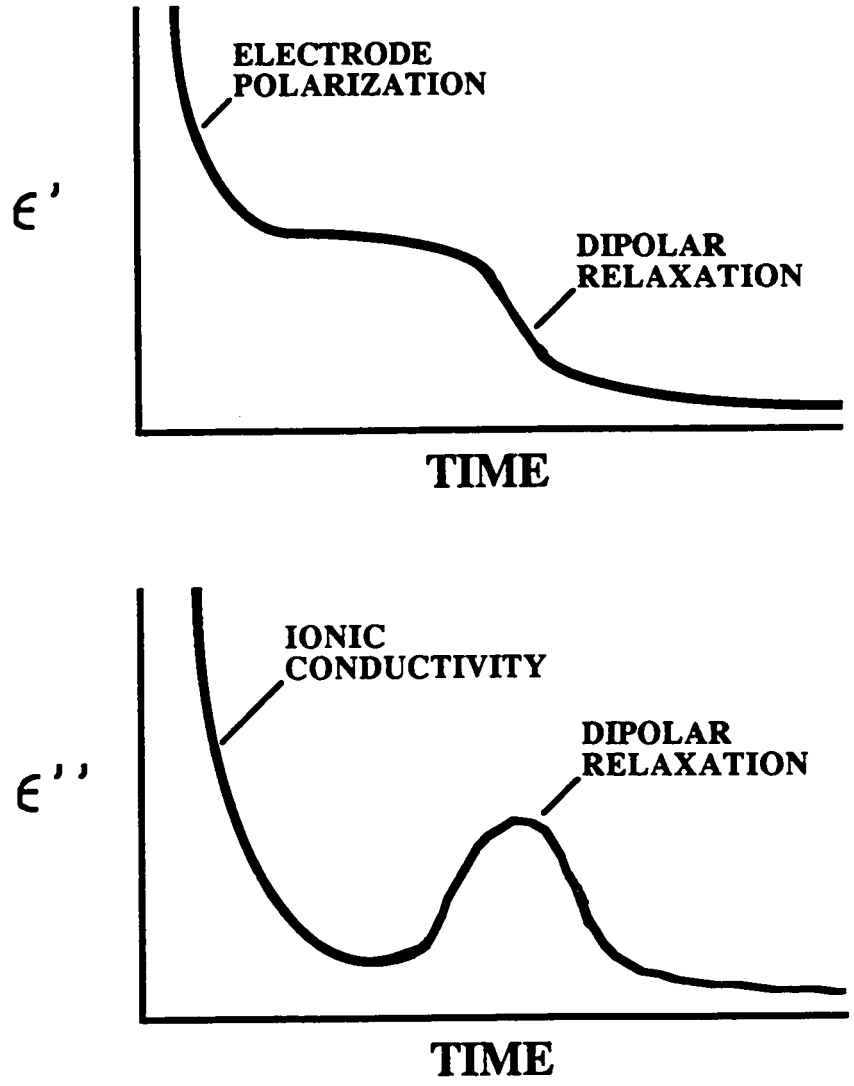

Figure 1.2 - Typical isofrequency dielectric responses of thermosetting polymers during isothermal cure.

Notes to Chapter 1

1. T-W. Chou, R.L. McCullough, and R.B. Pipes, Scientific American, 225, 192 (1986).

2. P.M. Hergenrother and N.J. Johnston, Polym. Matl. Sci. Eng., 59, 697 (1988).

3. J.C. Seferis and P.S. Theocaris, Eds., Interrelationships Between Processing, Structure, and Properties of Polymeric Materials, Elsevier, Amsterdam, 1984.

4. J.C. Seferis, Polym. Comp., 7, 158 (1986).

5. Polym. Comp., 28, (1988).

6. V. Wigotsky, Plast. Eng., 14, 25 (1988).

7. R.M. McLane, Proc. Ann. Tech. Conf., Am. Soc. Comp., 3, 23 (1988).

8. J.C. Seferis, SAMPE J., 24, 6 (1988).

9. M.A. Acitelli, R.B. Prime, and E. Sacher, Polymer, 12, 335 (1971).

10. R.B. Prime and E. Sacher, Polymer, 13, 455 (1972).

11. M.A. Golub, N.R. Lerner, and M.S. Hsu, J. Appl. Polym. Sci., 32, 5215 (1986).

12. G.A. George and D.P. Schweinsberg, J. Appl. Polym. Sci., 33, 2281 (1987).

13. S.F. Scarlata and J.A. Ors, Polym. Comm., 27, 41 (1986).

14. F.W. Wang, A.J. Bur, R.E. Lowry, and B.N. Fanconi, Polym. Matl. Sci. Eng., 59, 600 (1988).

15. M. Shmorhun, A.M. Jamieson, and R. Simha, Polymer, 29, 1960 (1988).

16. R.L. Levy, Polym. Matl. Sci. Eng., 50, 124 (1984).

17. C.S.P. Sung, I-J. Chen, and W-C. Yu, Macromol., 18, 1510 (1985).

18. R.L. Levy and S.D. Schwab, ACS Symp. Ser., 367, 113 (1988).

19. S.D. Schwab and R.L. Levy, Polym. Matl. Sci. Eng., 59, 591 (1988).

20. E. Turi, Ed., Thermal Characterization of Polymeric Materials, Academic Press, New York, 1981.

21. F. Zitomer, Anal. Chem., 40, 1091 (1968).

22. S.M. Dyszel, Thermochim. Acta., 61, 169 (1983).

23. J. Khorami, G. Chauvette, A. Lemieux, H. Menard, and C. Jolicoeur, Thermochim. Acta, 103, 221 (1986).

24. G.A. Sofer and E.A. Hauser, J. Polym. Sci., 8, 611 (1952).

25. R.G.C. Arridge and J.H. Speake, Polymer, 13, 443 (1972).

26. A.M. Lindrose, Exp. Mech., 18, 227 (1978).

27. H.T. Hahn, Nondestructive Methods for Material Property Determination, C. Rund, Ed., Plenum, New York, 1983.

28. E.M. Woo and J.C. Seferis, J. Comp. Matl., 21, 262 (1987).

29. R.T. Harrold and Z.N. Sanjana, Proc. Ann. Tech. Conf., Soc. Plast. Eng., 31, 331 (1985).

30. A. Torres-Filho, C.F. Perondi, and L.C. Miranda, J. Appl. Polym. Sci., 35, 103 (1988).

31. E.A. Cooper, M.W. Urban, and T. Provder, Polym. Matl. Sci. Eng., 59, 316 (1988).

32. L.H. Baekelund, Ind. Eng. Chem., 1, 149 (1909).

33. R.W. Warfield, Testing of Polymers, Vol. 1, J.V. Schmitz, Ed., Interscience, New York, 1965.

34. R.H. Keinle and H.H. Race, Trans. Electrochem. Soc., 65, 87 (1934).

35. M.N. Fineman and I.E. Puddington, Ind. Eng. Chem., 39, 1288 (1947).

36. M.N. Fineman and I.E. Puddington, Can. J. Research, B25, 101 (1947).

37. J.A. Aukward, R.W. Warfield and M.C. Petree, J. Polym. Sci., 27, 199 (1958).

38. R.W. Warfield and M.C. Petree, J. Polym. Sci., 37, 305 (1959).

39. R.W. Warfield and M.C. Petree, Macromol. Chem., 58, 139 (1962).

40. J.A. Uutratu, J. Polym. Sci., Polym. Chem. Ed., 27, 1609 (1986).

41. D.J. Crabtree, Proc. Ann. Conf., Soc. Adv. Matl. Proc. Eng., 22, 636 (1977).

42. S. Yalof, Adhesives Age, 18, 23 (1975).

43. Y.T. Jang, D. Parikla, and P.J. Phillips, J. Polym. Sci., Polym. Phys. Ed., 23, 2483 (1985).

44. S. Persson, Polym. Test., 6, 47 (1986).

45. C. Domenici, G. Levita, A. Marchetti, and V. Frosini, J. Appl. Polym. Sci., 34, 2285 (1987).

46. Y.P. Chen, J.F. Pollard, J.D. Graybeal, and T.C. Ward, Polym. Prepr., 29, 207 (1988).

47. J.D. Reid, W.H. Lawrence, and R.P. Buck, J. Appl. Polym. Sci, 31, 1771 (1986).

48. J.D. Reid and R.P. Buck, J. Appl. Polym. Sci, 33, 2293 (1987).

49. S.A. Yalof and W.J. Wrasidlo, J. Appl. Polym. Sci., 16, 2159 (1972).

50. C.A. May, Proc. Ann. Conf., Soc. Adv. Matl. Proc. Eng., 20, 108 (1975).

51. M.J. Yokota, Proc. Ann. Conf., Soc. Adv. Matl. Proc. Eng., 22, 416 (1977).

52. Y.A. Tajima, Polym. Comp., 3, 162 (1982).

53. C.A. May, M.R. Dusi, J.S. Fritzen, D.K. Hadad, M.G. Maximovich, K.G. Thrasher, and A. Wereta, ACS Symp. Series, 227, 1 (1983).

54. C.A. May, Pure Appl. Chem., 55, 811 (1983).

55. C. Carlini, A. Rolla, and E. Tombari, J. Polym. Sci., Polym. Let. Ed., 23, 5 (1985).

56. W.X. Zukas and S.E. Wentworth, Proc. Ann. Tech. Conf., Soc. Plast. Eng., 32, 336 (1986).

57. D.E. Kranbuehl, S.E. Delos, and P.K. Jue, Polymer, 27, 11 (1986).

58. R.D. Hoffman, J.J. Godfrey, D.E. Kranbuehl, L. Weller, and M.S. Hoff, J. Reinf. Plast. Comp., 6, 223 (1987).

59. D.E. Kranbuehl, S.E. Delos, M.S. Hoff, M.E. Whitham, L.W. Weller, P.D. Haverty, and T. Freeman, Proc. Sixth Intl. Conf. Comp. Matl., 1, 70 (1987).

60. W.X. Zukas and S.E. Wentworth, Polym. Comp., 8, 232 (1987).

61. G.W. Bogan, M.E. Lyssy, G.A. Monnerat, and E.P. Woo, SAMPE J., 24(6), 19 (1988).

62. J.W. Lane, J.C. Seferis, and M.A. Bachmann, Polym. Eng. Sci., 26, 346 (1986).

63. D.R. Day, Polym. Eng. Sci., 26, 362 (1986).

64. W.W. Bidstrup, N.F. Sheppard, Jr., S.D. Senturia, Polym. Eng. Sci., 26, 358 (1986).

65. S.D. Senturia, N.F. Sheppard, Jr., H.L. Lee, and S.B. Marshall, SAMPE J., 19, 22 (1983).

66. Z.N. Sanjana, Polym. Eng. Sci., 26, 373 (1986).

67. D.E. Kranbuehl, S.E. Delos, E. Yi, J. Mayer, T. Jarvie, W. Winfree, and T. Hou, Polym. Eng. Sci., 26, 338 (1986).

68. D.E. Kranbuehl, S.E. Delos, M.S. Hoff, P. Haverty, R. Hoffman, J. Godfrey, and W. Freeman, Proc. Ann. Tech. Conf., Soc. Plast. Eng., 33, 1031 (1987).

69. D.E. Kranbuehl, M.S. Hoff, T. Hamilton, R. Clark, and W. Freeman, Polym. Matl. Sci. Eng., 59, 1116 (1988).

70. D.E. Kranbuehl, M.S. Hoff, D.A. Eichinger, A.C. Loos, and W.T. Freeman, Jr., Proc. Ann. Tech. Conf., Am. Soc. Comp., 3, 313 (1988).

71. J. Jow, M.C. Hawley, M. Finzel, and T. Kern, Polym. Eng. Sci., 28, 1450 (1988).

72. J. Jow, M.C. Hawley, and J.D. DeLong, Proc. Ann. Tech. Conf., Am. Soc. Comp., 3, 305 (1988).

73. N.G. McCrum, B.E. Read, and G. Williams, Anelastic and Dielectric Effects in Polymeric Solids, Wiley and Sons, London, 1967.

74. R.A. Fava and A.E. Horsfield, Brit. J. Appl. Phys. (J. Phys. D), Ser. 2, 1, 117 (1968).

75. M.E. Baird, Electrical Properties of Polymeric Materials, The Plastics Institute, London, 1973.

76. E.B. Stark, A.M. Ibrahim, T.E. Munns, and J.C. Seferis, J. Appl. Polym. Sci., 30, 1717 (1985).

77. D.R. Day, T.J. Lewis, H.L. Lee, and S.D. Senturia, J. Adhesion, 18, 73 (1985).

78. R.L. McCullough, Comp. Sci. Tech., 22, 3 (1985).

79. G. Bánhegyi, Colloid Polym. Sci., 266, 11 (1988).

80. S.A. Bidstrup, N.F. Sheppard, Jr., and S.D. Senturia, Proc. Ann. Tech. Conf., Soc. Plast. Eng., 33, 987 (1987).

81. M.L. Williams, R.F. Landel, and J.D. Ferry, J. Am. Chem. Soc., 77, 370 (1955).

82. A.T. DiBenedetto, J. Macromol. Sci., Rev. Macromol. Chem., C3, 69 (1969).

83. W.W. Bidstrup and S.D. Senturia, Proc. Ann. Tech. Conf., Soc. Plast. Eng., 33, 1035 (1987).

84. S.A. Bidstrup, N.F. Sheppard, Jr., and S.D. Senturia, Polym. Matl. Sci. Eng., 56, 173 (1987).

85. W.W. Bidstrup, S.A. Bidstrup, and S.D. Senturia, Proc. Ann. Tech. Conf., Soc. Plast. Eng., 34, 960 (1988).

86. B.W. Fuller, J.T. Gotro, and G.C. Martin, Polym. Matl. Sci. Eng., 59, 975 (1988).

87. G.C. Martin, A.V. Tungare, and J.T. Gotro, Polym. Matl. Sci. Eng., 59, 980 (1988).

88. W.M. Sanford and R.L. McCullough, Proc. Ann. Tech. Conf., Am. Soc. Comp., 2, 21 (1987).

89. P.B. Macedo and T.A. Litovitz, J. Chem. Phys., 42, 245 (1965).

90. A.J. Warner, ASTM Bull., 153, 60 (1948).

91. J.W. Lane and R.K. Khattak, Proc. Ann. Tech. Conf., Soc. Plast. Eng., 33, 982 (1987).

92. F. Bueche, Physical Properties of Polymers, Interscience, New York, 1962.

93. N.F. Sheppard and S.D. Senturia, Polym. Eng. Sci., 26, 354 (1986).

CHAPTER 2

EXPERIMENTAL STUDY

2.1 Introduction

Dielectric and calorimetric measurements were performed during the isothermal and nonisothermal cure of a model thermosetting resin. The model system is first introduced with a description of both the dielectric equipment and experimental conditions relating to composite processing. Comparison of the dielectric and calorimetric data permits qualitative explanation of the dielectric properties in terms of the chemical and physical events which occur during cure.

2.2 Model Thermosetting Matrix

2.2.1 Chemical Composition and Reactions

The thermosetting matrix system used in this study was a model high performance epoxy/amine resin system, consisting of tetraglycidyl 4,4'-diaminodiphenyl methane, TGDDM (MW = 422.49), cured with 4,4'-diaminodiphenyl sulfone hardener, DDS (MW = 248.31). The chemical structures of these components are shown in Figure 2.1. The resin composition used 25 phr (parts per hundred parts

resin) DDS, an epoxy-rich mixture of 43% amine stoichiometry.

This system is of particular interest since TGDDM and DDS are the primary components of several extensively used resins and carbon fiber prepregs for aerospace and electronic applications. Systems such as Narmco 5208, Hercules 3501-6, and Fiberite 934 are commercially available. Given their widespread usage, a large research effort has been placed toward characterizing the chemistry and properties of the TGDDM/DDS system and other epoxy/amine resins [1-28], especially by Seferis et al. [13-28].

Four reactions, summarized in Figure 2.2, have been identified to occur during the cure of epoxy/amine resins [1,2]: epoxide/primary amine addition, epoxide/secondary amine addition, epoxide homopolymerization, and epoxide/hydroxyl addition. The epoxide/amine reactions are the primary means of polymerization, although the epoxide/hydroxyl reaction becomes more important near the completion of cure. The reaction rates are affected by diffusion limitations as polymerization proceeds. The relative rates of the secondary amine, homopolymerization, and hydroxyl reactions compared to the primary amine reaction are 0.01, 0.01, and 0.005, respectively [5,7].

2.2.2 Resin Preparation

TGDDM and DDS were obtained commercially as Ciba-Geigy MY 720 and Ciba-Geigy HT 976 and used as received. The resin mixture was prepared to insure homogeneous mixing without pre-reaction [16]. TGDDM was first heated to 135°C in an oil bath and stirred for 10 minutes. DDS was added gradually during the next 12 minutes. After adding DDS, the mixture was stirred for an additional 5 minutes, removed from the oil bath, degassed at 95°C under 30mm Hg vacuum for 30 minutes, and stored at -10°C to prevent pre-reaction. Precautions were taken to minimize exposure of the resin to moisture.

2.3 Dielectric Spectroscopy

2.3.1 Equipment

The resin cure was monitored using a previously designed disposable two terminal dielectric cell [29], which is diagrammed in Figure 2.3. Aluminum foil electrodes were glued onto standard glass laboratory slides (1 x 3 in.) using quick curing epoxy cement. The effective area of each aluminum foil electrode was 4.0 cm^2. A Teflon^R dam provided a 0.159 cm (1/16 in.) spacing between the electrodes. This geometry produced electric field edging effects in the dielectric data of ~13% [30]. Approximately 1.0 cm^3 of

resin was poured into the cell. This volume of resin extended one centimeter beyond the electrode area.

In total, three different dielectric apparatus were used during the course of the study. The cure data presented in this chapter were obtained by a General Radio (GenRad) 1688 Precision Digibridge with a frequency range of 240 Hz to 20 KHz. A Hewlett Packard 9000 computer controlled data acquisition. The real and imaginary components of the dielectric constant were calculated from the measured values of capacitance, dissipation, and electrode geometry using Equations 1.6 and 1.7. Values of ε' and ε'' were calculated in real time and stored on floppy disk for subsequent analysis.

Special experiments used one of two other dielectric apparatus. Reproducibility and specific instrument experiments were performed using the Tetrahedron ADR-380 Automatic Dielectric Rheometer, which is suited for industrial cure monitoring rather than analytical applications. The ADR-380 has a frequency range of 1 Hz to 100 KHz. Data acquisition and storage were controlled by a dedicated AT-type computer. The ADR reported only capacitance and dissipation measurements. These data were converted to ε' and ε'' by modifying a version of the ADR data acquisition software.

Additional experiments were performed using the new

DuPont 2970 Dielectric Analyzer (DEA) [31]. The 2970 DEA is currently able to perform dielectric measurements using either specially designed three terminal parallel plate electrodes or single surface interdigitated electrodes. An integrated linear variable differential transducer (LVDT) performs real time measurements of electrode spacing, allowing experimental values of ε' and ε'' to be calculated in real time. Generally, the parallel plate electrodes were used for solid samples and the single surface electrodes were used for liquid samples.

2.3.2 Experimental Conditions

The dielectric properties of the TGDDM/DDS system were monitored by the GenRad 1688 during isothermal cure at 140, 150, 160, 170, 180, 190, 200, 210, and 220°C. Seferis and co-workers cured TGDDM/DDS isothermally for 2 hours at 177°C for complete reaction [13]. This cycle was used as a basis for determining the cure times at each temperature, which are summarized in Table 2.1. The experiments were performed in an Exocal HT 250 silicon oil bath. The filled two terminal cells were immersed in the bath for 30 seconds to equilibrate at the desired isothermal temperature. The dielectric properties were monitored at 240 Hz, 700 Hz, 2 KHz, 4 KHz, 10 KHz, and 20 KHz.

Samples of TGDDM/DDS resin were monitored during

nonisothermal cure using a modified version of the two terminal dielectric cell. The foil electrode dimensions were the same as in the isothermal experiments, but the electrodes were glued to 1 x 1 1/2 in. glass slides, rather than 1 x 3 in. slides, due to the size of the DMA heating chamber. The spacing between the electrodes was kept to 0.159 cm (1/16 in.) by a Teflon dam. The cells were again filled with 1.0 cm^3 of resin.

Nonisothermal temperature control was made possible by performing the experiments in the heating chamber of a DuPont 982 Dynamic Mechanical Analyzer (DMA) controlled by a DuPont 1090 Thermal Analyzer. The modified dielectric cell was placed inside the DMA sample area with the radiation heat shield installed. The DMA sample thermocouple was placed flush against the dielectric cell to minimize thermal lag between the resin and programmed chamber temperature. The TGDDM/DDS model system was dielectrically monitored at 240 Hz, 700 Hz, 2 KHz, 4 KHz, 10 KHz, and 20 KHz during nonisothermal cure from room temperature to 350°C at heating rates of 1, 5, and 10°C/minute.

2.3.3 Results

2.3.3.1 Isothermal Dielectric Response

The dielectric properties measured during isothermal

cure are presented in Figures 2.4 - 2.12. These data exhibit characteristics of the three dielectric phenomena described previously: ionic conductivity, electrode polarization, and dipolar relaxation. The initial decrease in ε'' results from the reduced conduction of ions impeded by the growing polymer network. In epoxy/amine resins, Na^+ and Cl^- impurities are the primary ionic charge carriers [32].

Ionic conductivity effects in the data were quantified by calculating the apparent conductivity at each temperature using ε'' data and Equation 1.8. These data are plotted in Figures 2.13 - 2.21. Curves of apparent conductivity at several frequencies collapse to a single curve when ionic conduction dominates ε''. As expected, ε'' is completely the result of ionic conductivity during the initial stages of cure when resin viscosity is low. The curves diverge as the dipolar contributions to ε'' become significant.

The initial low frequency decrease in ε' seen in Figures 2.4 - 2.12 is caused by electrode polarization, charge buildup at the electrodes. The subsequent plateau in ε' represents the dielectric constant of uncured resin, which is free of polarization. The simultaneous inflection in ε' and peak in ε'', easily observed in the high frequency data, are caused by dipolar relaxation. As seen in Figures 2.4 - 2.12, the location of the inflection is a function of

frequency and may indicate either resin gelation or vitrification [33].

The only difficulty encountered when running the dielectric experiments was resin bubbling at the beginning of the 220°C cure, as evidenced in the initial ε' data in Figure 2.12. Irregularities in the initial ε' cure data at other temperatures may have resulted from smaller amounts of bubble formation.

2.3.3.2 Nonisothermal Dielectric Response

The dielectric properties monitored during the nonisothermal cure of TGDDM/DDS at 1, 5, and 10°C are presented in Figures 2.22 - 2.24. The apparent conductivities at each heating rate are plotted in Figures 2.25 - 2.27. As seen in these curves, a variety of dielectric behaviors is exhibited during the heating and subsequent reaction of TGDDM with DDS. The observed dielectric properties may be understood by comparison to the thermal analysis experimental results.

2.4 Differential Scanning Calorimetry

The TGDDM/DDS resin extent of reaction during cure was determined by differential scanning calorimetry (DSC). In DSC, physical and chemical processes in materials, e.g. reaction, glass transition, crystallization, and melting,

are detected as enthalpic changes. These processes can be detected and characterized from heat flow data obtained as a function of time and temperature. Thermal analysis by DSC has become an important tool for investigating polymer physical behavior and polymerization reaction kinetics [34].

2.4.1 Equipment

DSC cure experiments were performed using a DuPont 910 Differential Scanning Calorimeter interfaced with either a 1090, 9900, or 2000 DuPont Thermal Analyzer. The 910 DSC measures the temperatures of a small aluminum pan containing sample material and an empty reference pan. The enthalpy of the sample is calculated using the temperature difference between the pans and a calibration constant [35].

2.4.2 Experimental Conditions

Isothermal DSC experiments were performed at each of the cure temperatures according to a method described by Prime [36]. In each experiment, the pan containing uncured resin was placed in the DSC cell, which was preheated to 20°C above the desired cure temperature and under a constant nitrogen purge. The cell cooled to the reaction temperature upon opening. Data acquisition was initiated immediately after adding the sample pan. After curing according to the times in Table 2.1, the scan was stopped, the sample pan was

removed and quenched to room temperature, preventing additional reaction. The "residual" heat from incomplete reaction was measured by reheating the cured samples from room temperature to 300°C at 10°C/minute.

Nonisothermal DSC experiments were performed from 30°C to 350°C at the same heating rates used in the dielectric experiments: 1, 5, and 10°C/minute. Reaction was assumed to be 100% complete by the onset of degradation, between 290°C and 350°C. Consequently, residual heat scans were not performed after completing the nonisothermal experiments.

2.4.3 Results

2.4.3.1 Isothermal Experiments

DSC scans of TGDDM/DDS resin during isothermal cure and the corresponding residual heat scans are presented in Figures 2.28 - 2.36. The extent of reaction at time t, α_t, was calculated from the data using the relationship [36]:

$$\alpha_t = \Delta H_t \; / \; \Delta H_{rxn} \qquad (2.1)$$

ΔH_t is the total amount of heat generated by reaction up to time t. ΔH_{rxn} represents the sum of the heat generated during the experiment, ΔH_{tot}, and during the residual heat scan, ΔH_{res}:

$$\Delta H_{rxn} = \Delta H_{tot} + \Delta H_{res} \qquad (2.2)$$

The DuPont DSC reports heat flow in units of power per gram of sample. Partial integration of the heat flow data with time provided values of ΔH_t, and therefore α_t, throughout reaction.

The extent of reaction calculated by Equation 2.1 is an apparent value. The reaction of TGDDM with DDS was treated as a single overall reaction; no assumptions were made regarding which of the four possible reactions listed in Figure 2.2 occurred. The consideration of an overall reaction is appropriate since the individual contributions of the four reactions cannot be determined a priori from the DSC data.

The value of ΔH_{rxn} used in the calculations was determined from the total heat generated during a nonisothermal DSC scan at 10°C/minute, 676.94 J/g. A representative extent of reaction curve is plotted in Figure 2.37 for the 140°C cure. The final extents of reaction for each isothermal cure experiment are summarized in Table 2.2. The apparent activation energy for the reaction of TGDDM with DDS calculated using the maximum peak time method [37], is 16.35 kcal/mole.

2.4.3.2 Nonisothermal Experiments

The TGDDM/DDS extent of reaction during nonisothermal cure was determined from the DSC data as a function of temperature by Equation 2.1. The nonisothermal DSC scans are presented in Figures 2.38 - 2.40. As an example, the calculated extent of reaction data for cure at 1°C/minute are plotted in Figure 2.41. The apparent activation energy of the TGDDM reaction with DDS at this stoichiometry, calculated using the peak exotherm temperature at each heating rate [36], is 15.31 kcal/mole. This value differs from the isothermal DSC activation energy by an acceptable 6.8%.

2.5 Thermal Lag Correction

The nonisothermal dielectric data obtained at 5 and 10°C/minute were corrected to account for the thermal lag between the dielectric cell and the DMA chamber. In this manner, the DSC reaction exotherms and dielectric data could be properly correlated. Data during cure at 1°C/minute, were assumed to be free of thermal lag effects.

The adjusted temperatures were calculated from the DMA thermocouple temperatures using a linear correction:

$$T_{correct} = aT_{DMA} + b \qquad (2.3)$$

By comparing two experimentally measured temperatures with known values, the parameters in Equation 2.3 were determined for each heating rate using a two point slope-intercept method. The most accurate correction was achieved by choosing reference points at both low and high temperatures.

The low temperature reference point was chosen by assuming the low temperature transition seen in Figures 2.23 and 2.24 to be independent of heating rate. Differences between the transition temperatures at each heating rate were attributed to thermal lag. The uncured resin peak at 41.7°C in 20 KHz ε'' data obtained at 1°C/minute was chosen arbitrarily as the low temperature reference point.

The onset of resin degradation was used as the high temperature reference point. As seen in the DSC data in Figures 2.38 - 2.40, the occurrences of cure and degradation are heating rate dependent. The locations of the high temperature minima in both ε' and ε'' were correlated to the DSC degradation onset temperatures.

The correction parameters of Equation 2.3, summarized in Table 2.3, were determined from the reference and DMA thermocouple temperatures. The dielectric data at 5 and 10°C/minute were then appropriately adjusted. The results presented below refer only to temperature-corrected data.

2.6 Comparison of Nonisothermal Dielectric and DSC Data

The changes in the dielectric properties evident in the nonisothermal dielectric data may be understood in qualitative terms when compared to calorimetric data. The dielectric data monitored at 20 KHz for each of the heating rates are superimposed with the calculated extent of reaction data in Figures 2.42 - 2.44. These curves suggest that the nonisothermal dielectric response may be divided into three regions: pre-reaction, reaction, and post-reaction.

2.6.1 Pre-Reaction Region and Glass Transition of Uncured Resin

At temperatures below ~140°C, changes in the dielectric properties arise from sources other than chemical reaction. The glass transition temperature, T_g, measured by DSC for an uncured mixture of TGDDM and 25 phr DDS was -7°C [38]. Therefore, the frequency dependent changes in ε' and ε'' just above room temperature result from the subsidence of the uncured resin glass transition.

At temperatures above T_g, the dielectric properties of the liquid resin are functions of temperature. The influence of ionic conductivity in the dielectric response is observed in Figures 2.25 - 2.27. The convergent curves indicate that the dielectric loss is completely due to ionic

conduction until reaction begins. As expected in the presence of significant amounts of ionic conduction, electrode polarization influences ε' at low frequencies, as seen in Figures 2.22 - 2.24. The decrease in high frequency values of ε' with increasing temperature is due to thermal agitation of the dipoles, which randomizes the net dipolar orientation and decreases the capacitance of the resin [39].

The temperature dependence of conductivity is revealed when the data is plotted in Arrhenius fashion, as in Figures 2.45 - 2.47. Ionic conduction in the liquid is expected to follow the Arrhenius expression for activated processes [40]; however, this behavior is observed in the TGDDM/DDS system only at temperatures less than 100°C above the uncured glass transition. The conductivity curves in Figures 2.45 - 2.47 appear to approach asymptotic values which may depend on the heating rate.

Non-Arrhenius and asymptotic behavior have been reported for the resistivity of a variety of nonreacting liquid polymers, including several epoxy/amine resins, at temperatures "considerably" above T_g [40]. The temperature dependence of the resistivity was also reported to vary with heating rate. While Arrhenius behavior is observed at low temperatures, high temperature conduction is hampered by thermally agitated polymer segmental motion.

2.6.2 Reaction Region

The initiation of resin cure causes abrupt changes in the values of both ε' and ε''. However, the general form of the reaction portions of the nonisothermal data in Figures 2.42 - 2.44 is essentially identical to the isothermal data in Figures 2.4 - 2.12. As in the isothermal experiments, the dielectric properties are initially dominated by ionic conductivity and electrode polarization. Dipolar contributions to both ε' and ε'' become significant as ionic conductivity decreases with reaction.

2.6.3 Post-Reaction Region and Degradation

Upon completion of cure, the dielectric properties again change due to resin degradation. The minima in both ε' and ε'' immediately following reaction result from the completion of cure and the onset of resin degradation. Analysis of the post-reaction dielectric data is hampered by the onset of degradation of both the resin and the epoxy cement used for the dielectric cell construction. Each two terminal cell was observed to be cracked open and charred with burnt cement upon completion of the experiment.

2.7 Conclusions

The dielectric properties of the TGDDM/DDS model high performance resin during both isothermal and nonisothermal

cure were presented. Differential scanning calorimetry experiments were performed in order to obtain values for the extent of reaction under both cure conditions. By comparison to the calorimetry data, the dielectric data were described in terms of chemical and physical events occurring during reaction.

The dielectric properties observed during isothermal reaction were related to changes in the contributions of ionic and dipolar species in the resin. Ionic impurities enhance dielectric loss via conduction and increase dielectric storage via electrode polarization. Relaxation of dipolar segments of the polymer molecules dominate the dielectric properties as ionic conduction and polarization subside with cure.

The nonisothermal dielectric properties were classified into pre-reaction, reaction, and post-reaction temperature regions. The pre-reaction behavior resulted from the glass transition of the uncured resin and temperature effects. Both ionic conduction and dipolar orientation were found to be affected by thermal agitation. The dielectric responses during nonisothermal reaction were nearly identical in form to those obtained during isothermal reaction. Post-reaction properties were affected by resin degradation.

These qualitative descriptions of the dielectric properties aid in applying dielectric spectroscopy as a

method of polymer thermal analysis. However, a more sophisticated treatment is required. The next step in developing dielectric thermal analysis is the development of methods for calculating kinetic and thermodynamic parameters from dielectric data.

Table 2.1

Isothermal reaction temperatures and times for the TGDDM/DDS (25 phr) system

Temperature (°C)	Reaction time (mins.)
140	600
150	480
160	267
170	210
180	150
190	120
200	83
210	60
220	50

Table 2.2

Final extents of reaction measured by DSC for isothermal cure of TGDDM/DDS (25 phr)

Temperature (°C)	α_f
140	0.63
150	0.74
160	0.78
170	0.79
180	0.85
190	0.91
200	0.93
210	0.98
220	0.99

Table 2.3

Thermal lag correction factors

Rate (°C/min)	Tg_o (°C)	Degradation Onset (°C) 20 KHz	DSC
1	41.7	-----	-----
5	51.7	301.4	290.7
10	59.5	340.0	318.3

$$T_{correct} = aT_{DMA} + b$$

Rate (°C/min)	a	b (°C)
5	0.997	-9.78
10	1.008	-18.28

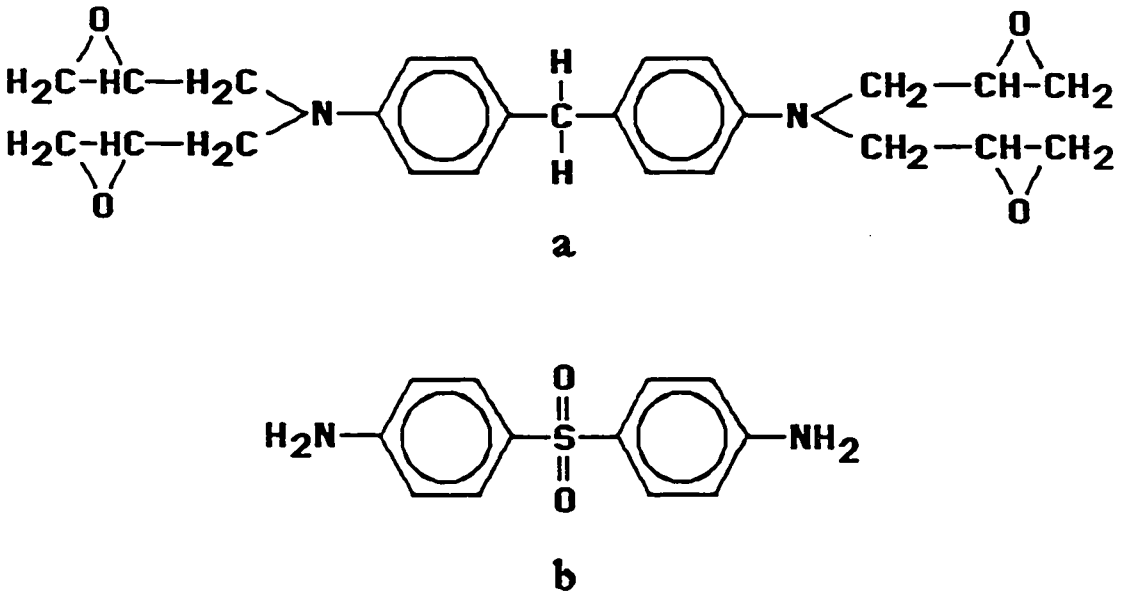

Figure 2.1 - Chemical structures of the components of the model epoxy/amine system: a) tetraglycidyl 4,4'-diaminodiphenyl methane (TGDDM), b) 4,4'-diaminodiphenyl sulfone (DDS).

PRIMARY AMINE-EPOXIDE ADDITION

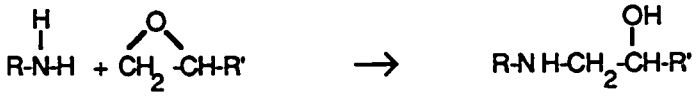

SECONDARY AMINE-EPOXIDE ADDITION

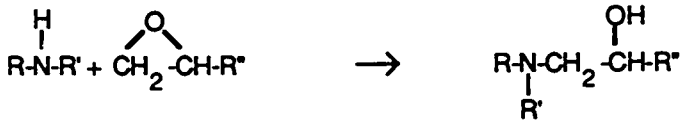

EPOXIDE HOMOPOLYMERIZATION

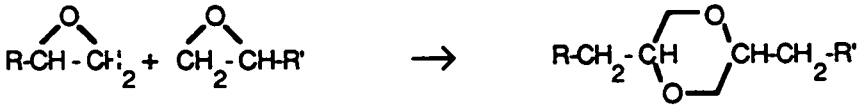

HYDROXY-EPOXIDE ETHERIFICATION

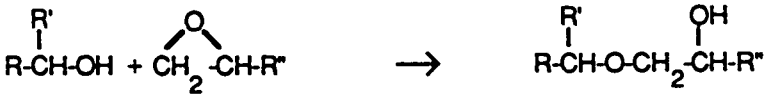

Figure 2.2 - Main reactions which occur during the cure of epoxy/amine resins [1,2].

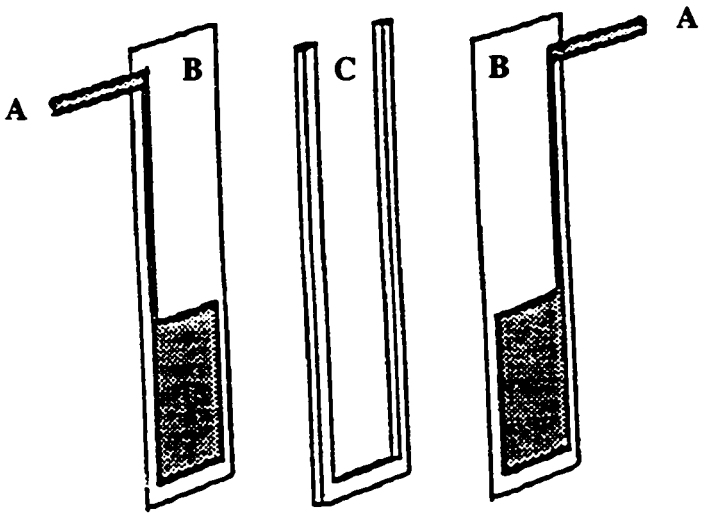

Figure 2.3 - Two terminal dielectric cell (exploded view): a) aluminum foil electrode, b) 1" x 3" glass slide, c) 1/16 " Teflon® dam.

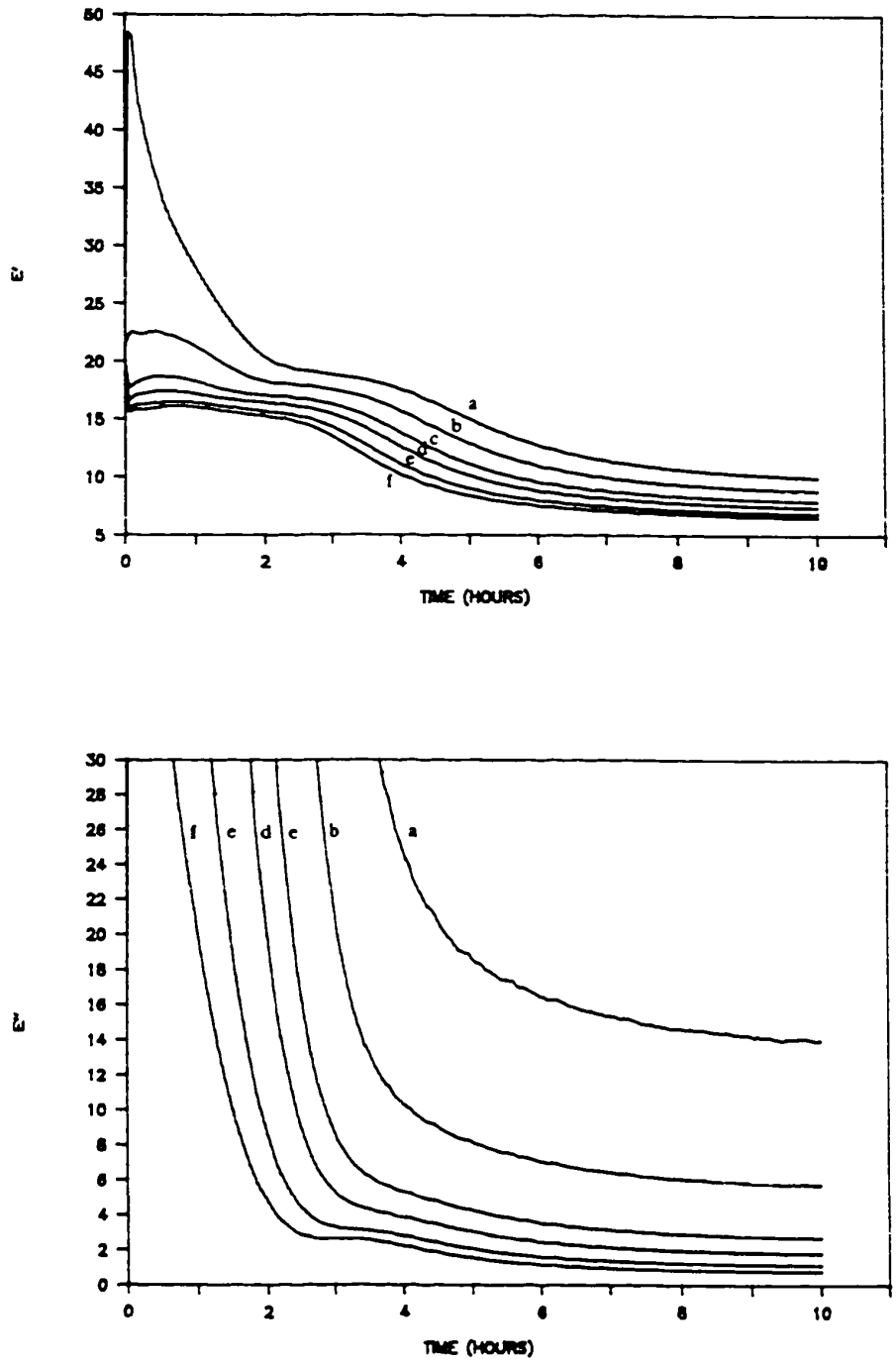

Figure 2.4 - Dielectric properties of TGDDM/DDS during isothermal cure at 140°C: a) 240 Hz, b) 1 KHz, c) 2 KHz, d) 4 KHz, e) 10 KHz, f) 20 KHz.

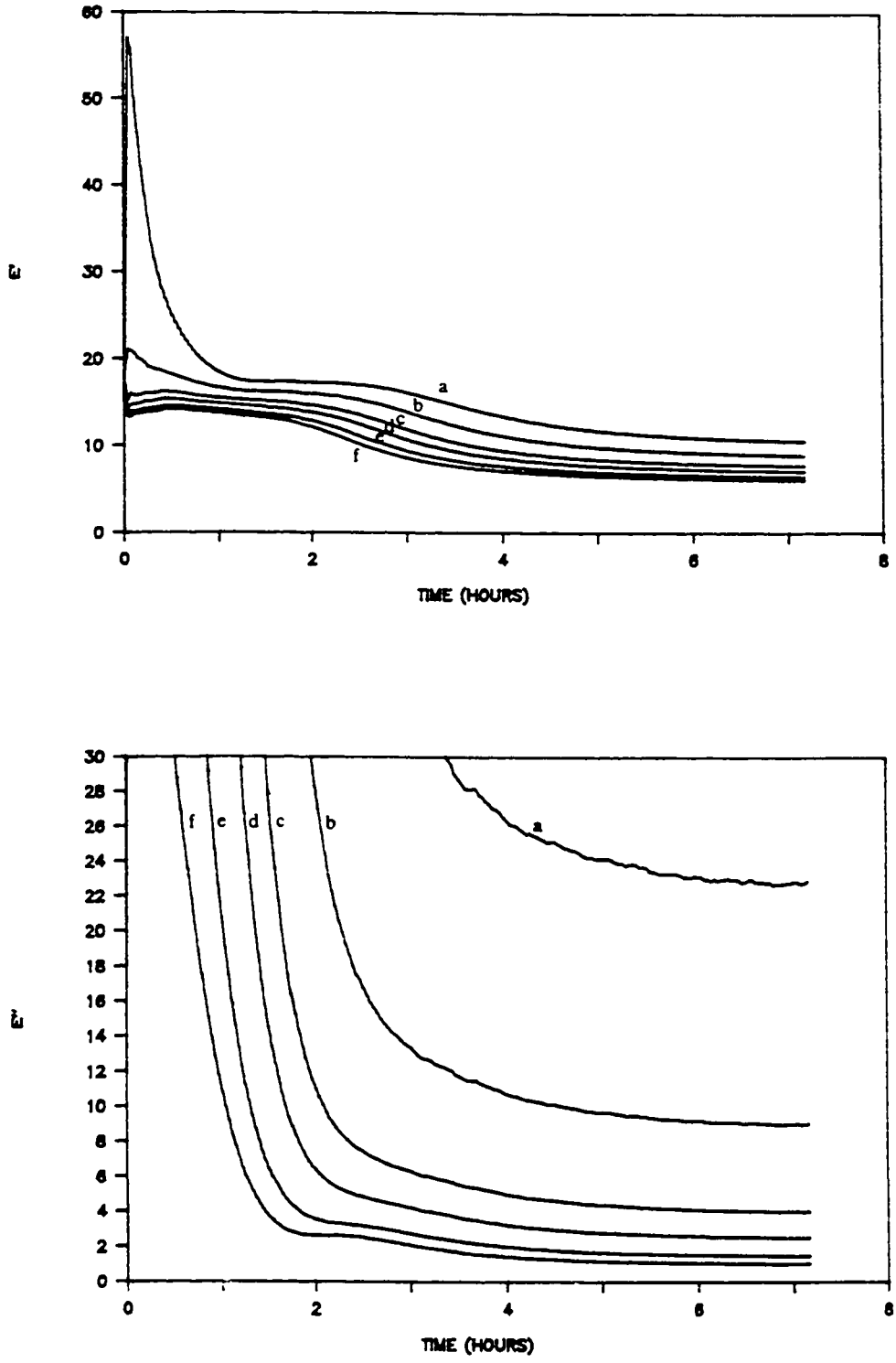

Figure 2.5 - Dielectric properties of TGDDM/DDS during isothermal cure at 150°C: a) 240 Hz, b) 1 KHz, c) 2 KHz, d) 4 KHz, e) 10 KHz, f) 20 KHz.

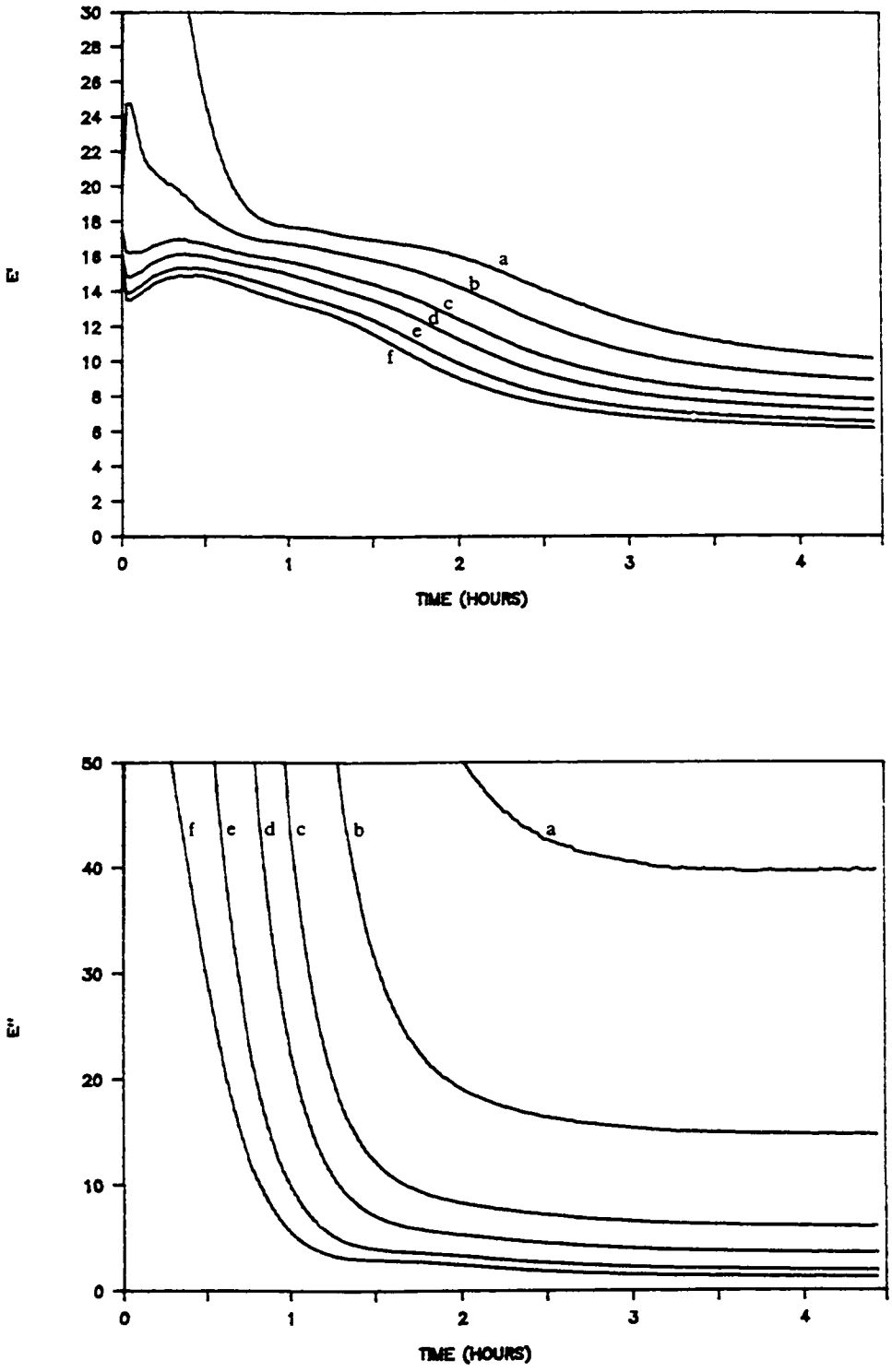

Figure 2.6 - Dielectric properties of TGDDM/DDS during isothermal cure at 160°C: a) 240 Hz, b) 1 KHz, c) 2 KHz, d) 4 KHz, e) 10 KHz, f) 20 KHz.

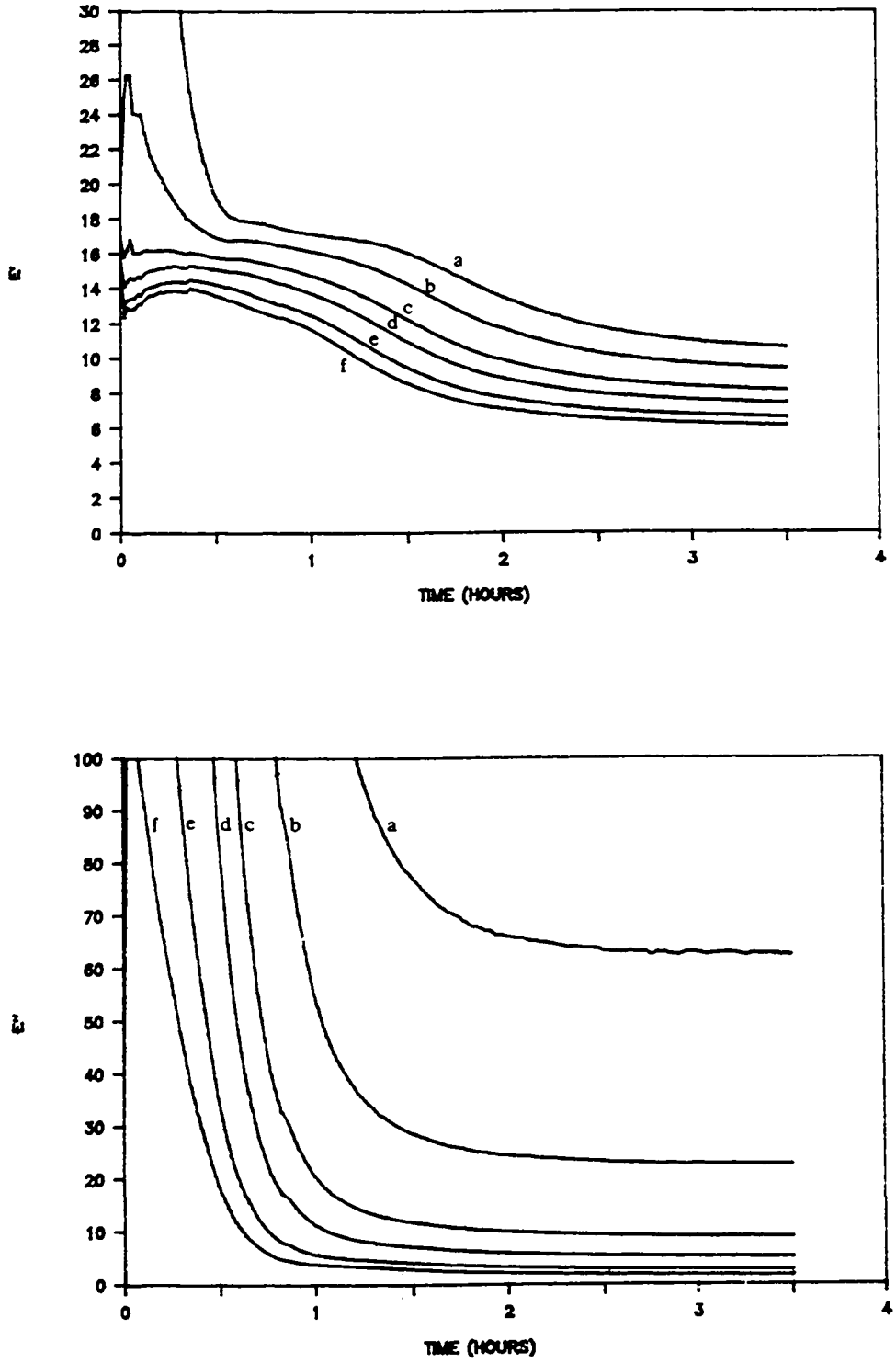

Figure 2.7 - Dielectric properties of TGDDM/DDS during isothermal cure at 170°C: a) 240 Hz, b) 1 KHz, c) 2 KHz, d) 4 KHz, e) 10 KHz, f) 20 KHz.

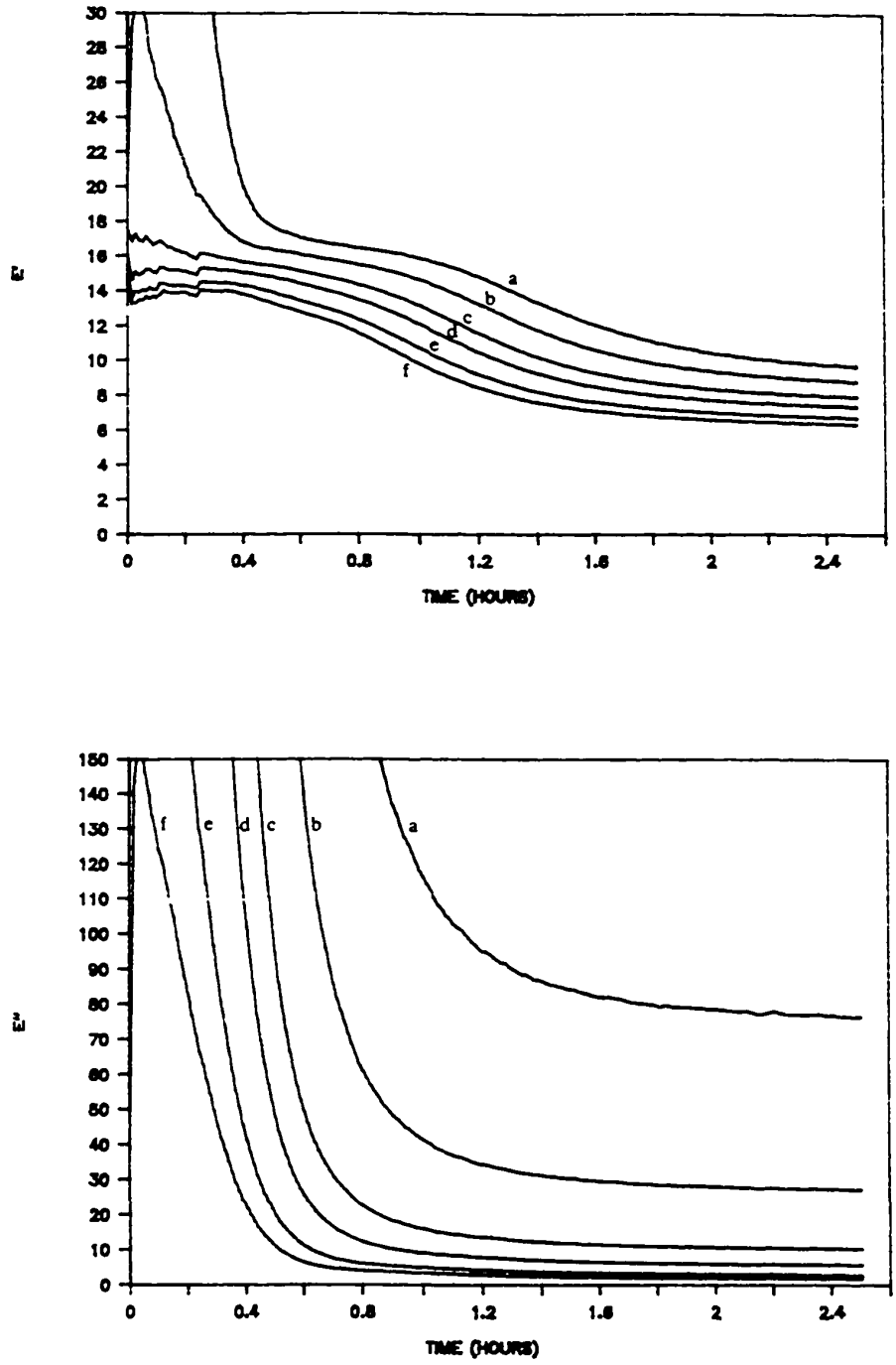

Figure 2.8 - Dielectric properties of TGDDM/DDS during isothermal cure at 180°C: a) 240 Hz, b) 1 KHz, c) 2 KHz, d) 4 KHz, e) 10 KHz, f) 20 KHz.

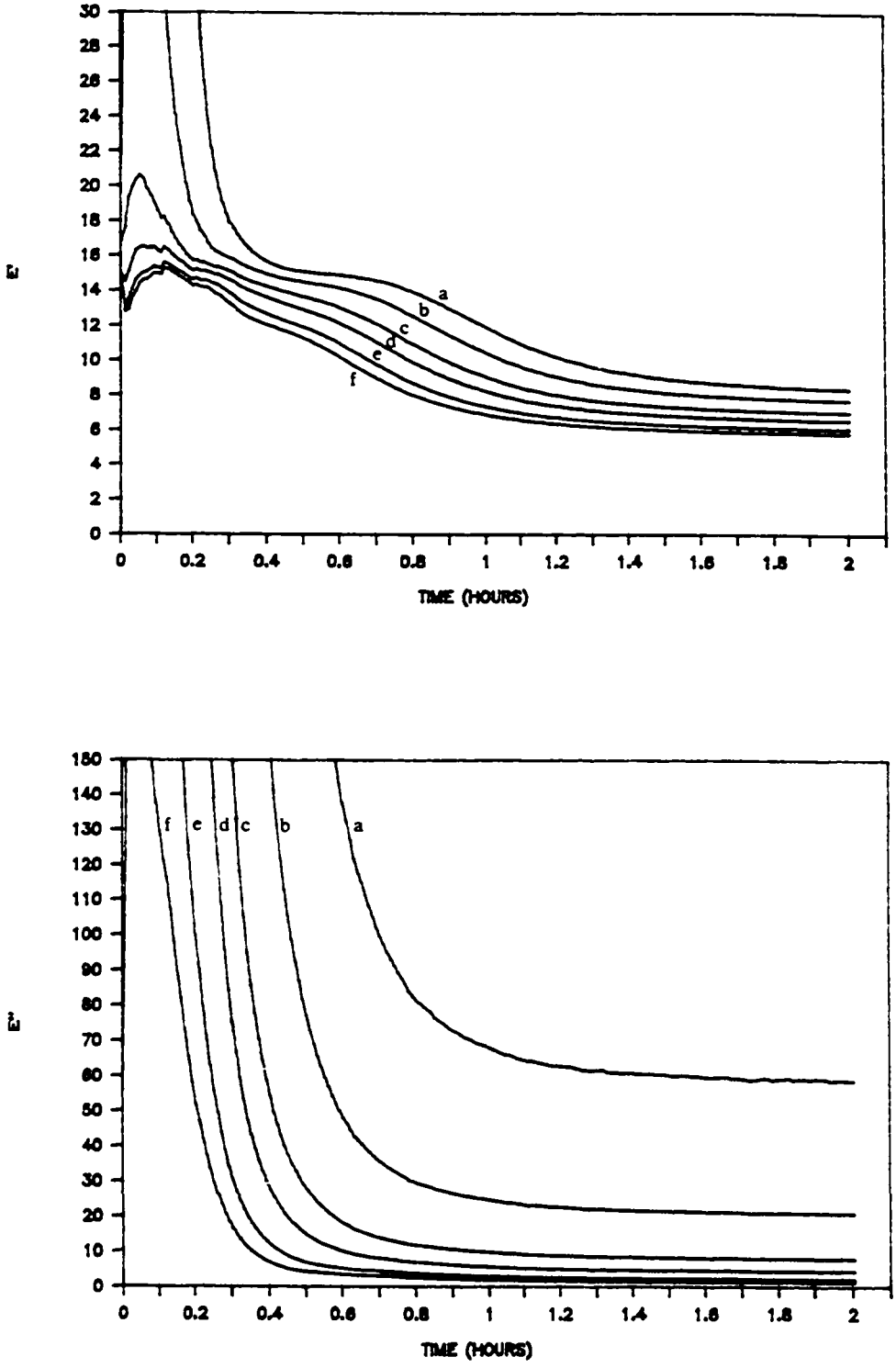

Figure 2.9 - Dielectric properties of TGDDM/DDS during isothermal cure at 190°C: a) 240 Hz, b) 1 KHz, c) 2 KHz, d) 4 KHz, e) 10 KHz, f) 20 KHz.

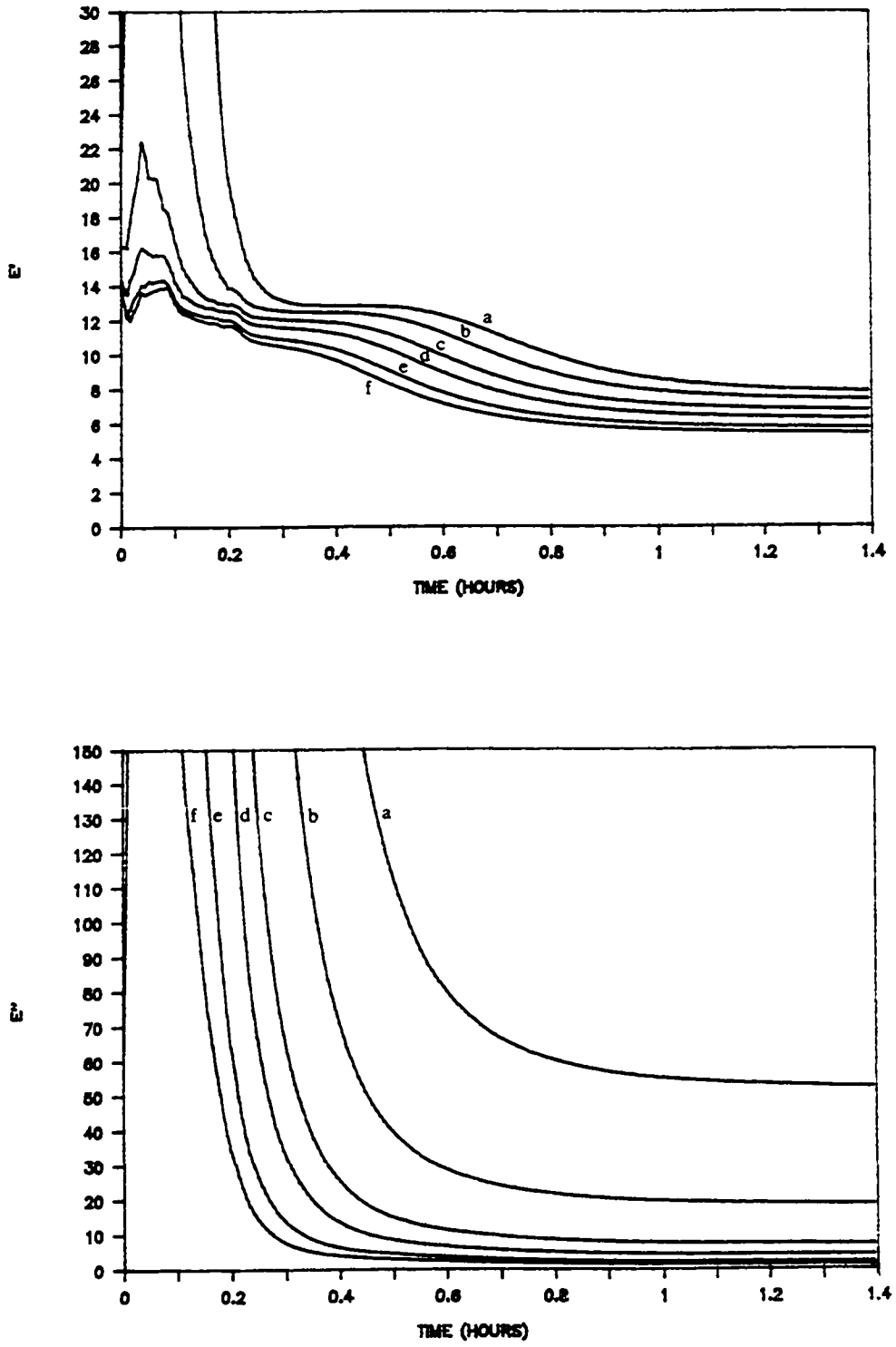

Figure 2.10 - Dielectric properties of TGDDM/DDS during isothermal cure at 200°C: a) 240 Hz, b) 1 KHz, c) 2 KHz, d) 4 KHz, e) 10 KHz, f) 20 KHz.

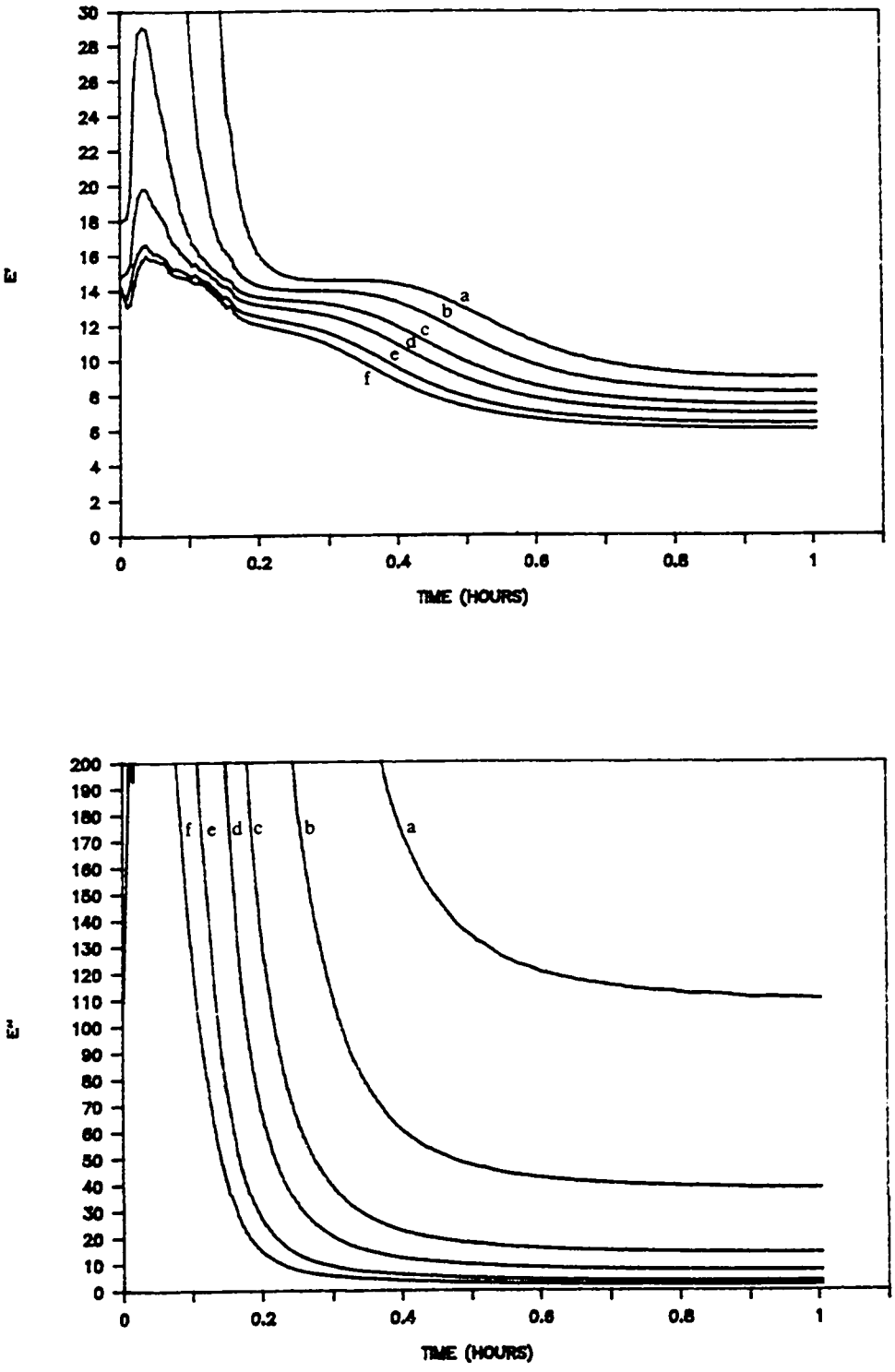

Figure 2.11 - Dielectric properties of TGDDM/DDS during isothermal cure at 210°C: a) 240 Hz, b) 1 KHz, c) 2 KHz, d) 4 KHz, e) 10 KHz, f) 20 KHz.

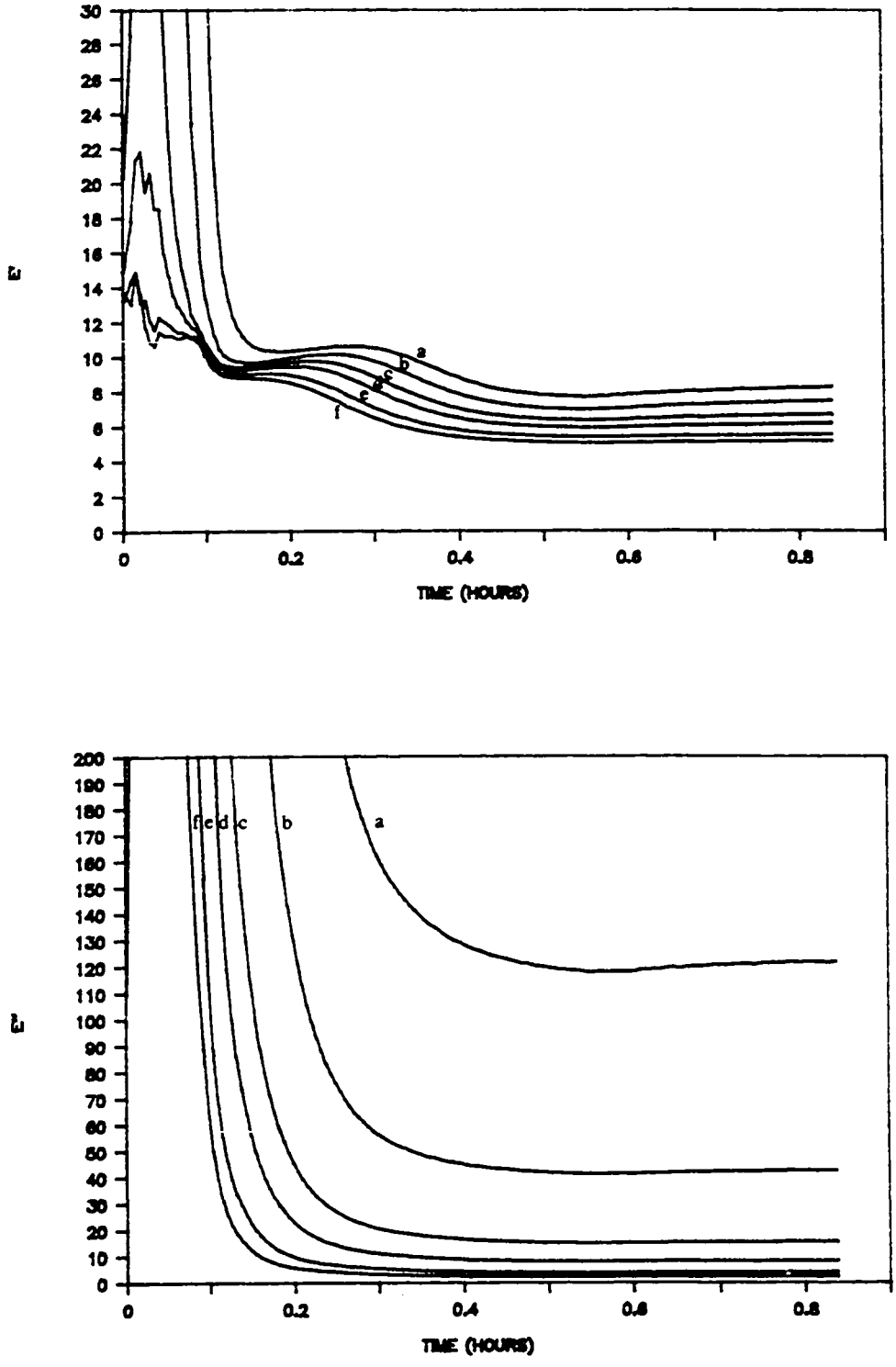

Figure 2.12 - Dielectric properties of TGDDM/DDS during isothermal cure at 220°C: a) 240 Hz, b) 1 KHz, c) 2 KHz, d) 4 KHz, e) 10 KHz, f) 20 KHz.

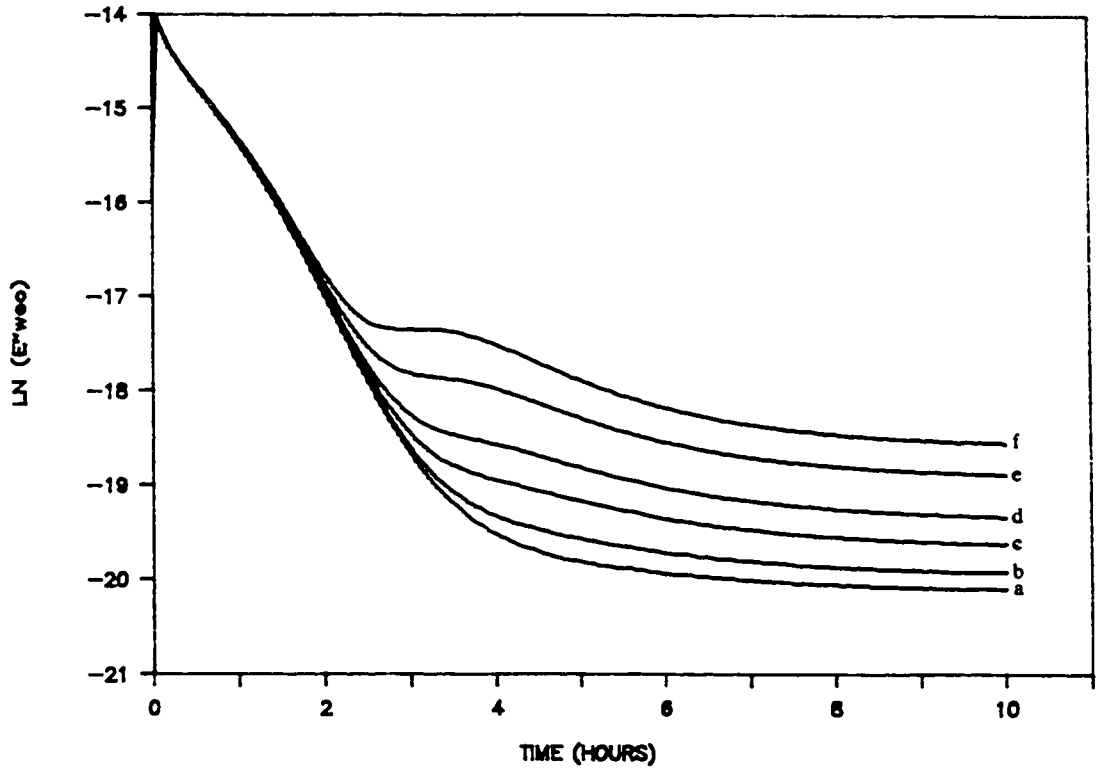

Figure 2.13 - Apparent conductivity of TGDDM/DDS during isothermal cure at 140°C: a) 240 Hz, b) 1 KHz, c) 2 KHz, d) 4 KHz, e) 10 KHz, f) 20 KHz.

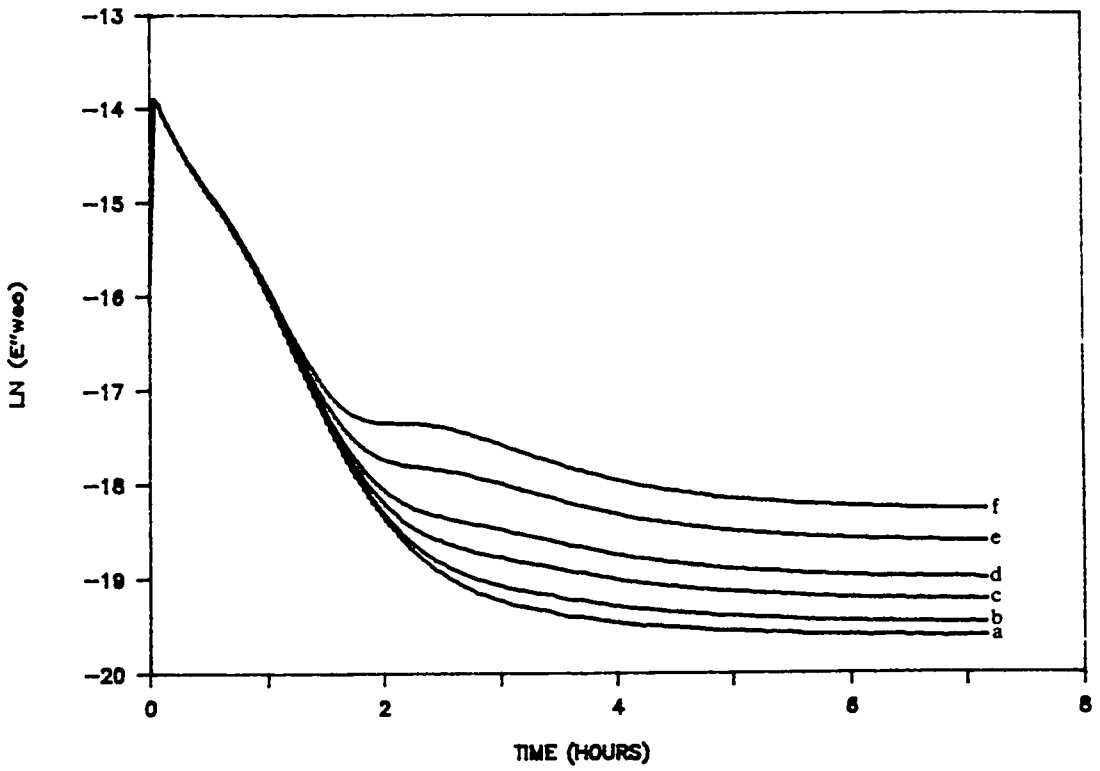

Figure 2.14 - Apparent conductivity of TGDDM/DDS during isothermal cure at 150°C: a) 240 Hz, b) 1 KHz, c) 2 KHz, d) 4 KHz, e) 10 KHz, f) 20 KHz.

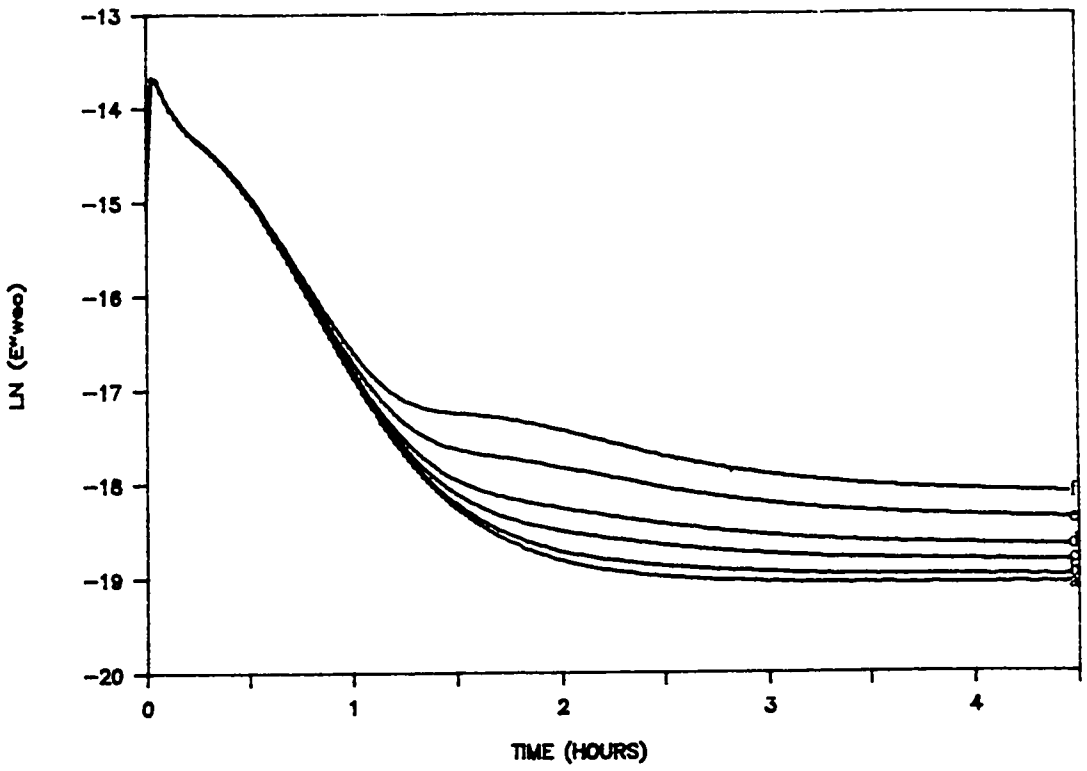

Figure 2.15 - Apparent conductivity of TGDDM/DDS during isothermal cure at 160°C: a) 240 Hz, b) 1 KHz, c) 2 KHz, d) 4 KHz, e) 10 KHz, f) 20 KHz.

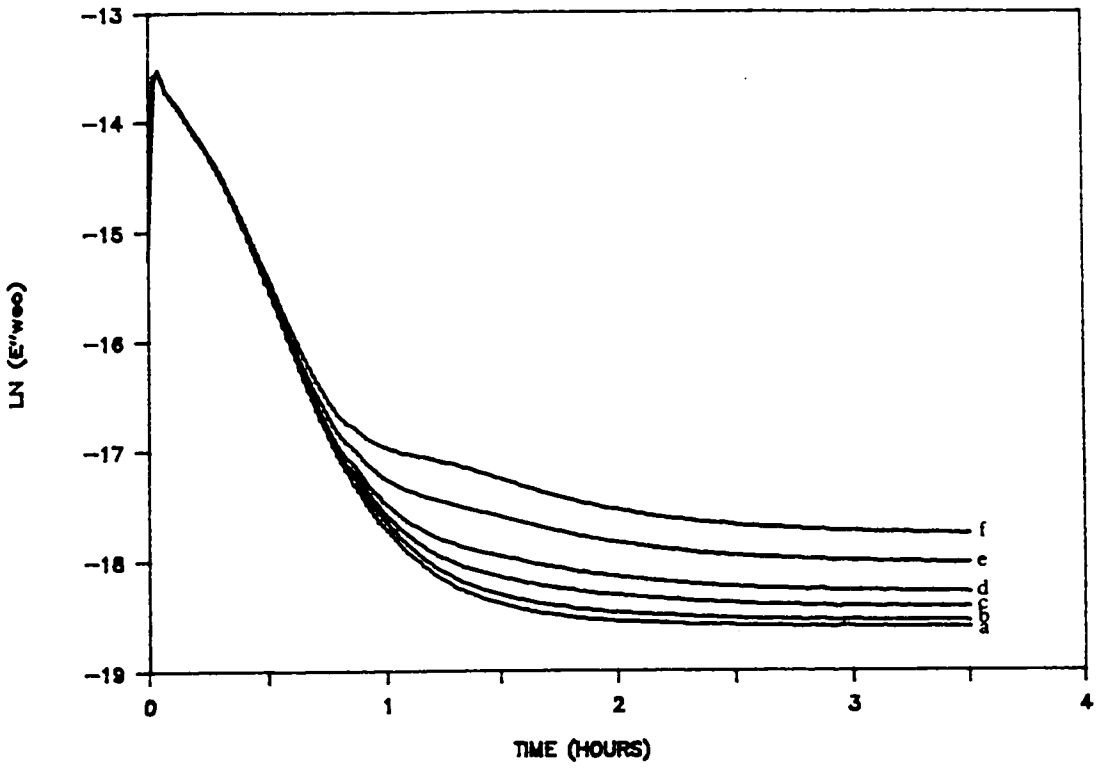

Figure 2.16 - Apparent conductivity of TGDDM/DDS during isothermal cure at 170°C: a) 240 Hz, b) 1 KHz, c) 2 KHz, d) 4 KHz, e) 10 KHz, f) 20 KHz.

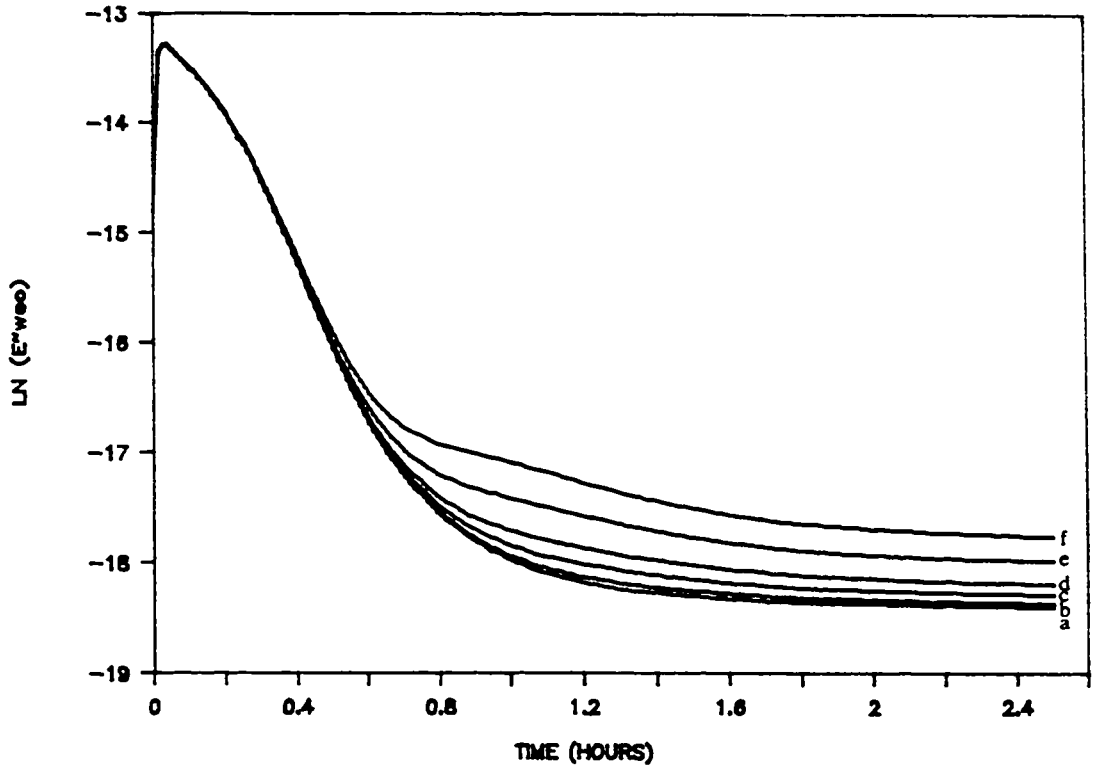

Figure 2.17 - Apparent conductivity of TGDDM/DDS during isothermal cure at 180°C: a) 240 Hz, b) 1 KHz, c) 2 KHz, d) 4 KHz, e) 10 KHz, f) 20 KHz.

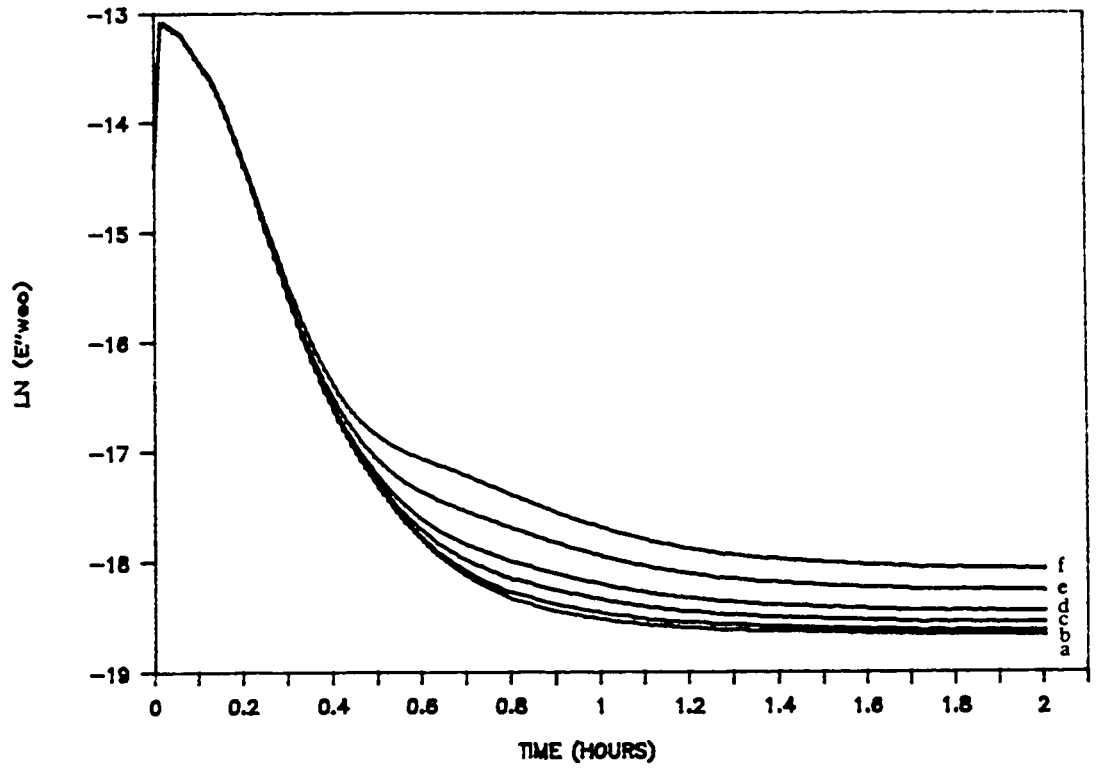

Figure 2.18 - Apparent conductivity of TGDDM/DDS during isothermal cure at 190°C: a) 240 Hz, b) 1 KHz, c) 2 KHz, d) 4 KHz, e) 10 KHz, f) 20 KHz.

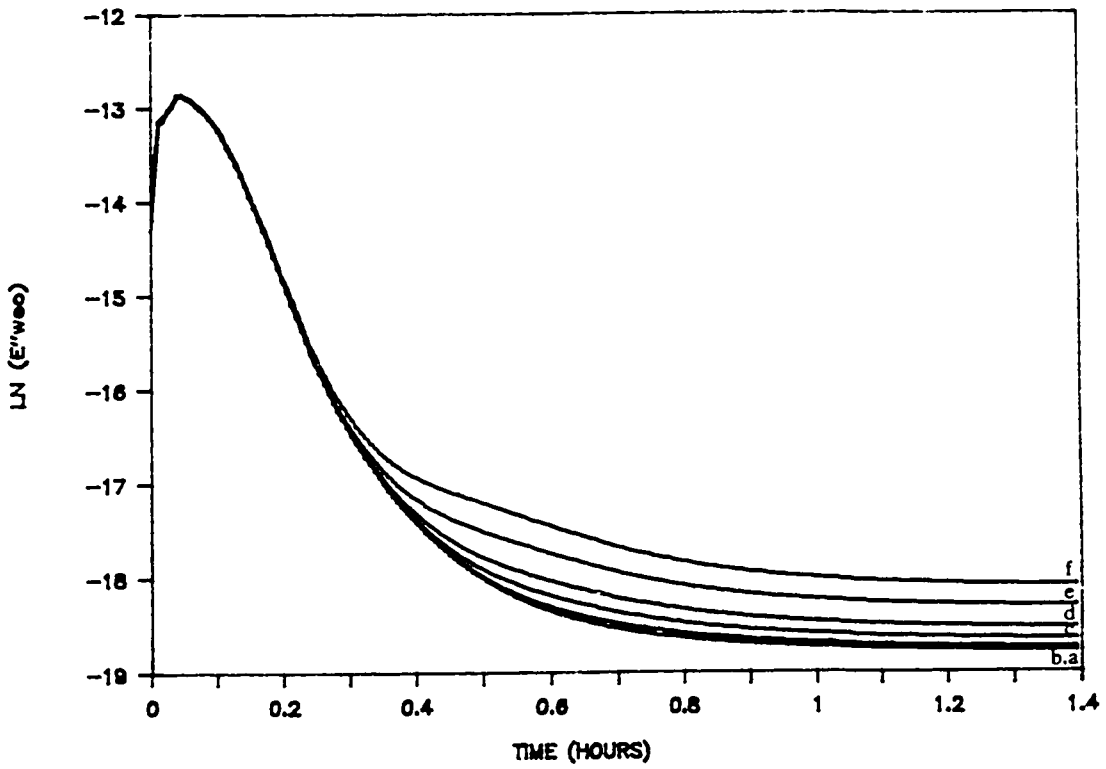

Figure 2.19 - Apparent conductivity of TGDDM/DDS during isothermal cure at 200°C: a) 240 Hz, b) 1 KHz, c) 2 KHz, d) 4 KHz, e) 10 KHz, f) 20 KHz.

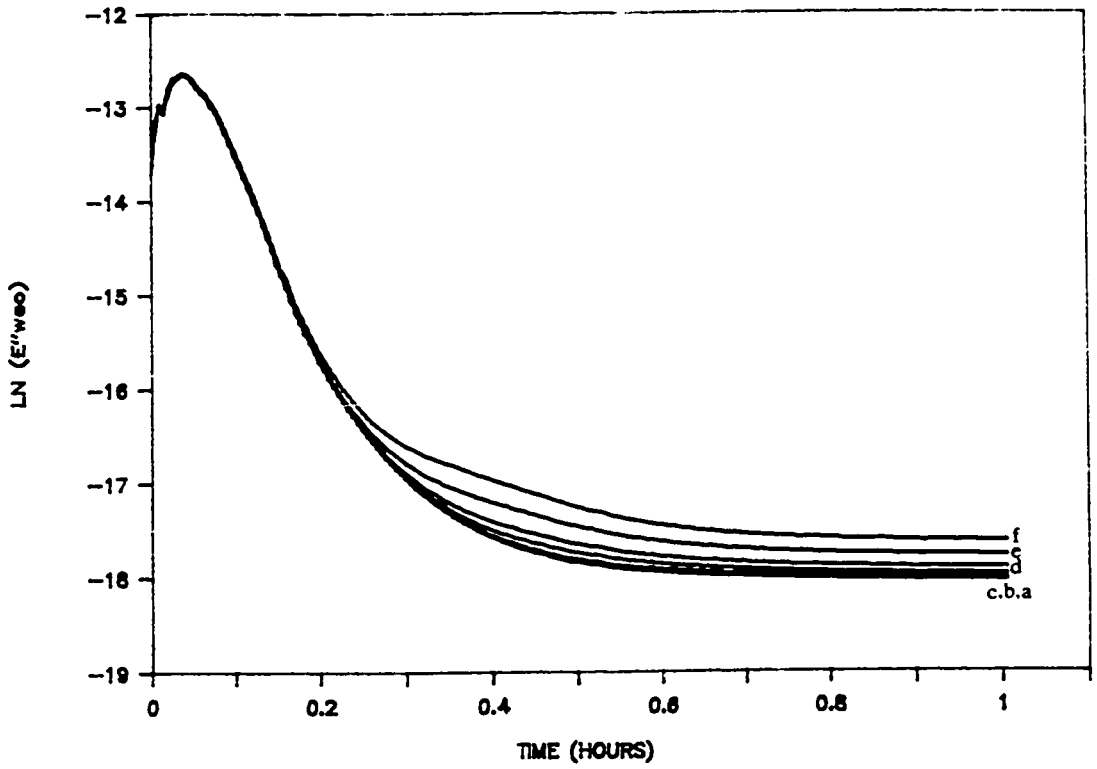

Figure 2.20 - Apparent conductivity of TGDDM/DDS during isothermal cure at 210°C: a) 240 Hz, b) 1 KHz, c) 2 KHz, d) 4 KHz, e) 10 KHz, f) 20 KHz.

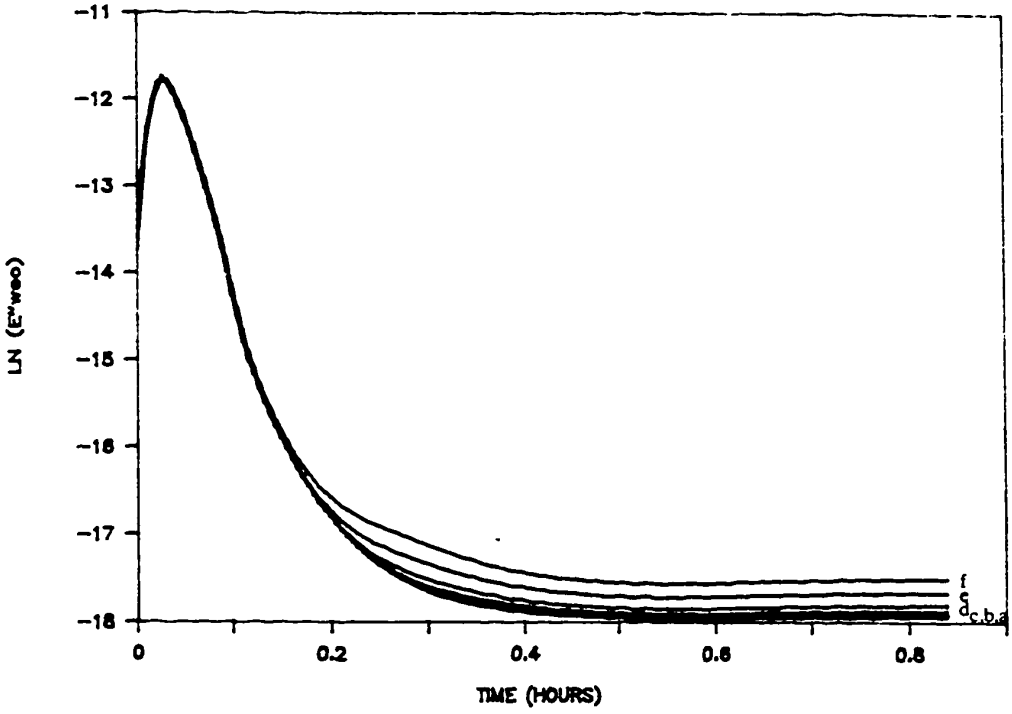

Figure 2.21 - Apparent conductivity of TGDDM/DDS during isothermal cure at 220°C: a) 240 Hz, b) 1 KHz, c) 2 KHz, d) 4 KHz, e) 10 KHz, f) 20 KHz.

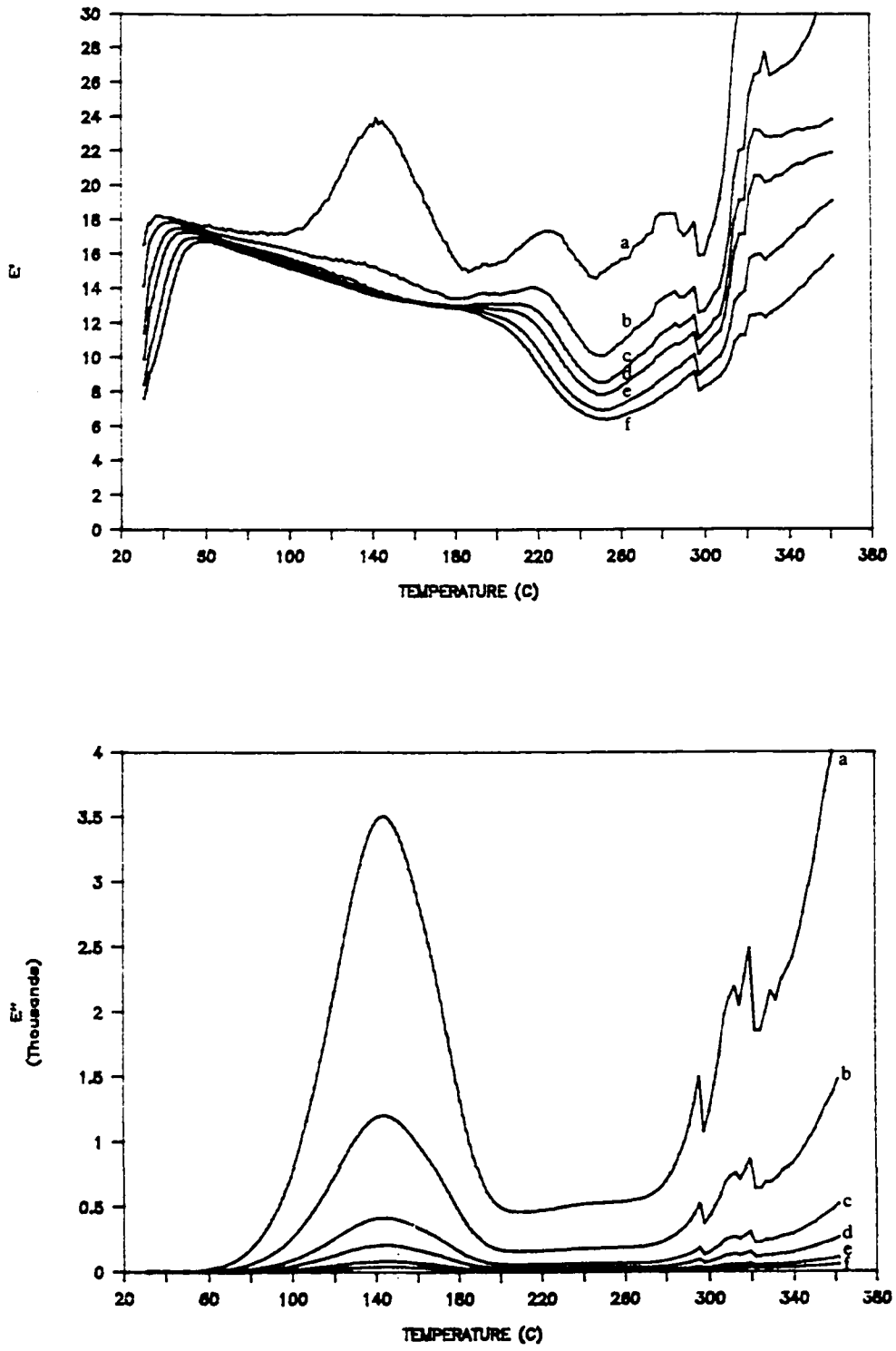

Figure 2.22 - Dielectric properties of TGDDM/DDS during cure at 1°C/minute: a) 240 Hz, b) 1 KHz, c) 2 KHz, d) 4 KHz, e) 10 KHz, f) 20 KHz.

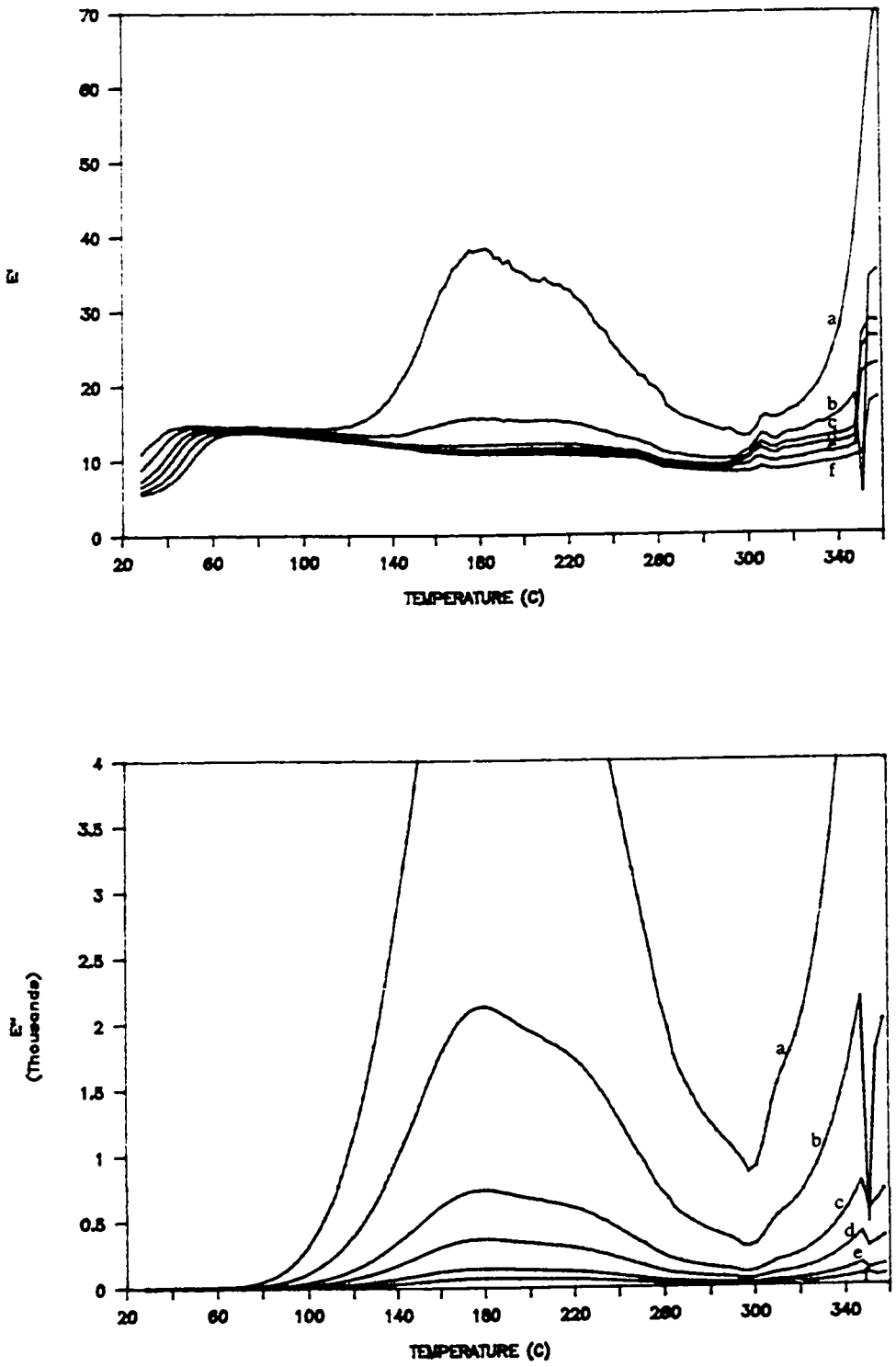

Figure 2.23 - Dielectric properties of TGDDM/DDS during cure at 5°C/minute: a) 240 Hz, b) 1 KHz, c) 2 KHz, d) 4 KHz, e) 10 KHz, f) 20 KHz.

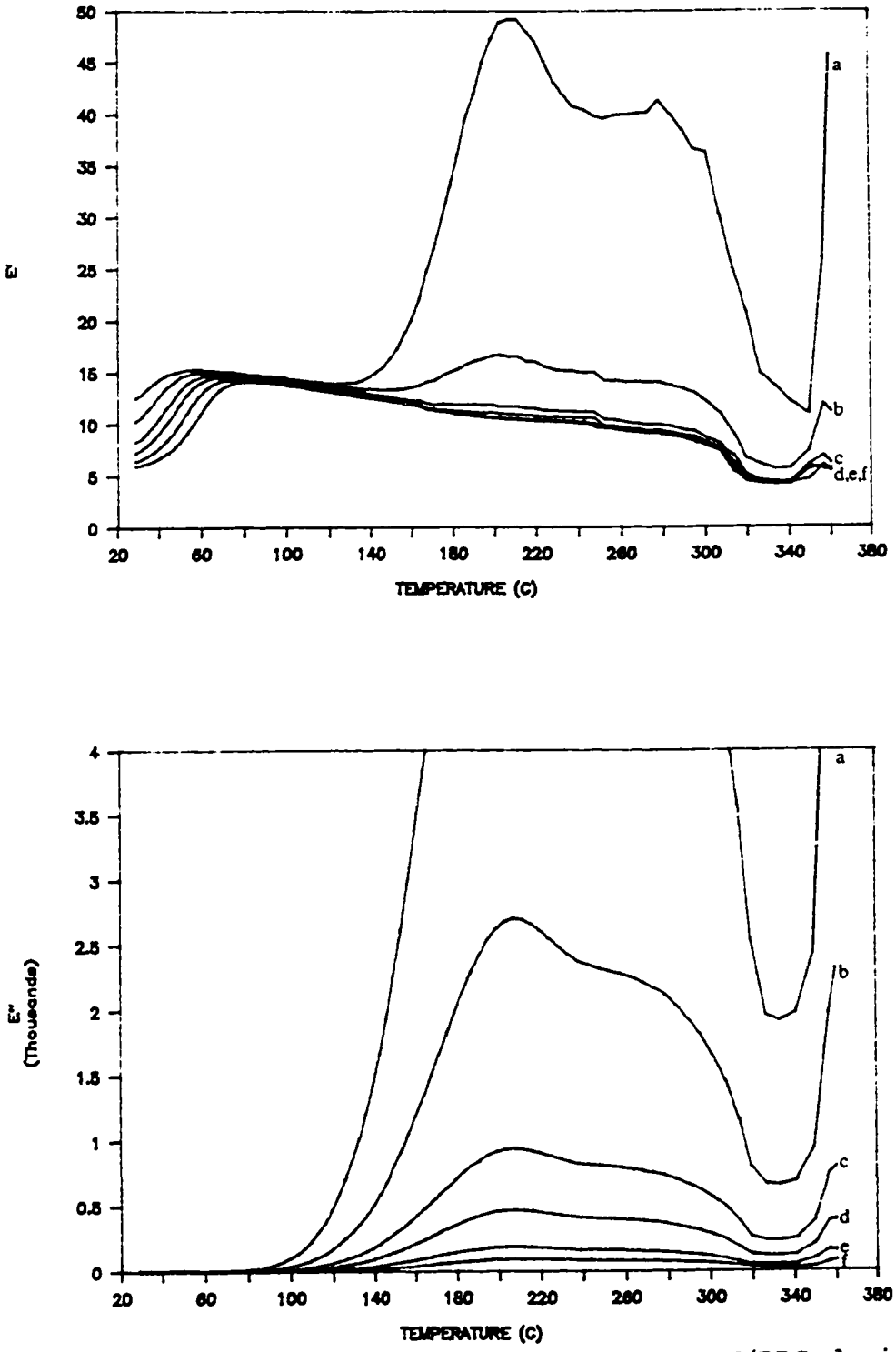

Figure 2.24 - Dielectric properties of TGDDM/DDS during cure at 10°C/minute: a) 240 Hz, b) 1 KHz, c) 2 KHz, d) 4 KHz, e) 10 KHz, f) 20 KHz.

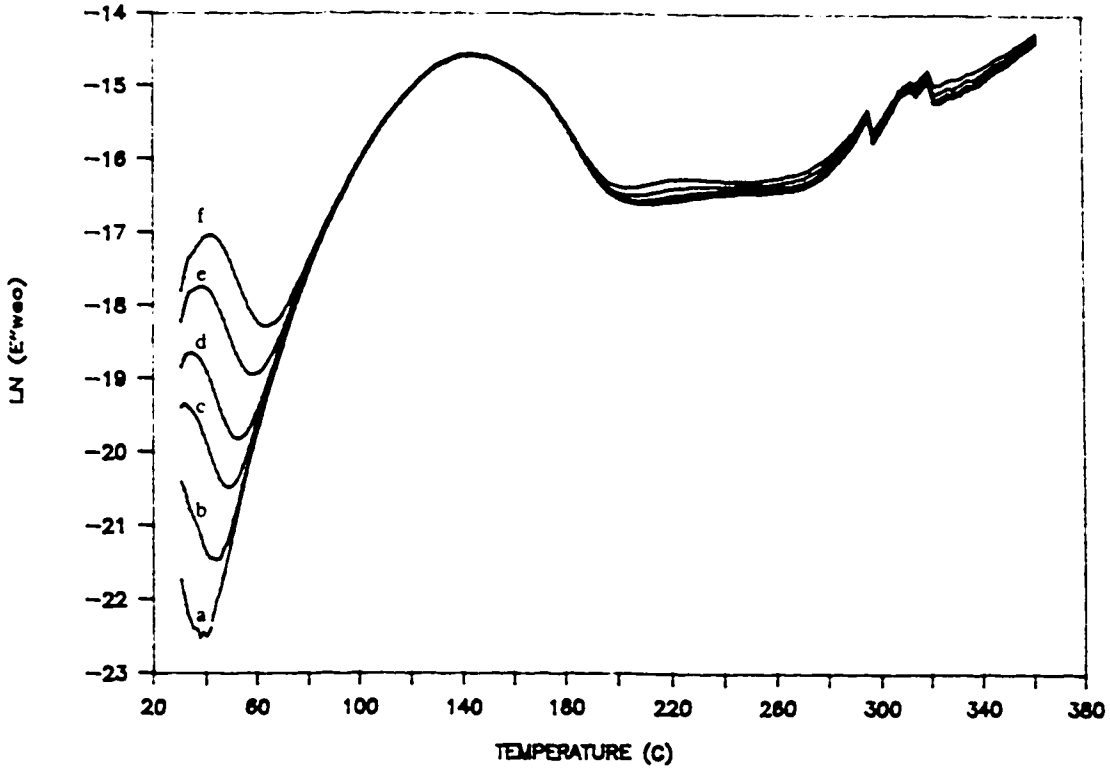

Figure 2.25 - Apparent conductivity of TGDDM/DDS during nonisothermal cure at 1°C/minute: a) 240 Hz, b) 1 KHz, c) 2 KHz, d) 4 KHz, e) 10 KHz, f) 20 KHz.

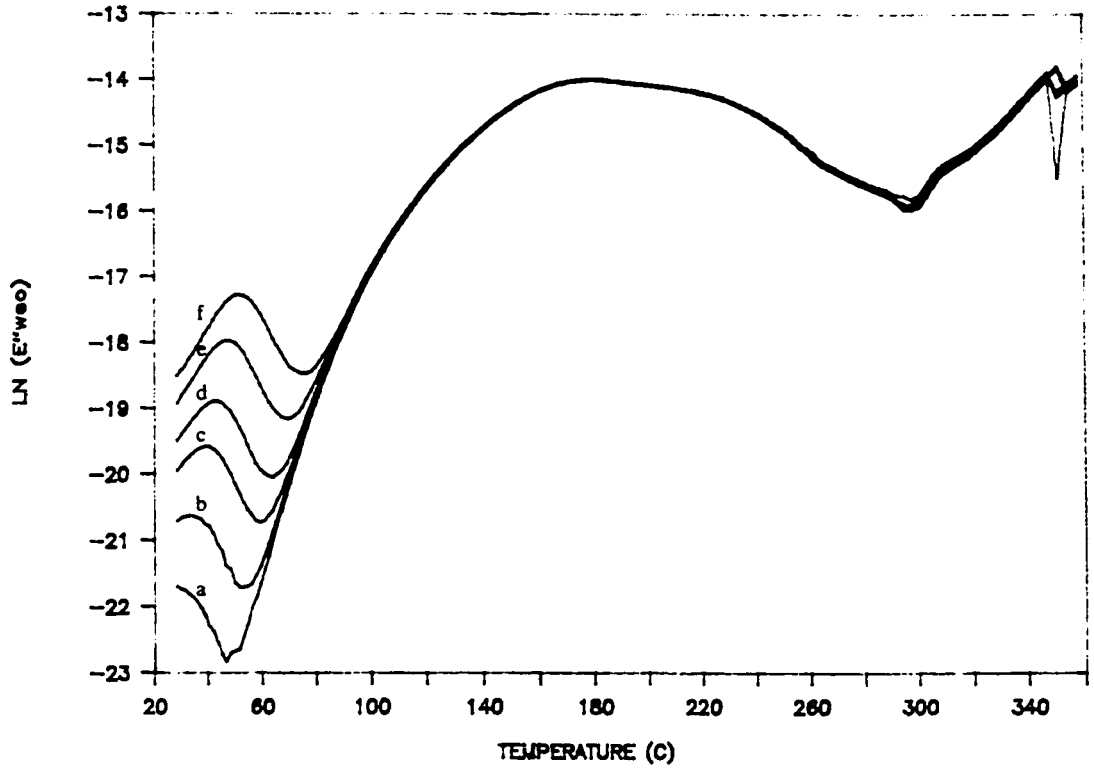

Figure 2.26 - Apparent conductivity of TGDDM/DDS during nonisothermal cure at 5°C/minute: a) 240 Hz, b) 1 KHz, c) 2 KHz, d) 4 KHz, e) 10 KHz, f) 20 KHz.

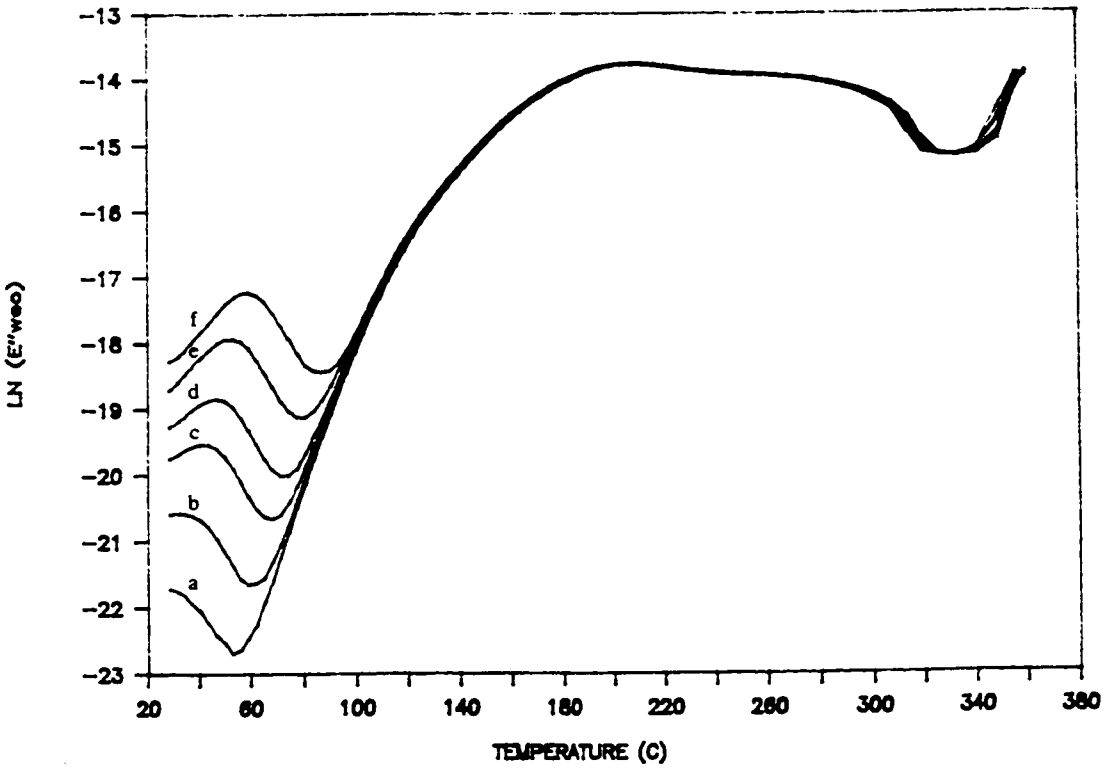

Figure 2.27 - Apparent conductivity of TGDDM/DDS during nonisothermal cure at 10°C/minute: a) 240 Hz, b) 1 KHz, c) 2 KHz, d) 4 KHz, e) 10 KHz, f) 20 KHz.

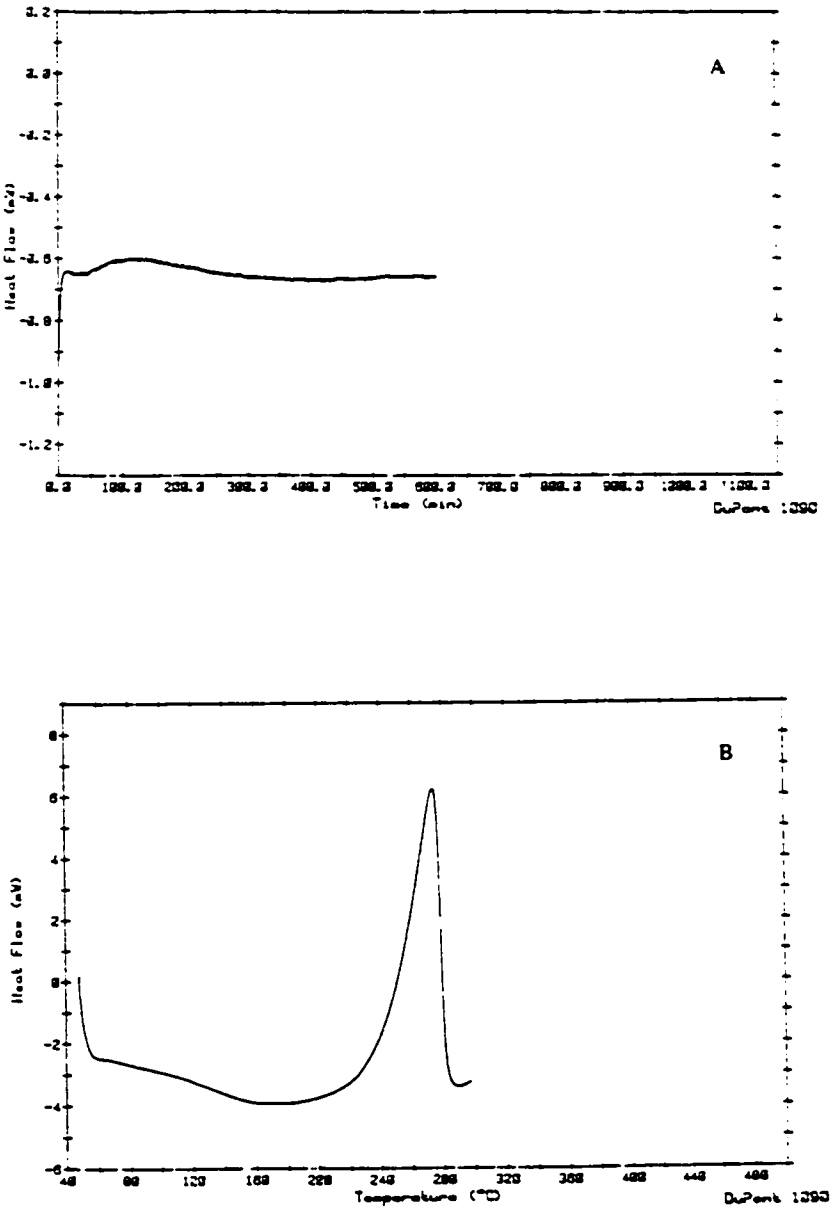

Figure 2.28 - a) DSC scan of TGDDM/DDS during isothermal cure at 140°C, b) residual heat scan.

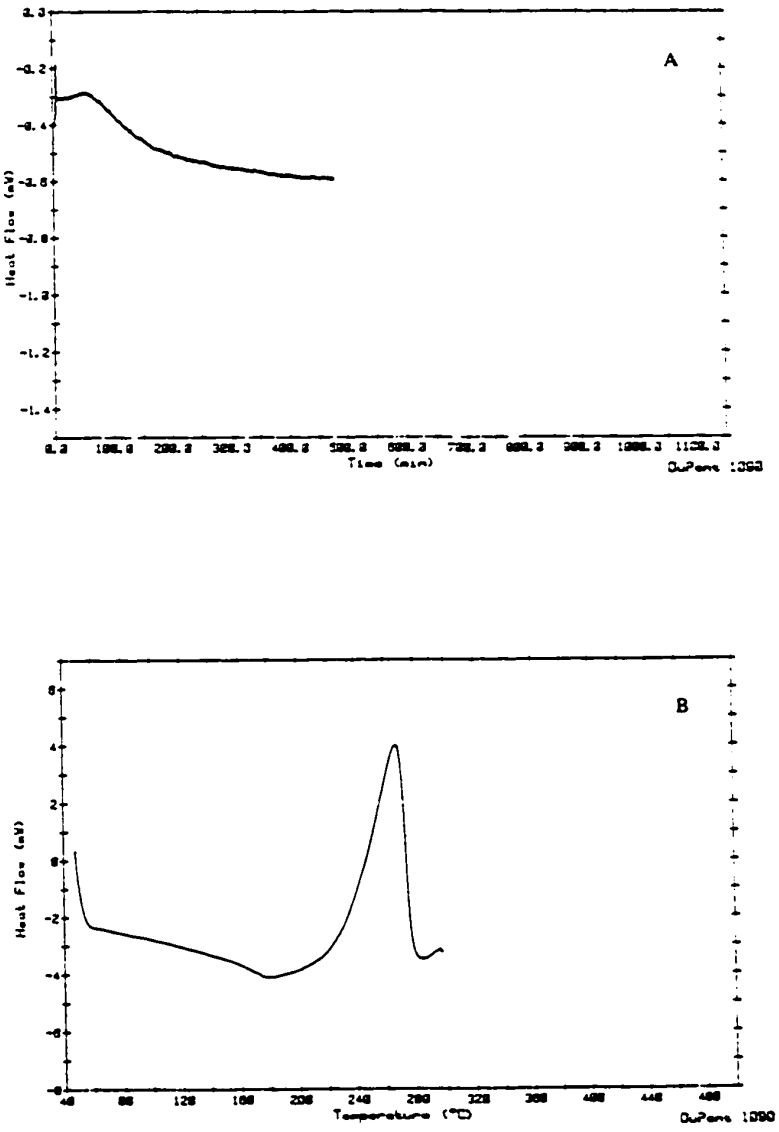

Figure 2.29 - a) DSC scan of TGDDM/DDS during isothermal cure at 150°C, b) residual heat scan.

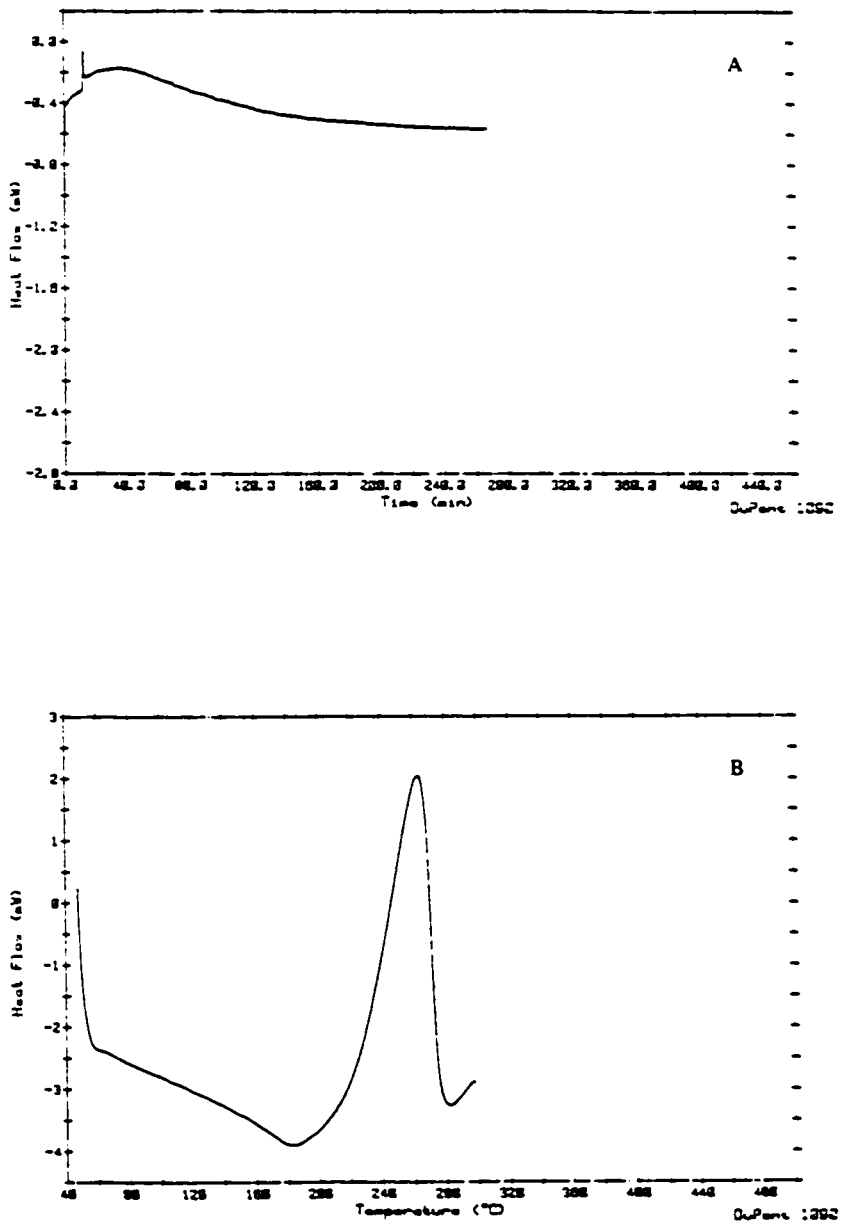

Figure 2.30 - a) DSC scan of TGDDM/DDS during isothermal cure at 160°C, b) residual heat scan.

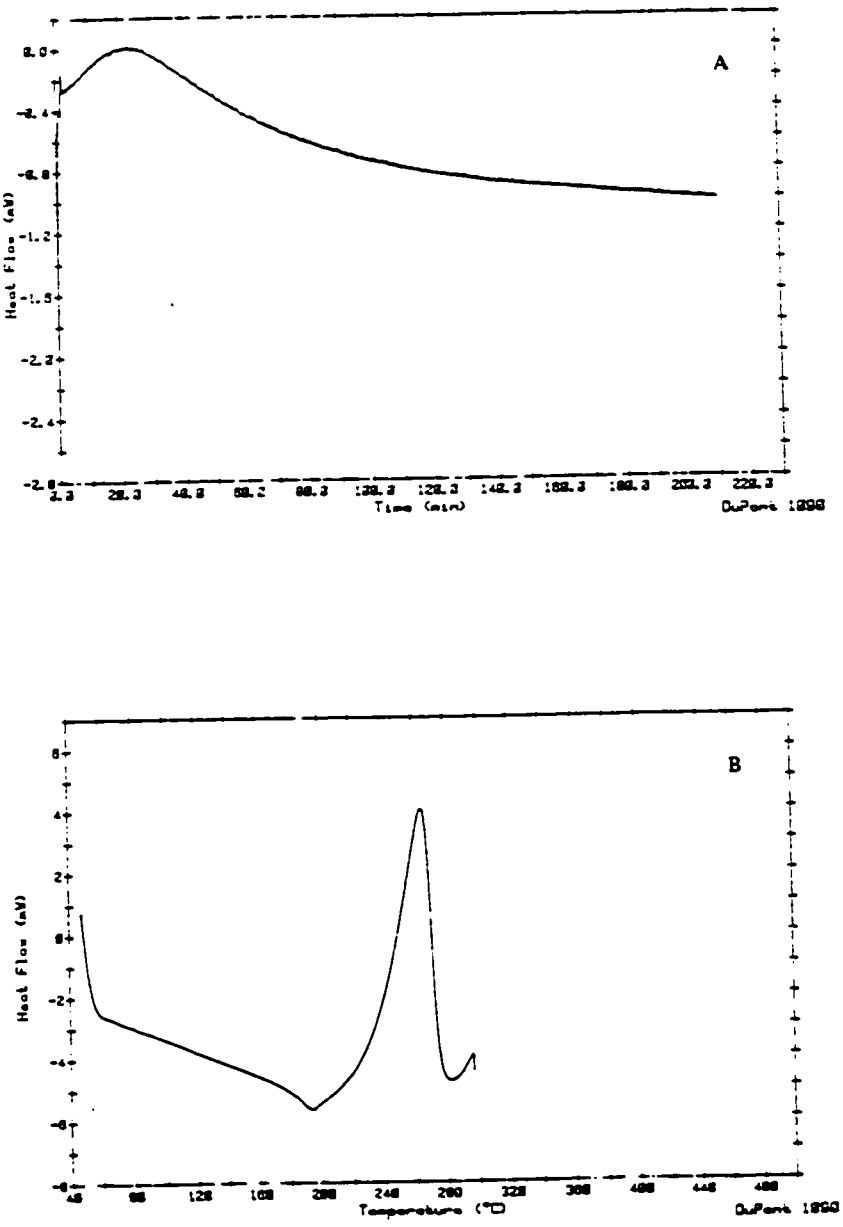

Figure 2.31 - a) DSC scan of TGDDM/DDS during isothermal cure at 170°C, b) residual heat scan.

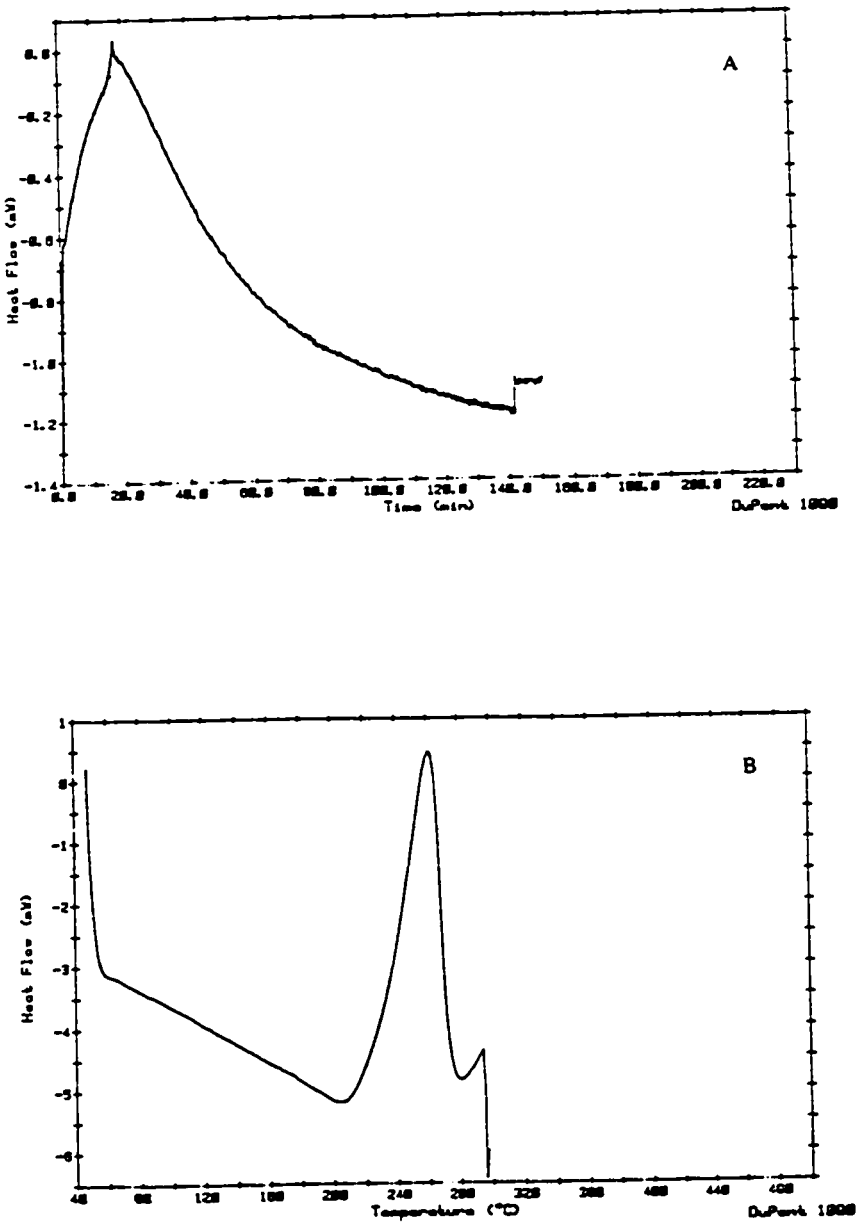

Figure 2.32 - a) DSC scan of TGDDM/DDS during isothermal cure at 180°C, b) residual heat scan.

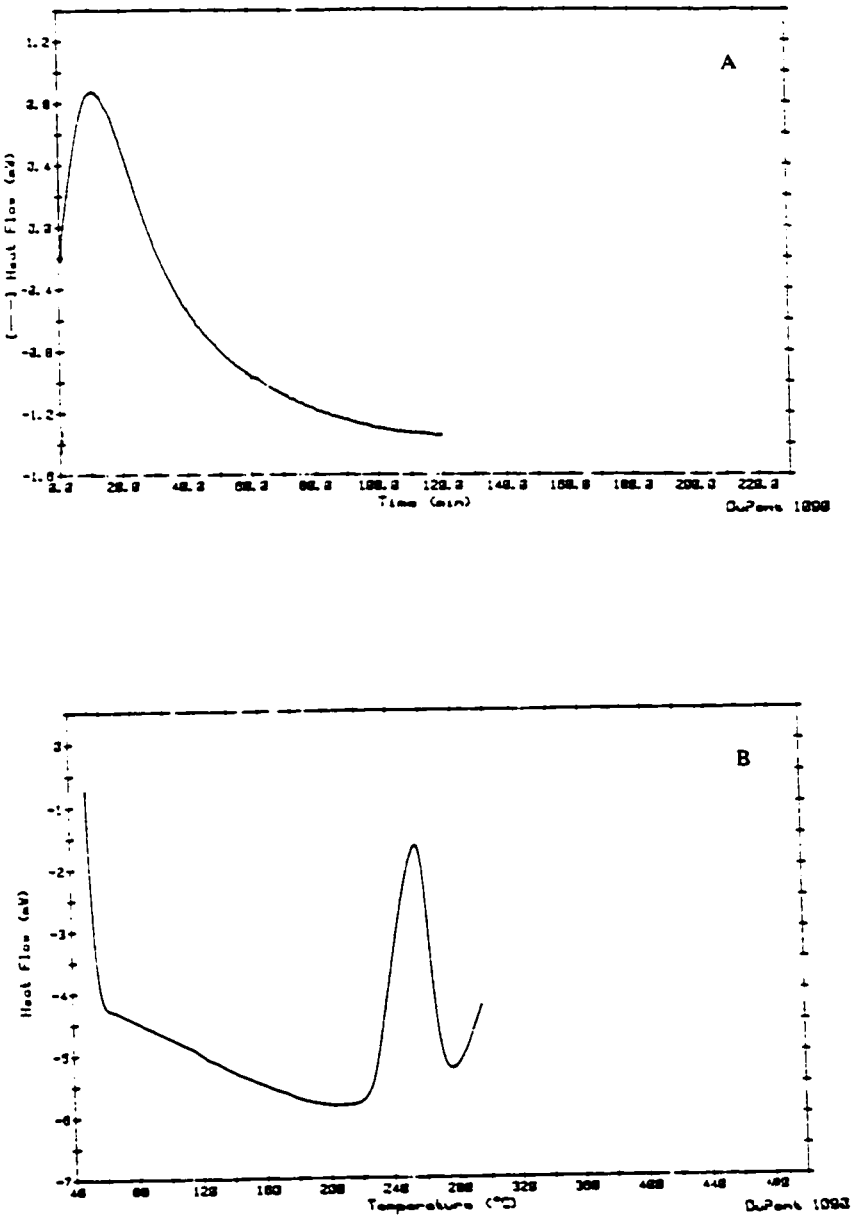

Figure 2.33 - a) DSC scan of TGDDM/DDS during isothermal cure at 190°C, b) residual heat scan.

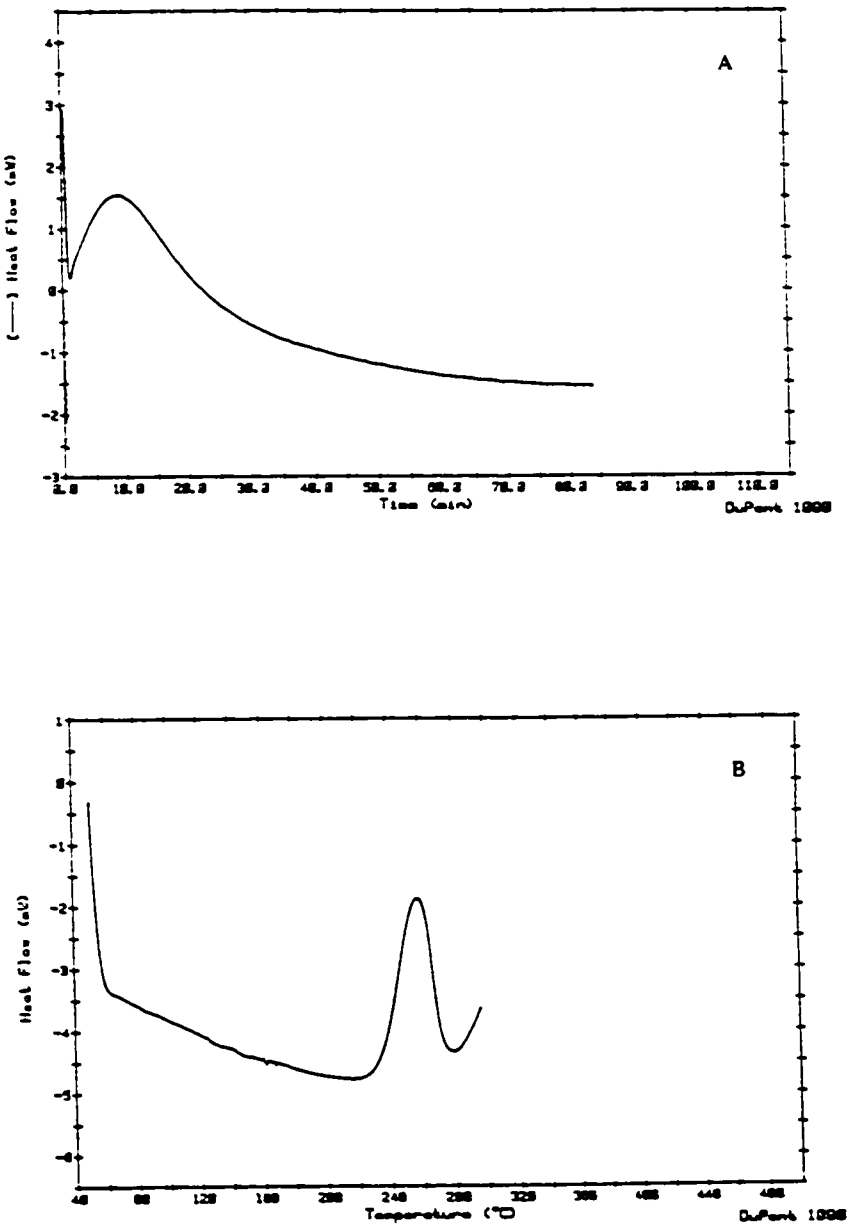

Figure 2.34 - a) DSC scan of TGDDM/DDS during isothermal cure at 200°C, b) residual heat scan.

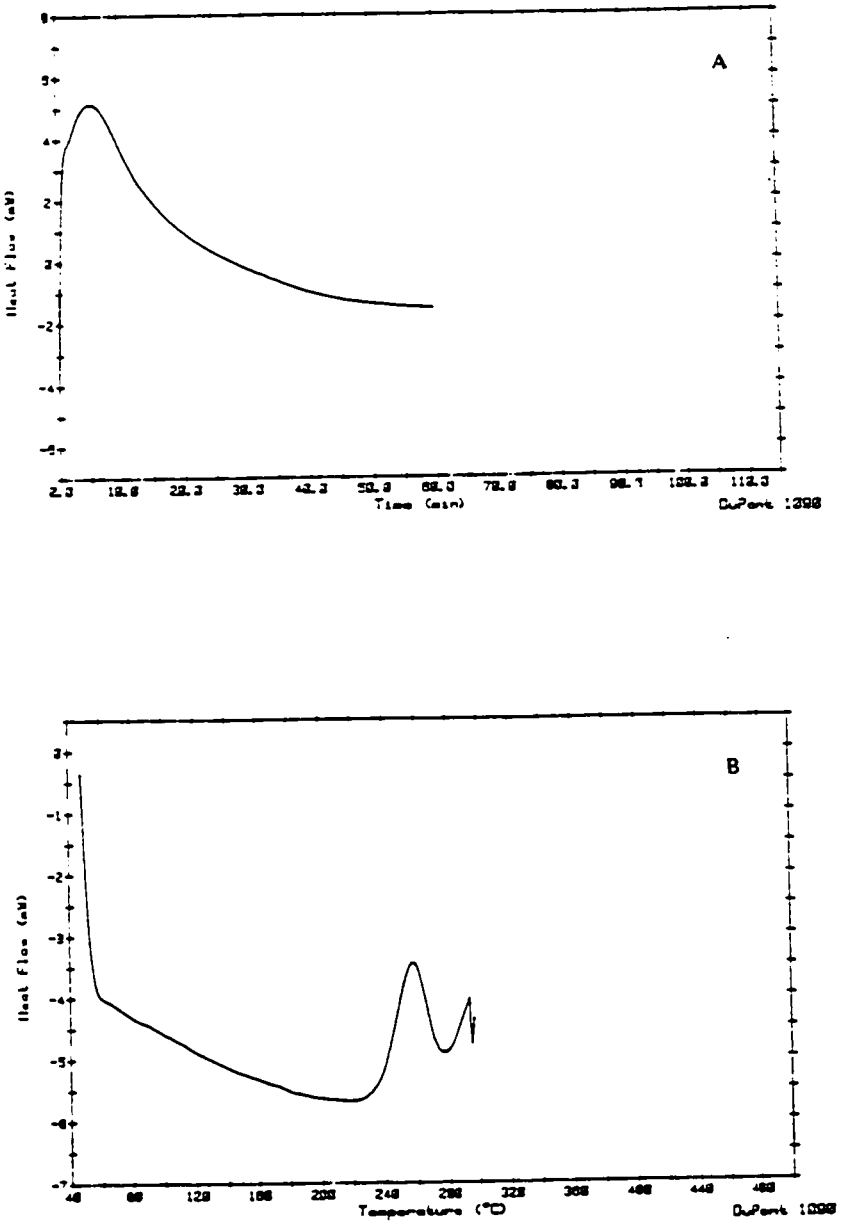

Figure 2.35 - a) DSC scan of TGDDM/DDS during isothermal cure at 210°C, b) residual heat scan.

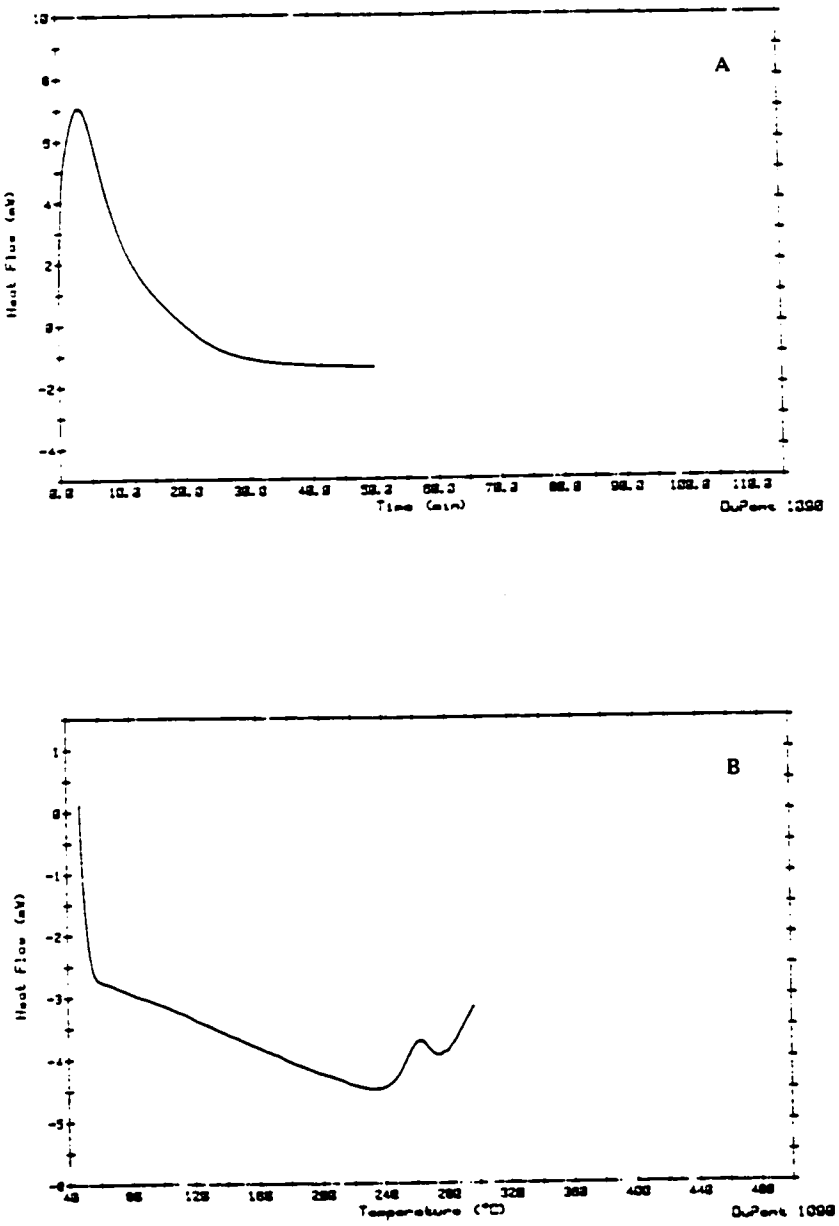

Figure 2.36 - a) DSC scan of TGDDM/DDS during isothermal cure at 220°C, b) residual heat scan.

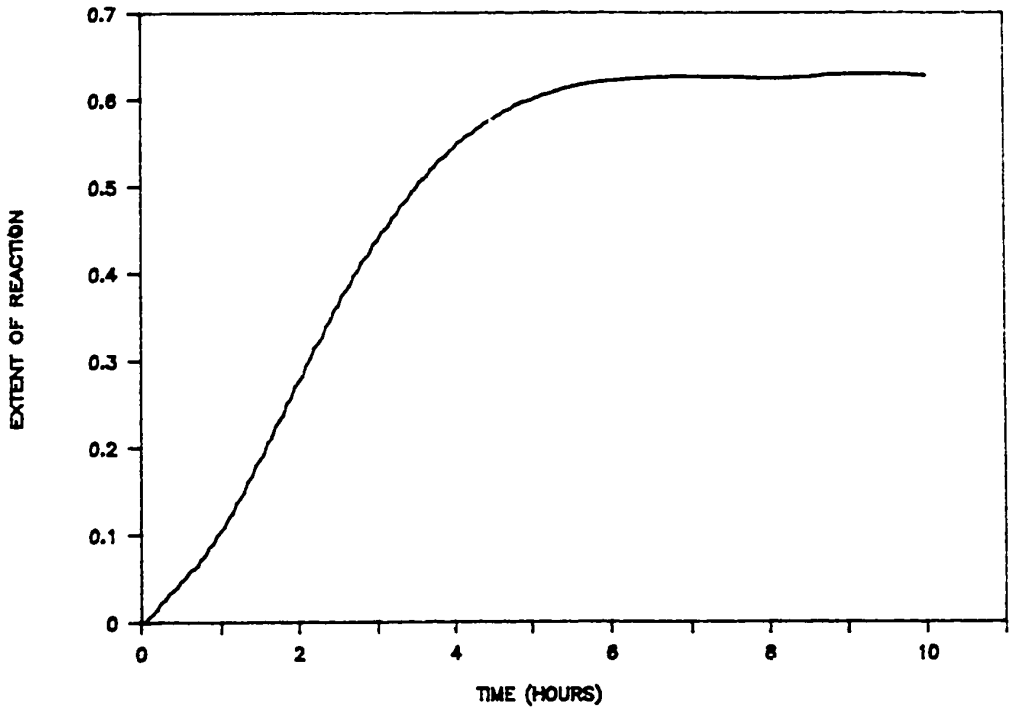

Figure 2.37 - Extent of reaction measured by DSC during isothermal cure of TGDDM/DDS at 140°C.

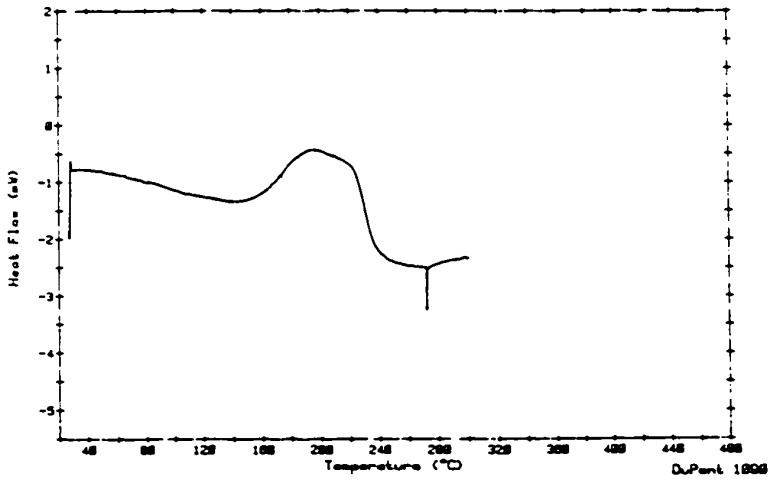

Figure 2.38 - DSC scan of TGDDM/DDS during nonisothermal cure at 1°C/minute.

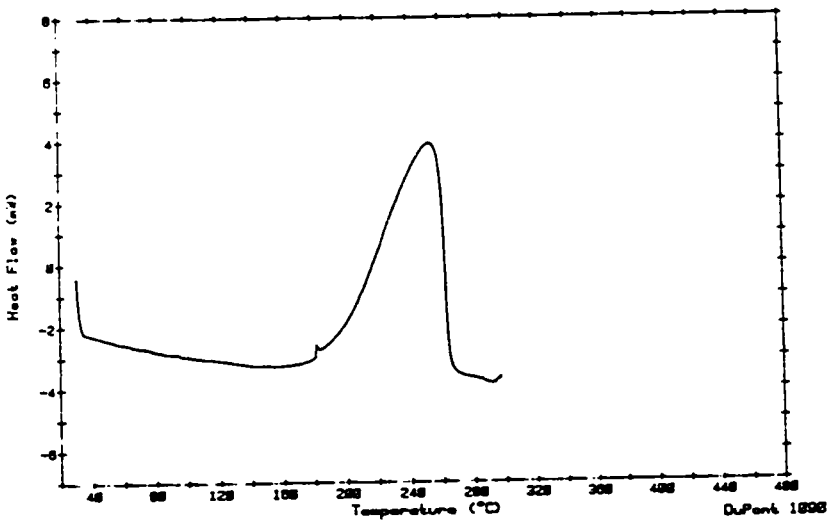

Figure 2.39 - DSC scan of TGDDM/DDS during nonisothermal cure at 5°C/minute.

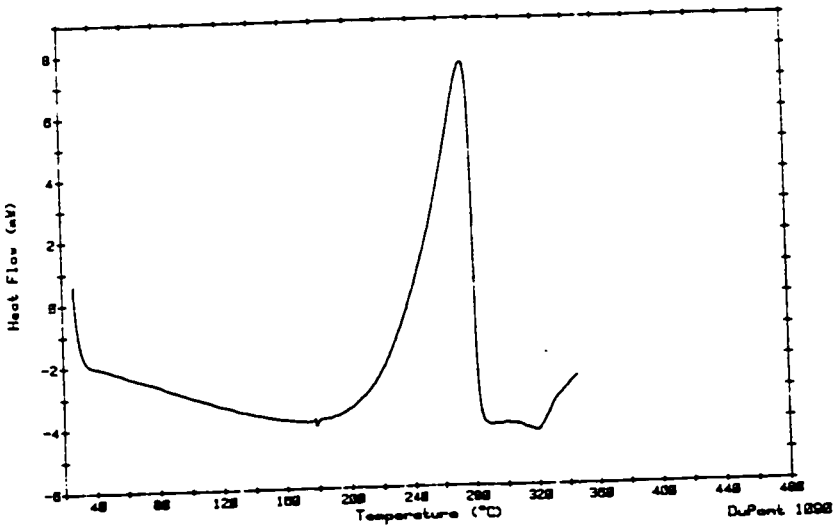

Figure 2.40 - DSC scan of TGDDM/DDS during nonisothermal cure at 10°C/minute.

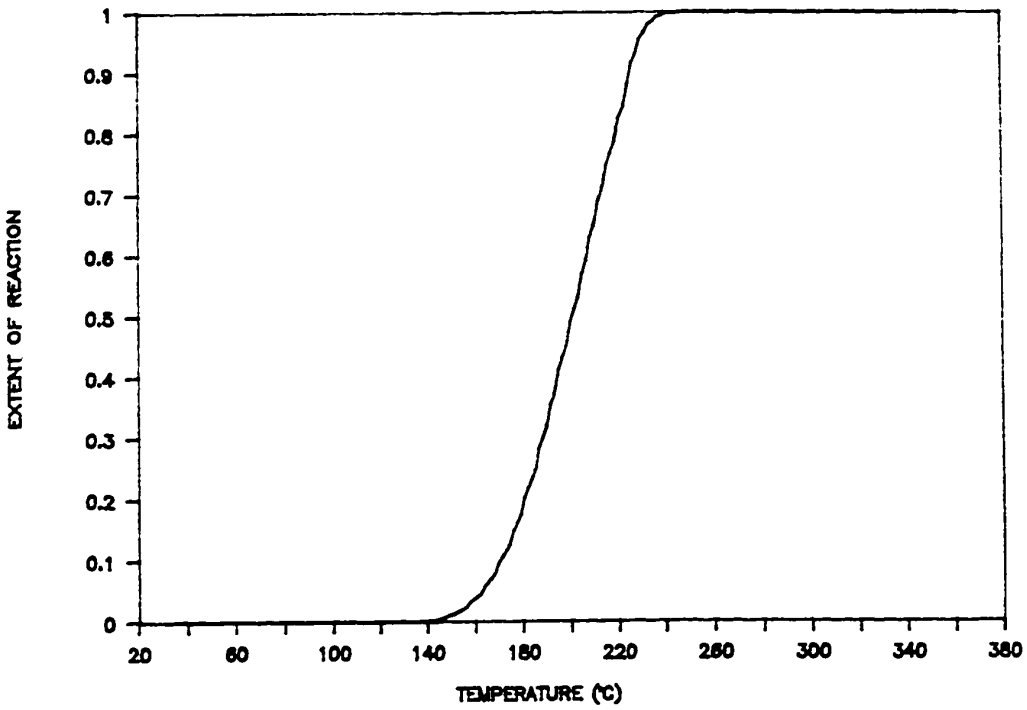

Figure 2.41 - Extent of reaction measured by DSC during nonisothermal cure of TGDDM/DDS at 1°C/minute.

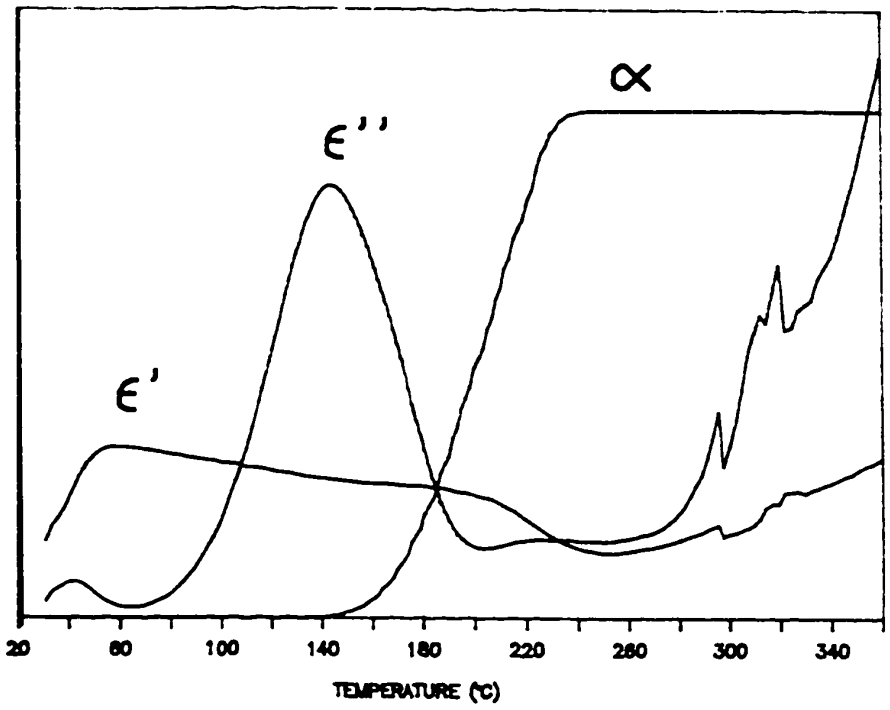

Figure 2.42 - Dielectric responses of TGDDM/DDS compared with the DSC extent of reaction during cure at 1°C/minute.

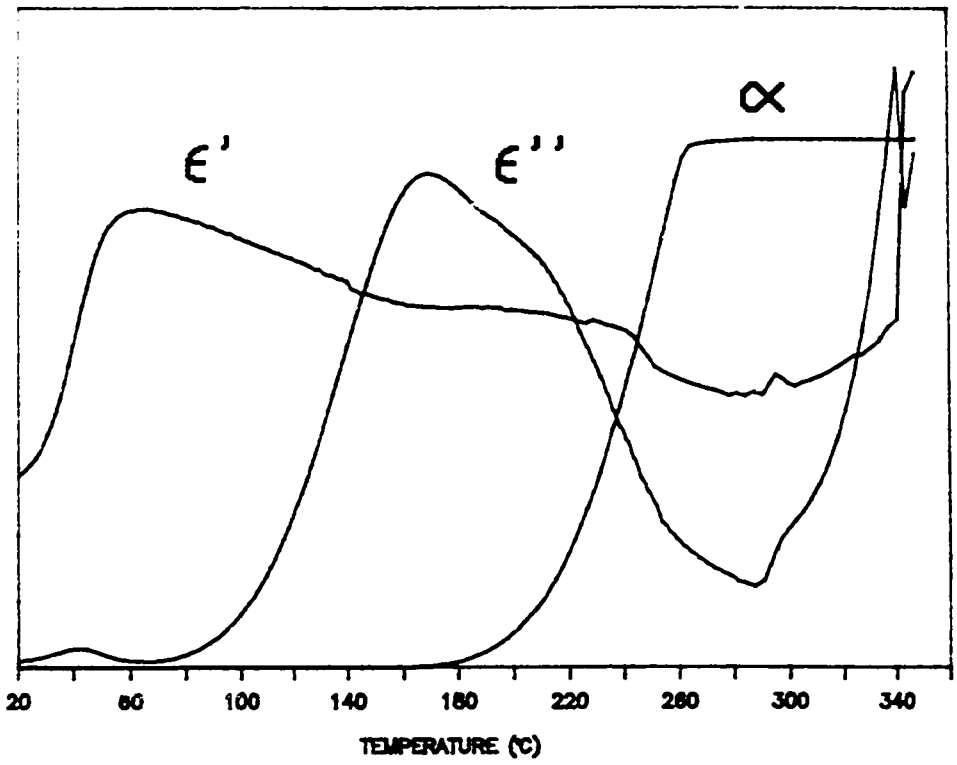

Figure 2.43 - Dielectric responses of TGDDM/DDS compared with the DSC extent of reaction during cure at 5°C/minute.

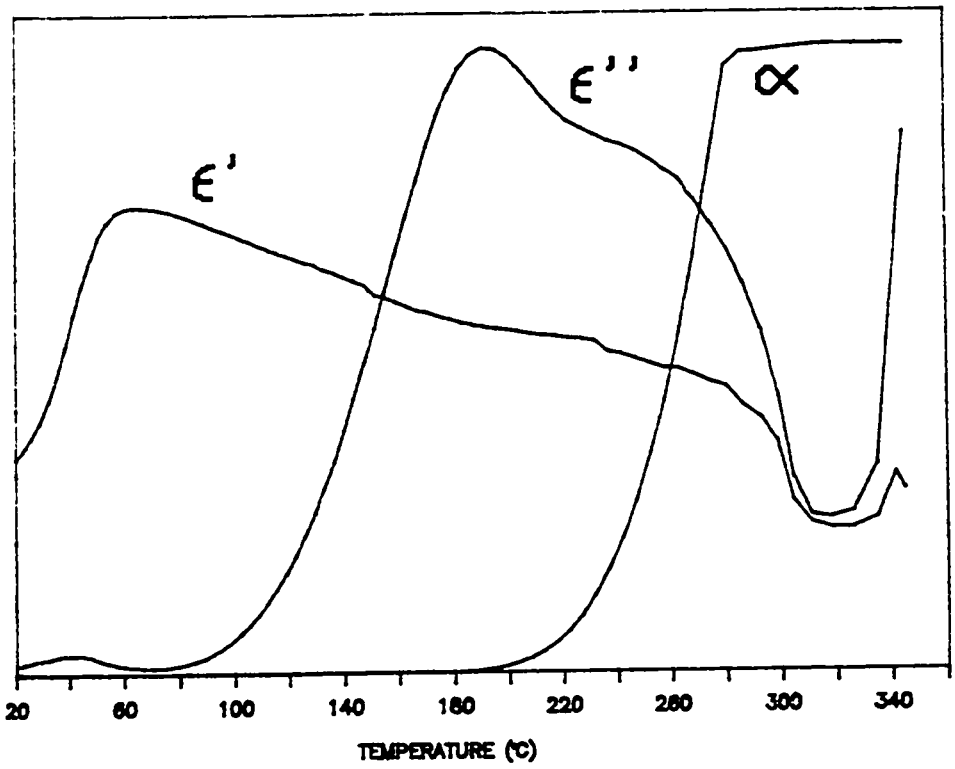

Figure 2.44 - Dielectric responses of TGDDM/DDS compared with the DSC extent of reaction during cure at 10°C/minute.

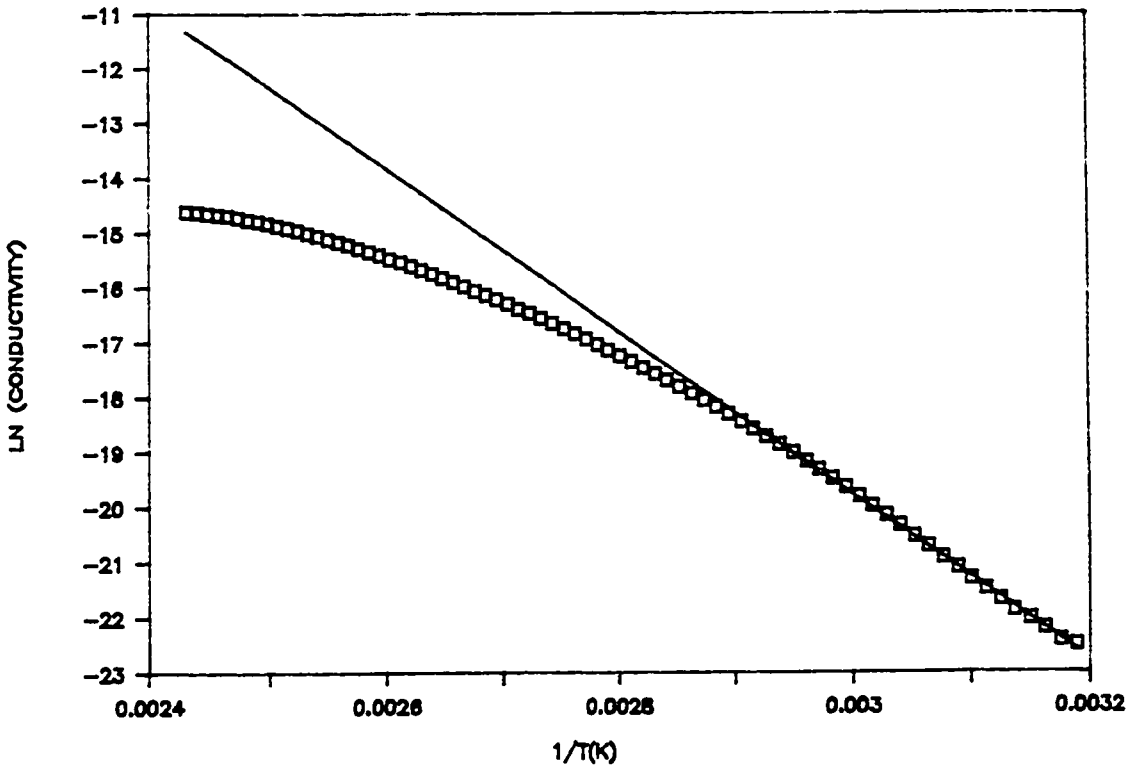

Figure 2.45 - Arrhenius plot of conductivity data of uncured resin above T_g, 1°C/minute heating rate.

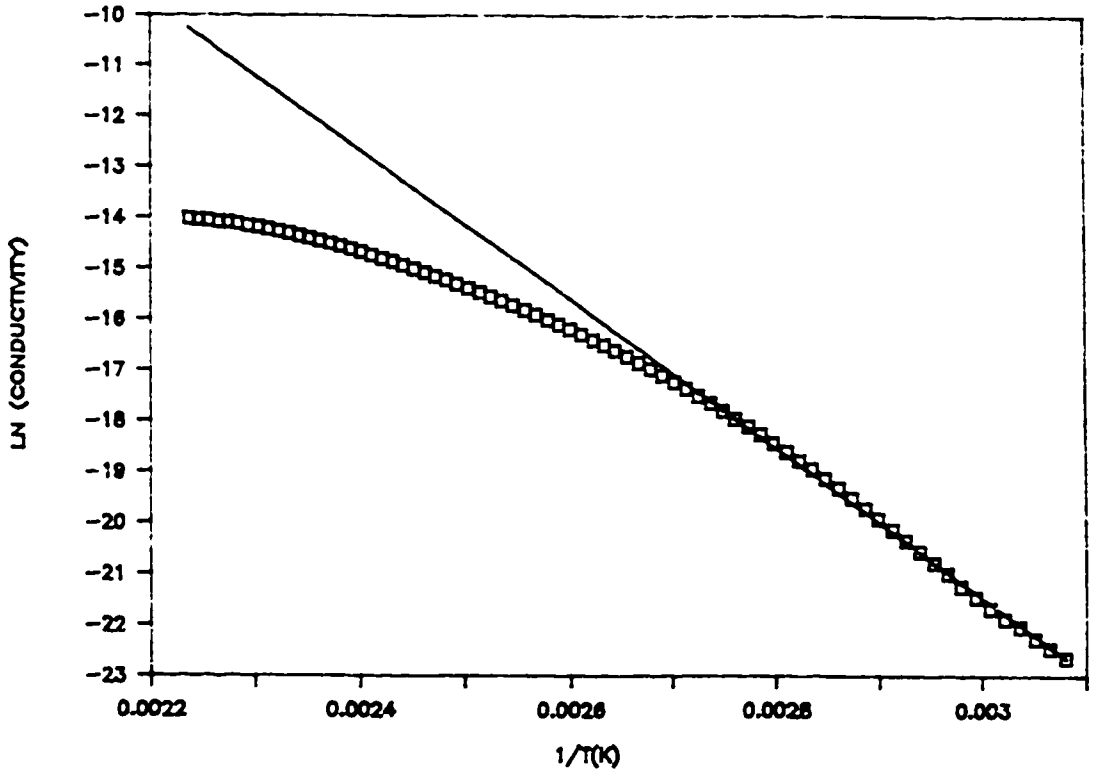

Figure 2.46 - Arrhenius plot of conductivity data of uncured resin above T_g, 5°C/minute heating rate.

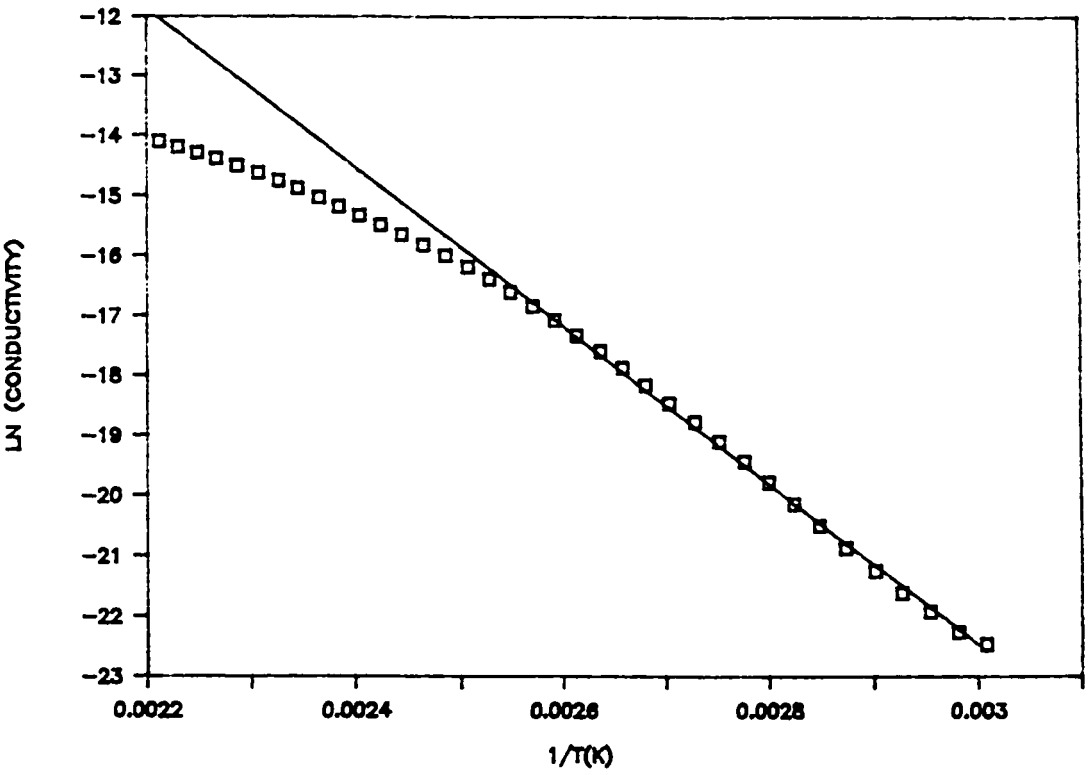

Figure 2.47 - Arrhenius plot of conductivity data of uncured resin above T_g, 10°C/minute heating rate.

Notes to Chapter 2

1. E.B. Stark, Doctoral Dissertation, University of Washington, 1985.

2. W.A. Romanchuk, J.E. Sohan, and J.F. Geibel, ACS Symp. Ser., 227, 85 (1983).

3. R.A. Fava, Polymer, 9, 137 (1968).

4. S. Souroor and M.R. Kamal, Thermochim. Acta, 14, 41 (1976).

5. L.J. Morgan and E.T. Mones, Polym. Prepr., 21, 921 (1980).

6. M. Shimbo, M. Ochi, and H. Iesako, J. Polym. Sci.: Polym. Phys. Ed., 22, 1461 (1984).

7. C. Walkup, R.J. Morgan, and T.H. Hoheisel, Polym. Prepr., 25, 187 (1984).

8. J. Mijovic, J.G. Williams, and T. Donnellan, J. Appl. Polym. Sci., 30, 2351 (1985).

9. W-L. Liu, E.M. Pearce, and T.K. Kwei, J. Appl. Polym. Sci., 30, 2907 (1985).

10. M. Cizmecioglu, A. Gupta, and R.F. Fedors, J. Appl. Polym. Sci., 32, 6177 (1986).

11. C-S. Chern and G.W. Poehlein, Polym. Eng. Sci., 27, 788 (1987).

12. P.L. Ku, Adv. Polym. Tech., 8, 81 (1988).

13. J.D. Keenan, J.C. Seferis, and J.T. Quinlivan, J. Appl. Polym. Sci., 24, 2375 (1979).

14. W.J. Mikols, J.C. Seferis, A. Apicella, L. Nicolais, Polym. Comp., 3, 118 (1982).

15. W.J. Mikols and J.C. Seferis, ACS Symp. Series, 227, 95 (1983).

16. H.S. Chu and J.C. Seferis, The Role of the Polymer Matrix in the Processing and Structural Properties of Composite Materials, J.C. Seferis and L. Nicolais, Eds., Plenum, New York, 1983.

17. T.E. Munns and J.C. Seferis, J. Appl. Polym. Sci., 28, 2227 (1983).

18. E.B. Stark, J.C. Seferis, A. Apicella, and L. Nicolais, Thermochimica Acta, 77, 19 (1984).

19. H.S. Chu and J.C. Seferis, Polym. Comp., 5, 125 (1984).

20. A.M. Ibrahim and J.C. Seferis, Interrelationships Between Processing, Structure, and Properties of Polymeric Materials, J.C. Seferis and P.S. Theocaris, Eds., Elsevier, Amsterdam, 1984.

21. E.B. Stark, A.M. Ibrahim, and J.C. Seferis, Interrelationships Between Processing, Structure, and Properties of Polymeric Materials, J.C. Seferis and P.S. Theocaris, Eds., Elsevier, Amsterdam, 1984.

22. T.E. Munns and J.C. Seferis, Analytical Calorimetry, Vol. 5, J.F. Johnson and P.S. Gill, Eds., Plenum, New York, 1984.

23. A.M. Ibrahim and J.C. Seferis, Proc. Ann. Conf., Soc. Adv. Matl. Proc. Eng., 29, 1405 (1985).

24. E.B. Stark, A.M. Ibrahim, T.E. Munns, and J.C. Seferis, J. Appl. Polym. Sci., 30, 1717 (1985).

25. A.M. Ibrahim and J.C. Seferis, Polym. Comp., 6, 47 (1985).

26. E.M. Woo, L.B. Chen, and J.C. Seferis, J. Mat. Sci., 22, 3665 (1987).

27. E.M. Woo, J.C. Seferis, and L.D. Bravenec, Proc. Ann. Tech. Conf., Am. Soc. Comp., 2, 569 (1987).

28. C.L. Loechelt, E.M. Woo,and J.C. Seferis, Proc. Ann. Tech. Conf., Soc. Plast. Eng., 34, 1645 (1988).

29. J.W. Lane, J.C. Seferis, and M.A. Bachmann, J. Appl. Polym. Sci., 31, 1155 (1986).

30. L. Hartshorn and W.H. Ward, J. Inst. Elect. Eng., 79, 597 (1936).

31. T. Grentzer and J. Leckenby, Amer. Lab., 21, 82 (1989).

32. R.A. Fava and A.E. Horsfield, Brit. J. Appl. Phys. (J. Phys. D), Ser. 2, 1, 117 (1968).

33. N.F. Sheppard, Jr., M.C.W. Coln, and S.D. Senturia, Proc. Ann. Conf., Soc. Adv. Matl. Proc. Eng., 29, 1243 (1984).

34. M.J. Richardson, Polymer Testing, 4, 101 (1984).

35. W.W. Wendlandt and P.K. Gallagher, Thermal Characterization of Polymeric Materials, E. Turi, Ed., Academic Press, New York, 1981.

36. R.B. Prime, Thermal Characterization of Polymeric Materials, E. Turi, Ed., Academic Press, New York, 1981.

37. W.J. Sichina, DuPont Instruments Thermal Analysis Applications Brief, TA-93.

38. W.W. Bidstrup, S.A. Bidstrup, and S.D. Senturia, Proc. Ann. Tech. Conf., Soc. Plast. Eng., 34, 960 (1988).

39. M.E. Baird, Electrical Properties of Polymeric Materials, The Plastics Institute, London, 1973.

40. R.W. Warfield and M.C. Petree, Macromol. Chem., 58, 139 (1962).

CHAPTER 3

ACTIVATION ENERGY DETERMINATIONS USING DIELECTRIC METHODS

3.1 Introduction

Traditional thermal analysis techniques yield quantitative information about the physical and chemical processes which occur in polymers and polymeric composites during processing. Information such as the activation energy is useful not only for characterization purposes, e.g. detecting resin aging or morphological changes, but also for understanding polymer molecular behavior. As described in Chapter 2, dielectric spectroscopy also detects these processes, requiring quantitative techniques for extracting material parameters from dielectric data. Methods for calculating the activation energies of mechanical transitions and chemical reactions, from both isothermal and nonisothermal dielectric data, are presented in this chapter.

3.2 Viscoelastic Transitions

The transformation of polymers from glassy to rubbery solids, the glass transition, is easily detected as a distinct change in the viscoelastic properties, such as

creep compliance or stress relaxation modulus, when plotted as functions of temperature. Transitions observed at temperatures below the glass transition temperature have been correlated to the relaxation of segments within the polymer molecules [1]. The time scale of the relaxation determines the frequency behavior of the transition when observed using dynamic techniques, such as dynamic mechanical analysis. Correspondingly, the relaxation of dipolar segments during transitions causes distinct changes in the dielectric properties of polymers [2]. Dielectric transitions may be characterized by analyzing their frequency (dispersion) and temperature behavior.

3.2.1 Isothermal Frequency Response of Nonreacting Polymers

The dispersion behavior of nonreacting polymers may be observed in complex plane (Cole-Cole) plots of the dielectric properties [2]. In these plots of ε'' plotted against ε', each data point corresponds to the dielectric properties at one frequency. The curves have been described mathematically as functions of the product of angular frequency and relaxation time, $w\tau$.

3.2.1.1 Phenomenological Dispersion Equations

The ideal frequency behavior of polymers has been described using a single relaxation time, τ_o. The complex

dielectric constant, ε^*, is related to $w\tau_o$ by [2]:

$$\varepsilon^* = \varepsilon_\infty + \frac{(\varepsilon_o - \varepsilon_\infty)}{1 + iw\tau_o} \qquad (3.1)$$

ε_o and ε_∞ are the values of ε' at $w = 0$ and ∞ rad/sec. This equation is analogous to the Voigt model describing the dynamic compliance. When rearranged and expressed in terms of ε' and ε'', Equation 3.1 describes a semicircle centered on the ε' axis at $(\varepsilon_o + \varepsilon_\infty)/2$, as shown in Figure 3.1. The maximum value of ε'' occurs when $w\tau_o = 1$.

Real polymers, however, are polydisperse and heterogeneous systems which possess distributions of relaxation times. Therefore, the experimental dispersion curves of polymers are either broader than the ideal curve, asymmetric at high frequencies, or both. Cole and Cole [3] modified Equation 3.1 by adding a parameter, $\underline{\beta}$, to produce a broad dispersion curve:

$$\varepsilon^* = \varepsilon_\infty + \frac{(\varepsilon_o - \varepsilon_\infty)}{1 + (iw\tau)^{\underline{\beta}}} \qquad (3.2)$$

$$0 < \underline{\beta} \leq 1$$

In this equation, τ is considered the mean value of the

dipolar relaxation time. The curve generated by the Cole-Cole equation is presented in Figure 3.2. As seen in the figure, the dispersion is broadened, but still symmetric about the value of ε'' where $w\tau = 1$. Davidson and Cole [4] described asymmetric high frequency broadening via a different modification of Equation 3.1 using another parameter, γ:

$$\varepsilon^* = \varepsilon_\infty + \frac{(\varepsilon_o - \varepsilon_\infty)}{(1 + iw\tau)^\gamma} \qquad (3.3)$$

$$0 < \gamma \leq 1$$

As seen in Figure 3.3, this equation produces deviation from the ideal curve at high frequencies.

3.2.1.2 Havriliak-Negami Equation

Polymer dispersion behavior which is both broadened and asymmetric was described by a constitutive equation proposed by Havriliak and Negami [5,6]. Their equation incorporates the features of the Cole-Cole and Davidson-Cole equations by using two parameters, α and β:

$$\varepsilon^* = \varepsilon_\infty + \frac{(\varepsilon_o - \varepsilon_\infty)}{(1 + (iw\tau)^{1-\alpha})^\beta} \qquad (3.4)$$

$$0 \leq \alpha < 1, \quad 0 < \beta \leq 1$$

Equations 3.1 - 3.3 may be generated by assigning a value of one to either α or β. The dispersion behavior predicted by this equation is plotted in Figure 3.4.

Expressions for ε' and ε'' in terms of $w\tau$ are obtained from Equation 3.4 by applying DeMoivre's Theorem twice:

$$\varepsilon' = \varepsilon_\infty + \frac{(\varepsilon_o - \varepsilon_\infty)\cos(\beta\varphi)}{[1+2(w\tau)^{(1-\alpha)}\cos((1-\alpha)\pi/2)+(w\tau)^{2(1-\alpha)}]^{\beta/2}} \tag{3.5}$$

$$\varepsilon'' = \frac{(\varepsilon_o - \varepsilon_\infty)\sin(\beta\varphi)}{[1+2(w\tau)^{(1-\alpha)}\cos((1-\alpha)\pi/2)+(w\tau)^{2(1-\alpha)}]^{\beta/2}} \tag{3.6}$$

The parameter φ is a collection of terms:

$$\varphi = \tan^{-1}\left[\frac{(w\tau)^{(1-\alpha)}\sin((1-\alpha)\pi/2)}{1 + (w\tau)^{(1-\alpha)}\cos((1-\alpha)\pi/2)}\right] \tag{3.7}$$

Values of α and β may be determined from dielectric data by a combination of graphical and iterative methods, which are explained in detail elsewhere [5,7,8].

Several features of the dispersion behavior in Figure 3.4 are worth noting. The angle formed by the intersection of the high frequency tail with the ε' axis, φ_L, is related to the dispersion parameters:

$$\varphi_L = (1-\alpha)\beta(\pi/2) \qquad (3.8)$$

The maximum value of ε'' does not occur when $w\tau = 1$, as with symmetric dispersions. The intersection of the bisector of φ_L with the dispersion curve corresponds to $w\tau = 1$, as illustrated in Figure 3.4.

The dispersion relationships expressed by Equations 3.1 - 3.4 are phenomenological, the exact physical significances of the dispersion parameters have not been established. Efforts to interpret the parameters in molecular terms have begun through statistical experimental design [9,10]. The equations may be used, however, to accurately determine the activation energy of dielectric transitions.

3.2.2 Temperature Dependence of Dipolar Relaxation

The activation energy of a dielectric transition is related to the temperature dependence of the relaxation time. If assumed to be an activated process, dipolar relaxation can be described by the Arrhenius expression [2]:

$$\tau = \tau' \exp (E_\tau/RT) \qquad (3.9)$$

E_τ represents the activation energy of the transition. The key to determining the transition activation energy from dielectric data is through the combination of Equation 3.9 with the dispersion relationships.

3.2.2.1 Previously Developed Methods for Calculating Activation Energy

Two methods relate the activation energy of transition to either the area or the half-width of ε'' curves plotted versus 1/T [2]. Each method, however, requires symmetric dispersion behavior, such as those predicted by Equation 3.1 and 3.2. Therefore, neither is applicable to the asymmetric dispersions described by Equations 3.3 and 3.4.

A third method, the peak temperature method, is valid for any type of dispersion. This method assumes that the maximum value of ε'' at each frequency occurs when $w\tau$ reaches a characteristic value. As the temperature increases, τ decreases and the maximum value shifts to higher frequencies. The frequency at which ε'' is a maximum at a given temperature is denoted as w_{max}. Under this assumption and Equation 3.9, Arrhenius curves of w_{max} are linear. The activation energy is calculated from [1]:

$$E_\tau \approx - R \frac{d(\ln w_{max})}{d(1/T)} \qquad (3.10)$$

This method may be applied to both symmetric and asymmetric dispersions since the ε'' maximum occurs when wτ reaches a value particular to the type of dispersion, e.g. wτ = 1 for symmetric dispersions. However, dielectric data must be obtained over a wide range of frequencies in order to obtain an accurate value of E_τ. Alternately, the temperature at which ε' data exhibits an inflection for each frequency may be used to determine w_{max} [11].

3.2.2.2 ε'' Ratio Method

In this study, an alternate method was developed for calculating the activation energy of asymmetric dielectric transitions. The method relates the ratios of ε'' values to the maximum value, ε''_m, in isofrequency dielectric data. The activation energy is calculated from the slope of Arrhenius-type curves of the ratios and appropriate dispersion parameter values.

Several assumptions were made in the derivation of the activation energy equation. First, dielectric dispersion was described using the generalized Havriliak-Negami equation, Equation 3.5. Secondly, the values of α and β were assumed to be independent of temperature. While both α

and β have been observed to vary with temperature [6,12], the temperature ranges of transition are typically small enough that these parameters may be assumed constant. In addition, the value of wτ was assumed to be less than one at temperatures higher than ε'' peak temperature of each frequency.

Under these assumptions, the following relationship was derived (Appendix A):

$$\ln \frac{\varepsilon''}{\varepsilon''_m} \approx \frac{(1-\alpha)E_\tau}{RT} + f(\alpha,\beta,w,\tau') \qquad (3.11)$$

According to this equation, Arrhenius curves of $\varepsilon''/\varepsilon''_m$ will be linear when the model assumptions are valid. The activation energy of the transition may be calculated from:

$$E_\tau \approx \frac{R}{(1-\alpha)} \frac{d[\ln(\varepsilon''/\varepsilon''_m)]}{d[1/T]} \qquad (3.12)$$

This method was tested by using Equation 3.12 to calculate the activation energy of a model dielectric transition. Model transition data were generated using Equations 3.6, 3.7, and 3.9 and representative dispersion parameter values. An activation energy of 40.00 kcal/mole was used, the other parameter values are summarized in

Table 3.1. Figure 3.5 contains the generated ε'' values plotted as a function of temperature. An Arrhenius plot of the ε'' ratios in Figure 3.6 exhibits the expected linearity at temperatures above the peak transition temperature. The activation energy calculated from the slope of the line in Figure 3.6 is 39.91 kcal/mole. The agreement between this and the "real" value validates the assumptions made. The activation energy of asymmetric transitions may then be calculated using Equation 3.12 and a limited amount of dielectric data.

3.3 Chemical Reaction

Polymer analysis via dielectric spectroscopy may be extended further by developing methods for determining the activation energy of polymerization. Dielectric spectroscopy is unique in that two types of information, ionic conduction and dipolar relaxation, may be analyzed. Activation energies may be determined from both isothermal and nonisothermal dielectric cure experiments.

3.3.1 Activation Energy from Isothermal Ionic Conduction Data

One method of calculating the reaction activation energy is to analyze ionic conductivity data at the beginning of cure at several isothermal temperatures [13].

Two assumptions form the basis of this technique. The temperature dependence of resistivity, p, was first described by the Arrhenius equation:

$$p(T) = p_o \exp (E_p/RT) \tag{3.13}$$

The activation energy of resistance, E_p, was then assumed to be directly proportional to the extent of polymerization, permitting dE_p/dt to be expressed as a function of the reaction activation energy, E_a. After substitution and rearrangement, the relationship between experimentally measured values of p and E_a was obtained:

$$\ln \left[\frac{d (\ln p)}{dt} \right]_{t=0} = B - \frac{E_a}{RT} \tag{3.14}$$

This equation may be used to describe conductivity during cure, σ, by substituting the definition:

$$\sigma = 1/p \tag{3.15}$$

to obtain:

$$\ln \left[\frac{d (-\ln \sigma)}{dt} \right]_{t=0} = B - \frac{E_a}{RT} \tag{3.16}$$

Accordingly, the activation energy of polymerization may be calculated from an Arrhenius plot of the initial time derivatives of isothermal ionic conductivity cure data. Nonisothermal conductivity data cannot be analyzed using this method without iterating.

3.3.2 Activation Energy from Dipolar Relaxation Data

In addition to conduction, the dipolar contribution to the dielectric properties during polymerization can be used to calculate an apparent value of the reaction activation energy. In this study, techniques used to determine activation energy from differential scanning calorimetry experiments were adapted for dielectric experiments [14,15]. This adaptation was made possible by assuming that the inflection in ε' and corresponding maximum in ε'' at each frequency occur at a particular value of extent of reaction during cure, in analogous fashion to the assumption that w_T has a characteristic value at the maximum in ε'' during dielectric transition. Methods for calculating the reaction activation energy from isothermal and nonisothermal dielectric experiments were then derived.

3.3.2.1 Isothermal Reaction

A method for extracting activation energy information from the time at which ε'' reaches a maximum value during

isothermal cure was first suggested by Lane, Seferis, and Bachmann [8], using a method described by Prime for isothermal DSC experiments [14]. The relationship was derived from a generalized polymerization rate equation:

$$\frac{d\alpha}{dt} = k\, f(\alpha) \tag{3.17}$$

This equation was then rearranged and integrated to the time at which the peak in ε'' occurred:

$$\int_0^{\alpha_p} \frac{d\alpha}{f(\alpha)} = k \int_0^{t_p} dt \tag{3.18}$$

The integral on the left side has a specific value for each value of α_p, allowing Equation 3.18 to be evaluated:

$$C(\alpha_p) = kt_p \tag{3.19}$$

Substituting the Arrhenius expression for the rate constant, k, and taking derivatives, the final expression for activation energy and peak time was obtained:

$$\ln (1/t_p) = \ln (k'C(\alpha_p)) - E_a/RT \tag{3.20}$$

In DSC experiments, this equation is used to calculate the activation energy of polymers which exhibit autocatalytic kinetic behavior, i.e. which produce a peak exotherm during isothermal reaction. Since ε'' reaches a peak value at some frequency during polymerization, Equation 3.20 may be applied to dielectric data, regardless of the reaction kinetics. In systems where the peak in ε'' is obscured by ionic conductivity, the time to the inflection in ε' may be used as t_p.

3.3.2.2 Nonisothermal Reaction

Extension of the above analysis permits the reaction activation energy to be calculated from the dielectric properties during cure at different heating rates. For nonisothermal DSC experiments, Equation 3.17 was modified by incorporating the heating rate, φ, and an Arrhenius expression for the rate constant [14]:

$$\varphi \frac{d\alpha}{dT} = [k'\exp(-E_a/RT)]\ f(\alpha) \qquad (3.21)$$

When integrated from the initial temperature, T_o, to the temperature at which the reaction exotherm reaches a maximum, T_p, this equation became:

$$\int_0^{\alpha_p} \frac{d\alpha}{f(\alpha)} = \frac{k'}{\varphi} \int_{T_o}^{T_p} \exp(-E_a/RT)\, dT \qquad (3.22)$$

As before, the integral on the left side has a particular value for each α_p. After evaluating the integral on the right side by approximation [14], the relationship between nonisothermal DSC data and activation energy was obtained:

$$\ln \varphi \approx -1.052\, E_a/RT + C(\alpha) \qquad (3.23)$$

Subsequently,

$$E_a \approx -\frac{R}{1.052} \frac{d(\ln \varphi)}{d(1/T_p)} \qquad (3.24)$$

Again, this equation is applicable to dielectric data by assuming that the inflection in ε' and maximum in ε'' signal a particular point in the cure. Therefore, the reaction activation energy may be calculated from an Arrhenius-type plot of heating rate versus the corresponding single frequency ε'' peak temperatures and Equation 3.24.

3.4 Analysis of the Model Thermosetting Resin

As outlined above, Equations 3.10 and 3.12 allow the

activation energy of dielectric transitions to be determined. Together, Equations 3.16, 3.20, and 3.24 provide means for evaluating the apparent reaction activation energy from isothermal and nonisothermal dielectric cure data. The success in applying these methods to real dielectric data was demonstrated by calculating the activation energies of transition and reaction for the TGDDM/DDS model resin system.

3.4.1 Uncured Glass Transition

The activation energy of the glass transition of uncured TGDDM/DDS was calculated from the nonisothermal pre-reaction region dielectric data using both the w_{max} and ε'' ratio methods. As required by the w_{max} method, Arrhenius plots of the peak transition frequencies were constructed for each set of heating rate data, as in Figure 3.7. The linearity of these curves reinforces the assumptions made in the method development. The activation energies calculated from these curves are summarized in Table 3.2. The exceptionally low value of E_τ at 10°C/minute is likely due to thermal lag at the beginning of the experiment when the glass transition is coincidentally observed.

Before applying the ε'' ratio method to the dielectric data, the dispersion parameters were determined for the

TGDDM/DDS uncured glass transition. Figure 3.8 contains an example of the isothermal complex plane plot of the dielectric properties at 30.65°C, during heating at 1°C/minute. From the slope of the high frequency dispersion and procedures outlined elsewhere [5], values of $\alpha = 0.273$ and $\beta = 0.487$ were calculated. These values were assumed to be constant with temperature and independent of heating rate.

Since the ratio method holds only for dipolar relaxation during transition, the contribution from ionic conduction was removed from the ε'' data. The apparent conductivity data in Figures 2.25 - 2.27 shows that ε'' monitored at 240 Hz is essentially the result of ionic conduction. Therefore, these data were used to calculate the amount of conductivity during the transition and to obtain conductivity-free values of ε'' at other frequencies:

$$\varepsilon''_{dipolar}(w) = \varepsilon''(w) - \frac{\varepsilon''(240\ Hz)\cdot(240)}{f} \qquad (3.25)$$

An example of 20 KHz ε'' data with and without conductivity effects is given in Figure 3.9.

Isofrequency conduction-free ε'' data were then ratioed to the maximum value and plotted in Arrhenius fashion, shown in Figure 3.10 for the 20 KHz data in Figure 3.9. As

predicted by Equation 3.12, this curve is linear at temperatures above the transition temperature. The activation energies calculated from the slopes of the curves at several frequencies are summarized in Table 3.2.

These values show good agreement with those calculated by the w_{max} method at 1 and 5°C/minute, differing by only a few percent. The excellent agreement between the values of E_τ calculated at different frequencies validates the model assumptions. Therefore the ε'' ratio method may be used to determine dielectric transition activation energies.

3.4.2 TGDDM/DDS Polymerization

3.4.2.1 Isothermal Reaction

The reaction activation energy was calculated from the isothermal dielectric cure data by both the ionic conductivity and dipolar relaxation methods. The initial slopes of the conductivity plots in Figures 2.13 - 2.21 were plotted against inverse isothermal cure temperature in Figure 3.11. As predicted by Equation 3.16, plotting the slopes in this manner produced a line from which E_a was calculated. The reaction activation energy for the TGDDM/DDS system was found to be 15.79 kcal/mole.

The activation energy was also calculated from the dipolar contribution to the isothermal cure dielectric

properties using the peak time method in Equation 3.20. The peak in ε'' is obscured by ionic conductivity at nearly all frequencies, especially at high cure temperatures. Consequently, the inflection point in ε' was used to determine t_p.

The assumption that the inflection in ε' (and the peak in ε'') occur at a particular point in the cure was checked by comparing the DSC extents of reaction at the 20 KHz values of t_p at each cure temperature. These values are summarized in Table 3.3. The extents of reaction are nearly identical, only α_p at 220°C differs greatly from the mean. Variations in α_p are primarily due to the difficulty in determining t_p precisely from the data. However, the primary assumption in the derivation of Equation 3.20 is appropriate.

Arrhenius curves of the inverse peak times at 240 Hz, 1 KHz, and 20 KHz at each cure temperature are presented in Figure 3.12. These curves are linear, further validating the model assumptions over a wide frequency range. The reaction activation energies calculated from these curves are presented in Table 3.4.

The reaction activation energies calculated using the ionic and dipolar methods are compared in Table 3.4 to the values calculated by DSC. The ionic conductivity value is in excellent agreement with the isothermal DSC value,

differing by only 3.4%. Those values calculated using the isothermal dipolar relaxation method are lower than the DSC values by approximately 20%, but still within the accepted range of 12-15 kcal/mole for epoxy/amine polymerization [16]. The differences may be attributed to experimental error.

3.4.2.2 Nonisothermal Reaction

The TGDDM/DDS reaction activation energy was also determined from the reaction portion of the nonisothermal dielectric data in Figures 2.22 - 2.24 using Equation 3.24. Conduction influences in mask the peak in ε'', so the ε' inflection point was used to determine T_p.

As with the isothermal data, the inflection and peak in ε' and ε'' were compared to the DSC data to check the primary assumption in the method derivation. Table 3.5 contains the values of α_p and T_p at 20 KHz for each heating rate. The values are scattered, but as seen in the DSC scans in Figures 2.38 - 2.40, the reaction exotherm is changing quickly at T_p. Therefore, the α_p assumption is difficult to check with any precision.

Figure 3.13 contains the Arrhenius curves of the heating rates plotted versus the ε' inflection temperatures at 240 Hz, 1 KHz, and 20 KHz. The reaction activation energies calculated from the slopes of these curves are

given in Table 3.4. The values of E_a are in excellent agreement with the value determined by DSC, supporting the assumptions made in deriving Equation 3.24. Dielectric data at additional heating rates are needed to further confirm the linearity of the curves in Figure 3.13.

As in the isothermal dipolar method, accurate values of the inflection temperature are difficult to determine. The inaccuracy is compounded by electrode polarization effects in nonisothermal ε' data, which are present throughout most of the reaction. In addition, Equation 3.24 holds only at constant heating rate, which may not be the case experimentally. The nonisothermal dielectric E_a values in Table 3.4 should then be considered as approximations, although these values are in good agreement with isothermal values.

3.5 Conclusions

Methods were developed for determining the activation energies of dielectric transition, E_t, and reaction, E_a, from dielectric data. These methods assume that the inflection in ε' and the simultaneous peak in ε'' occur at unique values of the relaxation time for each frequency. The transition activation energy may be calculated using the temperatures of the peak in ε'' at several frequencies with the developed expression.

An alternate technique for calculating E_τ, based on the temperature dependence of the dielectric properties of polymers which are described by the Havriliak-Negami dispersion equation, was developed in this study. This method allows E_τ to be calculated from ε'' data obtained at only one frequency. This method was shown to be valid by analyzing the glass transition of uncured TGDDM/DDS resin. The average value calculated from 10 and 20 KHz data, 43.85 kcal/mole, is in excellent agreement with the value calculated from 1°C/minute dielectric data, 44.51 kcal/mole.

Classical thermoanalytical expressions were developed for calculating the activation energy of reaction, E_a, from the dipolar portion of isothermal and nonisothermal cure dielectric properties. The reaction activation energy may be calculated from either the times or temperatures at which the ε' inflection or ε'' maximum occurs. For the TGDDM/DDS model system during isothermal cure, the average value of E_a calculated from the inflection times, 12.97 kcal/mole, compares well with values calculated using the ionic conductivity method, 15.79 kcal/mole, and the isothermal DSC value, 16.35 kcal/mole. The average value of E_a calculated from nonisothermal dipolar data, 16.09 kcal/mole, is in excellent agreement with the nonisothermal DSC value, 15.31 kcal/mole. The values in all cases are within or close to the accepted range of 12-15 kcal/mole.

The success of using dielectric spectroscopy to determine the activation energies of polymeric systems has been demonstrated. A further step in developing dielectric thermal analysis techniques is the description of the dielectric properties as functions of the extent of reaction during cure. The isothermal dielectric cure properties will be studied in Chapter 4; the nonisothermal cure properties will be discussed in Chapter 5.

Table 3.1

Parameters used to generate the model dielectric transition in Figure 3.5

$\alpha = 0.5$

$\beta = 0.5$

$\varepsilon_o = 5.0$

$\varepsilon_\infty = 10.0$

$\tau' = 1.0 \times 10^{-34}$ secs

$E_\tau = 40.0$ kcal/mole

Table 3.2

Comparison of activation energy calculations: uncured glass transition of TGDDM/DDS (25 phr)

	E_a (kcal/mole)		
φ (°C/min.)	w_{max}	ε'' ratio	
		10 KHz	20 KHz
1	44.51	47.00	45.01
5	41.70	42.89	43.05
10	(29.85)	41.60	43.52
AVERAGE	43.11	43.83	43.86

Table 3.3

Comparison of TGDDM/DDS (25 phr) extents of reaction at the 20 KHz ε' inflection during isothermal cure

Temperature (°C)	t_p(20 KHz) (secs)	α_p
140	11898	0.48
150	8532	0.42
160	5938	0.51
170	4302	0.46
180	3303	0.48
190	2214	0.51
200	1418	0.60
210	1278	0.61
220	898	0.71
	AVERAGE =	0.53

Table 3.4

Comparison of activation energy calculations: reaction of TGDDM/DDS (25 phr)

	E_a (kcal/mole)			
	Dielectric			DSC
	Ionic	Dipolar		
ISOTHERMAL	15.79	13.15	(240 Hz)	16.35
		12.82	(1 KHz)	
		12.94	(20 KHz)	
		12.97	AVERAGE	
NONISOTHERMAL	-----	16.25	(240 Hz)	15.31
		16.56	(1 KHz)	
		15.47	(20 KHz)	
		16.09	AVERAGE	

Table 3.5

Comparison of TGDDM/DDS (25 phr) extents of reaction at the 20 KHz ε' inflection during nonisothermal cure

φ (°C/min.)	T_p(20 KHz) (°C)	α_p
1	226	0.91
5	252	0.75
10	299	0.99
	AVERAGE =	0.88

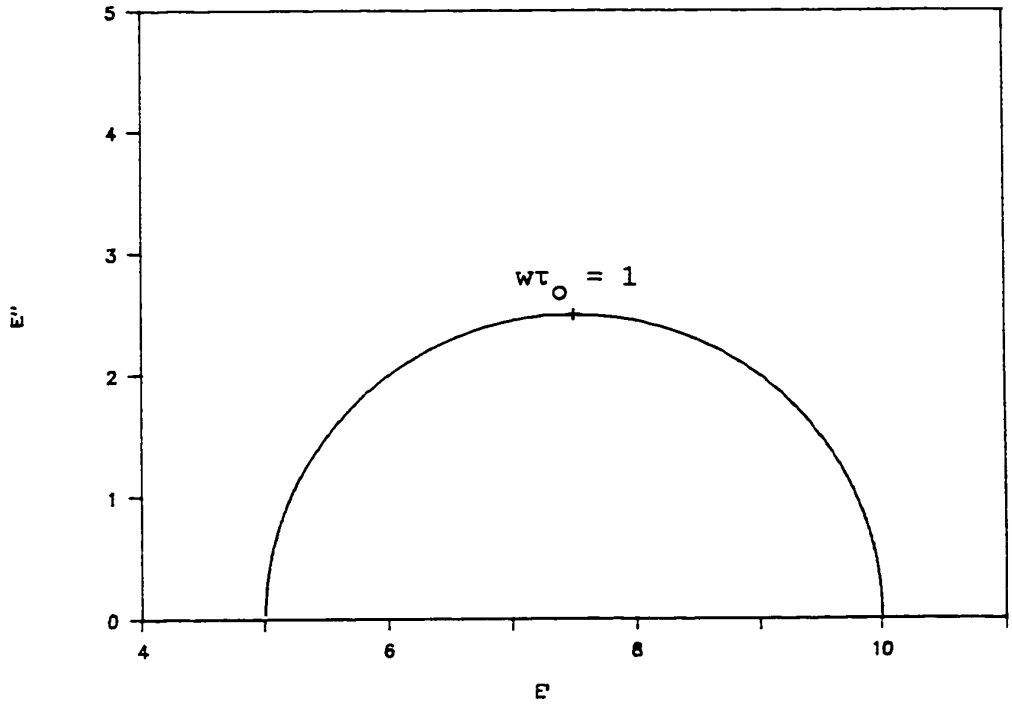

Figure 3.1 - Complex plane plot of Voigt model, Eq. 3.1, with τ_o = 0.1 secs, ε_o = 10, ε_∞ = 5.

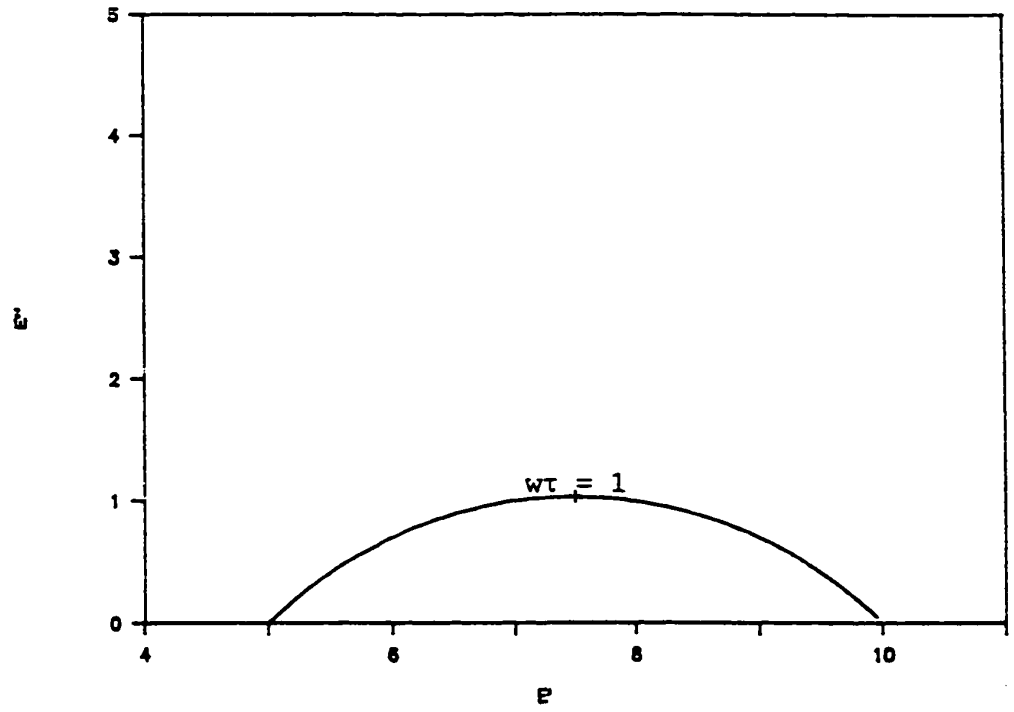

Figure 3.2 - Complex plane plot of Cole-Cole equation, Eq. 3.2, with τ = 0.1 secs, ε_o = 10, ε_∞ = 5.

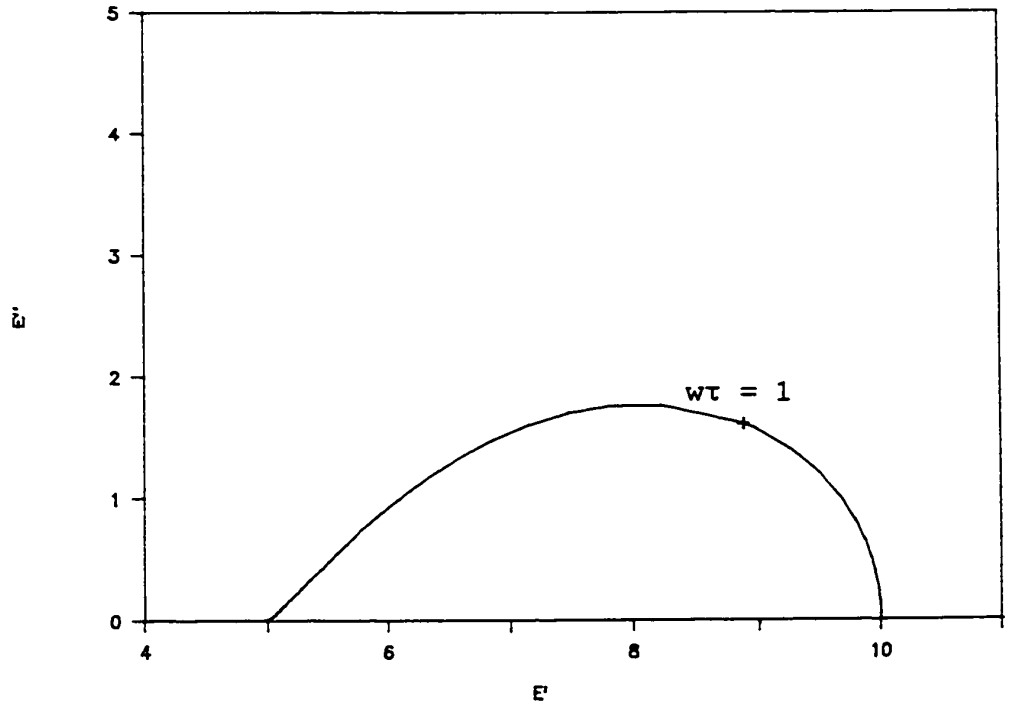

Figure 3.3 - Complex plane plot of Davidson-Cole equation, Eq. 3.3, wit τ = 0.1 secs, ε_o = 10, ε_∞ = 5.

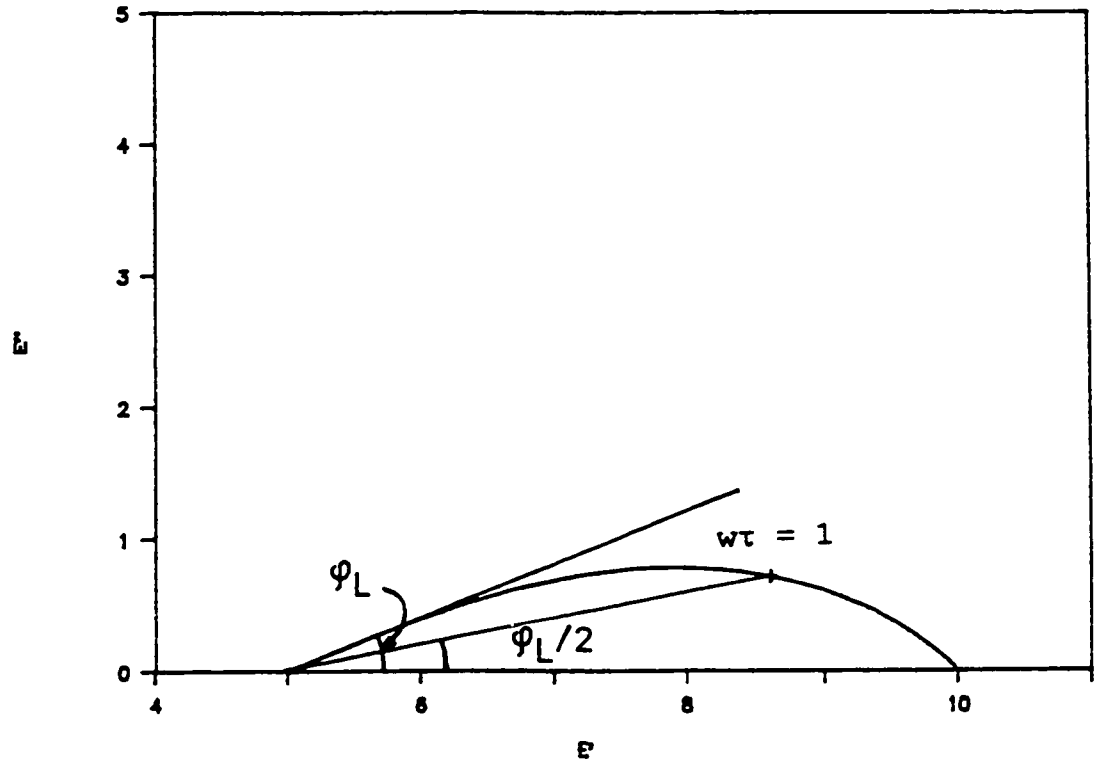

Figure 3.4 - Complex plane plot of Havriliak-Negami equation, Eq. 3.4, with τ = 0.1 secs, ε_o = 10, ε_∞ = 5.

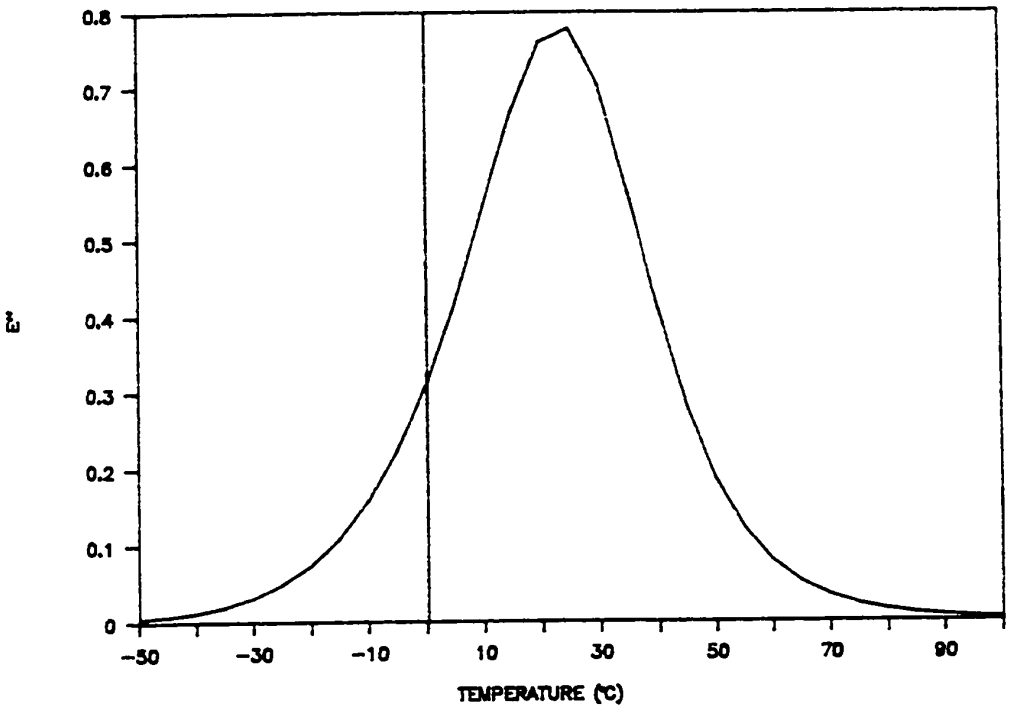

Figure 3.5 - Model dielectric transition generated by Havriliak-Negami equation, Eq. 3.4, and parameter values in Table 3.1.

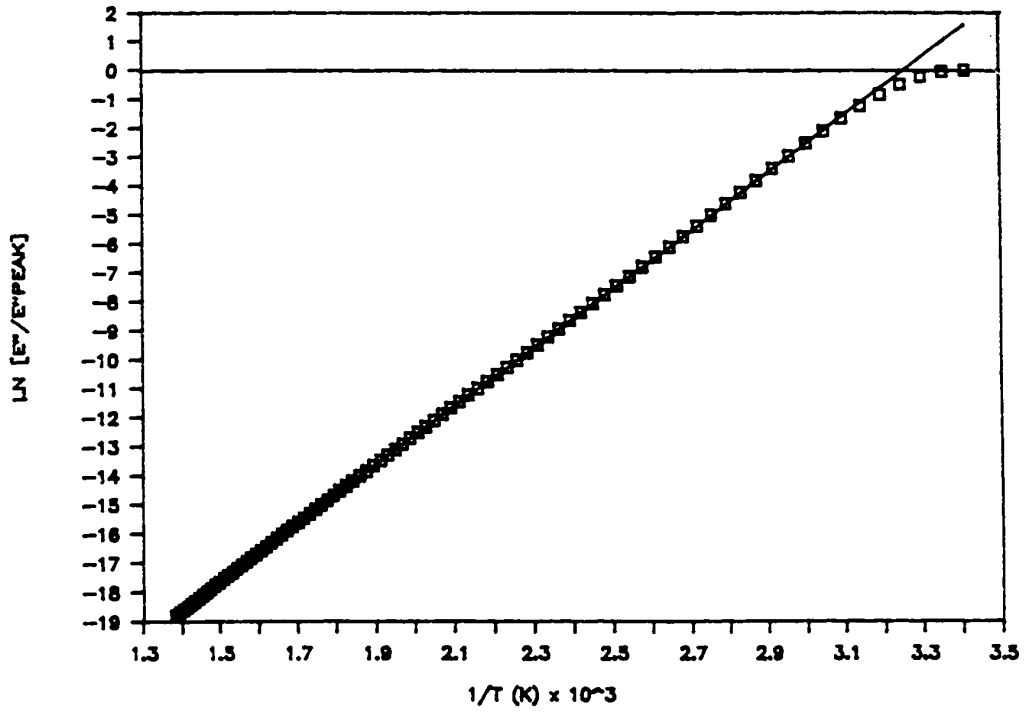

Figure 3.6 - Arrhenius plot of ε'' ratios from model Havriliak-Negami transition.

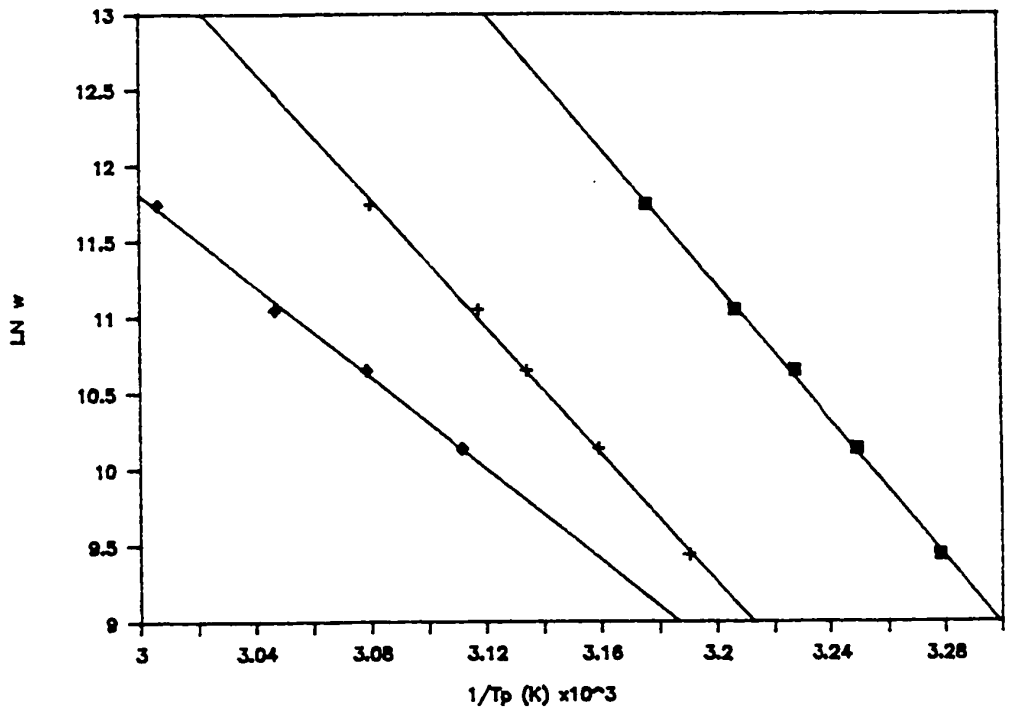

Figure 3.7 - Arrhenius plots of peak frequencies of T_g of uncured TGDDM/DDS (25 phr) at 1 (■), 5 (+), and 10 (♦)°C/minute.

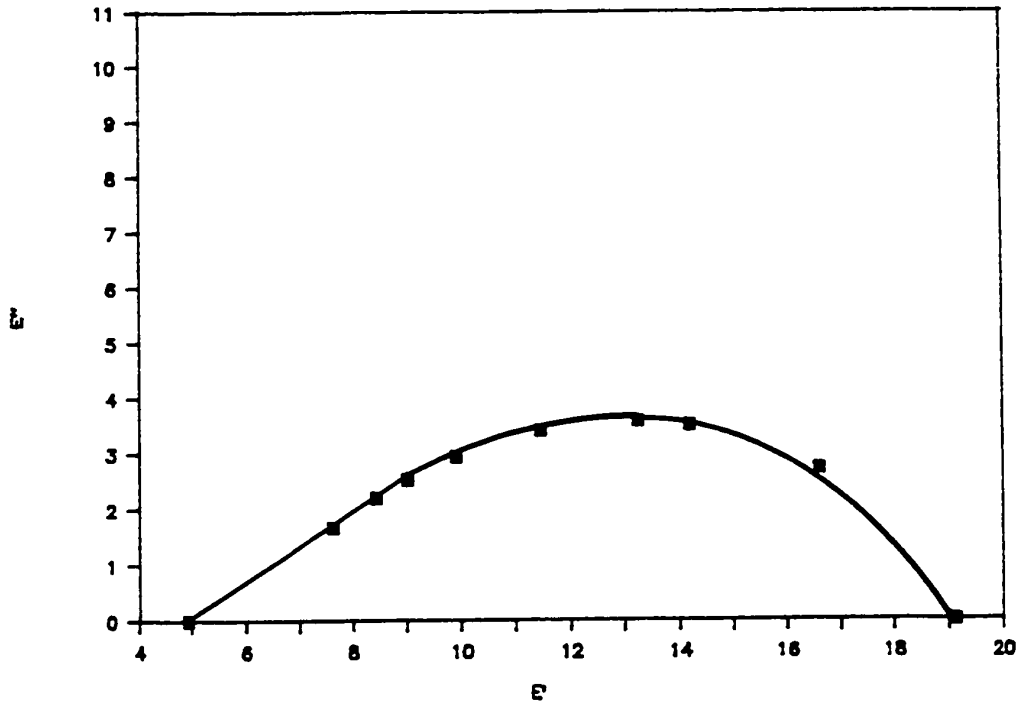

Figure 3.8 - Complex plane plot of dielectric properties of uncured TGDDM/DDS at 30.65°C.

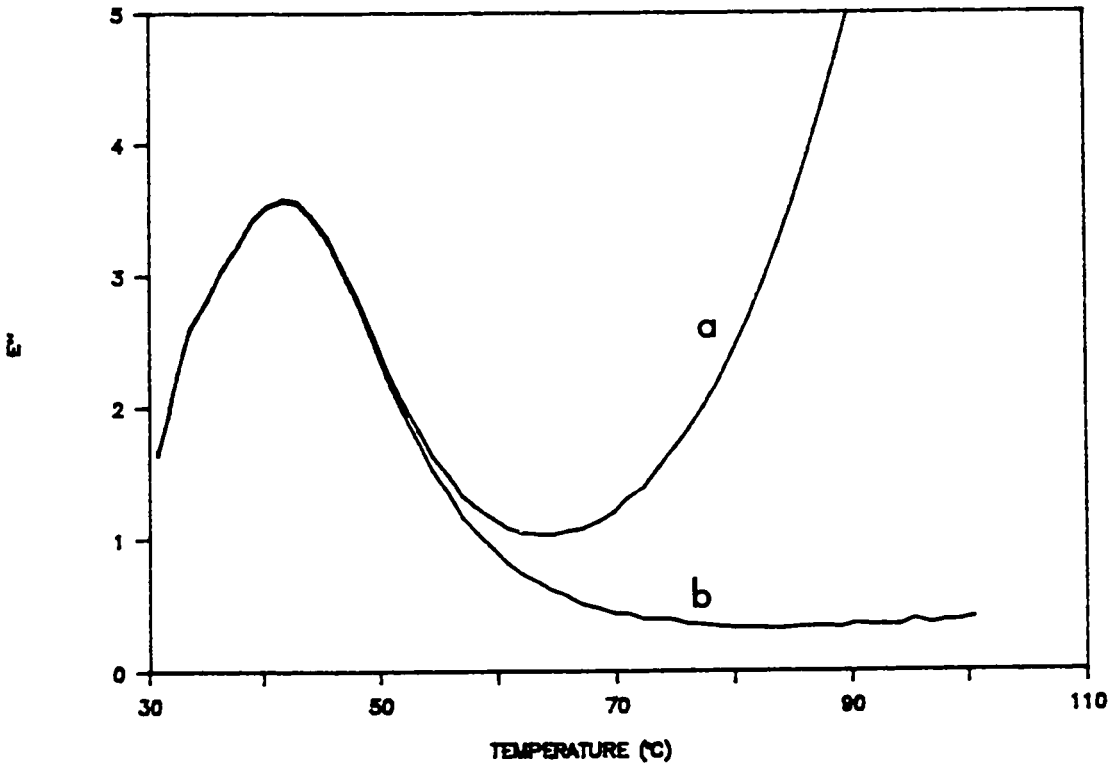

Figure 3.9 - Low temperature 20 KHz dielectric loss of uncured TGDDM/DDS at 1°C/minute:
a) experimental b) conduction subtracted.

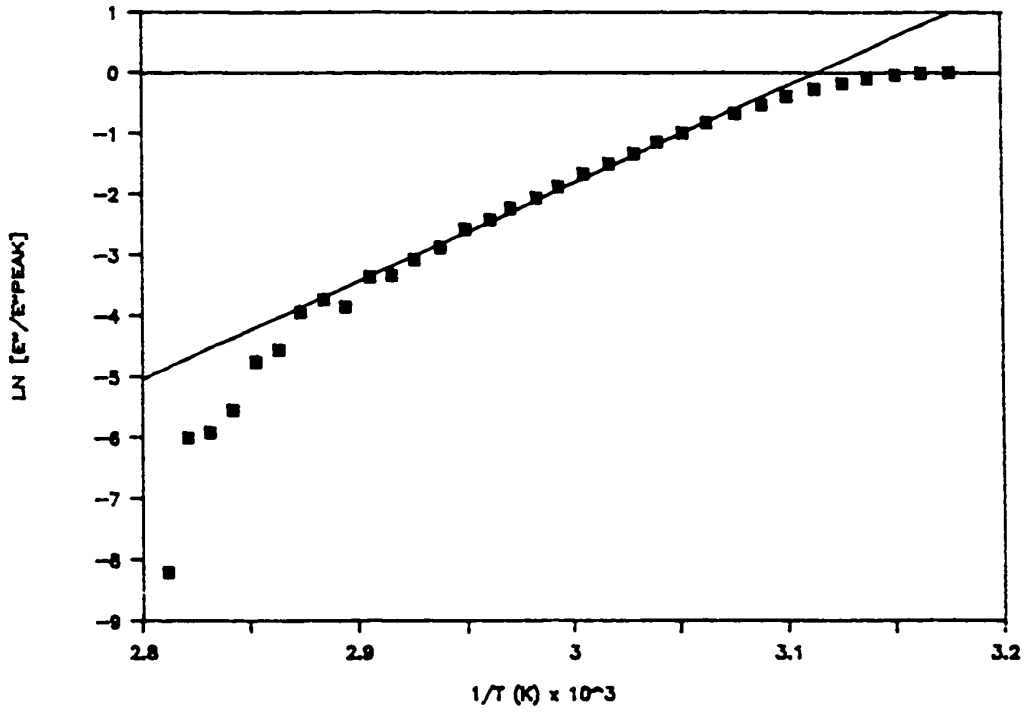

Figure 3.10 - Arrhenius plot of 20 KHz ε'' ratios for TGDDM/DDS uncured glass transition, E_τ = 45.01 kcal/mole.

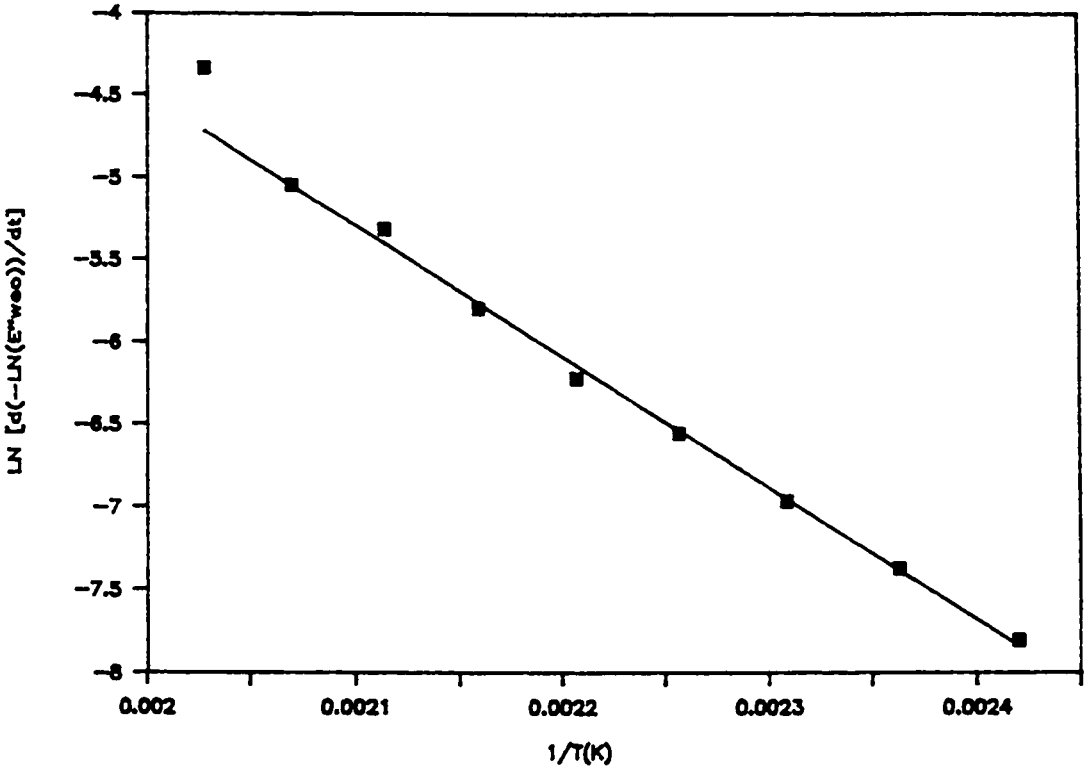

Figure 3.11 - Arrhenius plot of initial conductivity/time slopes during isothermal cure of TGDDM/DDS, E_a = 15.79 kcal/mole.

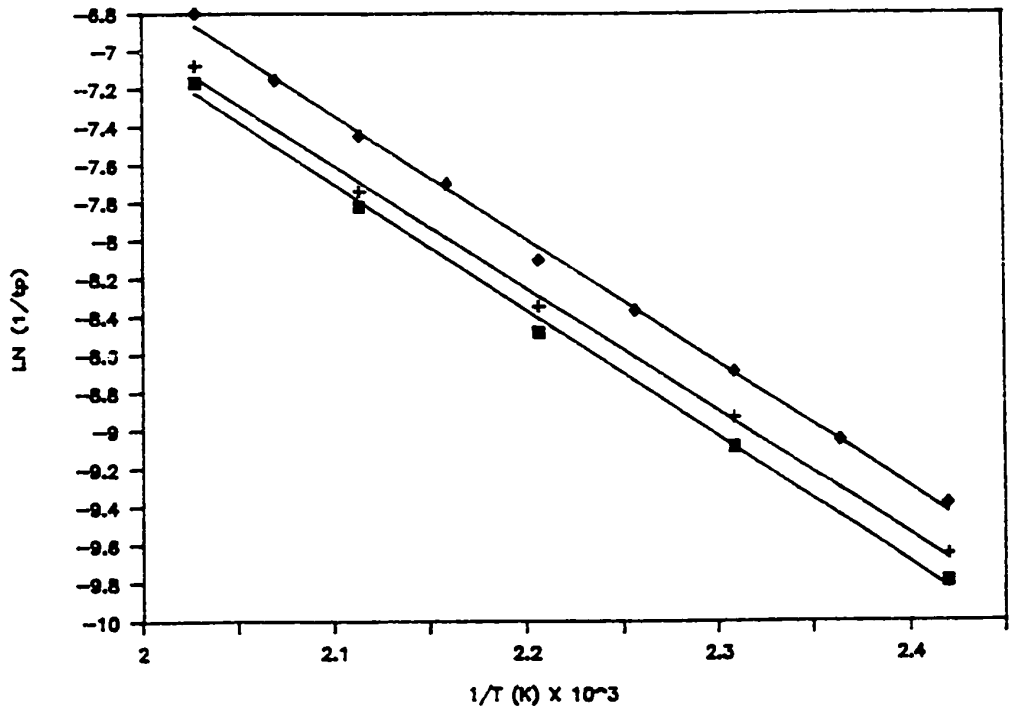

Figure 3.12 - Arrhenius plot of inverse ε' inflection times at 240 Hz (■), 1 KHz (+), and 20 KHz (♦) during isothermal cure of TGDDM/DDS.

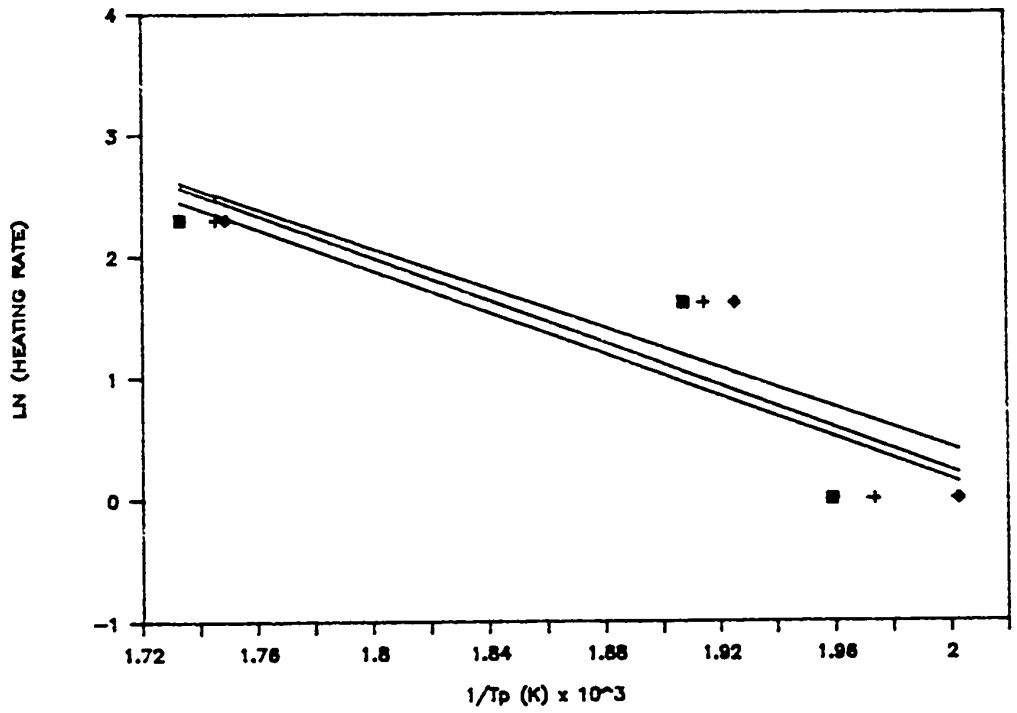

Figure 3.13 - Arrhenius-type plot of heating rate as a function ε' inflection temperature for curing TGDDM/DDS (25 phr) at 240 Hz (■), 1 KHz (+), and 20 KHz (♦).

Notes to Chapter 3

1. I.M. Ward, Mechanical Properties of Solid Polymers, 2nd Ed., Wiley-Interscience, New York, 1983.

2. N.G. McCrum, B.E. Read, and G. Williams, Anelastic and Dielectric Effects in Polymeric Solids, Wiley and Sons, London, 1967.

3. K.S. Cole and R.S. Cole, J. Chem. Phys., 9, 341 (1941).

4. D.W. Davidson and R.H. Cole, J. Chem. Phys., 18, 1417 (1950).

5. S. Havriliak and S. Negami, J. Polym. Sci.: Pt. C, 14, 99 (1966).

6. S. Havriliak and S. Negami, Polymer, 8, 161 (1967).

7. J.W. Lane, Masters Thesis, University of Washington, 1984.

8. J.W. Lane, J.C. Seferis, and M.A. Bachmann, J. Appl. Polym. Sci., 31, 1155 (1986).

9. S. Havriliak and D.G. Watts, Polymer, 27, 1509 (1986).

10. Y. Zhu and D.G. Watts, Polymer, 29, 325 (1988).

11. G. Bánhegyi, P. Hedvig, and F.E. Karasz, J. Appl. Polym. Sci., 35, 679 (1988).

12. S.H. Dillman and J.C. Seferis, J. Macromol. Sci., in press.

13. R.A. Fava and A.E. Horsfield, Brit. J. Appl. Phys. (J. Phys. D), Ser. 2, 1, 117 (1968).

14. R.B. Prime, Thermal Characterization of Polymeric Materials, E. Turi, Ed., Academic Press, New York, 1981.

15. W.J. Sichina, DuPont Instruments Thermal Analysis Applications Brief, TA-93.

16. R.B. Prime and E. Sacher, Polymer, 13, 455 (1972).

CHAPTER 4

DIELECTRIC RESPONSE OF A MODEL THERMOSETTING MATRIX DURING ISOTHERMAL REACTION

4.1 Introduction

The dielectric properties measured during the isothermal reaction of thermosetting polymers were investigated further. A mathematical model was developed which described the components of the complex dielectric constant in terms of the extent of reaction during cure. The model is a complete description of the properties, combining both ionic and dipolar sources during cure.

The success of the model is demonstrated for the model resin at several isothermal reaction temperatures. Electrode polarization effects were removed from the experimental data using a method developed in the study. The model resin parameters are presented and their temperature dependences are discussed.

4.2 Theoretical Model Development

A complete description of the dielectric behavior during reaction must account for the effects of both ionic conductivity and dipolar relaxation. Although the sources of these phenomena differ, the extent of polymerization

dictates the responses of both ions and dipoles to the electric field. Accordingly, the link between developed models of conduction and relaxation is the resin cure kinetics.

4.2.1 Equivalent Dielectric Circuit Representation

The electrical properties of curing thermosetting resin were described by constitutive expressions which represent an electric circuit containing a parallel arrangement of capacitive and resistive elements, as depicted in Figure 4.1. The mathematics of this configuration permitted the individual ionic and dipolar contributions to ε' and ε'' to be added to produce the total resin response:

$$\varepsilon'_{resin} = \varepsilon'_{ionic} + \varepsilon'_{dipolar} \qquad (4.1)$$

$$\varepsilon''_{resin} = \varepsilon''_{ionic} + \varepsilon''_{dipolar} \qquad (4.2)$$

During cure, these contributions are modelled as functions of extent of reaction.

4.2.2 Ionic Conductivity During Isothermal Reaction

The basis for ionic conductivity kinetic modelling was an empirical relationship between resistivity, p, and reaction proposed by Keinle and Race for alkyd resins [1]:

$$\frac{d(\ln p)}{dt} \alpha \frac{d\alpha}{dt} \qquad (4.3)$$

While empirical in nature, this relationship has been found to hold for a number of polymerization reactions [2-8]. An expression relating α and the conduction portion of ε'' was derived from Equation 4.3 by first substituting the definition of conductivity, σ, in terms of p:

$$\sigma = 1/p \qquad (4.4)$$

The relationship between ε' and conductivity, expressed in Equation 1.8, was substituted into Equation 4.3:

$$\frac{d[\ln(\varepsilon''we_o)]}{dt} \alpha \frac{d\alpha}{dt} \qquad (4.5)$$

By incorporating a proportionality constant, C_r, and integrating, an equation relating the ionic conduction contribution to ε'' and the extent of reaction was obtained:

$$\ln(\varepsilon''_{ionic}we_o) = C_r\alpha + C_o \qquad (4.6)$$

This equation predicts that a plot of $\ln(\varepsilon''we_o)$ versus the extent of reaction will be linear when the dielectric

response results primarily from ionic conduction.

4.2.3 Electrode Polarization Effects

The buildup of ions at the electrodes causes the measured value of ε' to be larger than the true value, especially at low frequencies. One way to account for these effects is to extrapolate ε' data to $t = 0$, obtaining the polarization-free dielectric constant of unreacted resin. However, a more rigorous method for removing electrode polarization effects from the data was developed in this study.

The contribution of electrode polarization to ε' was first investigated in 1951 using polar organic liquids [9]. Since the liquids did not react during the experiment, only the frequency dependence of electrode polarization was considered. Based on this analysis, simple methods have been developed for evaluating polarization effects in dielectric data [10].

These methods were adapted to relate polarization to ε' during reaction. As in the polar organic liquid study, electrode polarization was treated as a complex impedance, Z^*_{el}, in series with the resin and was modelled as a function of frequency using a power law expression:

$$Z^*_{el} = Z_o(iw)^{-n} \qquad (4.7)$$

The constant Z_o is a characteristic of each sample/electrode interface. The exponent n may have values between 0.0 and 1.0. The experimentally measured components of the dielectric constant were then related to their intrinsic values and to polarization by:

$$\varepsilon'_{obs} = \varepsilon'_{dipole} + Z_o \sin(n\pi/2) w^{-(n+1)} G^2/C_v \qquad (4.8)$$

$$\varepsilon''_{obs} = \varepsilon''_{ionic} + \varepsilon''_{dipole} - Z_o \cos(n\pi/2) w^{-n} G^2/C_v \qquad (4.9)$$

G, the conductance of the sample, is related to the resin conductivity measured using parallel plate electrodes:

$$G = \sigma A/d \qquad (4.10)$$

C_v is the capacitance of free space, which may be calculated from the cell geometry:

$$C_v = Ae_o/d \qquad (4.11)$$

Substituting Equations 4.10 and 4.11 into Equations 4.8 and 4.9 provided the contribution of electrode polarization to the dielectric properties in terms of the resin conductivity:

$$\varepsilon'_{obs} = \varepsilon'_{dipole} + Z_o \sin(n\pi/2) w^{-(n+1)} A\sigma^2/de_o \qquad (4.12)$$

$$\varepsilon''_{obs} = \varepsilon''_{ionic} + \varepsilon''_{dipole} - Z_o \cos(n\pi/2) w^{-n} A\sigma^2/de_o \qquad (4.13)$$

The final step in removing polarization from the data was the determination of the values of Z_o and n. The effects of polarization in ε'' are insignificant relative to those of ionic conductivity, so only ε' was considered. Curves of ε' plotted as a function of σ^2 will be linear according to Equation 4.12, when polarization is present, with:

$$\text{slope} = Z_o \sin(n\pi/2) w^{-(n+1)} A/de_o \qquad (4.14)$$

$$\text{intercept} = \varepsilon'_{dipole} \qquad (4.15)$$

The intercept value represents the initial value of ε' of uncured resin.

From the slopes and intercepts of σ^2 plots of ε' data obtained at several frequencies, the values of Z_o and n may be calculated. Taking the logarithm of Equation 4.14 produces:

$$\ln(\text{slope}) = \ln[Z_o \sin(n\pi/2) A/de_o] - (n+1) \ln w \qquad (4.16)$$

This equation suggests that a log-log plot of the slopes and angular frequencies is linear with:

$$\text{slope} = n+1 \tag{4.17}$$

$$\text{intercept} = \ln[Z_o \sin(n\pi/2)A/de_o] \tag{4.18}$$

The values of Z_o and n may be calculated using these equations and ε' and σ data obtained at several frequencies.

In isothermal dielectric cure experiments, ionic conductivity at the beginning of epoxy/amine polymerization is affected not only by network formation during reaction, but also by the temperature increase resulting from the highly exothermic reaction. In addition, resin conductivity decreases over several orders of magnitude during initial reaction. Consequently, the correct ε' region for performing linear regression according to Equation 4.12 is difficult to determine a priori.

Therefore, the appropriate data region for linear regression was obtained by first taking the derivative of Equation 4.12 with respect to σ:

$$d\varepsilon'/d\sigma = 2[Z_o \sin(n\pi/2)w^{-(n+1)}A/de_o]\sigma \tag{4.19}$$

and then taking the logarithm of both sides:

$$\ln(d\varepsilon'/d\sigma) = \ln(2Z_o \sin(n\pi/2) w^{-(n+1)} A/de_o) + \ln \sigma \quad (4.20)$$

According to this equation, a log-log plot of $d\varepsilon'/d\sigma$ and σ is linear with a slope equal to 1.0 and is easy to identify. This region may then be used to find the slopes and intercepts of Equation 4.12 by linear regression.

4.2.4 Isothermal Dipolar Relaxation During Reaction

Kinetic modelling of ε^* resulting from dipolar relaxation was achieved by first describing the dielectric properties during cure in terms of the average dipolar relaxation time, τ. The mathematical development used to describe the dielectric properties reflects the viscoelastic nature of the dipolar dielectric response. The relaxation time during cure was then related to the extent of reaction, thus providing the complete relationship between dielectric properties and reaction.

4.2.4.1 Isofrequency Time Response of Reacting Polymers

Complex plane plots of the isofrequency dielectric properties of reacting polymers are analogous in appearance to the dispersion curves of nonreacting polymers [11]. In nonreacting polymers, each point on the curve represents the dielectric properties at a given frequency; in reacting polymers, each represents the properties at a given time.

Lane, Seferis, and Bachmann extended the two parameter Havriliak-Negami dispersion equation [11], Equation 3.4, to describe the complex plane plots of polymers having a relaxation time distribution which change with time, such as in curing thermosets [12].

Using this approach, the independent variable in Equation 3.4 was the relaxation time rather than frequency. The definitions of ε_o and ε_∞ were changed to represent the values of ε' at $\alpha = 0$ and 1. Rewritten to reflect this difference in application, Equation 3.4 becomes:

$$\varepsilon^* = \varepsilon_{\alpha=1} + \frac{(\varepsilon_{\alpha=o} - \varepsilon_{\alpha=1})}{(1 + (i\omega\tau)^{\beta'})^{\alpha'}} \qquad (4.21)$$

$$0 < \alpha' \leq 1, \; 0 < \beta' \leq 1$$

Expressions for ε' and ε'' in terms of $\omega\tau$ are obtained by applying DeMoivre's Theorem twice:

$$\varepsilon' = \varepsilon_{\alpha=1} + \frac{(\varepsilon_{\alpha=o} - \varepsilon_{\alpha=1}) \cos \alpha'\varphi}{[1+2(\omega\tau)^{\beta'}\cos(\beta'\pi/2)+(\omega\tau)^{2\beta'}]^{\alpha'/2}} \qquad (4.22)$$

$$\varepsilon'' = \frac{(\varepsilon_{\alpha=o} - \varepsilon_{\alpha=1}) \sin \alpha'\varphi}{[1+2(\omega\tau)^{\beta'}\cos(\beta'\pi/2)+(\omega\tau)^{2\beta'}]^{\alpha'/2}} \qquad (4.23)$$

The parameter φ is a collection of terms:

$$\varphi = \tan^{-1}\left[\frac{(w\tau)^{\beta'}\sin(\beta'\pi/2)}{1 + (w\tau)^{\beta'}\cos(\beta'\pi/2)}\right] \qquad (4.24)$$

4.2.4.2 Kinetic Viscoelasticity and Relaxation Time

The final step in describing the dielectric properties during cure is to relate the dipolar relaxation time to the extent of reaction. Being a viscoelastic process, dipolar relaxation during reaction was modelled in the same manner as are other viscoelastic phenomena during reaction. Dillman and Seferis took this same approach by modifying viscosity models to describe "kinetic viscoelasticity," i.e. viscoelastic property changes resulting from reaction [13]. Their success in modelling dynamic mechanical behavior during cure suggested using a similar approach to model dipolar relaxation during reaction.

The basis for kinetic viscoelastic modelling is the Dusi-May-Seferis equation, which describes resin cure using n^{th} order kinetics and defines viscosity as an activated process [14]. The viscosity of reacting polymers is expressed as a function of time and temperature, $\eta(t,T)$, by:

$$\ln \eta(t,T) = \ln \eta_o(T) + \frac{\Phi}{n-1} \ln [1 + (n-1)k_x t] \quad (4.25)$$

$\eta_o(T)$ is the viscosity of uncured resin. The parameters n and k_x represent the reaction order and rate constant; Φ is an entanglement factor and is constant for each resin system and stoichiometry. Dillman and Seferis used Equation 4.25 to model relaxation time during cure, viz.:

$$\ln \tau(t,T) = \ln \tau_o(T) + \frac{\Phi}{n-1} \ln [1 + (n-1)k_x t] \quad (4.26)$$

However, activated models such as Equation 4.26 predict infinite, rather than finite, properties as $t \rightarrow \infty$. Consequently, a physically meaningless, infinite relaxation time is predicted by Equation 4.26 at the completion of reaction. Dillman and Seferis corrected this shortcoming by including the relaxation time at complete reaction, τ_∞ [13]:

$$\ln \left[\frac{\frac{1}{\tau_o} - \frac{1}{\tau_\infty}}{\frac{1}{\tau} - \frac{1}{\tau_\infty}} \right] = \frac{\Phi}{n-1} \ln [1 + (n-1)k_x t] \quad (4.27)$$

This equation predicts that the relaxation time approaches

τ_∞ at infinite reaction times. The values of Φ, k_x, and n cannot be individually determined from relaxation time data because of the manner in which they appear in this equation. By substituting DSC extent of reaction data in place of the kinetic equation, the kinetic relaxation model parameters may be determined from relaxation data for any curing polymer and for any reaction mechanism. After substitution and rearrangement, the final relationship between relaxation time and cure was expressed as:

$$\frac{1}{\tau} = \frac{1}{\tau_\infty} + \left[\frac{1}{\tau_o} - \frac{1}{\tau_\infty}\right](1-\alpha)^{\Phi} \qquad (4.28)$$

This equation was then used to describe the average dipolar relaxation time during cure in terms of the relaxation times of uncured resin, τ_o, and fully cured resin, τ_∞; the extent of reaction, α; and the entanglement parameter, Φ.

4.2.5 Physical Interpretation of the Entanglement Parameter

The entanglement parameter, Φ, appearing in the above kinetic viscoelasticity equations has previously alluded physical interpretation. The incorporation of kinetic models in previous studies [13,14] precluded mathematical determination of the value of Φ and hence any discussion of

its significance. Analogies to the Mark-Houwink exponent [15] have been made in order to estimate that Φ is equal to 3.4 in thermoplastic polymers [15] and 15.0 in crosslinked thermosetting polymers [16]. Also, connections between Φ and other polymer properties have not been discussed in the literature. Incorporating experimental kinetic data in this study allowed the direct determination of Φ and therefore the first opportunity for interpreting its physical significance. Equation 4.28 was compared to another viscoelastic property model, allowing Φ to be expressed in terms of the model parameters.

Meissonnier and Seferis [18], in an attempt to consolidate differing approaches to viscosity modelling, related the viscosity of curing polymers to the glass transition temperature using the WLF equation:

$$\ln \eta(T) = \ln \eta_o(T) - \frac{C_1(T - T_g)}{C_2 + (T - T_g)} \qquad (4.29)$$

The increase in the glass transition temperature of reacting polymers from the uncured value, T_{go}, to the fully cured value, $T_{g\infty}$, was described using the Bueche equation [19]:

$$\frac{1}{T_g(\alpha)} = \frac{1 - \alpha}{T_{go}} + \frac{\alpha}{T_{g\infty}} \qquad (4.30)$$

Meissonnier and Seferis substituted an n^{th} order kinetic model for α during reaction. Means of calculating Φ were produced by substituting Equation 4.30 into Equation 4.29 and expressing viscosity as a function of α directly:

$$\ln \eta(\alpha,T) = \ln \eta_o(T) - \frac{C_1 T_{g\infty}(T-T_{go}) - C_1 T(T_{g\infty}-T_{go})\alpha}{T_{g\infty}(C_2+T-T_{go}) - (C_2+T)(T_{g\infty}-T_{go})\alpha} \quad (4.31)$$

The kinetic viscoelasticity equation, Equation 4.28, was applied to viscosity and compared to Equation 4.31 after expanding both in power series of α. The mathematical details are presented in Appendix B. Equating coefficients of the two series provided a relationship between Φ and the WLF equation parameters:

$$\Phi = C_1 C_2 \, (T_{go}/T_{g\infty}) \, \frac{(T_{g\infty} - T_{go})}{(C_2 + T - T_{go})^2} \quad (4.32)$$

According to this analysis, Φ is related to changes in the resin free volume and is a complex combination of the effects of network structure formation and cure temperature. Further implications of Equation 4.32 will be discussed after determining the dielectric model parameters for the TGDDM/DDS system.

4.2.6 Kinetic Dielectric Model Combining Conduction and Relaxation

The final form of the dielectric model combines the ionic conductivity contribution to ε'' in Equation 4.6 with the dipolar relaxation contributions to ε' and ε'' from Equations 4.22 and 4.23:

$$\varepsilon' = \varepsilon_{\alpha=1} + \frac{(\varepsilon_{\alpha=0} - \varepsilon_{\alpha=1}) \cos \alpha'\varphi}{[1+2(w\tau)^{\beta'}\cos(\beta'\pi/2)+(w\tau)^{2\beta'}]^{\alpha'/2}} \quad (4.33)$$

$$\varepsilon'' = \frac{\exp(C_r\alpha+C_o)}{we_o} + \frac{(\varepsilon_{\alpha=0} - \varepsilon_{\alpha=1}) \sin \alpha'\varphi}{[1+2(w\tau)^{\beta'}\cos(\beta'\pi/2)+(w\tau)^{2\beta'}]^{\alpha'/2}} \quad (4.34)$$

The parameter φ is defined by Equation 4.24. For isothermal experiments, the relaxation time, τ, was expressed as an explicit function of extent of reaction using Equation 4.28. The complete dielectric response of thermosetting polymers during reaction may be predicted by determining the appropriate values of the parameters in Equations 4.28, 4.33, and 4.34.

4.3 Discussion

4.3.1 Model Parameter Determination

4.3.1.1 Ionic Conductivity Parameters

The parameters C_r and C_o in the ionic conductivity term of Equation 4.34 were determined for each cure temperature by regression of the initial linear portion of semi-log plots of apparent conductivity, $\varepsilon''we_o$, versus DSC extent of reaction data. Linear regression was performed on only the 240 Hz data. Ionic conductivity influences the dielectric response at this frequency to a greater extent than at higher frequencies, allowing C_r and C_o to be accurately determined. Regression was typically performed on the data in the range $0.10 \leq \alpha \leq 0.40$. For $\alpha < 0.10$ heat transfer effects in the data were significant.

These values of C_r and C_o are presented in Table 4.1. The linearity of the data predicted by Equation 4.6 is reflected in the high values of the correlation coefficients. The significant deviation of C_o at 220°C may be the result of substantial bubble formation in the resin at the beginning of the experiment. These data were therefore discarded.

4.3.1.2 Electrode Polarization Parameters

The contribution of electrode polarization was determined from ε' data using the method developed in Equations 4.12 - 4.20. An example of this procedure will be discussed for data generated during cure at 140°C. First, the data region used to find the polarization parameters was determined using Equation 4.20. The derivative of ε' with respect to conductivity was calculated from the data using a two point formula [20]:

$$\left.\frac{d\varepsilon'}{d\sigma}\right|_i = \frac{\varepsilon'_{i+1} - \varepsilon'_i}{\sigma_{i+1} - \sigma_i} \qquad (4.35)$$

Log-log plots of the derivatives and conductivities, as in Figure 4.11, contained a linear region with slope ≈ 1, as predicted by Equation 4.20.

ε' data in this region were then plotted as a function of σ^2, as shown in Figure 4.12. The polarization parameters were calculated using the slope and intercept of the lines and Equations 4.14 and 4.15. The impedance constant Z_o and exponent n were then determined from the polarization parameters at several frequencies using Equations 4.16 - 4.20.

The complete set of polarization parameters calculated by this procedure are presented for each isothermal cure

temperature in Table 4.2. These values are presented merely for reference purposes since they are characteristic only of each experiment and are not material parameters. The impedance caused by electrode polarization varies over several orders of magnitude, but increased with temperature.

The most significant result of the analysis is the accurate determination of polarization-free values of $\varepsilon_{\alpha=o}$. Examination of $\varepsilon_{\alpha=o}$ with frequency, as plotted in Figure 4.13 for 140°C data, suggested the following relationship:

$$\varepsilon_{\alpha=o} = C \ln w + D \qquad (4.36)$$

The values of C and D found by linear regression are summarized in Table 4.3.

4.3.1.3 Dipolar Relaxation Parameters

With the contributions of ionic conduction and electrode polarization to the dielectric properties described, only the dipolar relaxation parameters remained to be found. The values for each temperature were determined either directly from the data or numerically. Data at 20 KHz were used to find the parameters in Equations 4.28, 4.33, and 4.34. These data were used since dipolar relaxation effects are masked by conduction and polarization at low frequencies.

The values of $\varepsilon_{\alpha=o}$ were calculated using Equation 4.36 and the parameters in Table 4.3. The values of $\varepsilon_{\alpha=\infty}$ were found directly from the experimental data. The parameters α', τ_o, and τ_∞ were determined by nonlinear regression using the method of steepest descent. The value of Φ is calculated by Equation 4.28 from known values of α, τ_o, and τ_∞. The value of β' may be calculated from α' and the complex plane angle φ_L, which is formed by the intersection of the long time linear dispersion and the ε' axis, using [11]:

$$\varphi_L = \alpha'\beta'(\pi/2) \tag{4.37}$$

In summary, only three of the seven model parameters were determined by numerical methods. The remainder of the parameters were found by direct analysis of the data or through constraints. The parameters describing the relationships between dipolar relaxation time, reaction, and the dielectric properties for each of the isothermal cure temperatures are listed in Table 4.4.

4.3.2 Model Prediction of Experimental Results

The parameters listed Tables 4.1 and 4.4 and experimental extent of reaction data were used to generate the model response of TGDDM/DDS during cure, combining ionic

conductivity, dipolar relaxation, and electrode polarization. The ability of the combined model to describe the dielectric properties at 20 KHz is demonstrated for each cure temperature in Figures 4.14 - 4.21. As seen in these plots, the model describes both ε' and ε'' data very well.

The combined model was tested by using the isothermal parameters listed in Tables 4.1 and 4.4 to predict data obtained at other frequencies, without any additional fitting. For specific comparison, the model prediction and data obtained at 240 Hz are presented in Figures 4.22 - 4.29. The excellent agreement between the model and the data indicate that the parameters determined from the 20 KHz data are consistent for describing the data at all frequencies and that the assumptions used were valid.

4.3.3 Dependence of Parameters on Temperature

The temperature dependences of the conductivity parameters C_r and C_o were determined using the Arrhenius plots shown in Figures 4.30 and 4.31. The parameter C_r, which relates ionic mobility to the network formation state, shows no clear functionality with temperature; the average value was -11.27. C_o, which represents the conductivity of unreacted resin, follows Arrhenius-type behavior. This type of behavior is expected, since conductivity in nonreacting systems is an activated process [21]. The apparent

activation energy for conduction in uncured resin is 15.33 kcal/mole.

The dipolar relaxation parameters are presented as functions of cure temperature in Figures 4.32 and 4.33. The value of α' increased at higher isothermal cure temperatures, while β' remained approximately constant at 0.70. These results indicate that long time dispersion was less severe at higher temperatures while the symmetry properties of the complex plane plot remained unchanged. The value of α' also increased with temperature in dynamic mechanical experiments during cure [13] and in unreacting systems [22]. Differing trends have been observed for β' in the literature [13,22]. Since reaction is more complete at higher temperatures, a more symmetric distribution of relaxation times may result at high cure temperatures. Also, dipolar orientation is aided by the increased temperature, which may produce a narrower distribution of relaxation times and a less broadened dispersion curve.

The entanglement parameter Φ decreased with temperature, as seen in Figure 4.34. This behavior is consistent with the interpretation of Φ in terms of the glass transition temperature, Equation 4.32. The ratio of Φ values at two cure temperatures is given by:

$$\frac{\Phi(T_2)}{\Phi(T_1)} = \frac{Tg_{\infty 1}\,(Tg_{\infty 2}-Tg_o)\,(C_2+T_1-Tg_o)^2}{Tg_{\infty 2}\,(Tg_{\infty 1}-Tg_o)\,(C_2+T_2-Tg_o)^2} \qquad (4.38)$$

This equation predicts that $\Phi(T_2)$ is less than $\Phi(T_1)$, since both T_2 and $Tg_{\infty 2}$ are greater than T_1 and $Tg_{\infty 1}$. Physically, Φ is related to the ability of dipoles to orient as crosslinking occurs. At higher cure temperatures, network development is more extensive, the glass transition temperature is higher, and the dipolar relaxation time changes more slowly.

The temperature behavior of dipolar relaxation in unreacted and in fully cured resin were investigated in Figures 4.35 and 4.36, Arrhenius plots of τ_∞ and τ_o. The linearity of Figure 4.35 indicates that relaxation in fully cured resin is an activated process, which was expected [23]. The dipolar relaxation activation energy in fully cured TGDDM/DDS calculated from the data is 8.97 kcal/mole.

A similar trend was also expected, but not observed, in the uncured resin data of Figure 4.36. In the early stages of cure, τ is approximately equal to τ_o. Consequently, ε' is essentially constant and the dipolar contribution to ε'' is insignificant. The scatter in the fitted values of τ_o possibly results from the difficulty in obtaining parameters from data that is unaffected by dipolar relaxation.

4.4 Conclusions

The primary dielectric phenomena observed during the isothermal cure of thermosetting polymers, conduction of ionic impurities and relaxation of dipolar molecular segments, have been related to the polymerization kinetics. Complete representation of the dielectric properties of curing systems was modelled as a parallel arrangement of capacitive and resistive elements, allowing the individual contributions of conductivity and relaxation to be added in Equations 4.33 and 4.34.

This strategy was successfully applied to the model high performance epoxy/amine thermosetting resin, TGDDM cured with 25 phr DDS, isothermally cured over a wide temperature range and monitored dielectrically over a wide frequency range. The modelling approach incorporated independent experimental kinetic information obtained by differential scanning calorimetry, rather than kinetic model equations, for determining the model parameters. A method was also developed to account for electrode polarization effects in dielectric cure data.

The experimentally observed correlation between resistivity and polymerization rate was used to relate the contribution of ionic conductivity and the extent of reaction. The developed model equation, Equation 4.6, was shown to be valid for the model system. The activation

energy for ionic conduction in uncured resin was 15.33 kcal/mole.

Electrode polarization effects in the data were determined using a method specifically developed for curing systems, Equations 4.12 - 4.20. The equations were based on an analysis originally designed for polarization in nonreacting polar organic liquids. Although the parameters in the polarization equations are not material constants, the presence of polarization in individual dielectric experiments can be determined precisely. The polarization-free dielectric constant of uncured resin may be easily found, even from low frequency data.

The portion of the dielectric polymer cure properties arising from dipolar relaxation was described using a characteristic relaxation time in Equation 4.21. The complex plane behavior of nonreacting polymers provided the basis for interpreting the behavior of curing systems. The principles of kinetic viscoelasticity were applied in Equation 4.28 to link the dipolar relaxation time to reaction.

Of the two relaxation time distribution parameters, α' increased with temperature, while β' remained constant. The decrease in the entanglement parameter with temperature was explained by the increase in the glass transition temperature as the cure temperature increased. This trend

was predicted by expressing Φ in terms of the WLF equation parameters in Equation 4.32. Additional work is needed to fully characterize the physical significance of Φ.

The approach taken in this study allows dielectric spectroscopy to be used as a means of analyzing isothermally reacting polymer systems to obtain kinetic and physical property information.

Table 4.1

Isothermal conductivity/reaction parameters for TGDDM/DDS (25 phr)

Temperature (°C)	C_r	C_o	r2
140	-10.17	-14.21	0.999
150	-12.66	-13.57	0.996
160	-10.40	-13.32	0.994
170	-12.53	-12.83	1.000
180	-11.77	-12.35	0.998
190	-11.38	-12.35	0.999
200	-10.77	-11.70	0.997
210	-10.50	-11.40	0.995
220	-12.19	-9.90	0.993

Table 4.2

Electrode polarization parameters for isothermal dielectric experiments

Temperature (°C)	Z_o (ohms)	n
140	4.85×10^3	0.14
150	1.57×10^2	0.27
160	1.27×10^5	0.00
170	2.17×10^4	0.55
180	1.99×10^4	0.54
190	5.16×10^4	0.68
200	1.75×10^5	0.90
210	7.78×10^4	0.76

Table 4.3

Parameters describing the ε' frequency behavior of unreacted TGDDM/DDS (25 phr)

Temperature (°C)	C	D	r2
140	-1.07	26.85	0.998
150	-1.00	24.50	0.999
160	-0.85	23.78	0.999
170	-0.79	23.14	0.993
180	-0.77	22.68	0.999
190	-0.59	20.56	0.999
200	-0.65	18.80	0.999
210	-0.51	18.17	0.999

Table 4.4

Kinetic dipolar relaxation model parameters for isothermal cure of TGDDM/DDS (25 phr)

Temp. (°C)	τ_o (secs)	τ_∞ (secs)	α'	β'	Φ
140	3.18×10^{-9}	52.25	0.30	0.78	14.36
150	1.28×10^{-9}	34.34	0.35	0.74	18.33
160	8.11×10^{-10}	27.60	0.44	0.59	14.52
170	6.80×10^{-9}	13.88	0.46	0.61	14.06
180	1.38×10^{-8}	16.49	0.45	0.68	10.75
190	1.46×10^{-8}	15.93	0.40	0.81	9.74
200	1.03×10^{-8}	10.63	0.56	0.65	8.20
210	3.11×10^{-8}	10.16	0.52	0.74	6.82

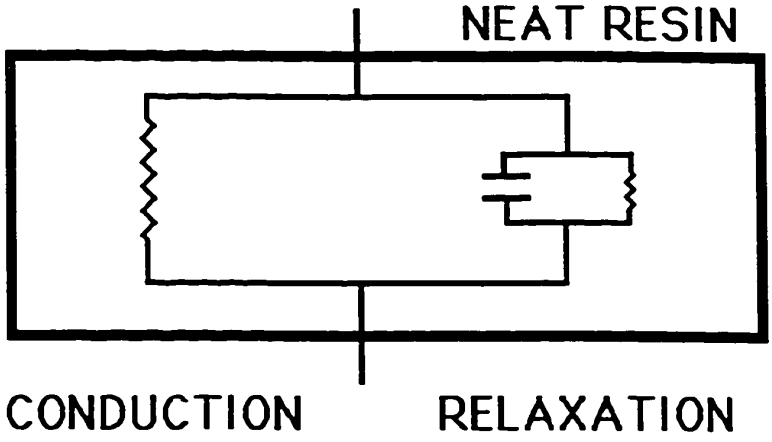

Figure 4.1 - Equivalent electric circuit representation of curing resin.

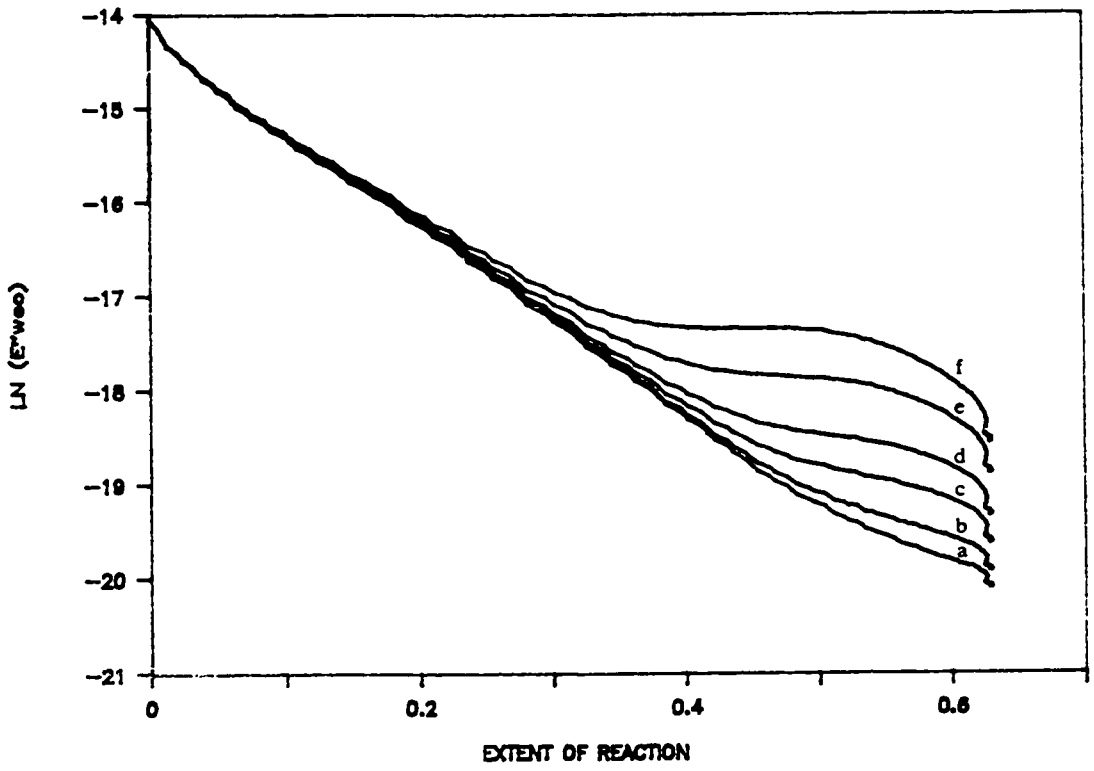

Figure 4.2 - Keinle-Race plot of TGDDM/DDS during isothermal cure at 140°C: a) 240 Hz, b) 1 KHz, c) 2 KHz, d) 4 KHz, e) 10 KHz, f) 20 KHz.

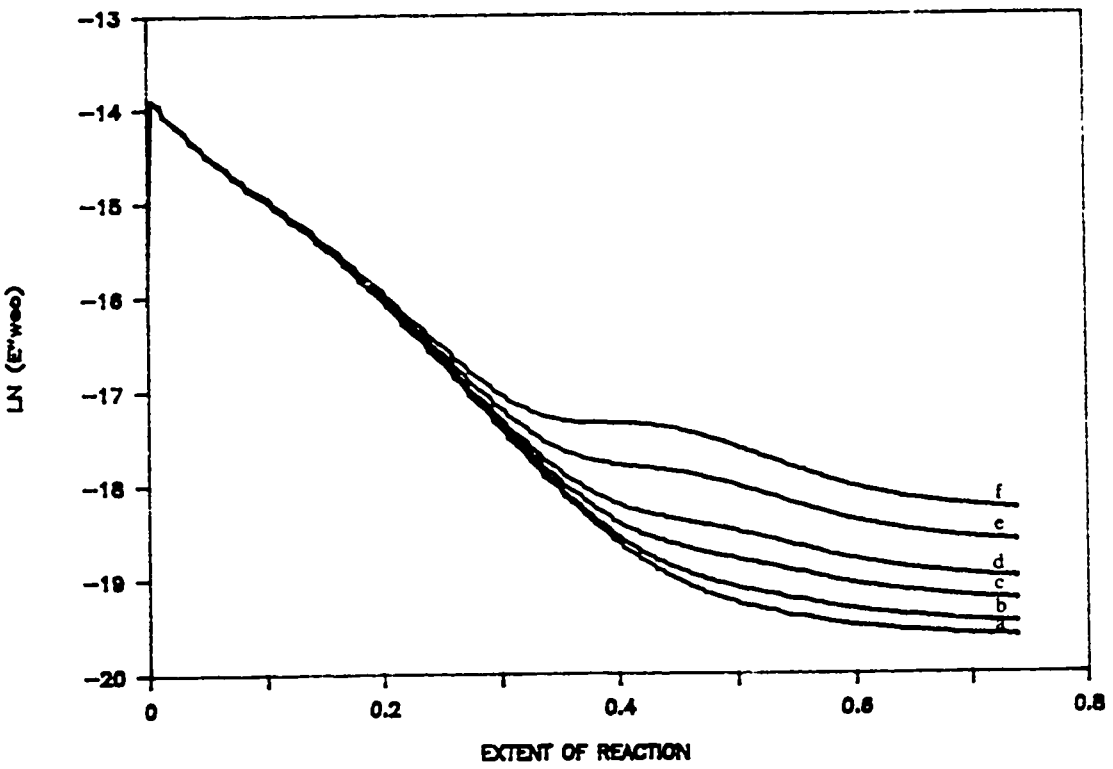

Figure 4.3 - Keinle-Race plot of TGDDM/DDS during isothermal cure at 150°C: a) 240 Hz, b) 1 KHz, c) 2 KHz, d) 4 KHz, e) 10 KHz, f) 20 KHz.

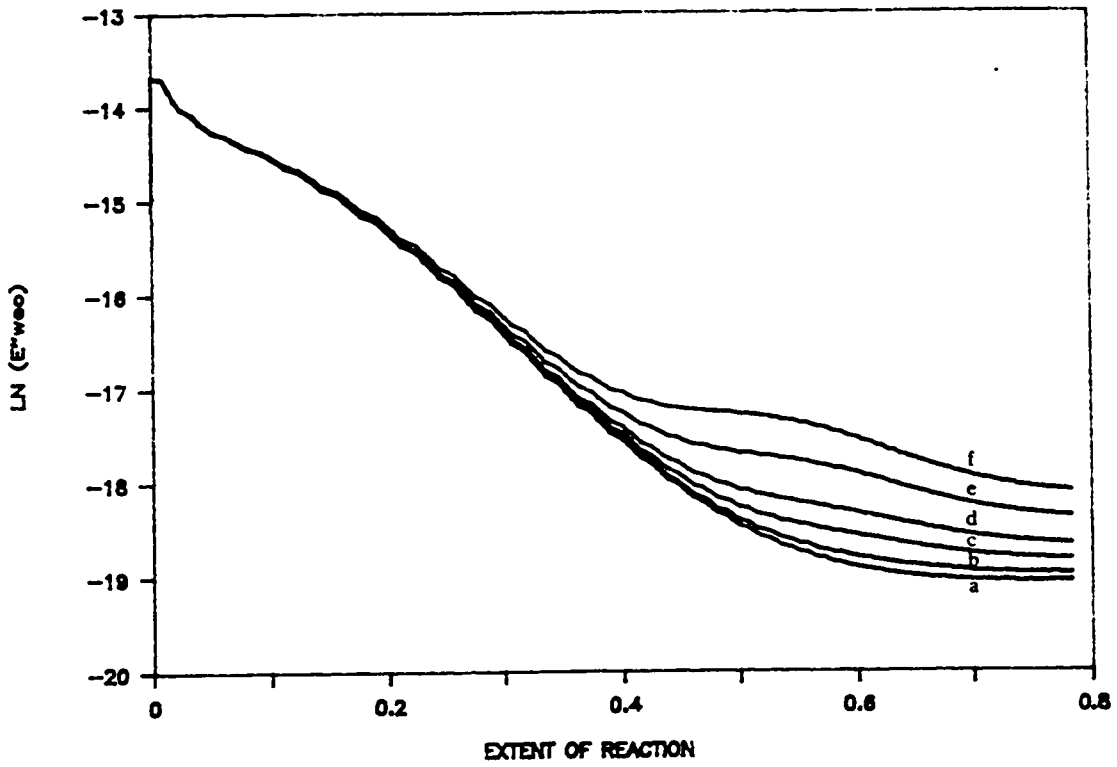

Figure 4.4 - Keinle-Race plot of TGDDM/DDS during isothermal cure at 160°C: a) 240 Hz, b) 1 KHz, c) 2 KHz, d) 4 KHz, e) 10 KHz, f) 20 KHz.

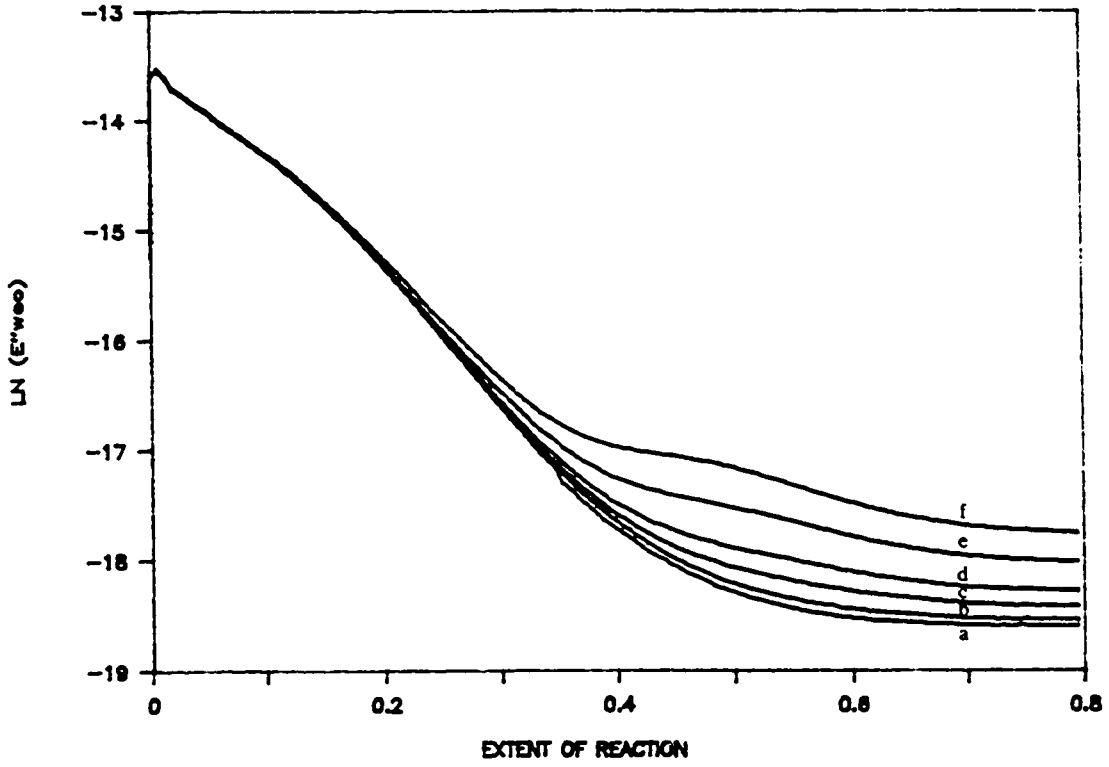

Figure 4.5 - Keinle-Race plot of TGDDM/DDS during isothermal cure at 170°C: a) 240 Hz, b) 1 KHz, c) 2 KHz, d) 4 KHz, e) 10 KHz, f) 20 KHz.

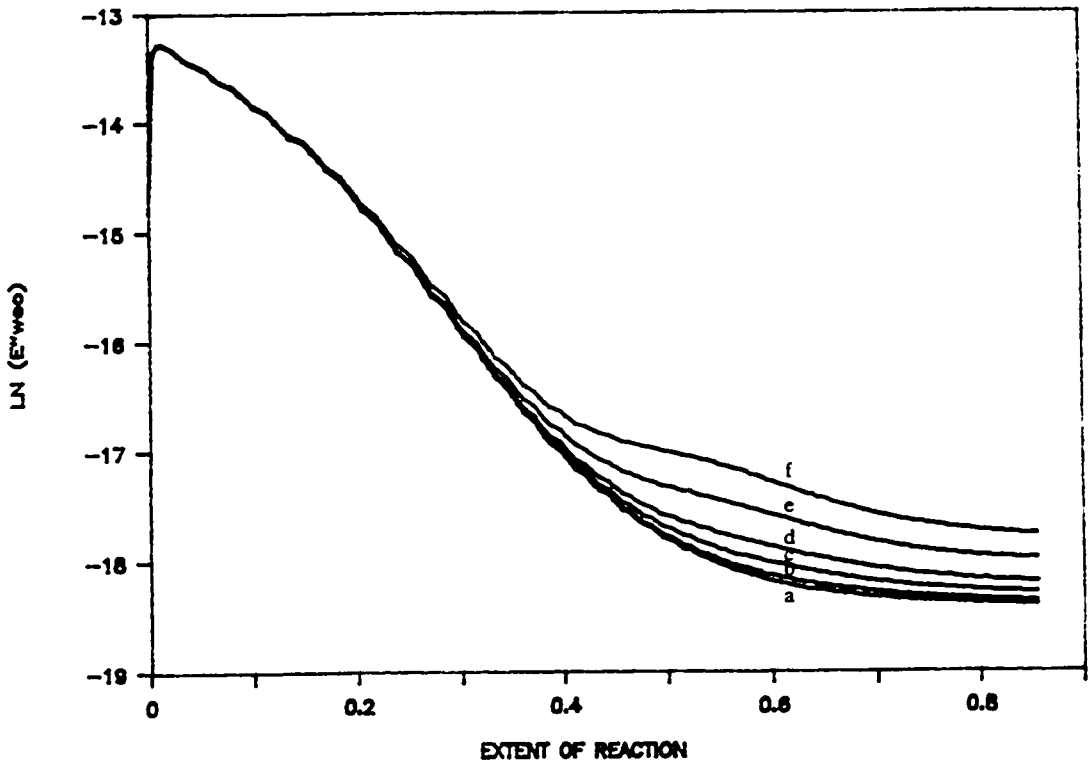

Figure 4.6 - Keinle-Race plot of TGDDM/DDS during isothermal cure at 180°C: a) 240 Hz, b) 1 KHz, c) 2 KHz, d) 4 KHz, e) 10 KHz, f) 20 KHz.

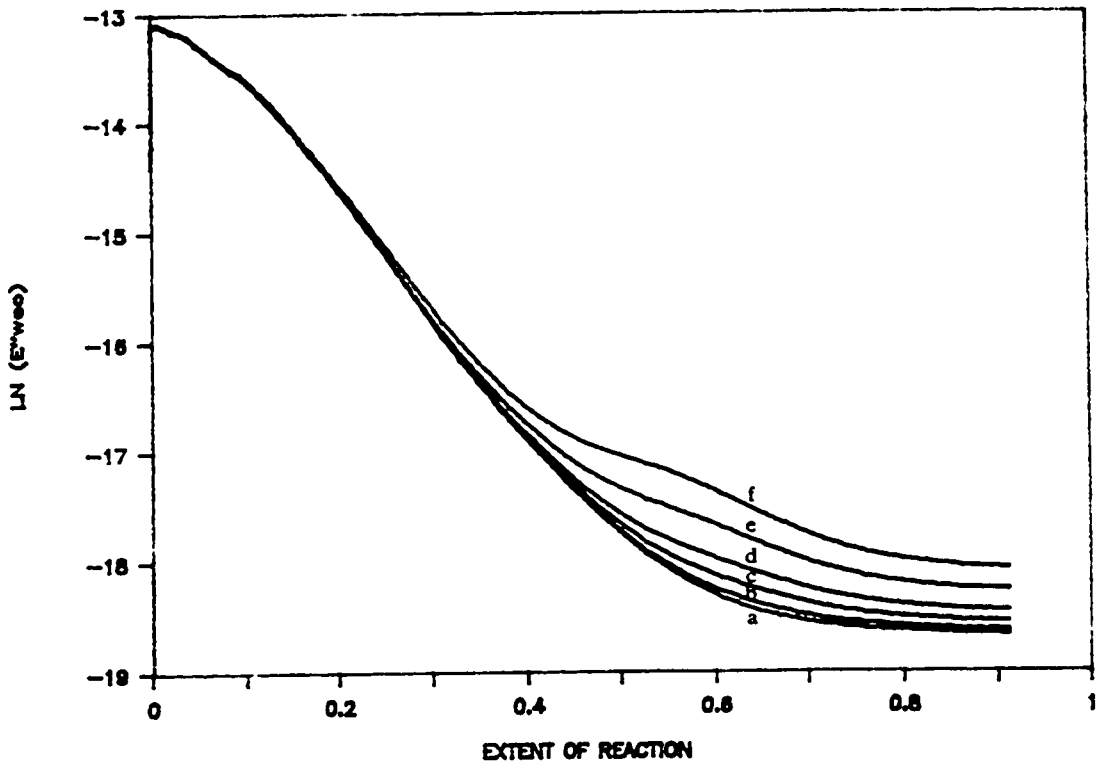

Figure 4.7 - Keinle-Race plot of TGDDM/DDS during isothermal cure at 190°C: a) 240 Hz, b) 1 KHz, c) 2 KHz, d) 4 KHz, e) 10 KHz, f) 20 KHz.

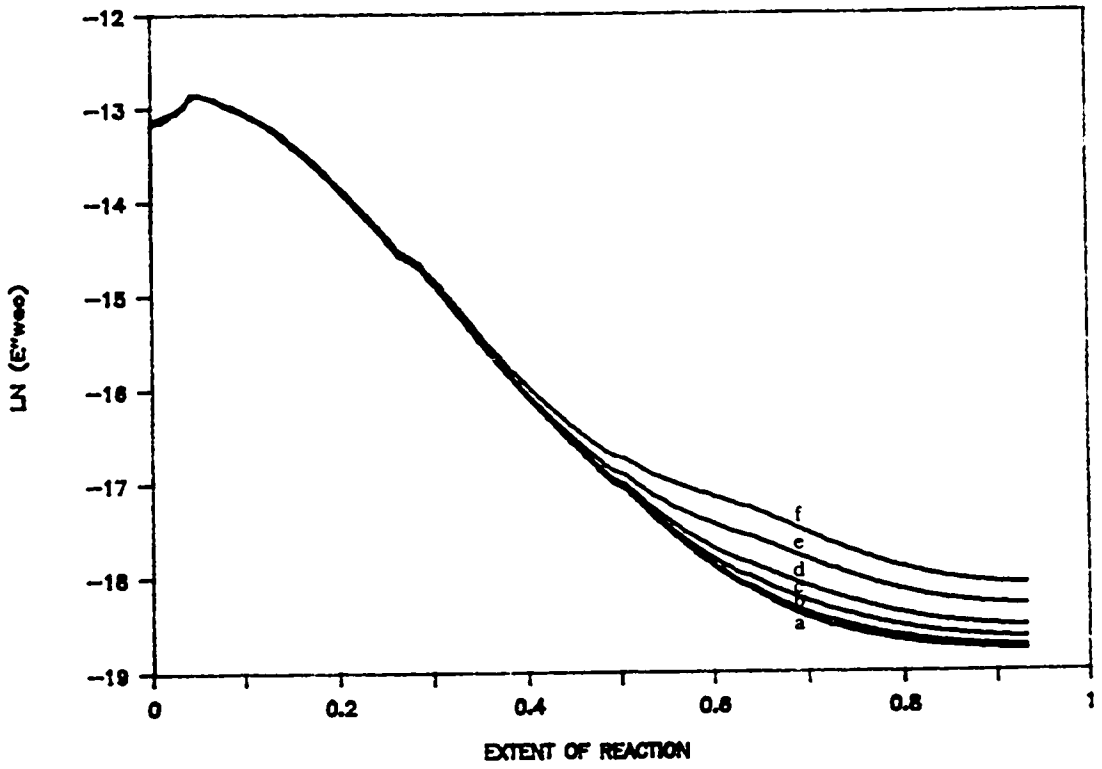

Figure 4.8 - Keinle-Race plot of TGDDM/DDS during isothermal cure at 200°C: a) 240 Hz, b) 1 KHz, c) 2 KHz, d) 4 KHz, e) 10 KHz, f) 20 KHz.

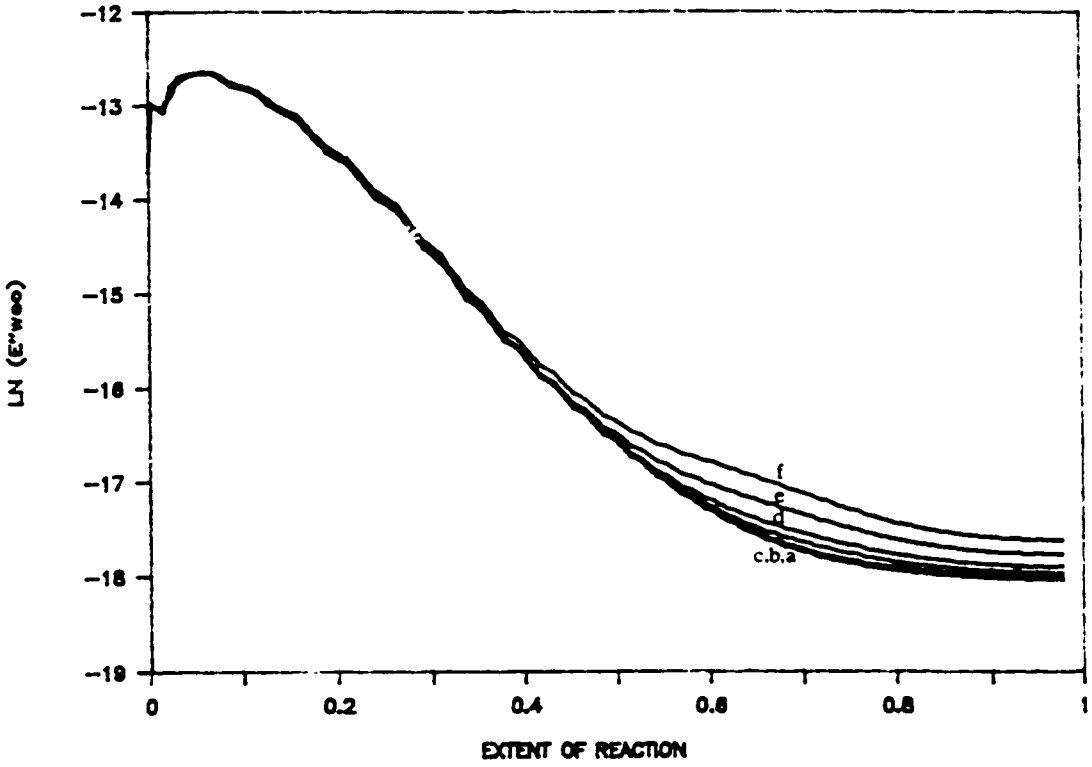

Figure 4.9 - Keinle-Race plot of TGDDM/DDS during isothermal cure at 210°C: a) 240 Hz, b) 1 KHz, c) 2 KHz, d) 4 KHz, e) 10 KHz, f) 20 KHz.

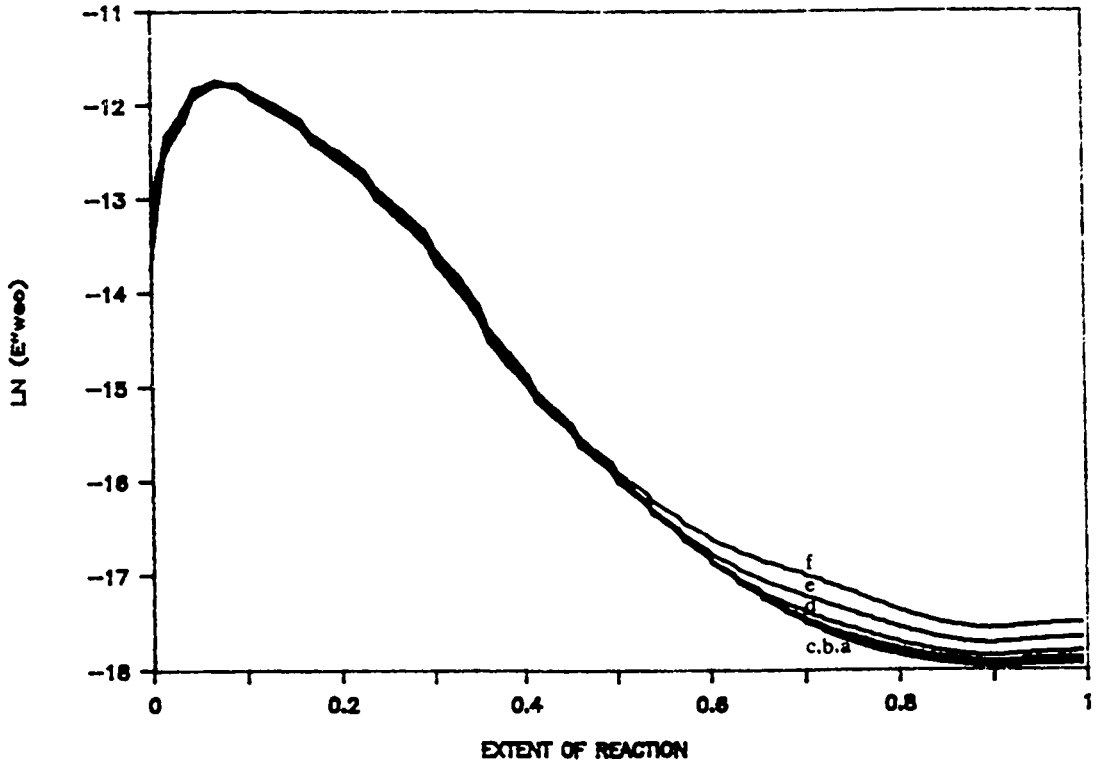

Figure 4.10 - Keinle-Race plot of TGDDM/DDS during isothermal cure at 220°C: a) 240 Hz, b) 1 KHz, c) 2 KHz, d) 4 KHz, e) 10 KHz, f) 20 KHz.

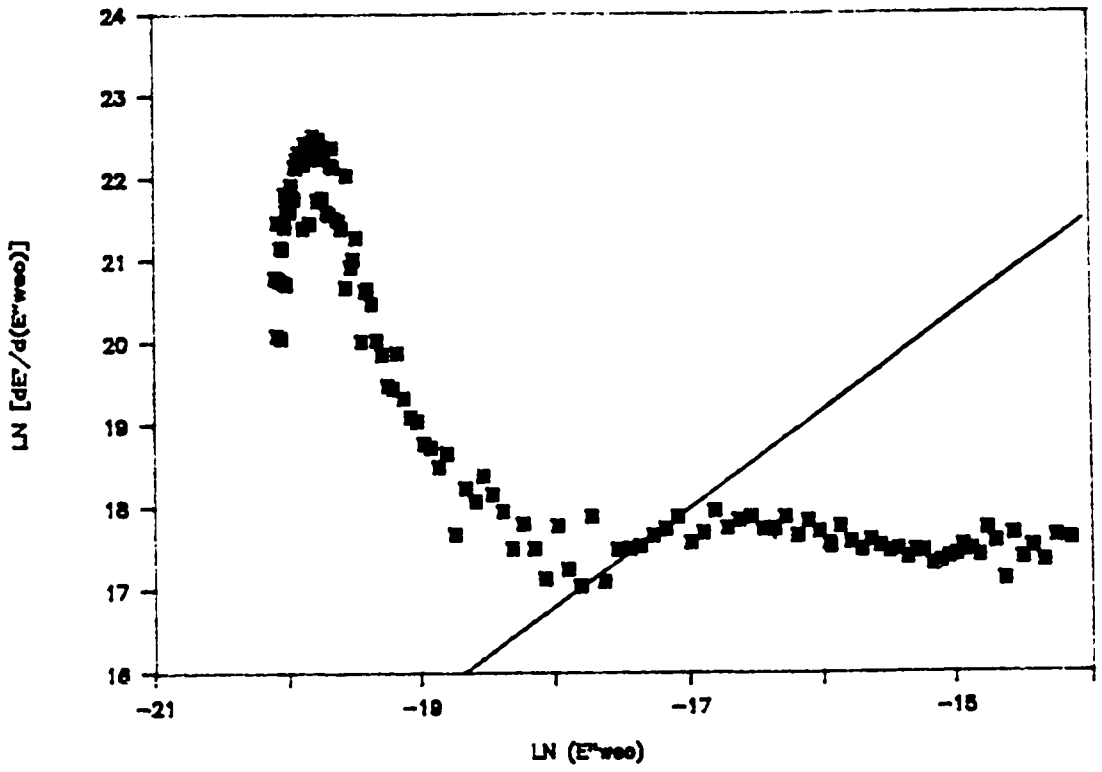

Figure 4.11 - Conductivity/ε' data at 140°C plotted according to Equation 4.20 for determining polarization regression region, slope of linear portion = 1.02.

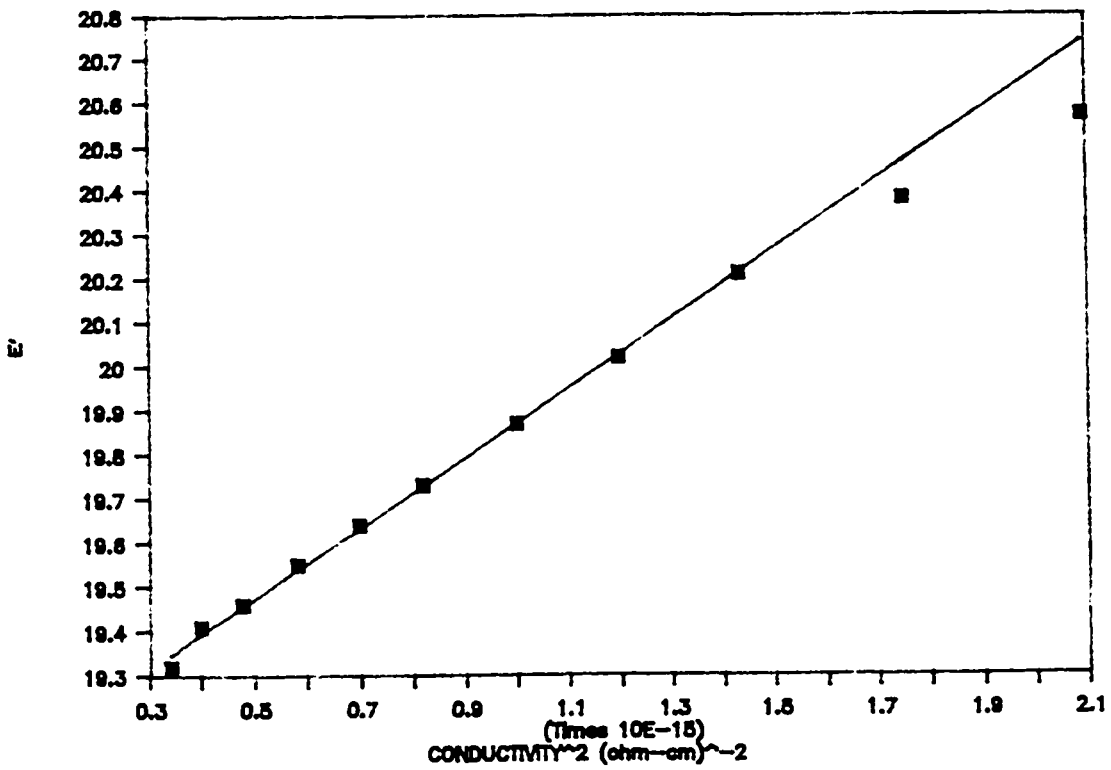

Figure 4.12 - Conductivity/ε' data at 140°C in linear region of Figure 4.11, plotted according to Equation 4.12 to determine electrode polarization parameters.

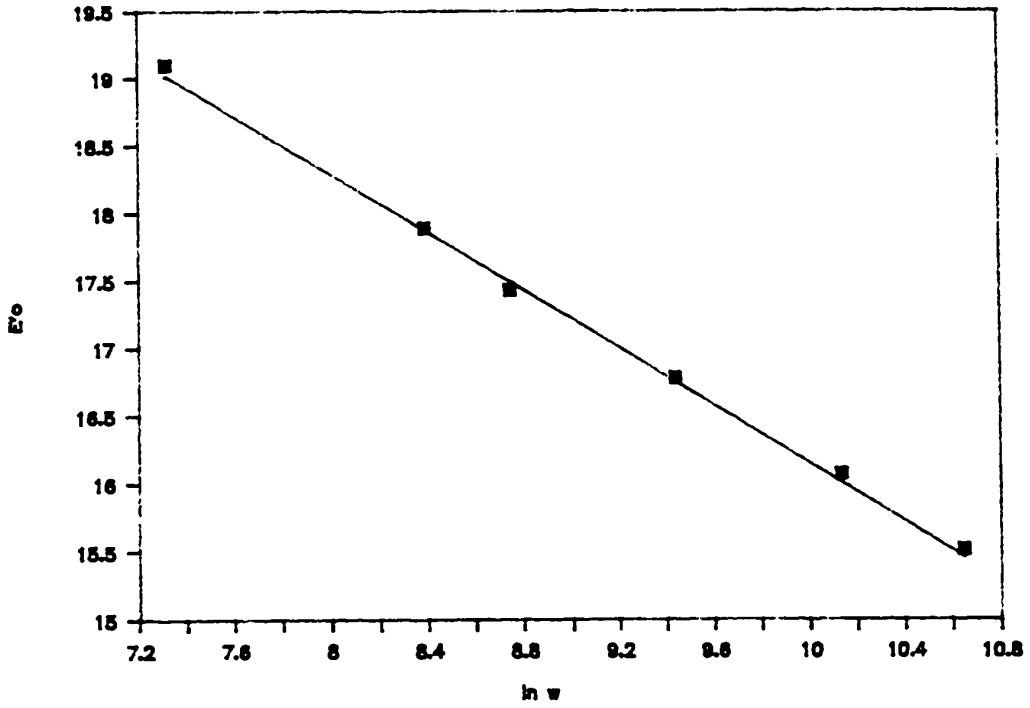

Figure 4.13 - Frequency dependence of ε' of uncured TGDDM/DDS at 140°C.

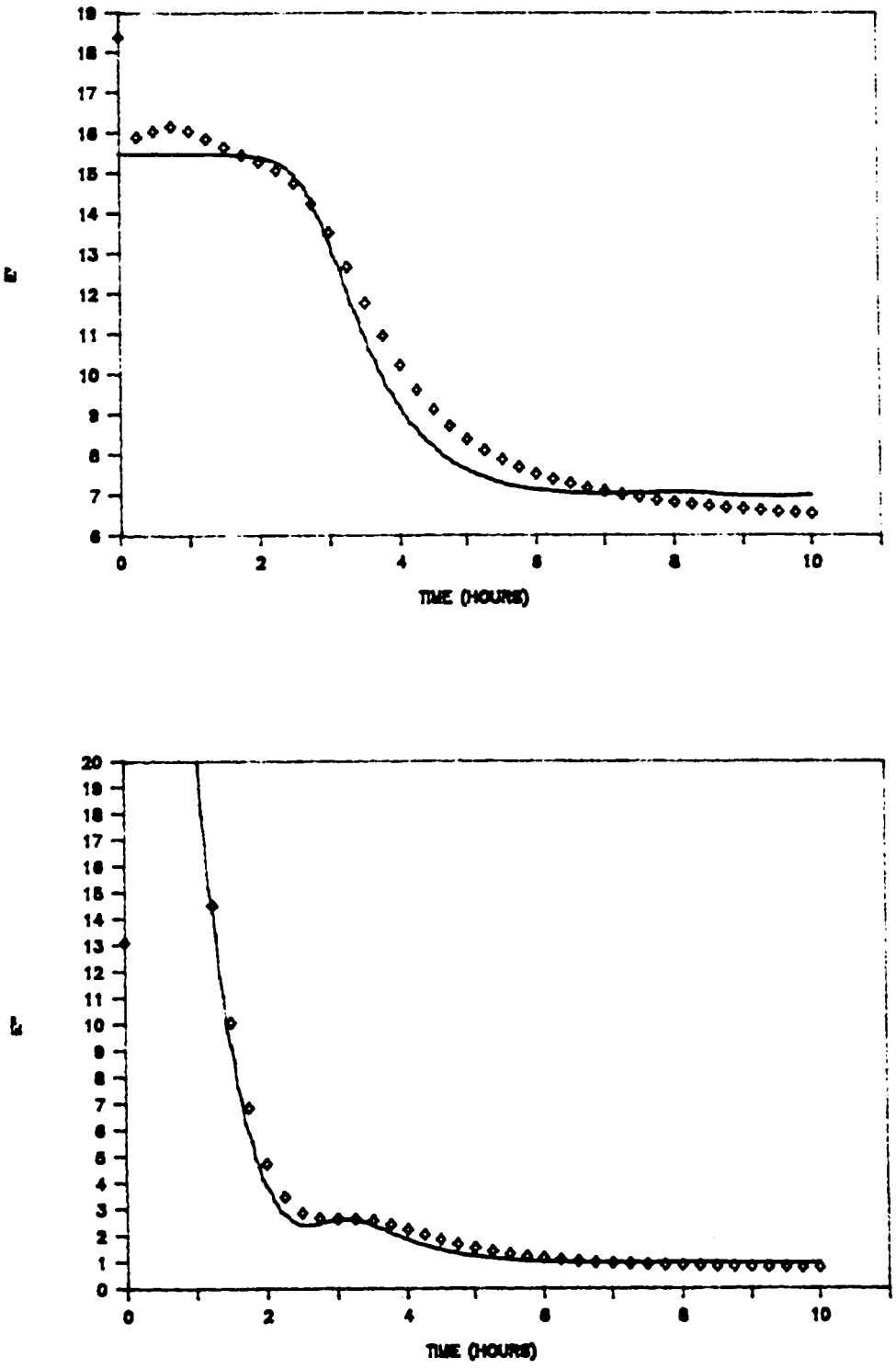

Figure 4.14 - Comparison of combined dielectric model (—) and experimental data at (♦) 20 KHz during isothermal cure of TGDDM/DDS at 140°C.

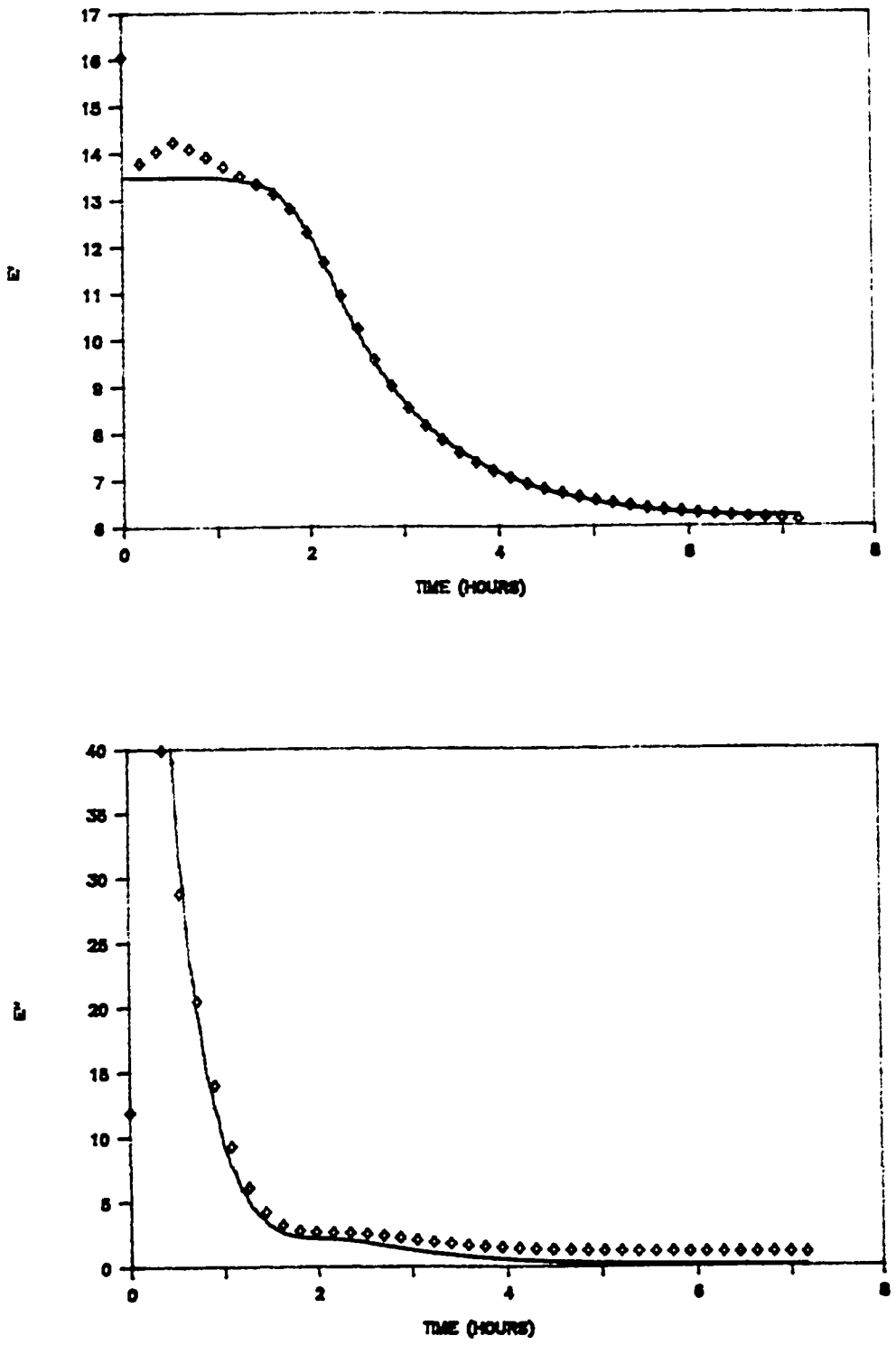

Figure 4.15 - Comparison of combined dielectric model (—) and experimental data at (♦) 20 KHz during isothermal cure of TGDDM/DDS at 150°C.

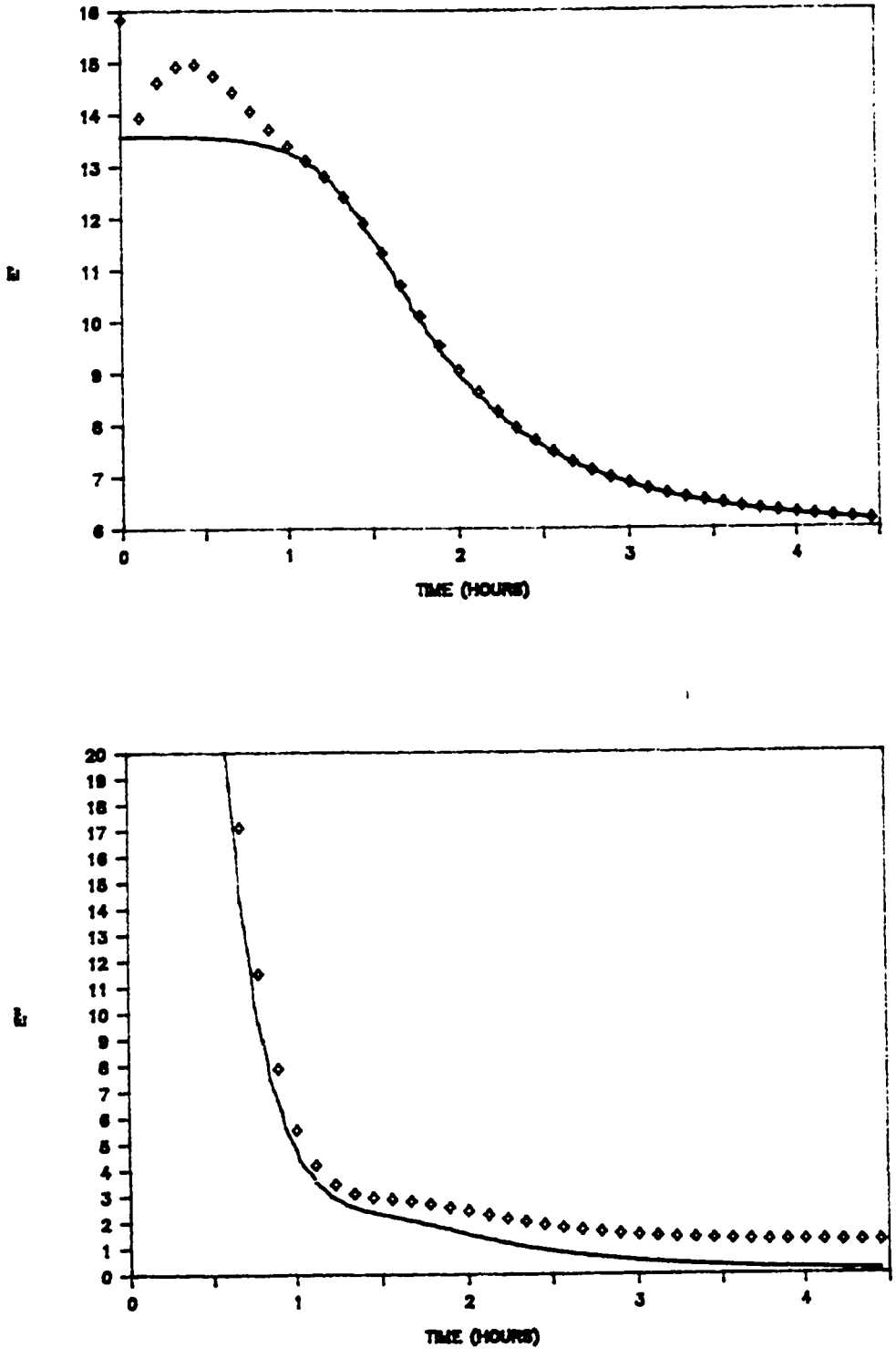

Figure 4.16 - Comparison of combined dielectric model (—) and experimental data at (♦) 20 KHz during isothermal cure of TGDDM/DDS at 160°C.

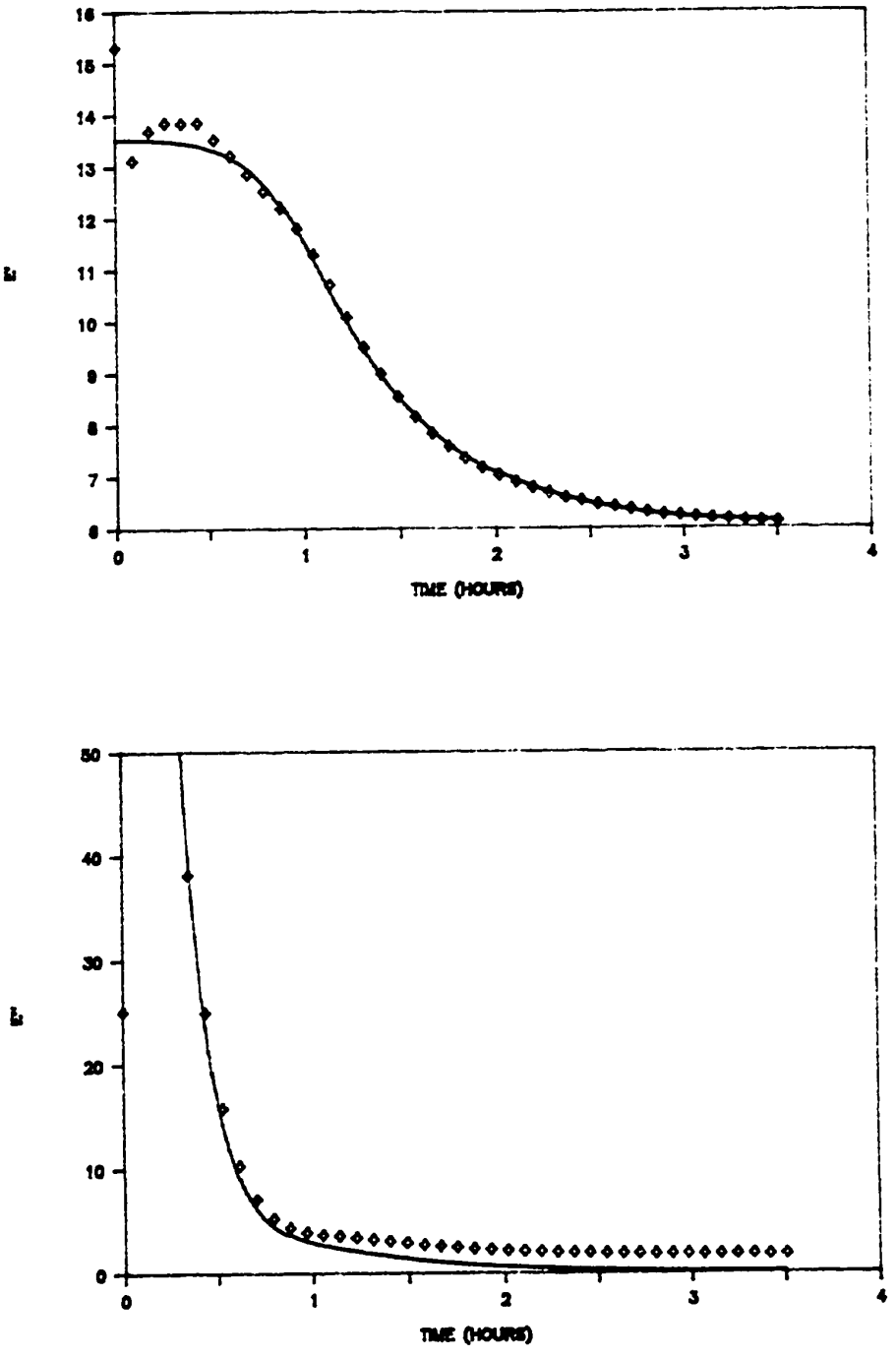

Figure 4.17 - Comparison of combined dielectric model (—) and experimental data at (♦) 20 KHz during isothermal cure of TGDDM/DDS at 170°C.

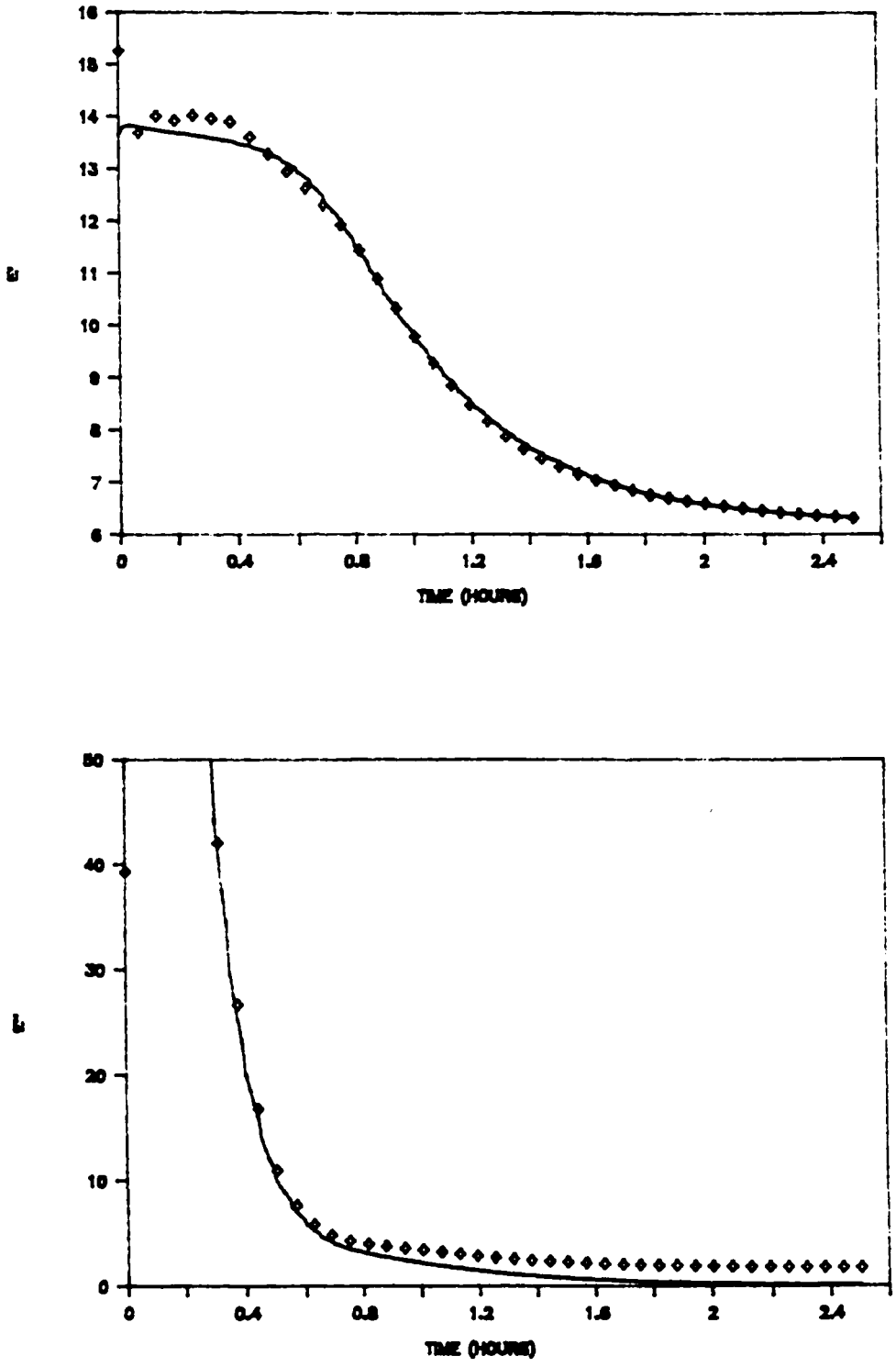

Figure 4.18 - Comparison of combined dielectric model (—) and experimental data at (♦) 20 KHz during isothermal cure of TGDDM/DDS at 180°C.

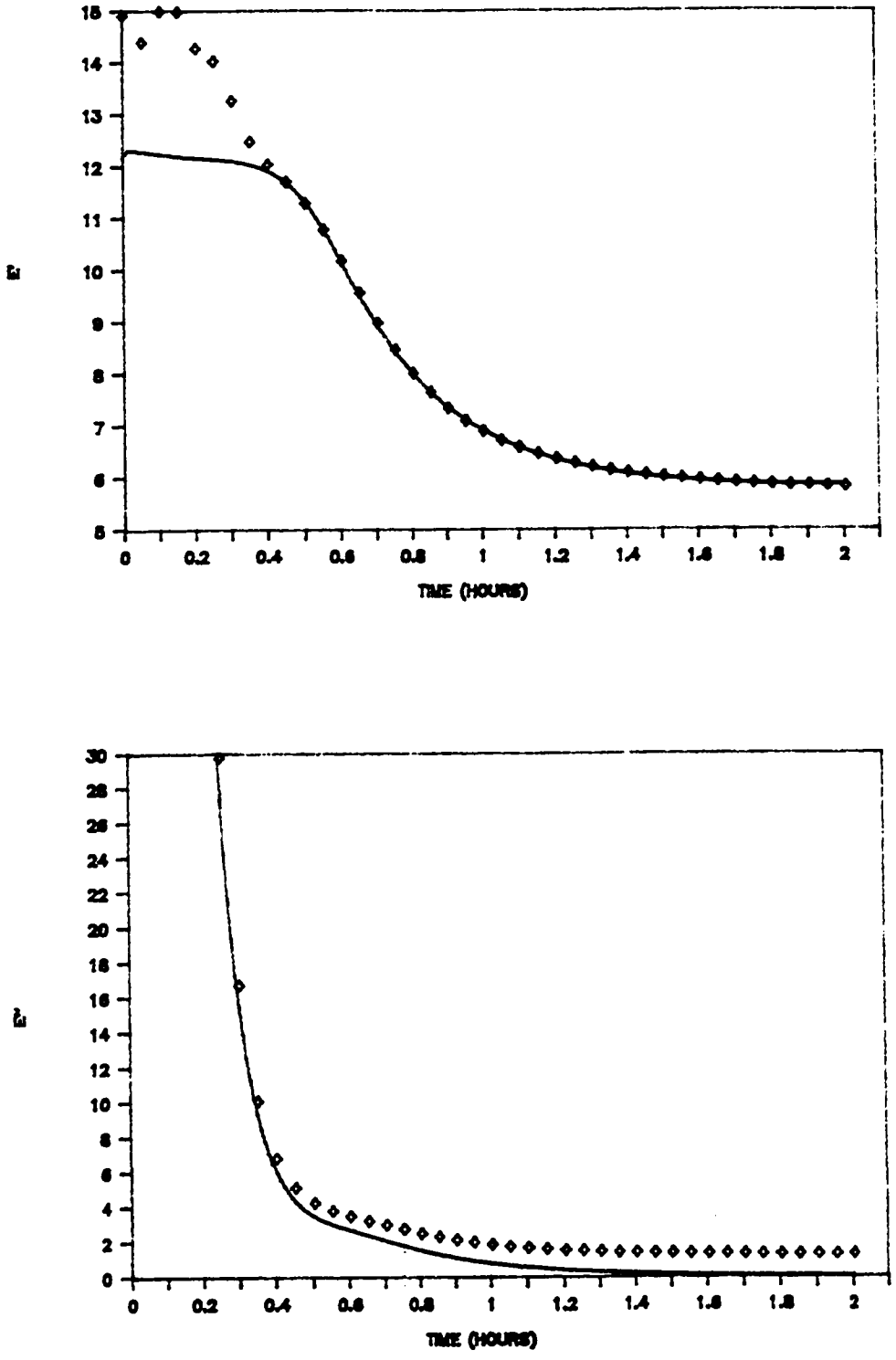

Figure 4.19 - Comparison of combined dielectric model (—) and experimental data at (♦) 20 KHz during isothermal cure of TGDDM/DDS at 190°C.

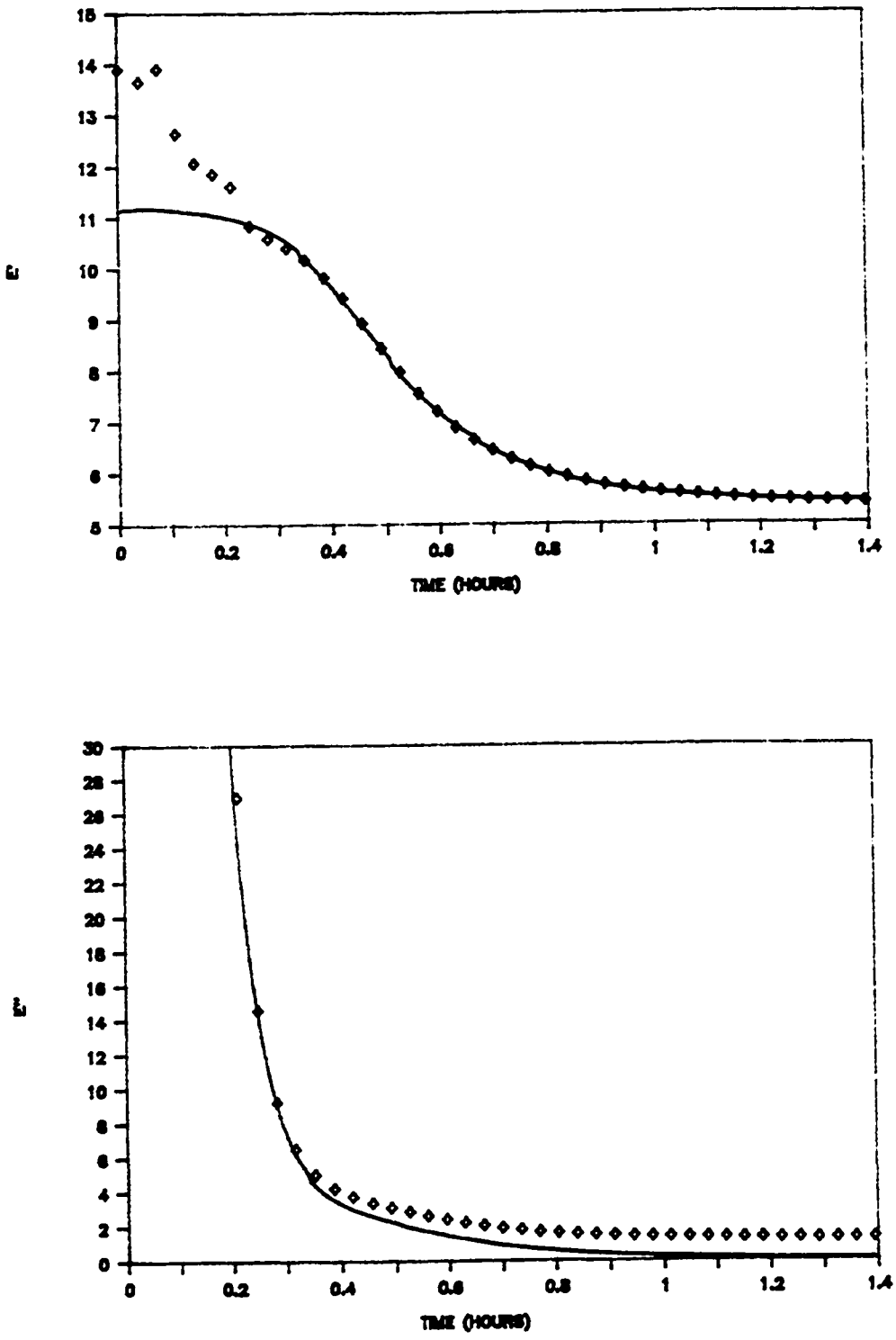

Figure 4.20 - Comparison of combined dielectric model (—) and experimental data at (♦) 20 KHz during isothermal cure of TGDDM/DDS at 200°C.

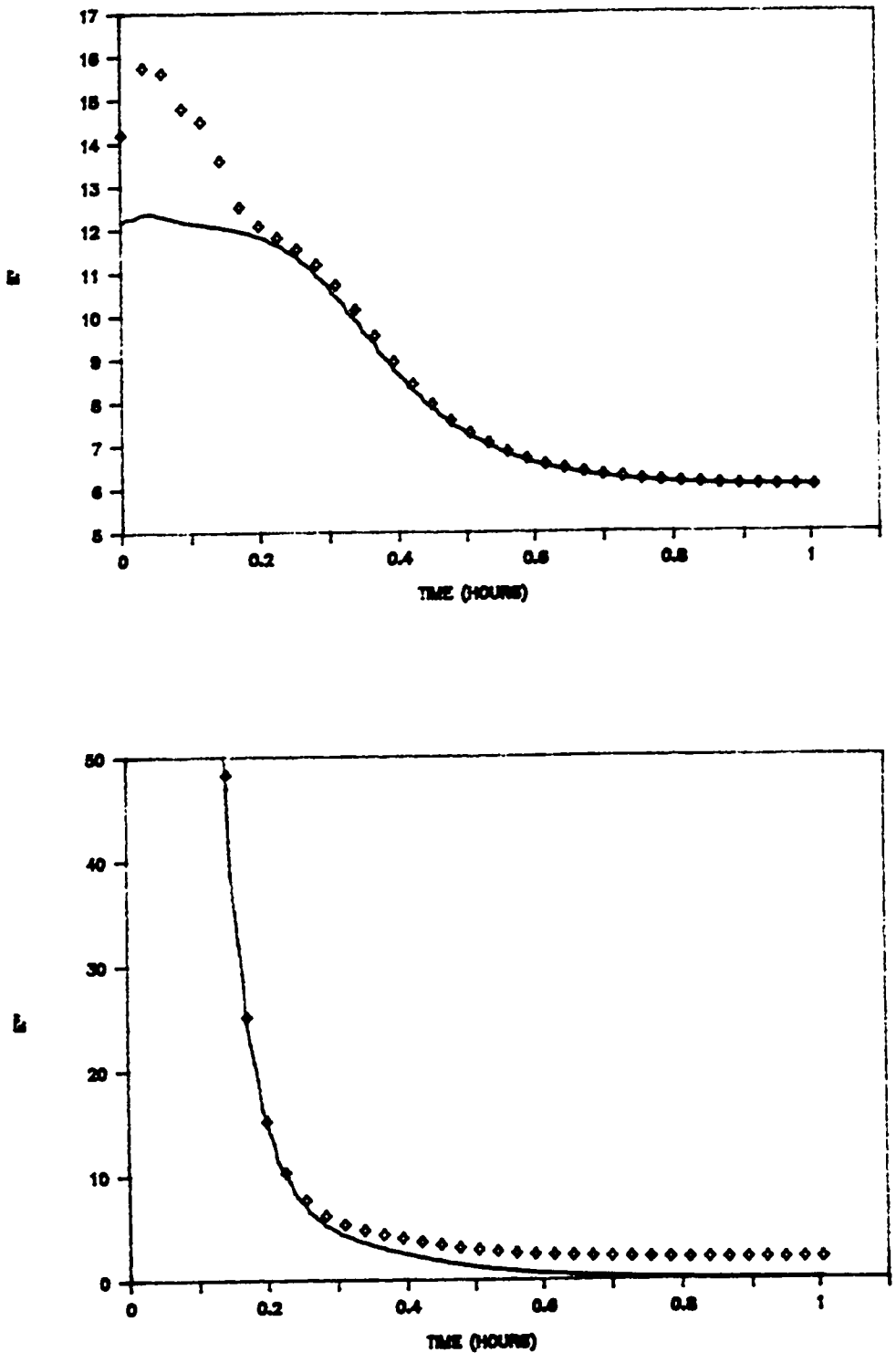

Figure 4.21 - Comparison of combined dielectric model (—) and experimental data at (♦) 20 KHz during isothermal cure of TGDDM/DDS at 210°C.

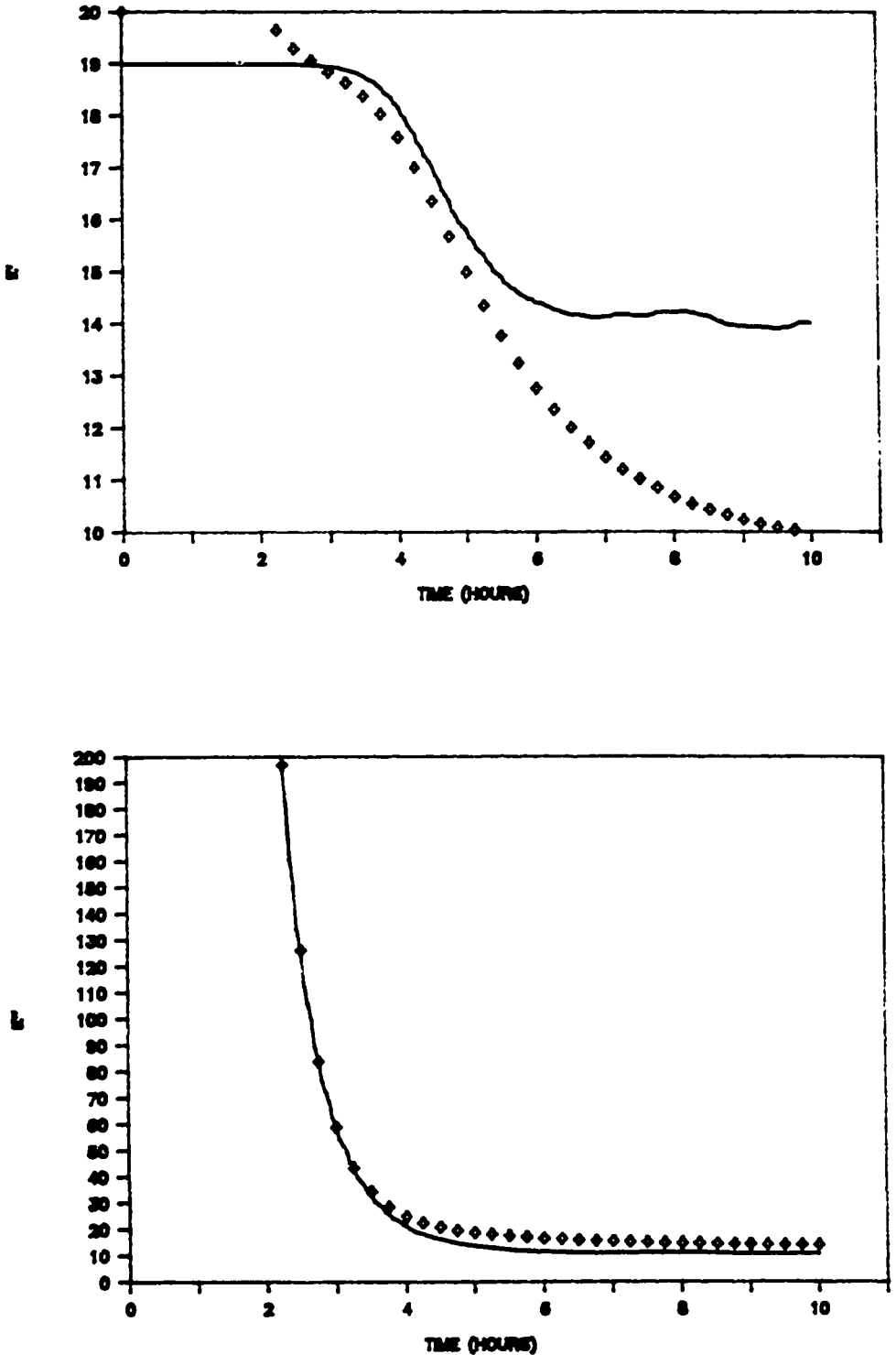

Figure 4.22 - Prediction of dielectric properties (—) of TGDDM/DDS at 240 Hz during isothermal cure at 140°C, experimental data (♦).

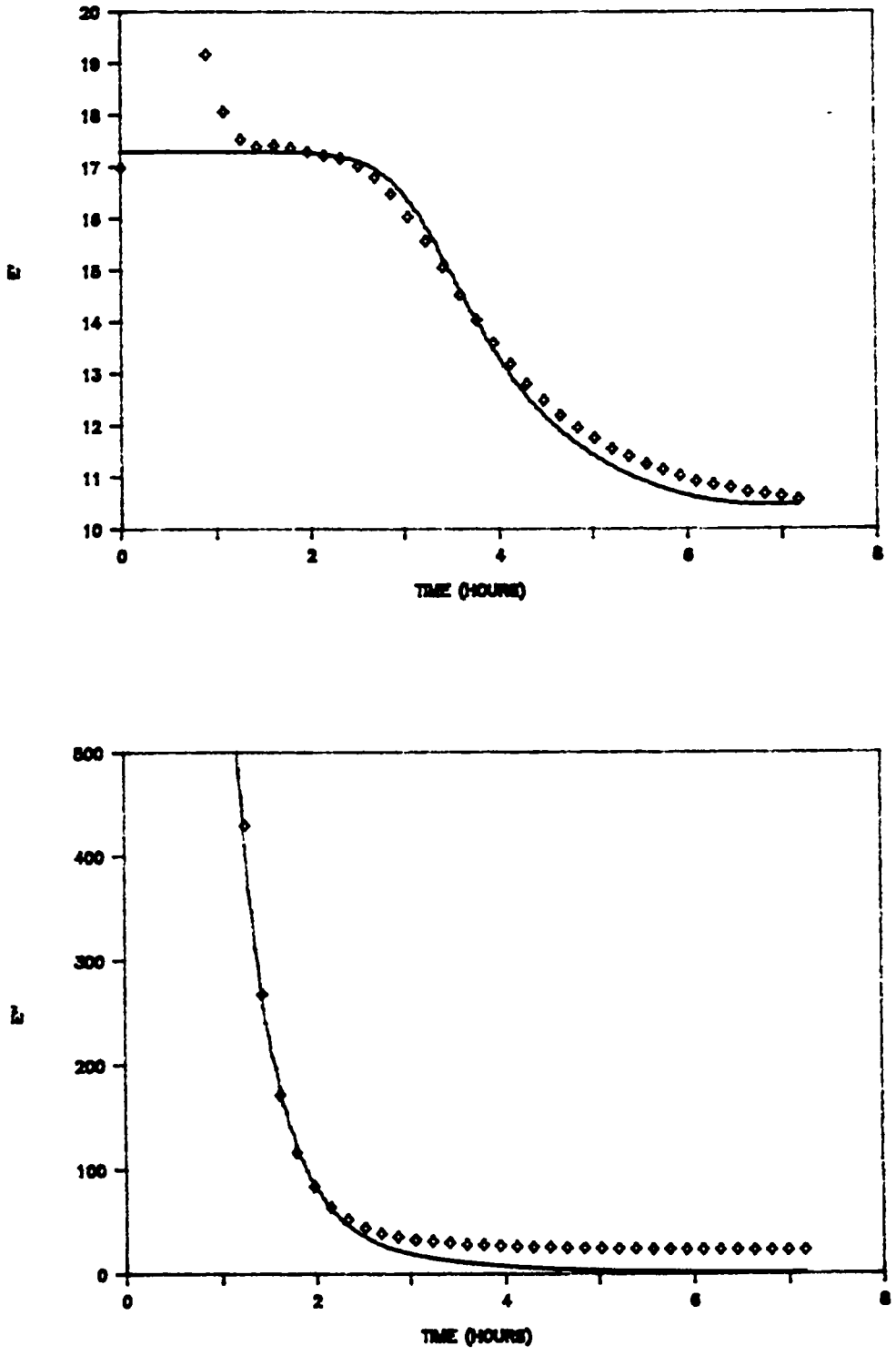

Figure 4.23 - Prediction of dielectric properties (—) of TGDDM/DDS at 240 Hz during isothermal cure at 150°C, experimental data (♦).

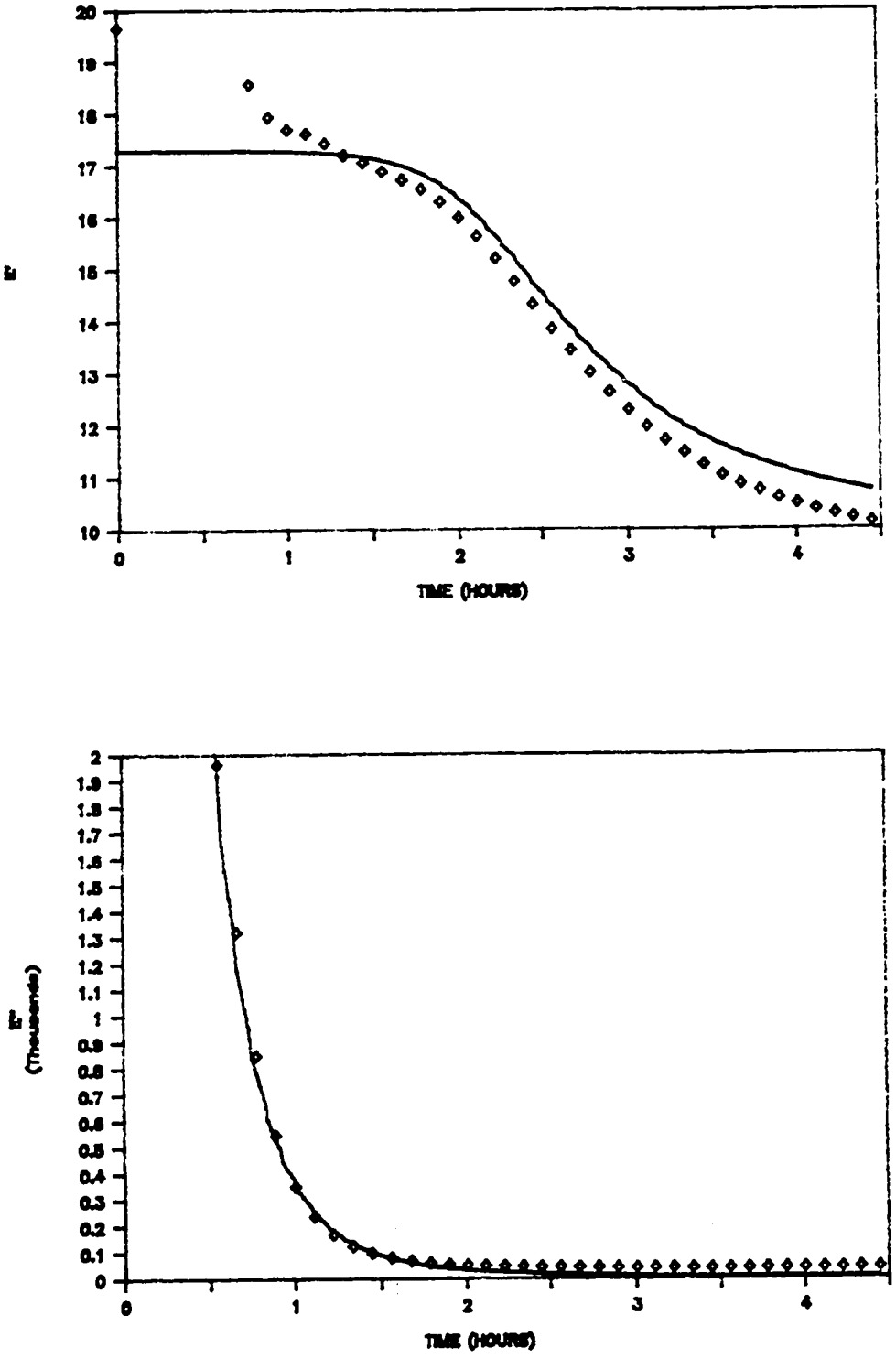

Figure 4.24 - Prediction of dielectric properties (—) of TGDDM/DDS at 240 Hz during isothermal cure at 160°C, experimental data (♦).

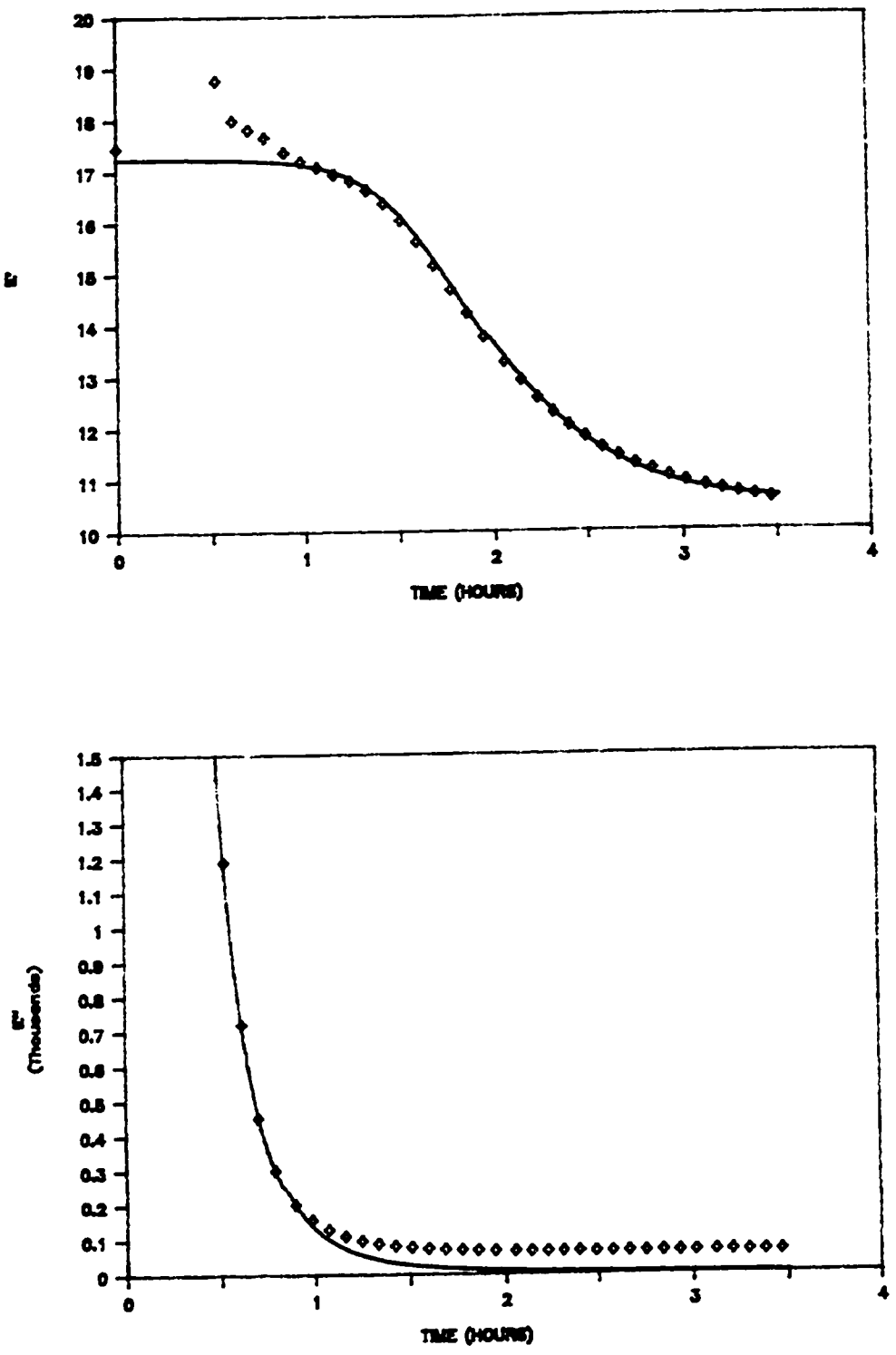

Figure 4.25 - Prediction of dielectric properties (—) of TGDDM/DDS at 240 Hz during isothermal cure at 170°C, experimental data (♦).

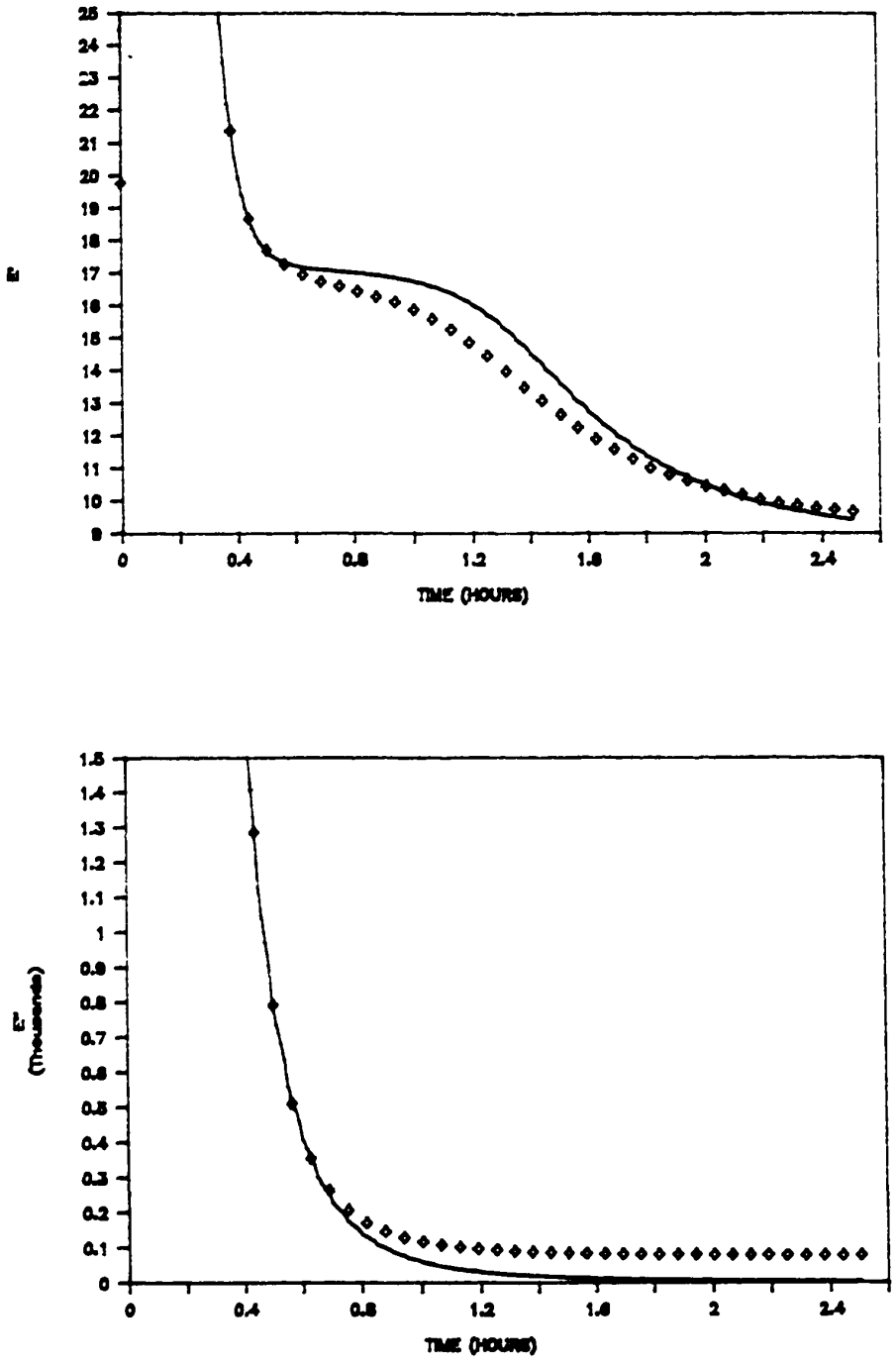

Figure 4.26 - Prediction of dielectric properties (—) of TGDDM/DDS at 240 Hz during isothermal cure at 180°C, experimental data (♦).

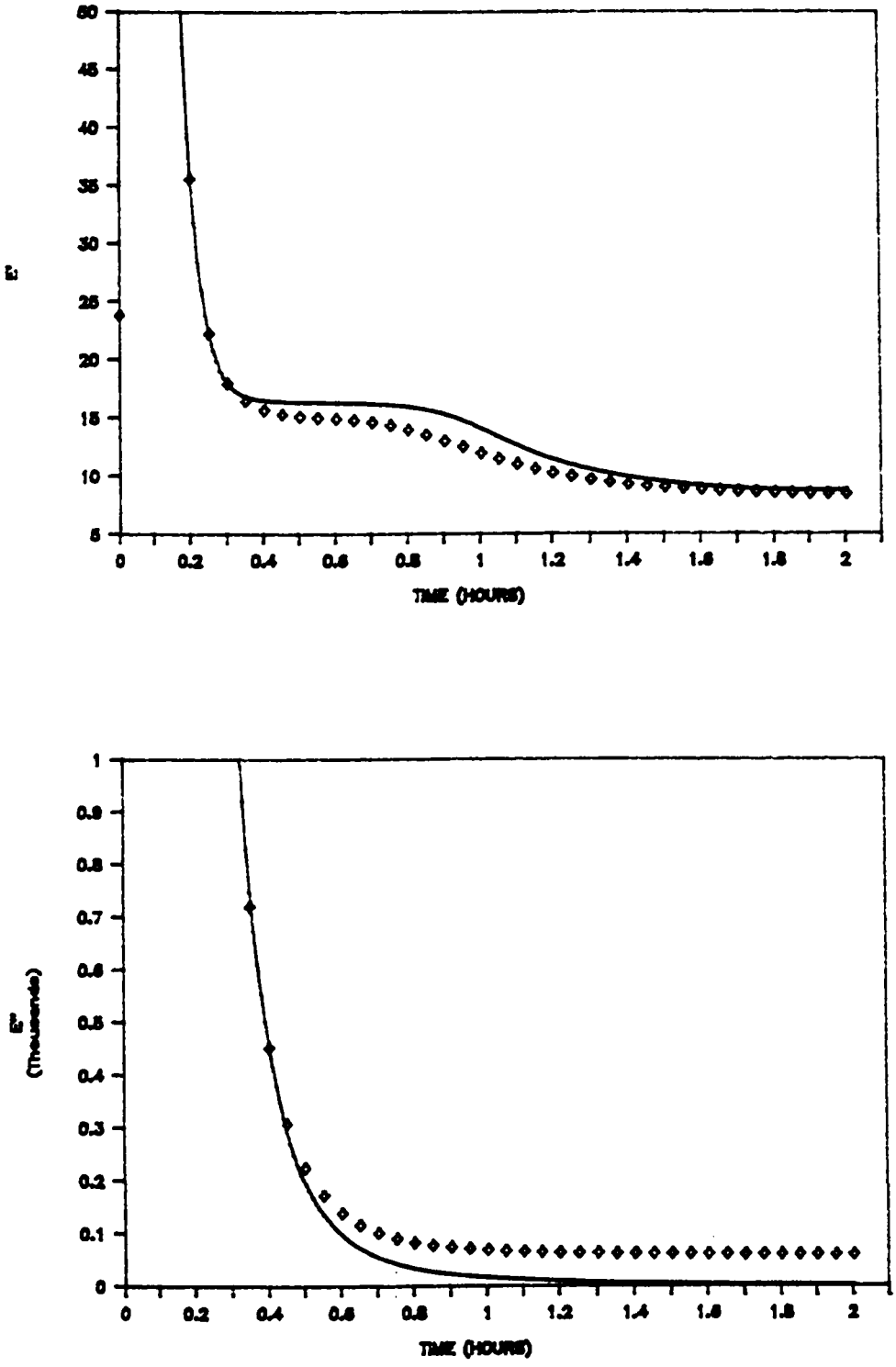

Figure 4.27 - Prediction of dielectric properties (—) of TGDDM/DDS at 240 Hz during isothermal cure at 190°C, experimental data (♦).

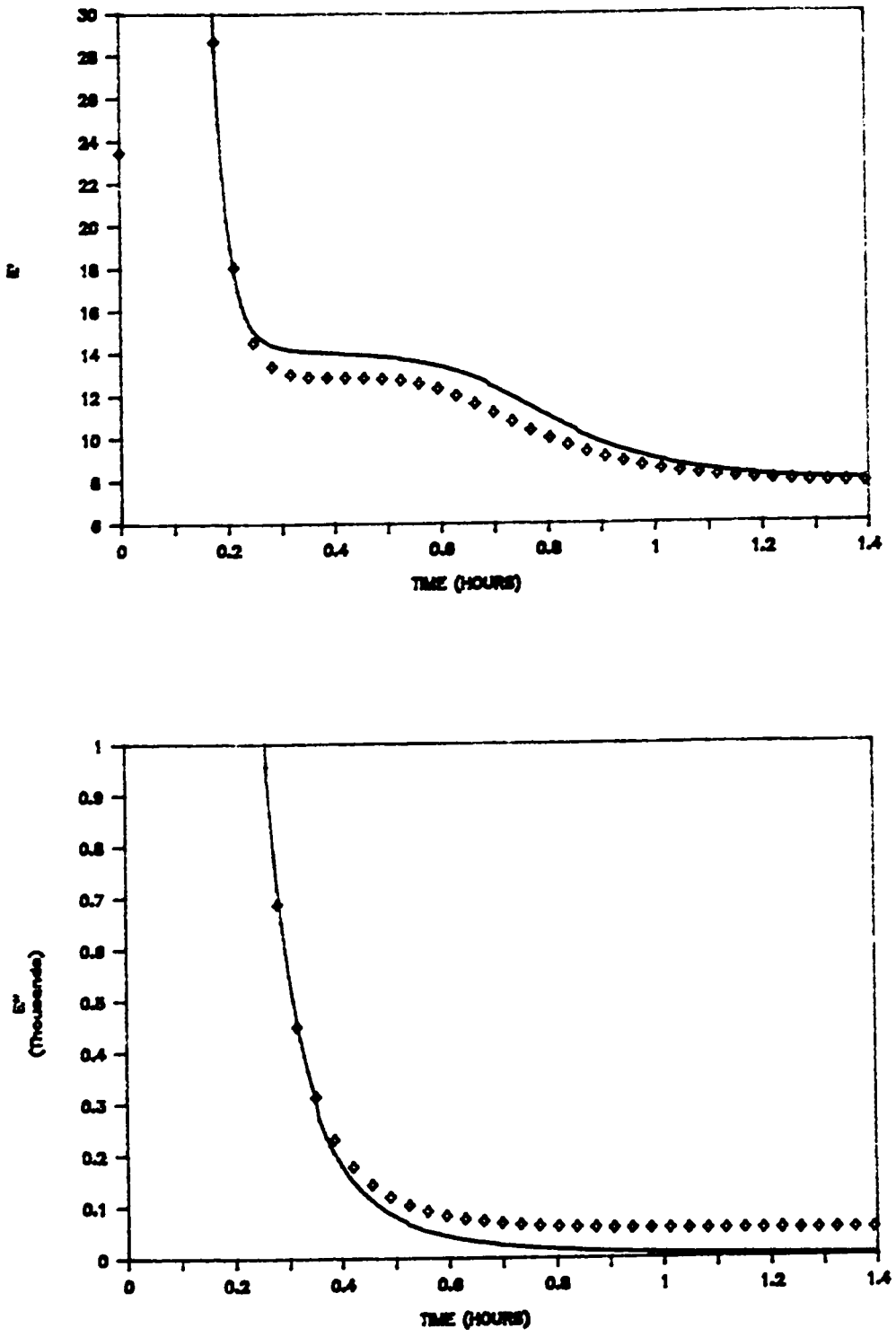

Figure 4.28 - Prediction of dielectric properties (—) of TGDDM/DDS at 240 Hz during isothermal cure at 200°C, experimental data (♦).

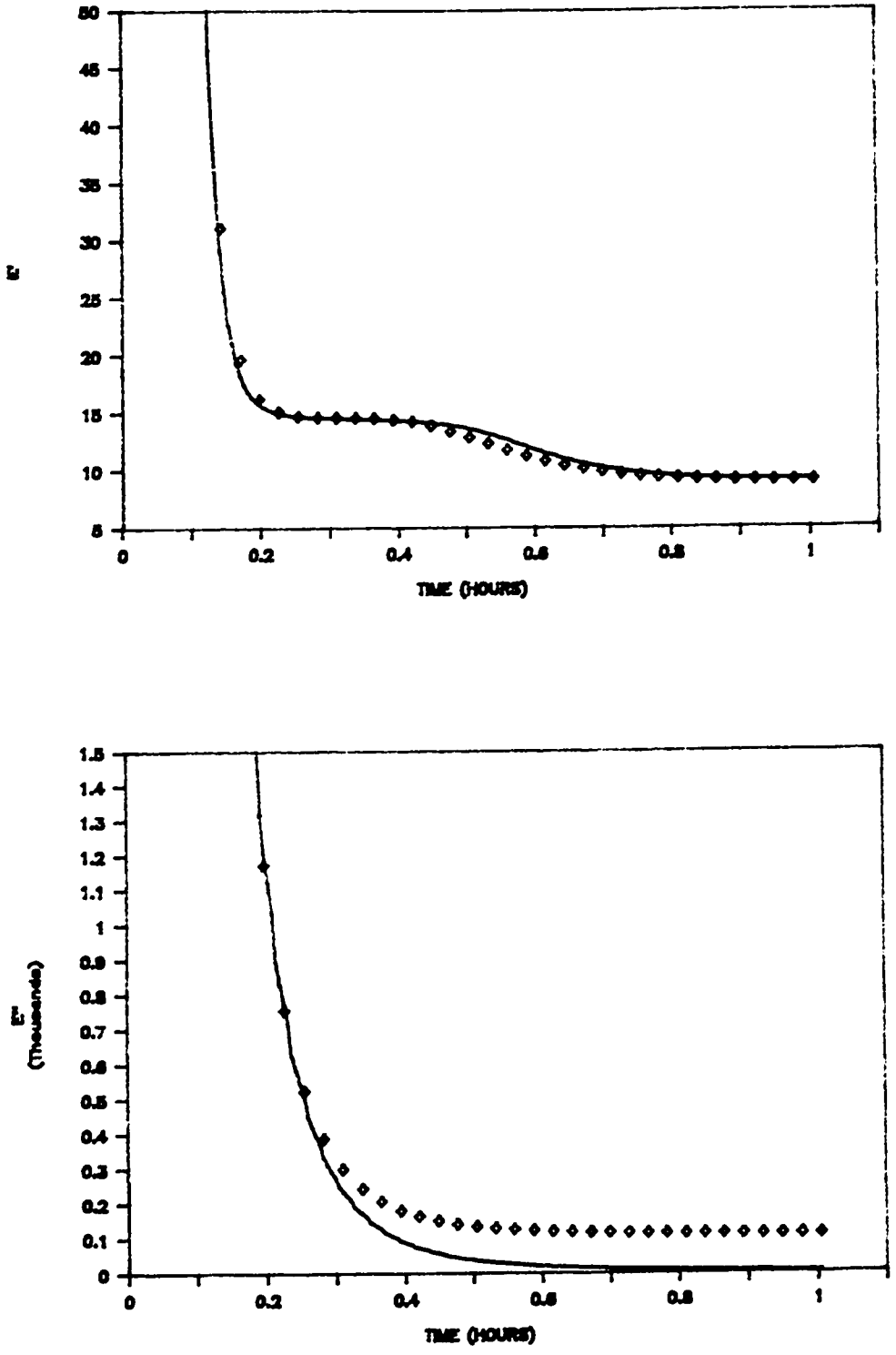

Figure 4.29 - Prediction of dielectric properties (—) of TGDDM/DDS at 240 Hz during isothermal cure at 210°C, experimental data (♦).

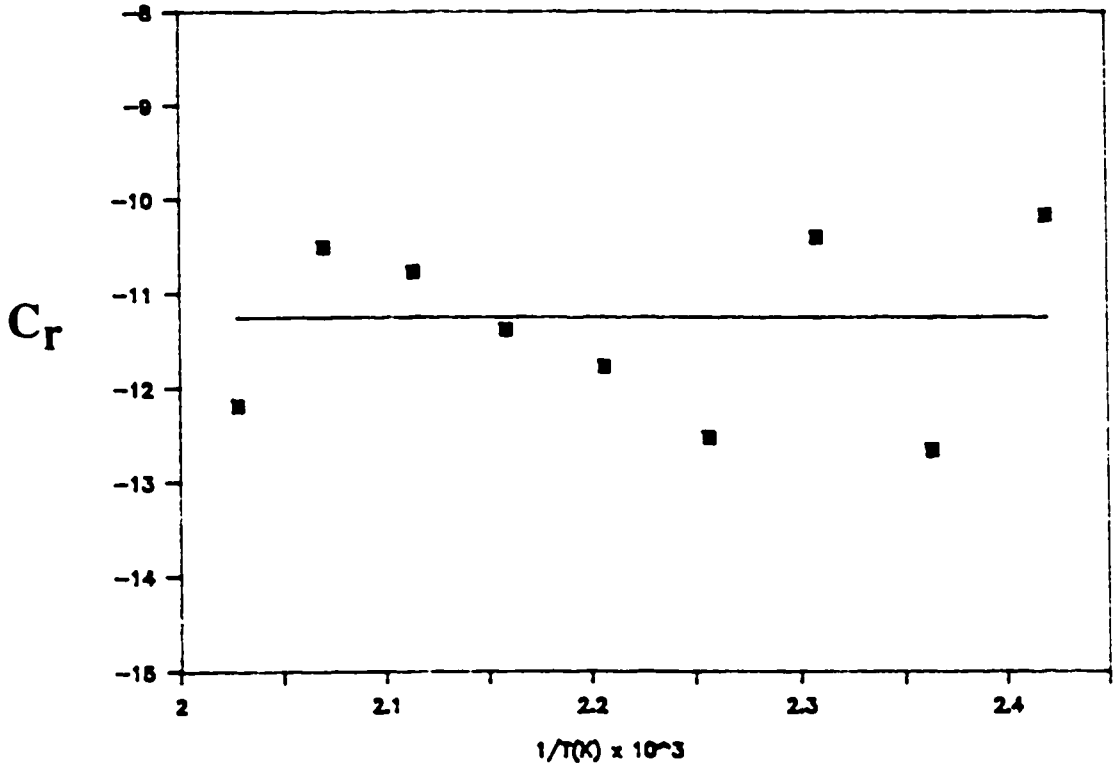

Figurc 4.30 - Temperature dependence of conduction parameter C_r, average value = -11.27.

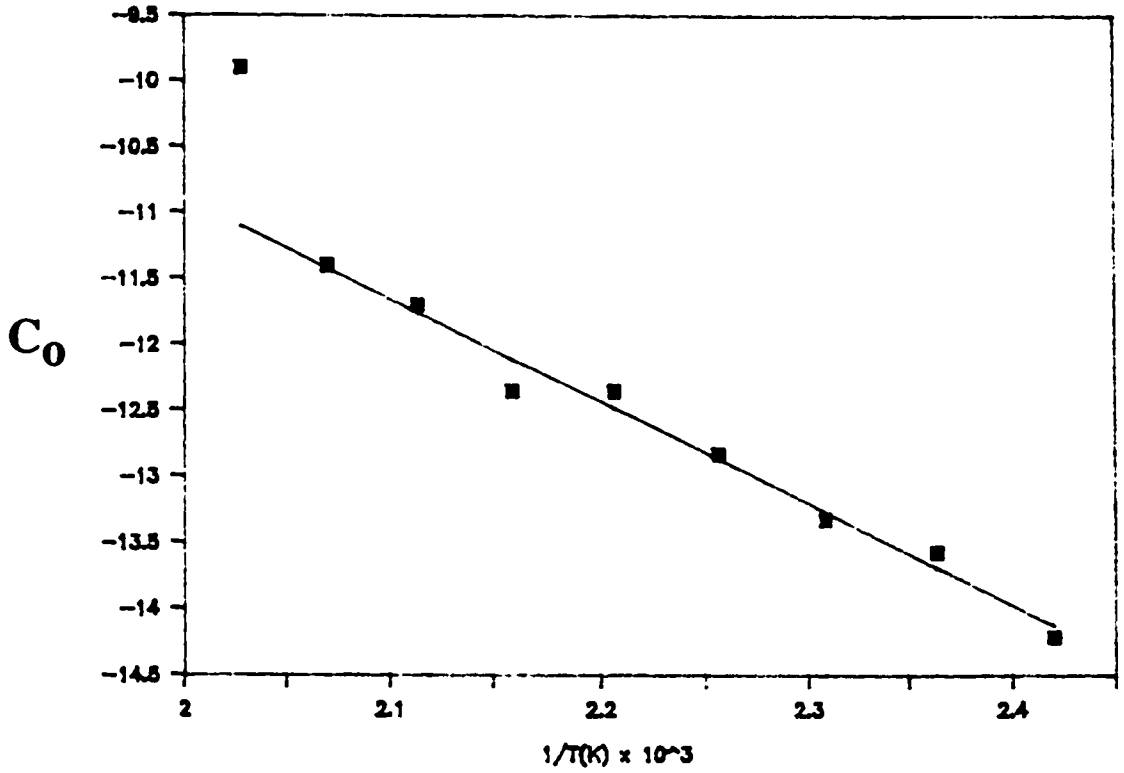

Figure 4.31 - Temperature dependence of conduction parameter C_o, activation energy of conduction in uncured resin = 15.33 kcal/mole.

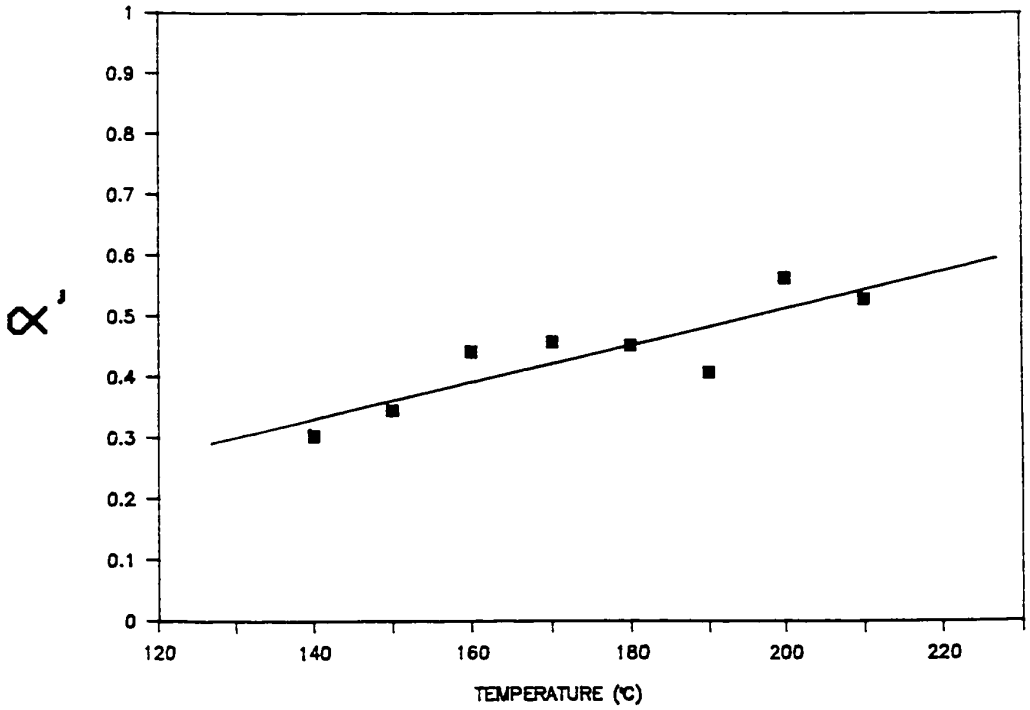

Figure 4.32 - Temperature dependence of α' dispersion parameter.

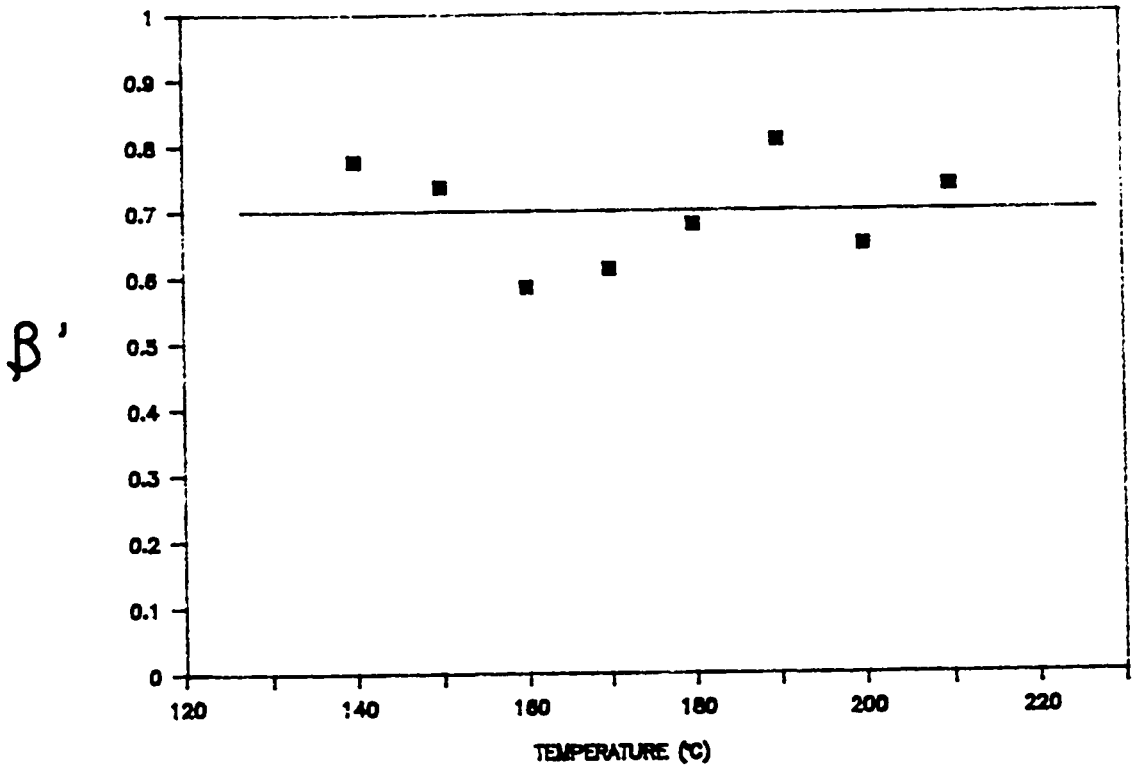

Figure 4.33 - Temperature dependence of β' dispersion parameter, average value = 0.7.

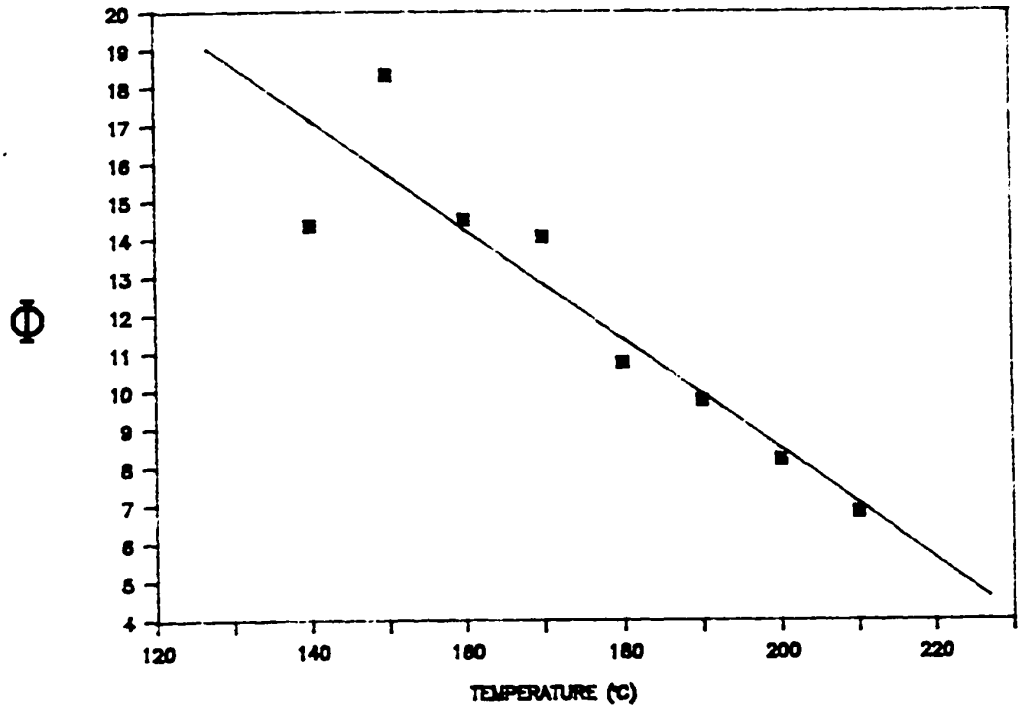

Figure 4.34 - Temperature dependence of entanglement parameter Φ.

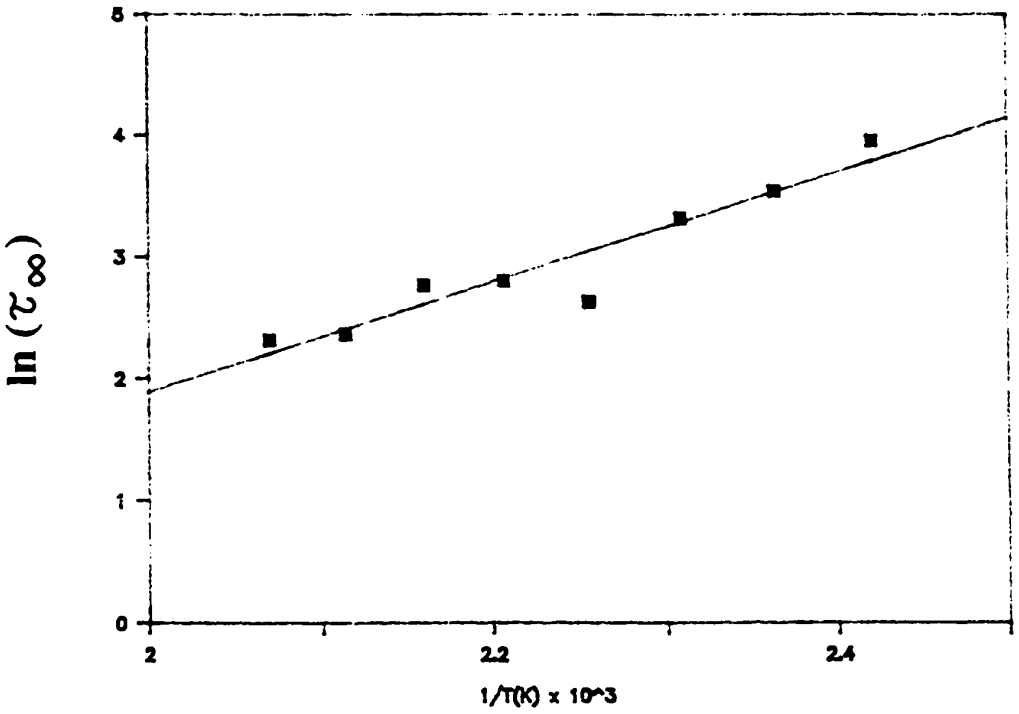

Figure 4.35 - Temperature dependence of final dipolar relaxation time, τ_∞, E_τ = 8.97 kcal/mole.

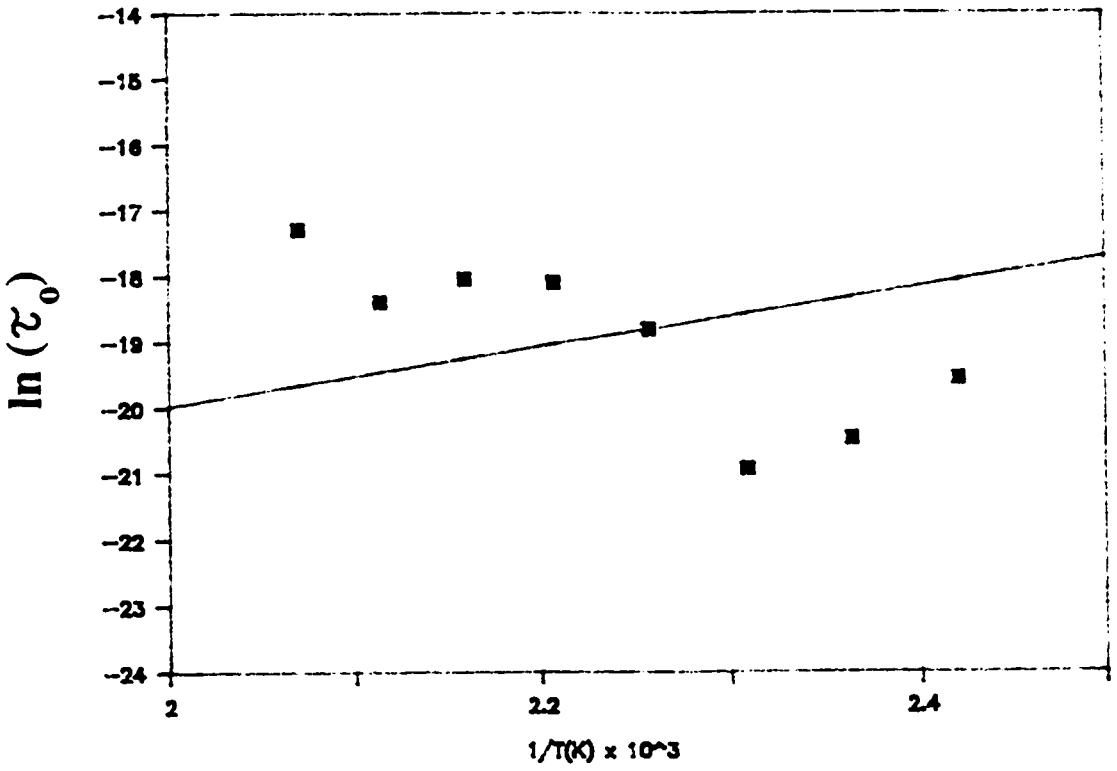

Figure 4.36 - Temperature dependence of initial dipolar relaxation time, τ_o.

Notes to Chapter 4

1. R.H. Keinle and H.H. Race, Trans. Electrochem. Soc., 65, 87 (1934).

2. M.N. Fineman and I.E. Puddington, Ind. Eng. Chem., 10, 1288 (1947).

3. M.N. Fineman and I.E. Puddington, Can. J. Research, B25, 101 (1947).

4. J.A. Aukward, R.W. Warfield and M.C. Petree, J. Polym. Sci., 27, 199 (1958).

5. R.W. Warfield and M.C. Petree, J. Polym. Sci., 37, 305 (1959).

6. R.W. Warfield and M.C. Petree, Macromol. Chem., 58, 139 (1962).

7. M.A. Acitelli, R.B. Prime, and E. Sacher, Polymer, 12, 335 (1971).

8. R.B. Prime and E. Sacher, Polymer, 13, 455 (1972).

9. J.F. Johnson and R.H. Cole, J. Am. Chem. Soc., 73, 4536 (1951).

10. P. Dansas and P. Sixou, Revue Générale de L'Electricité, 76, 726 (1967).

11. S. Havriliak and S. Negami, J. Polym. Sci.: Pt. C, 14, 99 (1966).

12. J.W. Lane, J.C. Seferis, and M.A. Bachmann, Polym. Eng. Sci., 26, 346 (1986).

13. S.H. Dillman and J.C. Seferis, J. Macromol. Sci., in press.

14. M.R. Dusi, C.A. May, and J.C. Seferis, ACS Symp. Ser., 227, 302 (1983).

15. L.E. Nielsen, Polymer Rheology, Marcel Dekker, New York, 1977.

16. C. Huraux and A. Sellaimia, C. R. Acad. Sci. Paris, 277, Ser. B, 691 (1973).

17. J. Meissonnier and J.C. Seferis, J. Makromol. Chemie, in press.

18. M.L. Williams, R.F. Landel, and J.D. Ferry, J. Am. Chem. Soc., 77, 370 (1955).

19. F. Bueche, Physical Properties of Polymers, Interscience, New York, 1962.

20. B.A. Finlayson, Nonlinear Analysis in Chemical Engineering, McGraw-Hill, New York, 1980.

21. R.A. Fava and A.E. Horsfield, Brit. J. Appl. Phys. (J. Phys. D), Ser. 2, 1, 117 (1968).

22. S. Havriliak and S. Negami, J. Polym. Sci.: Pt. C, 14, 99 (1966).

23. N.G. McCrum, B.E. Read, and G. Williams, Anelastic and Dielectric Effects in Polymeric Solids, Wiley and Sons, London, 1967.

CHAPTER 5

DIELECTRIC RESPONSE OF A MODEL THERMOSETTING MATRIX DURING NONISOTHERMAL REACTION

5.1 Introduction

The dielectric properties of an isothermally curing model thermosetting resin were experimentally measured and successfully modelled in work presented in Chapter 4. However, thermosetting matrices are also processed under nonisothermal conditions. The development of dielectric spectroscopy for thermal analysis applications therefore requires understanding the relationships between the dielectric properties and the nonisothermal cure state.

Viscoelastic, especially viscous and dynamic mechanical, property development in nonisothermally reacting thermosetting polymers has been the focus for several studies [1-12]. To improve the processing characteristics of thermosets, rheological properties during nonisothermal cure have been experimentally measured and modelled [1-8]. However, experimental measurements of viscosity are only possible below the gel point. Therefore, information regarding reaction beyond the gel point to the completion of cure is unattainable by viscometric techniques.

Nonisothermal dynamic mechanical analysis has also been performed during reaction, but the experimental results have been presented with limited analysis [9,10]. In contrast to viscosity measurements, dynamic mechanical measurements are generally possible only above the gel point. Information about material changes at low levels of conversion is lost. Dillman et al., however, developed a wire mesh technique which allows the dynamic mechanical properties of thermosetting polymers to be accurately measured from the uncured, liquid state through complete cure [11]. Dillman also qualitatively described and successfully modelled the dynamic mechanical behavior of TGDDM/DDS (35 phr) during nonisothermal reaction [12].

In contrast to rheological experiments and the majority of dynamic mechanical techniques, dielectric measurements are easily and accurately made throughout the entire range of cure. Dielectric data obtained during the nonisothermal processing of several thermosetting resins have appeared in the literature, but were performed merely to demonstrate dielectric techniques [13-17]. The dielectric model descriptions proposed by a number of researchers for isothermal reaction, which are summarized in §1.4, have not yet been applied to reaction under nonisothermal conditions.

The quantitative description of the model thermosetting resin dielectric properties during nonisothermal reaction is

the focus of this chapter. The results of the isothermal dielectric investigation provide the basis for modelling the complex dielectric constant as a function of the extent of reaction. As with the previously developed isothermal model, the contributions from ionic impurities and dipolar segments of the molecules to the resin dielectric response were determined and related to the extent of reaction. Such information is crucial to the application of dielectric techniques for extracting chemical and physical information during the processing of thermosetting polymers.

5.2 Theoretical Model Development

The similarities between the responses of the model system during isothermal and nonisothermal cure, noted in §2.6.2, suggest that a single modelling approach may be applied to describe the dielectric properties during reaction, regardless of the thermal conditions. Accordingly, a model description of the nonisothermal reaction response was obtained by simple extension of the isothermal modelling concepts. The effects of ionic conductivity and dipolar relaxation were combined to produce the complete dielectric model response during nonisothermal reaction.

5.2.1 Equivalent Electric Circuit Representation

The dielectric properties of curing resin was again modelled with ionic conduction and dipolar relaxation effects treated as circuit elements in parallel, as diagrammed in Figure 4.1. The dielectric response of the resin is the sum of the individual responses:

$$\varepsilon'_{resin} = \varepsilon'_{ionic} + \varepsilon'_{dipolar} \tag{5.1}$$

$$\varepsilon''_{resin} = \varepsilon''_{ionic} + \varepsilon''_{dipolar} \tag{5.2}$$

The ionic and dipolar responses must then be understood in terms of the extent of reaction to completely describe the dielectric properties during nonisothermal cure.

5.2.2 Nonisothermal Ionic Conduction

Conduction of ionic impurities during nonisothermal cure may be described by the Keinle-Race expression developed for isothermal cure in Chapter 4:

$$\ln(\varepsilon''_{ionic} we_o) = C_r \alpha + C_o \tag{5.3}$$

In isothermal cure experiments, the conductivity of uncured resin, C_o, was found to follow Arrhenius behavior. However, as discussed in §2.6.1, nonisothermal ionic conductivity

approaches an asymptotic value which is a function of heating rate. These observations imply that Equation 5.3 also applies to nonisothermal cure conditions without explicit modification to include temperature. Accordingly, logarithmic plots of nonisothermal conductivity data versus extent of reaction will be linear. Temperature effects are incorporated through the values of C_r and C_o at each heating rate.

5.2.3 Nonisothermal Electrode Polarization

The contribution of electrode polarization to ε' measured at low frequencies is related to the resin ionic conductivity. In isothermal experiments, polarization was described using an expression proposed by Johnson and Cole for polar organic liquids [18]. The final polarization equation accounting for electrode area, A; electrode spacing, d; applied frequency, w; and the permittivity of free space, e_o, became:

$$\varepsilon'_{obs} = \varepsilon'_{dipole} + Z_o \sin(n\pi/2) w^{-(n+1)} A 2\sigma^2 / de_o \qquad (5.4)$$

Z_o and n describe the complex impedance behavior of polarization. The values of Z_o and n are specific to each dielectric cell and are not material properties. The exponent n has values between 0.0 and 1.0.

This approach may also be applied in describing nonisothermal polarization. Since the amount of ionic conductivity, σ, and the electrode geometry are known explicitly, ε' data may be analyzed directly to determine values of Z_o and n. According to Equation 5.4, curves of ε' plotted as a function of σ^2 will be linear with:

$$\text{slope} = Z_o \sin(n\pi/2) w^{-(n+1)} A/de_o \qquad (5.5)$$

$$\text{intercept} = \varepsilon'_{\text{dipole}} \text{ at onset of cure} \qquad (5.6)$$

As seen in Figures 2.25 - 2.27, conductivity changes during the early stages of nonisothermal reaction are smaller than those during isothermal reaction. Therefore, the data region for performing linear regression according to Equation 5.4 is easily determined.

Z_o and n were calculated from the slopes of ε' versus σ^2 data obtained over a range of frequencies. Closer inspection of Equation 5.5 reveals that log-log curves of these slopes plotted as functions of frequency are linear with:

$$\text{slope} = n + 1 \qquad (5.7)$$

$$\text{intercept} = \ln[Z_o \sin(n\pi/2) A/de_o] \qquad (5.8)$$

Using these parameters, electrode polarization effects may be removed from the nonisothermal dielectric data.

5.2.4 Nonisothermal Dipolar Relaxation

The contributions of dipolar relaxation to ε' and ε'' during isothermal cure were related to the mean dipolar relaxation time in Chapter 4. The proposed constitutive equation expressed the complex dielectric constant, ε^*, in terms of the relaxation time, τ, and two relaxation time distribution parameters, α' and β', by:

$$\varepsilon^* = \varepsilon_{\alpha=0} + \frac{(\varepsilon_{\alpha=0} - \varepsilon_{\alpha=1})}{(1 + (i\omega\tau)^{\beta'})^{\alpha'}} \qquad (5.9)$$

$$0 < \alpha', \beta' \leq 1$$

This equation may also be applied to describe the relationship between the nonisothermal dielectric properties and relaxation time. As a first approximation, the parameters α' and β' were assumed to be constant with temperature. This assumption was supported in part by the results of the isothermal experiments, which showed no significant change in β' with temperature. While α' did increase at higher temperatures, the changes are small enough so α' was treated as temperature independent.

The influence of nonisothermal reaction on the mean dipolar dielectric relaxation time was again modelled using kinetic viscoelasticity. In isothermal cure, the relaxation time expressed as a function of extent of reaction, α; the dipolar relaxation times of uncured and fully cured resin, τ_o and τ_∞; and an entanglement parameter, Φ:

$$\frac{1}{\tau} = \frac{1}{\tau_\infty} + \left[\frac{1}{\tau_o} - \frac{1}{\tau_\infty}\right](1-\alpha)^{\Phi} \qquad (5.10)$$

The relationship between dipolar relaxation and temperature must be included in the nonisothermal model since relaxation is an activated process [19]. Changes in the dielectric constant of nonreacting polymers are described by expressing the dipolar relaxation time as a function of temperature in Arrhenius form, viz. [19]:

$$\tau = \tau' \exp(E_\tau/RT) \qquad (5.11)$$

This equation may be substituted for τ_o and τ_∞ in Equation 5.10 to incorporate the effect of temperature:

$$\frac{1}{\tau} = \frac{-E_\infty/RT}{\tau'_\infty} - \left[\frac{E_o/RT}{\tau'_o} - \frac{E_\infty/RT}{\tau'_\infty}\right](1-\alpha)^\Phi \qquad (5.12)$$

As a first approximation, E_o and E_∞ were assumed to be equal and represented as E_τ:

$$\frac{1}{\tau} = \exp(-E_\tau/RT)\left[\frac{1}{\tau'_\infty} + \left[\frac{1}{\tau'_o} - \frac{1}{\tau'_\infty}\right](1-\alpha)^\Phi\right] \qquad (5.13)$$

However, E_o is expected to be less than E_∞, since relaxation is less hindered in an uncured, liquid environment. As a test of the modelling approach, the entanglement parameter Φ was assumed to be constant with temperature. The relationship between kinetics, temperature, and dipolar relaxation time during nonisothermal cure was expressed explicitly by Equation 5.13.

5.2.5 Combined Nonisothermal Dielectric Cure Model

The complete nonisothermal model describing the nonisothermal dielectric properties was obtained by combining the contributions to the complex dielectric constant from ionic conduction, expressed by Equation 5.3, and from dipolar relaxation, given by Equation 5.9:

$$\varepsilon' = \varepsilon_{\alpha=1} + \frac{(\varepsilon_{\alpha=0} - \varepsilon_{\alpha=1}) \cos \alpha'\varphi}{[1+2(w\tau)^{\beta'}\cos(\beta'\pi/2)+(w\tau)^{2\beta'}]^{\alpha'/2}} \quad (5.14)$$

$$\varepsilon'' = \frac{\exp(C_r\alpha+C_o)}{we_o} + \frac{(\varepsilon_{\alpha=0} - \varepsilon_{t=1}) \sin \alpha'\varphi}{[1+2(w\tau)^{\beta'}\cos(\beta'\pi/2)+(w\tau)^{2\beta'}]^{\alpha'/2}} \quad (5.15)$$

The parameter φ is a collection of the relaxation time distribution parameters:

$$\varphi = \tan^{-1}\left[\frac{(w\tau)^{\beta'}\sin(\beta'\pi/2)}{1 + (w\tau)^{\beta'}\cos(\beta'\pi/2)}\right] \quad (5.16)$$

The dependence of the dipolar relaxation time on temperature and the extent of reaction, assuming the model parameters to be constant with temperature, is given by Equation 5.13. With the correct values of the parameters in Equations 5.13, 5.14, and 5.15, the dielectric properties of thermosetting polymers may be predicted completely during nonisothermal reaction.

5.3 Discussion

5.3.1 Model Parameter Determination

5.3.1.1 Ionic Conduction Parameters

The parameters describing the contribution of ionic conduction to ε'' during nonisothermal cure were determined by linear regression according to Equation 5.3. The expected linearity of semi-log plots of conductivity versus extent of reaction is seen at each heating rate in Figures 5.1 - 5.3. As cure proceeds, additional contribution to the apparent conductivity from dipolar relaxation is observed in the 1 and 5°C/minute data.

Conductivity calculated from 240 Hz data were used to determine C_r and C_o in Equation 5.3 for each heating rate by linear regression. As in the isothermal determination, regression was typically performed on conductivity in the conversion range of 0.10 to 0.40. The parameter values obtained are presented in Table 5.1. The high values of the correlation coefficients justifies excluding explicit temperature dependences in Equation 5.3.

5.3.1.2 Electrode Polarization Parameters

The additional capacitance arising from electrode polarization by ionic charge buildup was determined for each

data set. The polarization contribution to ε' was related to the nonisothermal conductivity using Equation 5.4. According to this equation, plots of ε' versus σ^2 are linear, as exemplified by the 1°C/minute data in Figure 5.4. The slope and intercept of the linear region are described by Equations 5.5 and 5.6.

From the slopes for each frequency, the values of Z_o and n were found according to Equations 5.7 and 5.8. Table 5.2 contains a summary of the calculated parameter values. Z_o and n are specific to each two terminal cell, and are not material constants. These parameters are useful, however, to evaluate the extent of electrode polarization in the ε' data, thereby providing a more accurate determination of dipolar relaxation effects in the data.

5.3.1.3 Dipolar Relaxation Parameters

The final step in analyzing the nonisothermal dielectric cure responses is to determine the parameters in Equations 5.13, 5.14, and 5.15. As with the isothermal analysis, a nonlinear regression routine was used to find the set of parameters which best describe the data.

The constraints which allowed only three parameters to be fitted to the isothermal data could not be applied to the nonisothermal dielectric data without explicitly knowing the

activation energy for relaxation, E_τ. However, the number of fitted parameters was reduced by making several simplifications. The value of β' was assumed to be 0.70, the average value found from the isothermal data. The pre-exponential of the final dipolar relaxation time, τ_∞', was assumed to be equal to the value determined from the isothermal data, 7.93×10^{-4} secs. Values of $\varepsilon_{\alpha=0}$ and $\varepsilon_{\alpha=1}$ were taken directly from the experimental data. Consequently, only four parameters were found by nonlinear regression of the data: α', Φ, τ_o', and E_τ.

Since dipolar effects are most prevalent at high frequency, 20 KHz data were used to fit the parameters. However, only data obtained at heating rates of 1 and 5°C/minute heating rates were analyzed. The apparent conductivity curves for reaction at 10°C/minute, Figure 5.3, did not diverge, which would have revealed dipolar relaxation effects in the data. In addition, ε' did not change until very late in the cure. The analysis was also hampered by insufficient DSC data near the end of the reaction due to the fast heating rate. The parameters relating reaction, temperature, dipolar relaxation time, and the dielectric properties for cure at 1 and 5°C/minute are listed in Table 5.3.

5.3.2 Model Predictions of Experimental Results

The nonisothermal dielectric response of TGDDM/DDS at 20 KHz was generated from the combined model expressed in Equations 5.14 and 5.15, using the calculated parameters in Tables 5.1 and 5.3. The effects of electrode polarization were added to the plotted responses. Model curves of ε' and ε'' during cure at 1 and 5°C/minute are compared to experimental data in Figures 5.5 and 5.6. As seen in these figures, the model is able to reasonably describe the responses. The good agreement between the data and model supports the assumptions made in the model development.

These assumptions were further tested by comparing model predictions with experimental data obtained at the lowest applied frequency, 240 Hz, in Figures 5.7 and 5.8. No additional fitting was performed to generate these responses. The prediction agrees with the 240 Hz data for reaction at 5°C/minute. The 1°C/minute data displayed a maxima in ε' which was not observed for any other heating rate. The source of this maxima was unknown and, hence, the peak was not predicted the model. While differences between the model and data suggest fine tuning the model parameters, their similarities verify the model assumptions.

The constant model dielectric responses at the completion of cure reflect the insensitivity of differential scanning calorimetry to small thermal changes in reaction.

Dielectric property changes are observed to occur until the onset of degradation, while the DSC reaction exotherm ends abruptly. Correspondingly, the model calculations, which use experimental DSC extents of reaction, reach final values before the dielectric data indicate complete reaction.

5.3.3 Dependence of Model Parameters on Heating Rate and Comparison to Isothermal Values

Additional support for the model approach was provided by comparing the heating rate dependence of the parameters with expected behavior. The heating rate behavior of the conductivity parameter C_r reveals the expected effects of temperature on conductivity during cure. The decreasing value of C_r with increasing heating rate resulted from the competing effects of ionic mobility, network structure, and temperature. Crosslinking reduced the available volume for ion migration, while temperature increased ionic mobility. By this mechanism, ionic conductivity would decrease with cure, but less abruptly than in isothermal experiments. Since the DSC reaction exotherms indicate that reaction shifts to higher temperatures at higher heating rates, the value of C_r was therefore expected to be decrease at higher heating rates. Both of these effects are observed in the values of C_r in Table 5.1.

The dipolar relaxation parameters in Table 5.3 are not functions of the heating rate. If the assumptions made in the nonisothermal model development were grossly incorrect, maintaining β' and τ_∞' at the isothermal values would produce widely varying values of the nonisothermal parameters. As seen in Table 5.3, the dipolar parameters, especially τ_o' and Φ, were essentially constant, indicating that the assumptions are essentially correct. However, the values of E_τ and α' did vary slightly, indicating further refinement of the model parameters.

The differences between the nonisothermal and isothermal values of α' and Φ were expected since these parameters varied with the isothermal cure temperature. The parameter values, which were determined by regression, were influenced directly by the assumption that the activation energies of relaxation for uncured and fully cured resin are equal. The average value of E_τ, 14.56 kcal/mole, was higher than the activation energy found for fully cured resin in isothermal experiments, 8.97 kcal/mole. The expected value of τ_o' was difficult to evaluate since no clear trend was seen in τ_o in the isothermal experiments. While variations exist between the results of the isothermal and nonisothermal experiments, the satisfactory performance of the respective models validates this approach and its assumptions.

5.4 Conclusions

An approach for quantitatively describing the dielectric properties of thermosetting polymers during nonisothermal reaction was proposed and shown valid for the model high performance TGDDM/DDS system. The nonisothermal model, contained in Equations 5.13, 5.14, and 5.15, was based on previously developed model for isothermal cure. Qualitative similarities between the dielectric responses during reaction suggested applying the isothermal model to nonisothermal cure conditions.

Ionic conduction was described by the Keinle-Race equation, Equation 5.3. The nonisothermal conductivity data for the uncured resin suggested excluding explicit temperature effects from this equation. Dipolar relaxation was related to the dielectric properties and the mean dipolar relaxation time during cure using the Lane-Seferis-Bachmann equation, Equation 5.9. The relaxation time was related to reaction using the principles of kinetic viscoelasticity. The nonisothermal kinetic relaxation model was an extension of the isothermal model by including an Arrhenius expression for the uncured and fully cured resin dipolar relaxation times. A single activation energy for both processes was used to a first approximation.

Electrode polarization effects in ε' were evaluated using an approach developed for polar organic liquids.

Polarization was related to the measured resin conductivity by Equations 5.4 - 5.8. These effects were removed from the data before determining the best dipolar relaxation parameters.

The parameters describing conductivity during cure were calculated from apparent conductivity curves plotted as functions of the extent of reaction for each heating rate. The decrease in C_r with heating rate indicated that temperature is an implicit factor in the resin conductivity during reaction as ionic motion decreases with cure, but ionic mobility increases with temperature.

The dipolar relaxation parameters were calculated from 20 KHz dielectric data by nonlinear regression. The values of β' and τ_∞' were maintained at the isothermal data values, 0.70 and 7.93×10^{-4} secs, respectively. The model responses are in good agreement with the 20 KHz experimental data. The modelling approach was tested further testing by comparing the predicted response and experimental data for 240 Hz, without additional parameter fitting. While not exact, good qualitative agreement resulted. The values of τ_o' and Φ did not depend on heating rate, while E_τ and α' varied slightly. The nonisothermal parameter values differ from the isothermal values, but such behavior was expected with the simplifications used in the nonisothermal model development.

The success of the developed nonisothermal modelling approach is necessary for further development of dielectric techniques for thermal analysis applications. Discrepancies between the isothermal and nonisothermal model parameters for the model epoxy resin suggest that additional refinement before attempting to use this approach for dielectric process control.

Table 5.1

Nonisothermal conductivity/reaction parameters for TGDDM/DDS (25 phr)

φ (°C/min)	C_r	C_o	r2
1	-4.80	-14.57	0.990
5	-1.47	-13.99	0.999
10	-0.27	-13.87	0.976

Table 5.2

Electrode polarization parameters for nonisothermal dielectric experiments

φ (°C/min)	Z_o (ohms)	n
1	2.25×10^3	0.16
5	1.68×10^3	0.14
10	3.23×10^3	0.05

Table 5.3

Kinetic dipolar relaxation model parameters for nonisothermal cure of TGDDM/DDS (25 phr)

φ (°C/min)	τ_o' (secs)	τ_∞'(secs)	E_τ(kcal/mole)	α'	β'	Φ
1	6.00×10^{-14}	7.92×10^{-4}	14.15	0.19	0.70	5.10
5	6.20×10^{-14}	7.93×10^{-4}	14.97	0.25	0.70	5.08
AVERAGE	6.10×10^{-14}	7.93×10^{-4}	14.56	0.22	0.70	5.09

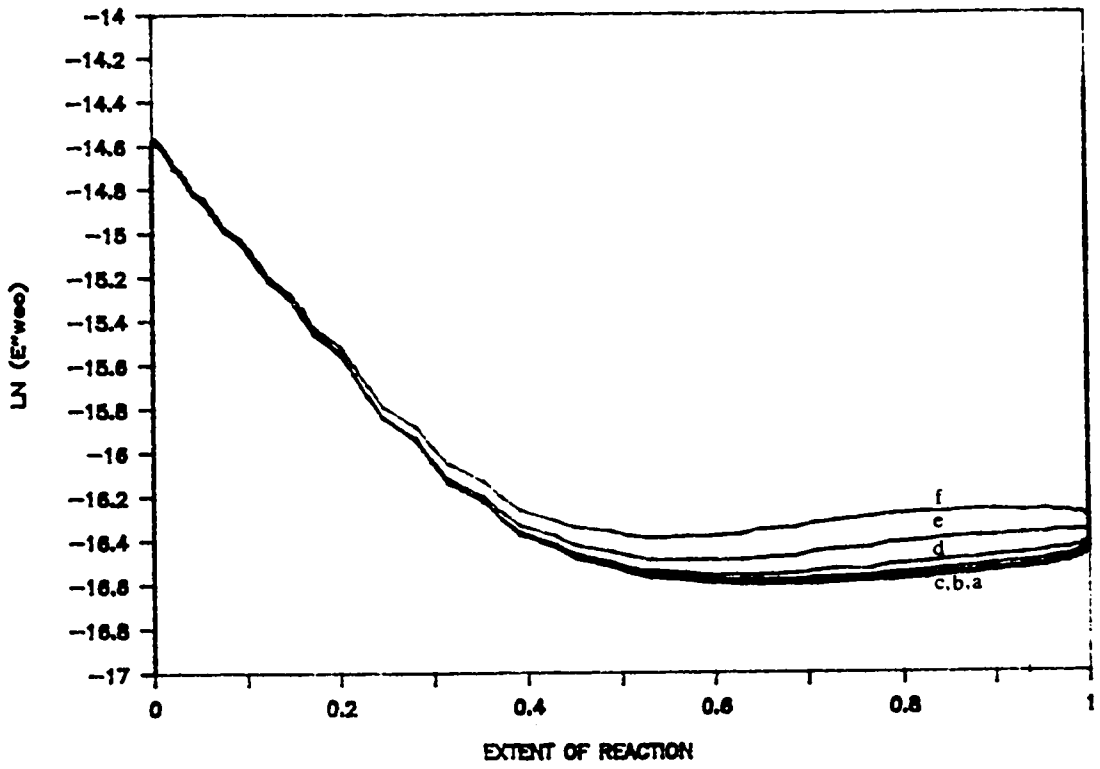

Figure 5.1 - Keinle-Race plot of TGDDM/DDS during nonisothermal cure at 1°C/minute: a) 240 Hz, b) 1 KHz, c) 2 KHz, d) 4 KHz, e) 10 KHz, f) 20 KHz.

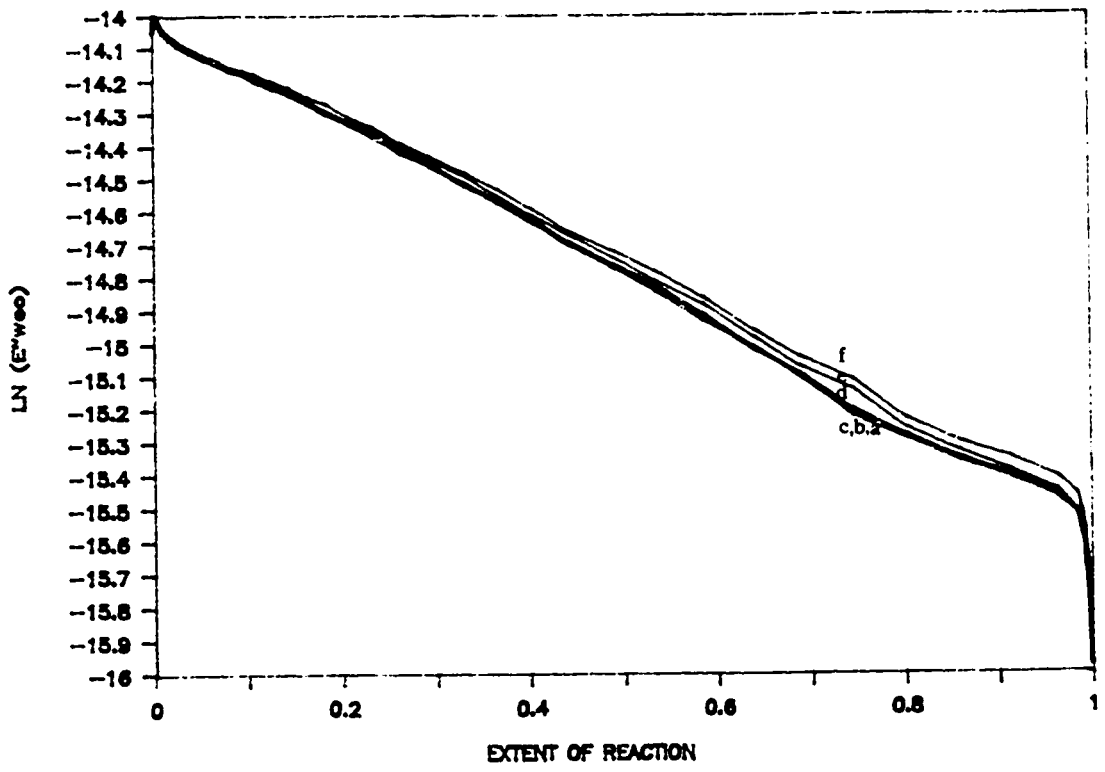

Figure 5.2 - Keinle-Race plot of TGDDM/DDS during nonisothermal cure at 5°C/minute: a) 240 Hz, b) 1 KHz, c) 2 KHz, d) 4 KHz, e) 10 KHz, f) 20 KHz.

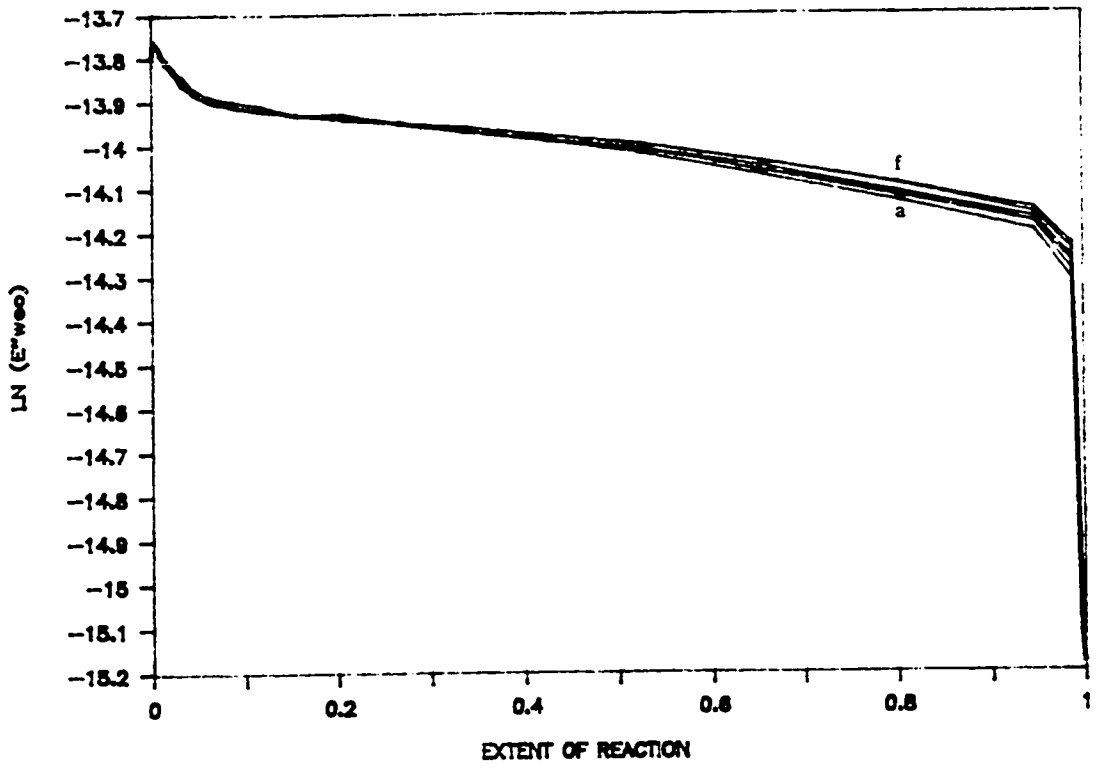

Figure 5.3 - Keinle-Race plot of TGDDM/DDS during nonisothermal cure at 10°C/minute: a) 240 Hz, b) 1 KHz, c) 2 KHz, d) 4 KHz, e) 10 KHz, f) 20 KHz.

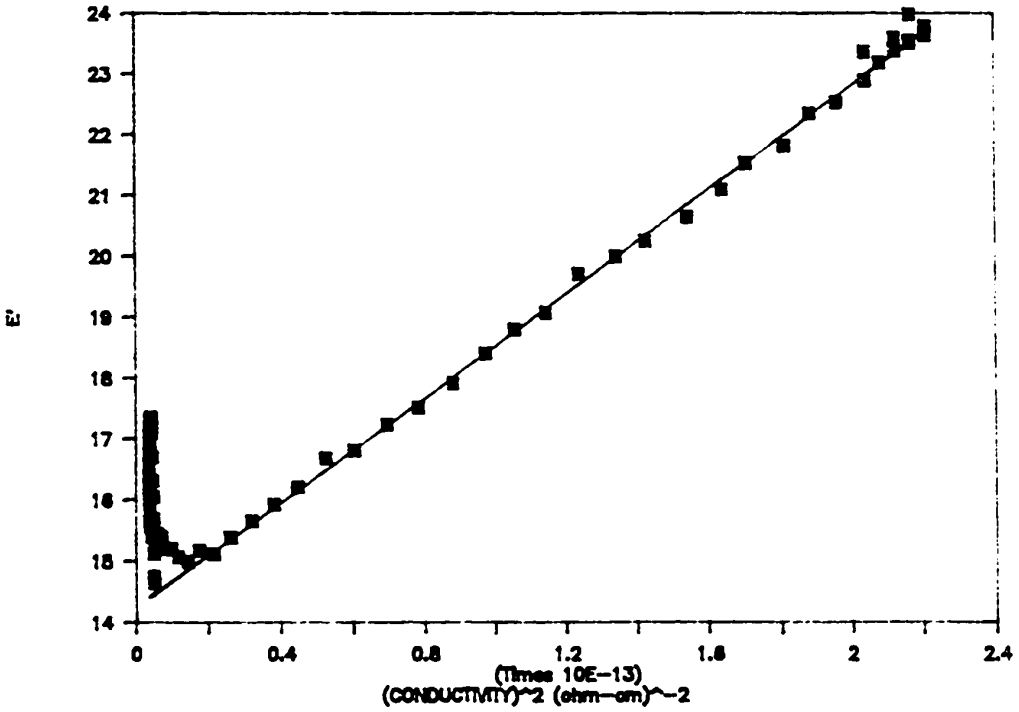

Figure 5.4 - Conductivity/ε' data during cure at 1°C/minute, plotted according to Equation 5.4 to determine electrode polarization parameters.

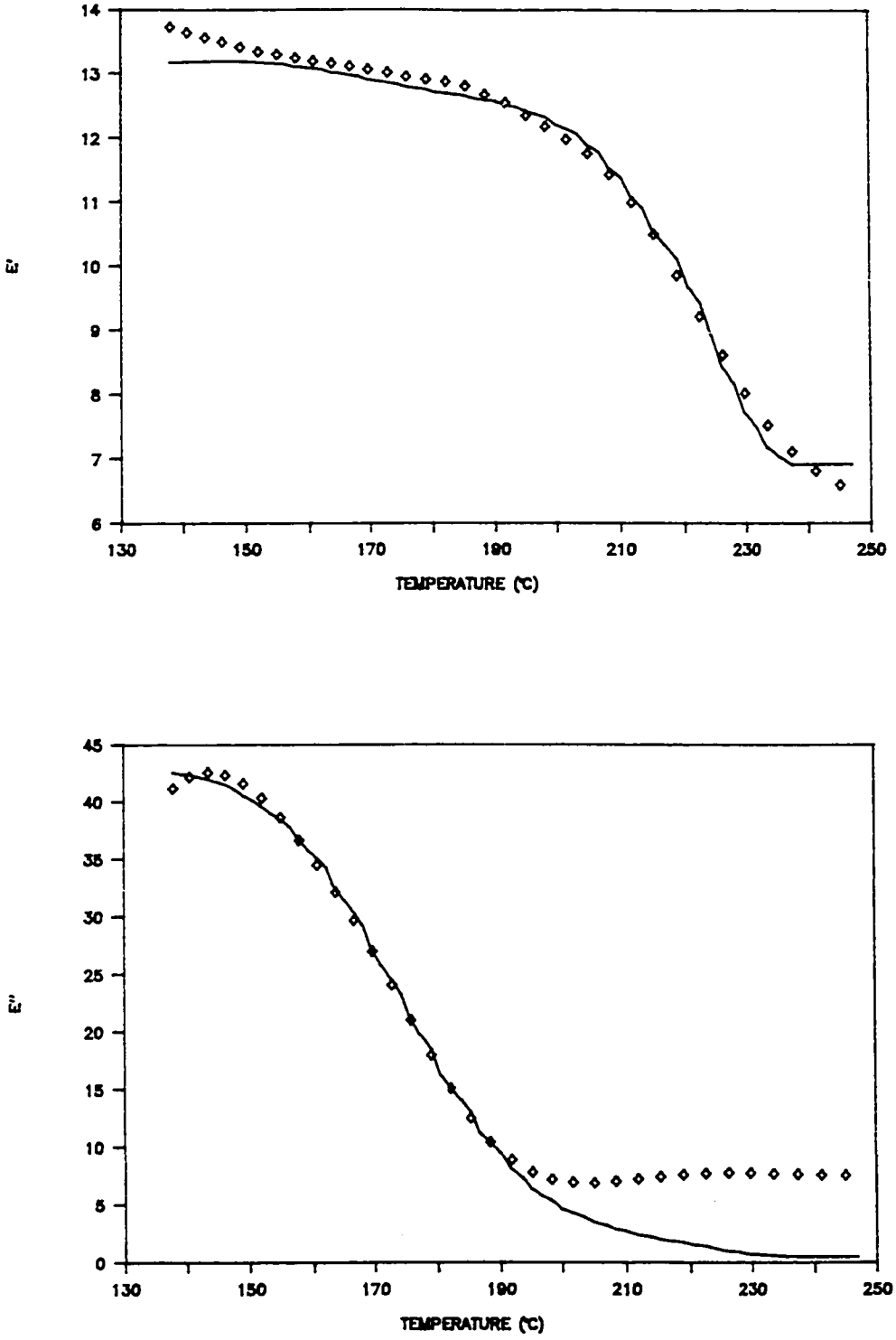

Figure 5.5 - Comparison of combined dielectric model (—) and experimental data (♦) at 20 KHz during nonisothermal cure of TGDDM/DDS at 1°C/minute.

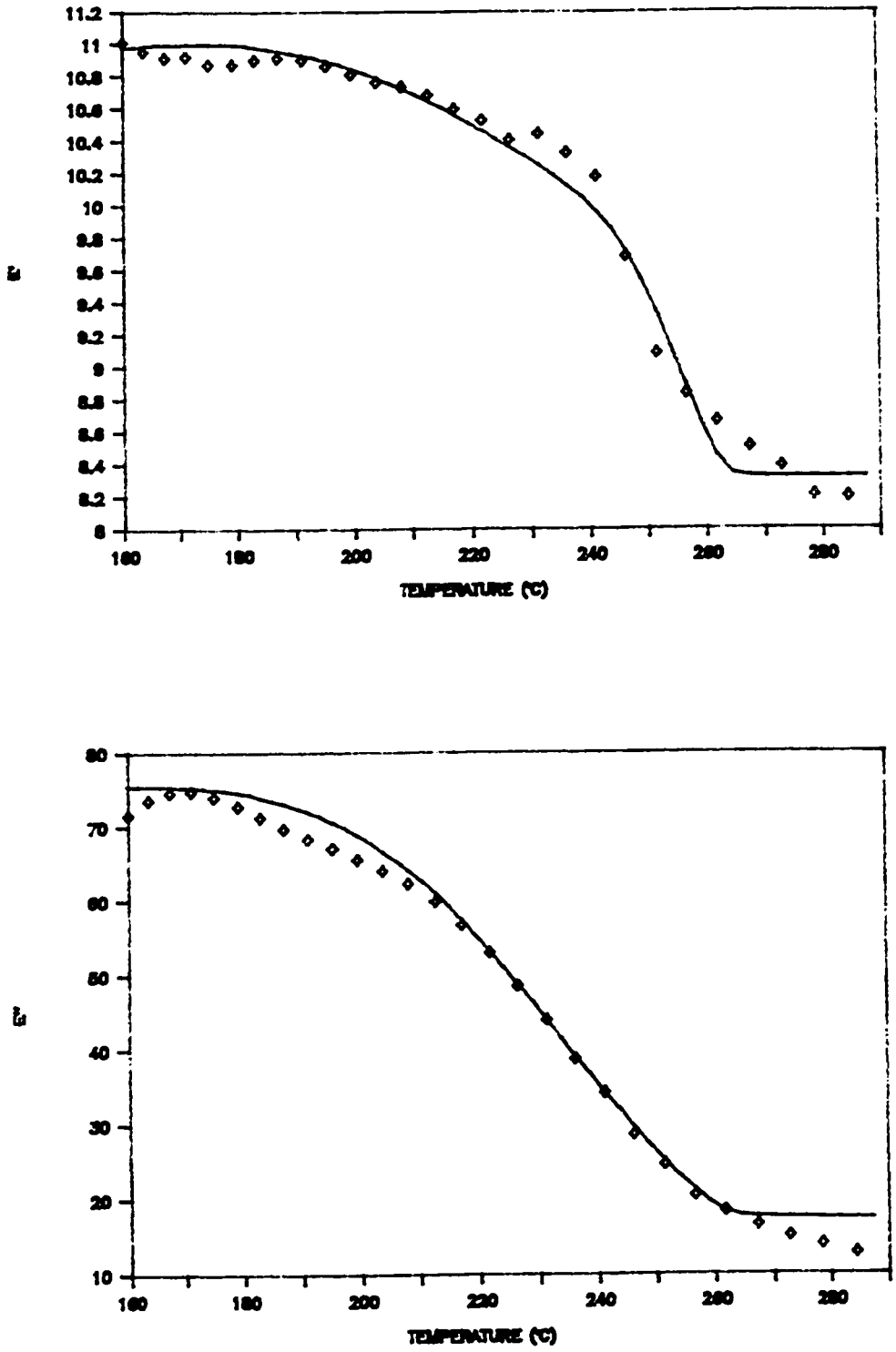

Figure 5.6 - Comparison of combined dielectric model (—) and experimental data (♦) at 20 KHz during nonisothermal cure of TGDDM/DDS at 5°C/minute.

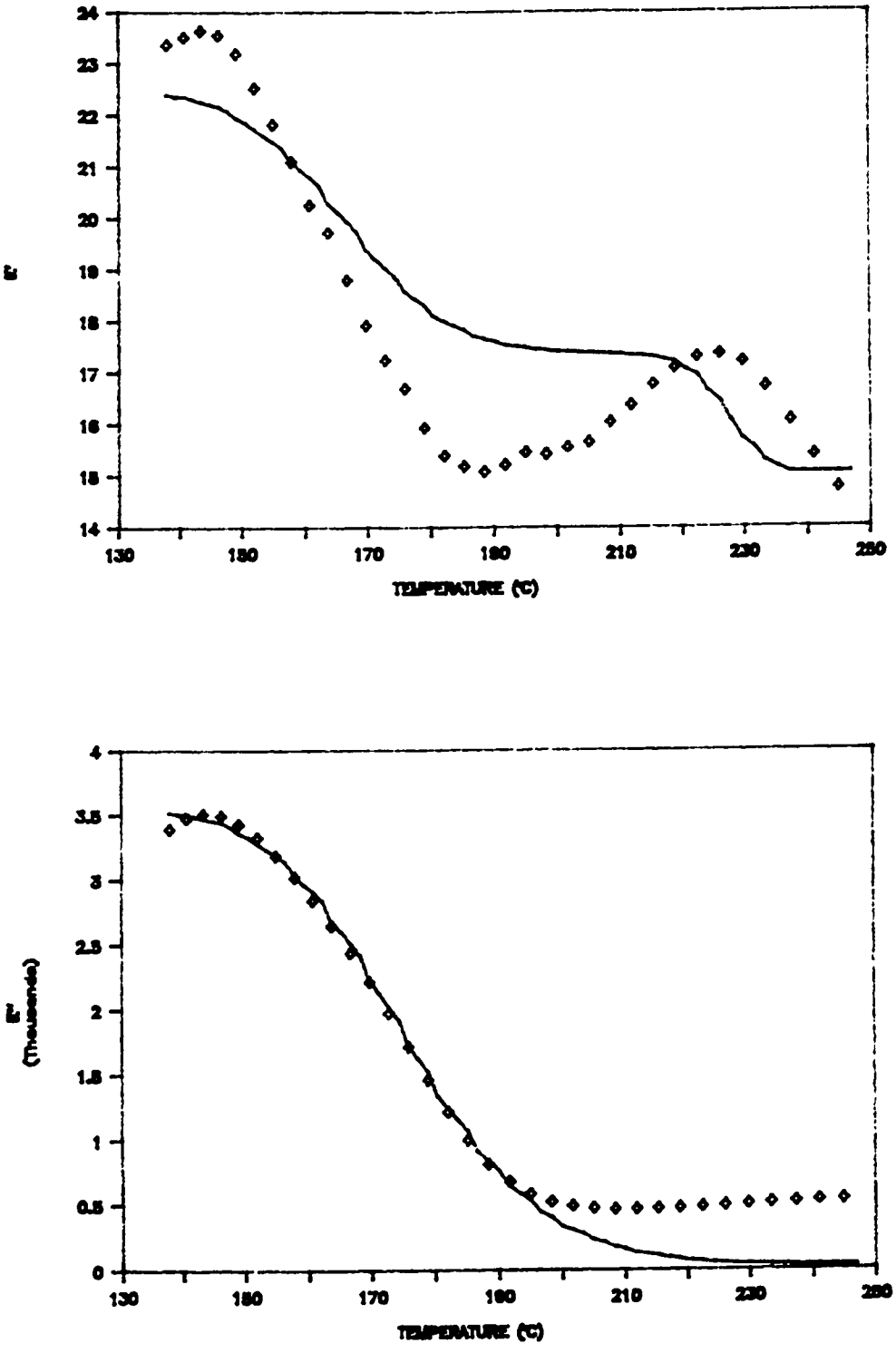

Figure 5.7 - Prediction of 240 Hz dielectric properties (—) during nonisothermal cure of TGDDM/DDS at 1°C/minute, experimental data (♦).

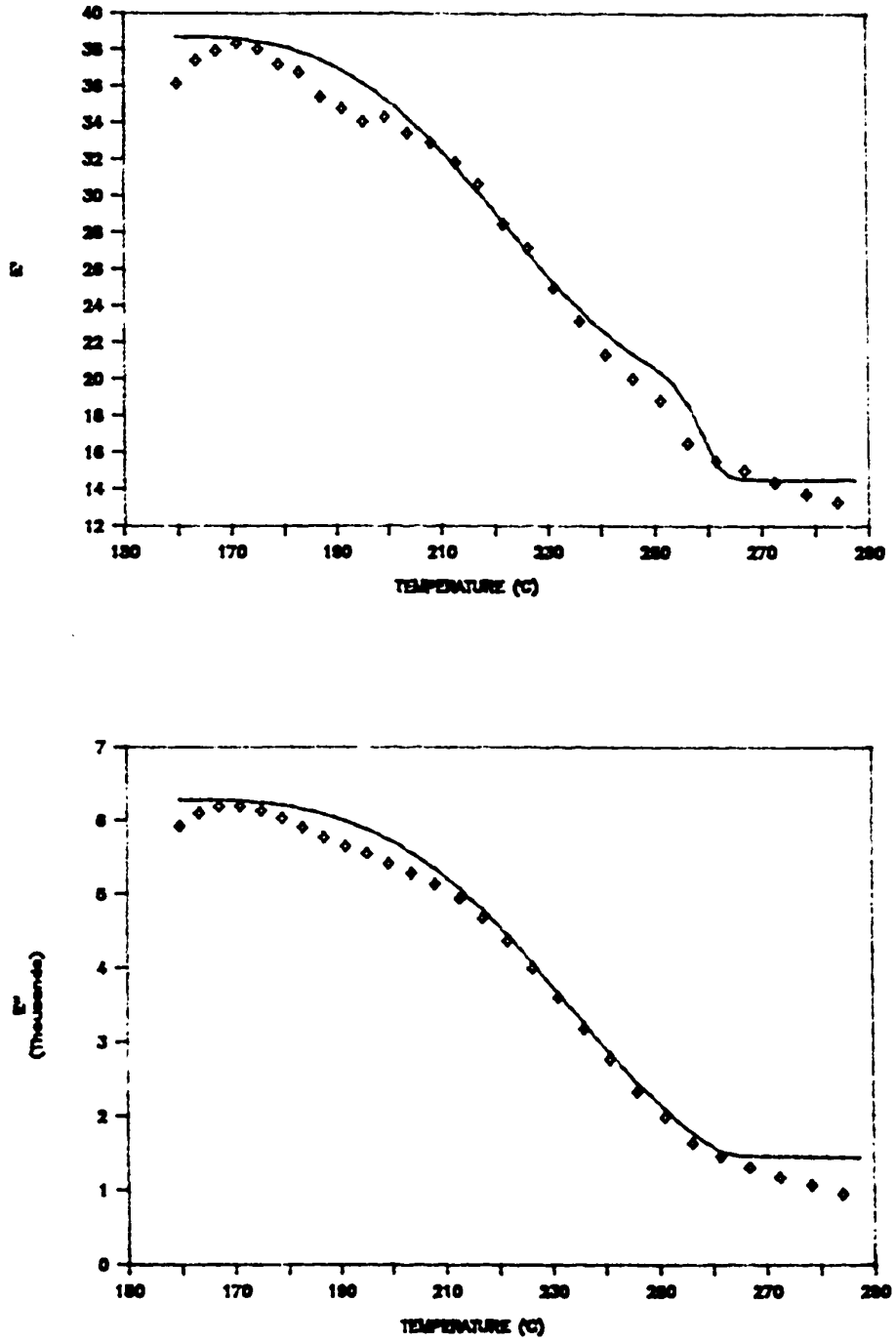

Figure 5.8 - Prediction of 240 Hz dielectric properties (—) during nonisothermal cure of TGDDM/DDS at 5°C/minute, experimental data (♦).

Notes to Chapter 5

1. M.B. Roller, Polym. Eng. Sci., 15, 406 (1975).

2. M.B. Roller, Polym. Eng. Sci., 26, 432 (1986).

3. J.C. Halpin, J.L. Kardos, and M.P. Dudukovic, Pure and Appl. Chem., 55, 893 (1983).

4. M.R. Dusi, C.A. May, and J.C. Seferis, ACS Symp. Ser., 227, 302 (1983).

5. E.B. Stark, Doctoral Dissertation, University of Washington, 1985.

6. Y.A. Tajima and D.G. Crozier, Polym. Eng. Sci., 26, 427 (1986).

7. Y.A. Tajima and D.G. Crozier, Polym. Eng. Sci., 28, 491 (1988).

8. J. Meissonnier and J.C. Seferis, J. Makromol. Chemie, in press.

9. C. Y-C. Lee and I.J. Goldfarb, Polym. Eng. Sci., 21, 951 (1981).

10. T. Provder, R.M. Holsworth, and T.H. Grentzer, Adv. Chem. Ser., 203, 77 (1983).

11. S.H. Dillman, J.C. Seferis, and R.B. Prime, Proc. Ann. Tech. Conf., N. Amer. Thermal Anal. Soc., 19, 429 (1987).

12. S.H. Dillman, Doctoral Dissertation, University of Washington, 1985.

13. C.A. May, Proc. Ann. Conf., Soc. Adv. Matl. Proc. Eng., 20, 108 (1975).

14. C.A. May, M.R. Dusi, J.S. Fritzen, D.K. Hadad, M.G. Maximovich, K.G. Thrasher, and A. Wereta, ACS Symp. Ser., 227, 1 (1983).

15. M.J. Yokota, Proc. Ann. Conf., Soc. Adv. Matl. Proc. Eng., 22, 416 (1977).

16. D.E. Kranbuehl, S.E. Delos, and P.K. Jue, Polymer, 27, 11 (1986).

17. D.E. Kranbuehl, S.E. Delos, E. Yi, J. Mayer, T. Jarvie, W. Winfree, and T. Hou, Polym. Eng. Sci., 26, 338 (1986).

18. J.F. Johnson and R.H. Cole, J. Am. Chem. Soc., 73, 4536 (1951).

19. N.G. McCrum, B.E. Read, and G. Williams, Anelastic and Dielectric Effects in Polymeric Solids, Wiley and Sons, London, 1967.

CHAPTER 6

SUMMARY AND RECOMMENDATIONS

6.1 Research Summary

This study considered dielectric spectroscopy as a technique suitable for thermal analysis of polymeric matrices, and conceivably, polymeric composite materials. The study sought to describe the experimentally measured dielectric properties of thermosetting polymers in terms of the chemical and physical phenomena which occur during processing. A unified approach was taken by considering the responses of the two types of electrically active species in polymers, ionic impurities and dipolar molecular segments. The behaviors of ions and dipoles in a changing molecular environment, such as during viscoelastic transition or chemical reaction, were considered. Several data analysis techniques were developed for extracting standard thermal analysis parameters, such as the activation energies of dielectric transitions and reactions, and to predict the dielectric properties during isothermal and nonisothermal polymerization.

This first step in describing the dielectric properties of curing thermosetting polymers has demonstrated the validity of the modelling approach. An exact fit of the

model parameters to the isothermal and nonisothermal data was not obtained, consequently the same sets of parameters were not for both types of cure conditions. At this point, the discrepancy appears to be the result of experimental errors in the data, rather than errors in the modelling approach. The development of instrumentation able to obtain reliable and reproducible dielectric data will allow the model to be examined more closely.

The components of the complex dielectric constant, ε^*, were experimentally measured during isothermal and nonisothermal processing of a model thermosetting resin, TGDDM cured with 25 phr DDS. In isothermal experiments, changes in the real component, ε', resulted from the ionic buildup at the electrode surfaces and the restriction of dipolar orientation by polymer network formation. The loss component, ε'', was influenced by the restriction of ionic motion and dipolar relaxation from resin reaction. During nonisothermal experiments, the glass transition of the uncured resin, reaction, and degradation of the cured resin were observed in the dielectric properties. The observed property changes were qualitatively similar to those which occurred during isothermal experiments, further supporting the unified approach taken in the research.

Methods were developed for determining E_τ, the activation energies of dielectric transitions such as the

uncured glass transition of the model resin. A new method for calculating E_τ from post-transition values of ε'' was developed by considering the temperature effect on the polymeric dispersion behavior. The frequency dependence of the dielectric properties was described using a generalized constitutive equation which related the mean dipolar relaxation time to the experimentally measured properties. An equation for E_τ was derived from this equation by including the temperature dependence of the dipolar relaxation time as an Arrhenius expression. The success of the equation in describing the post-transition ε'' data and in calculating E_τ, was demonstrated for the model system.

Techniques for analyzing both isothermal and nonisothermal dielectric data during cure were also developed. These techniques were based on methods commonly employed to analyze differential scanning calorimetry data. The reaction activation energy, E_a, was determined from isothermal data by comparing the times at which ε'' reached a maximum for a given frequency and cure temperature. For the nonisothermal data, the temperatures at which ε'' reached a maximum were used to determine E_a. Both of these methods were shown to be successful for the TGDDM/DDS system by comparison with the reaction activation energies determined from DSC.

The dielectric properties of curing thermosetting resins during cure were analyzed further by developing a model expression in terms of the extent of reaction. This model may be viewed as a parallel arrangement of capacitive and resistive elements corresponding to the contributions of ionic and dipolar species. This treatment allowed models of each behavior to be added together, producing a complete description of the resin properties during cure.

The decrease in ionic conduction during isothermal reaction was related to the extent of reaction using an empirical relationship found to hold for a variety of thermosetting polymers. Dipolar relaxation was considered by adapting a generalized dielectric dispersion model for nonreacting systems. The mean relaxation time was then related directly to the extent of reaction using the principles of kinetic viscoelasticity. The model equation developed relates the dipolar relaxation time to the values of uncured and fully cured resin and an entanglement parameter. An understanding of the physical significance of the entanglement parameter was obtained through its association with the WLF equation parameters.

The model parameters were determined for the isothermal cure of the TGDDM/DDS model system using high frequency data and DSC extent of reaction values. Electrode polarization effects were subtracted from the data by adapting a method

for removing similar effects from the dielectric properties of polar organic liquids. The temperature dependence of the model parameters were then determined. The most significant result noted was that the decrease in the entanglement parameter value with increasing temperature could be predicted by the WLF equation parameters. The success of the model was demonstrated by using the high frequency parameters to predict the dielectric cure data obtained at low frequencies.

The isothermal model was extended to describe the dielectric data obtained during nonisothermal cure by including a specific temperature dependence for the mean dipolar relaxation time. The model was simplified by assuming that the relaxation activation energies of uncured and fully cured resin did not differ appreciably and could therefore be represented by an average value. The experimentally observed ionic conduction contribution to the dielectric properties was observed to follow the same dependence on the extent of reaction as seen in the isothermal experiments. No explicit dependence on temperature was noted. The model parameters which remained constant with temperature in the isothermal experiments were put directly into the nonisothermal model. The remaining model parameters were determined from high frequency dielectric data and DSC extent of reaction data. The model

was shown to be successful in describing the dielectric properties during nonisothermal cure by using the determined parameters to accurately predict the low frequency dielectric properties.

Collectively, this work has provided a significant step in the development of dielectric spectroscopy as a thermoanalytical technique for reacting polymeric systems. By considering the contributions of ions and dipoles, expressions for the dielectric properties during both isothermal and nonisothermal processing were developed. This treatment also permitted the calculation of chemical and physical parameters from dielectric data. Such information is necessary if dielectric spectroscopy is to develop further as an in situ method of tracking polymers and polymeric composites during processing.

6.2 Recommendations for Future Research

The results of this study suggest several areas for further research. Perhaps the most crucial area is exploring the effects that carbon fibers and moisture have on the measured dielectric properties. Several of the references presented in Chapter 1 discuss experimental investigations of these effects, and yet no quantitative analysis was presented. The work presented in this study investigated an ideal thermosetting resin. Experiments were

performed on moisture- and fiber-free material. For dielectric spectroscopy to become a standard laboratory and production analysis technique, such effects must be fully understood. If the influence of carbon fibers cannot be removed from the data, alternate experimental techniques must be developed.

Secondly, the dielectric model descriptions proposed in Chapters 4 and 5 should be explored further, on a more fundamental basis. While the Keinle-Race expression relating resin conductivity to the extent of reaction has been found to hold for many thermosetting resins, the equation has not yet been derived in terms of the transport properties during reaction. Such a derivation would make the Keinle-Race expression more widely accepted.

Also, the concept of the entanglement parameter should be explored further, given the relationship between this parameter and the WLF equation parameters described in Chapter 4. The kinetic relaxation equation has been applied to dynamic mechanical data during reaction and, in theory, is applicable to viscosity measurements as well. A concerted analysis of the DMA, viscometric, and dielectric data for curing thermosetting polymers, combined with analyses of the vitrification and gelation behavior, would further substantiate the validity of this parameter.

Finally, the dielectric modelling approach presented here should be applied to other thermosetting and thermoplastic polymers. Events which occur during the reaction of other resin systems, such as volatile formation in curing polyimides, should be added to the model. Newly developed dielectric instruments, such as the DuPont 2970 DEA, will make quantitative experiments possible in the analytical laboratory. Processing experiments using the Tetrahedron ADR-380 would verify the results of smaller scale experiments. These experiments would provide further basis in developing dielectric spectroscopy for thermal analysis, eventually leading to quantitative process monitoring of both thermosetting and thermoplastic polymer systems.

BIBLIOGRAPHY

Acitelli, M.A., R.B. Prime, and E. Sacher, Polymer, 12, 335 (1971).

Arridge, R.G.C. and J.H. Speake, Polymer, 13, 443 (1972).

Aukward, J.A., R.W. Warfield and M.C. Petree, J. Polym. Sci., 27, 199 (1958).

Baekelund, L.H., Ind. Eng. Chem., 1, 149 (1909).

Baird, M.E., Electrical Properties of Polymeric Materials, The Plastics Institute, London, 1973.

Bånhegyi, G., Colloid Polym. Sci., 266, 11 (1988).

Bånhegyi, G., P. Hedvig, and F.E. Karasz, J. Appl. Polym. Sci., 35, 679 (1988).

Bidstrup, S.A., N.F. Sheppard, Jr., and S.D. Senturia, Proc. Ann. Tech. Conf., Soc. Plast. Eng., 33, 987 (1987).

Bidstrup, S.A., N.F. Sheppard, Jr., and S.D. Senturia, Polym. Matl. Sci. Eng., 56, 173 (1987).

Bidstrup, W.W., N.F. Sheppard, Jr., S.D. Senturia, Polym. Eng. Sci., 26, 358 (1986).

Bidstrup, W.W. and S.D. Senturia, Proc. Ann. Tech. Conf., Soc. Plast. Eng., 33, 1035 (1987).

Bidstrup, W.W., S.A. Bidstrup, and S.D. Senturia, Proc. Ann. Tech. Conf., Soc. Plast. Eng., 34, 960 (1988).

Bogan, G.W., M.E. Lyssy, G.A. Monnerat, and E.P. Woo, SAMPE J., 24(6), 19 (1988).

Bueche, F., Physical Properties of Polymers, Interscience, New York, 1962.

Carlini, C., A. Rolla, and E. Tombari, J. Polym. Sci., Polym. Let. Ed., 23, 5 (1985).

Chen, Y.P., J.F. Pollard, J.D. Graybeal, and T.C. Ward, Polym. Prepr., 29, 207 (1988).

Chern, C-S. and G.W. Poehlein, Polym. Eng. Sci., 27, 788 (1987).

Chou, T-W., R.L. McCullough, and R.B. Pipes, Scientific American, 225, 192 (1986).

Chu, H.S. and J.C. Seferis, The Role of the Polymer Matrix in the Processing and Structural Properties of Composite Materials, J.C. Seferis and L. Nicolais, Eds., Plenum, New York, 1983.

Chu, H.S. and J.C. Seferis, Polym. Comp., 5, 125 (1984).

Cizmecioglu, M., A. Gupta, and R.F. Fedors, J. Appl. Polym. Sci., 32, 6177 (1986).

Cole, K.S. and R.S. Cole, J. Chem. Phys., 9, 341 (1941).

Cooper, E.A., M.W. Urban, and T. Provder, Polym. Matl. Sci. Eng., 59, 316 (1988).

Crabtree, D.J., Proc. Ann. Conf., Soc. Adv. Matl. Proc. Eng., 22, 636 (1977).

Dansas, P. and P. Sixou, Revue Générale de L'Electricité, 76, 726 (1967).

Davidson, D.W. and R.H. Cole, J. Chem. Phys., 18, 1417 (1950).

Day, D.R., T.J. Lewis, H.L. Lee, and S.D. Senturia, J. Adhesion, 18, 73 (1985).

Day, D.R., Polym. Eng. Sci., 26, 362 (1986).

DiBenedetto, A.T., J. Macromol. Sci., Rev. Macromol. Chem., C3, 69 (1969).

Dillman, S.H. and J.C. Seferis, J. Macromol. Sci., in press.

Dillman, S.H., J.C. Seferis, and R.B. Prime, Proc. Ann. Tech. Conf., N. Amer. Thermal Anal. Soc., 19, 429 (1987).

Dillman, S.H., Doctoral Dissertation, University of Washington, 1985.

Domenici, C., G. Levita, A. Marchetti, and V. Frosini, J. Appl. Polym. Sci., 34, 2285 (1987).

Dusi, M.R., C.A. May, and J.C. Seferis, ACS Symp. Ser., 227, 302 (1983).

Dyszel, S.M., Thermochim. Acta, 61, 169 (1983).

Fava, R.A. and A.E. Horsfield, Brit. J. Appl. Phys. (J. Phys. D), Ser. 2, 1, 117 (1968).

Fava, R.A., Polymer, 9, 137 (1968).

Fineman, M.N. and I.E. Puddington, Ind. Eng. Chem., 39, 1288 (1947).

Fineman, M.N. and I.E. Puddington, Can. J. Research, B25, 101 (1947).

Finlayson, B.A., Nonlinear Analysis in Chemical Engineering, McGraw-Hill, New York, 1980.

Fuller, B.W., J.T. Gotro, and G.C. Martin, Polym. Matl. Sci. Eng., 59, 975 (1988).

George, G.A. and D.P. Schweinsberg, J. Appl. Polym. Sci., 33, 2281 (1987).

Golub, M.A., N.R. Lerner, and M.S. Hsu, J. Appl. Polym. Sci., 32, 5215 (1986).

Grentzer, T. and J. Leckenby, Amer. Lab., 21, 82 (1989).

Hahn, H.T., Nondestructive Methods for Material Property Determination, C. Rund, Ed., Plenum, New York, (1983).

Halpin, J.C., J.L. Kardos, and M.P. Dudukovic, Pure and Appl. Chem., 55, 893 (1983).

Harrold, R.T. and Z.N. Sanjana, Proc. Ann. Tech. Conf., Soc. Plast. Eng., 31, 331 (1985).

Hartshorn, L. and W.H. Ward, J. Inst. Elect. Eng., 79, 597 (1936).

Havriliak, S. and S. Negami, J. Polym. Sci.: Pt. C, 14, 99 (1966).

Havriliak, S. and S. Negami, Polymer, 8, 161 (1967).

Havriliak, S. and D.G. Watts, Polymer, 27, 1509 (1986).

Hergenrother, P.M. and N.J. Johnston, Polym. Matl. Sci. Eng., 59, 697 (1988).

Hoffman, R.D., J.J. Godfrey, D.E. Kranbuehl, L. Weller, and M.S. Hoff, J. Reinf. Plast. Comp., 6, 223 (1987).

Huraux, C. and A. Sellaimia, C. R. Acad. Sci. Paris, 277, Ser. B, 691 (1973).

Ibrahim, A.M. and J.C. Seferis, Interrelationships Between Processing, Structure, and Properties of Polymeric Materials, J.C. Seferis and P.S. Theocaris, Eds., Elsevier, Amsterdam, 1984.

Ibrahim, A.M. and J.C. Seferis, Polym. Comp., 6, 47 (1985).

Ibrahim, A.M. and J.C. Seferis, Proc. Ann. Conf., Soc. Adv. Matl. Proc. Eng., 29, 1405 (1985).

Jang, Y.T., D. Parikla, and P.J. Phillips, J. Polym. Sci., Polym. Phys. Ed., 23, 2483 (1985).

Johnson, J.F. and R.H. Cole, J. Am. Chem. Soc., 73, 4536 (1951).

Jow, J., M.C. Hawley, M. Finzel, and T. Kern, Polym. Eng. Sci., 28, 1450 (1988).

Jow, J. M.C. Hawley, and J.D. DeLong, Proc. Ann. Tech. Conf., Am. Soc. Comp., 3, 305 (1988).

Keenan, J.D., J.C. Seferis, and J.T. Quinlivan, J. Appl. Polym. Sci., 24, 2375 (1979).

Keinle, R.H. and H.H. Race, Trans. Electrochem. Soc., 65, 87 (1934).

Khorami, J., G. Chauvette, A. Lemieux, H. Menard, and C. Jolicoeur, Thermochim. Acta, 103, 221 (1986).

Kranbuehl, D.E., S.E. Delos, and P.K. Jue, Polymer, 27, 11 (1986).

Kranbuehl, D.E., S.E. Delos, E. Yi, J. Mayer, T. Jarvie, W. Winfree, and T. Hou, Polym. Eng. Sci., 26, 338 (1986).

Kranbuehl, D.E., S.E. Delos, M.S. Hoff, P. Haverty, R. Hoffman, J. Godfrey, and W. Freeman, Proc. Ann. Tech. Conf., Soc. Plast. Eng., 33, 1031 (1987).

Kranbuehl, D.E., S.E. Delos, M.S. Hoff, M.E. Whitham, L.W. Weller, P.D. Haverty, and T. Freeman, Proc. Intl. Conf. Comp. Matl., 6, 1.70 (1987).

Kranbuehl, D.E., M.S. Hoff, T. Hamilton, R. Clark, and W. Freeman, Polym. Matl. Sci. Eng., 59, 1116 (1988).

Kranbuehl, D.E., M.S. Hoff, D.A. Eichinger, A.C. Loos, and W.T. Freeman, Jr., Proc. Ann. Tech. Conf., Am. Soc. Comp., 3, 313 (1988).

Ku, P.L., Adv. Polym. Tech., 8, 81 (1988).

Lane, J.W., J.C. Seferis, and M.A. Bachmann, Polym. Eng. Sci., 26, 346 (1986).

Lane, J.W., J.C. Seferis, and M.A. Bachmann, J. Appl. Polym. Sci., 31, 1155 (1986).

Lane, J.W. and R.K. Khattak, Proc. Ann. Tech. Conf., Soc. Plast. Eng., 33, 982 (1987).

Lee, C. Y-C. and I.J. Goldfarb, Polym. Eng. Sci., 21, 951 (1981).

Levy, R.L., Polym. Matl. Sci. Eng., 50, 124 (1984).

Levy, R.L. and S.D. Schwab, ACS Symp. Ser., 367, 113 (1988).

Lindrose, A.M., Exp. Mech., 18, 227 (1978).

Liu, W-L., E.M. Pearce, and T.K. Kwei, J. Appl. Polym. Sci., 30, 2907 (1985).

Loechelt, C.L., E.M. Woo,and J.C. Seferis, Proc. Ann. Tech. Conf., Soc. Plast. Eng., 34, 1645 (1988).

Macedo, P.B. and T.A. Litovitz, J. Chem. Phys., 42, 245 (1965).

Martin, G.C., A.V. Tungare, and J.T. Gotro, Polym. Matl. Sci. Eng., 59, 980 (1988).

May, C.A., Proc. Ann. Conf., Soc. Adv. Matl. Proc. Eng., 20, 108 (1975).

May, C.A., Pure Appl. Chem., 55, 811 (1983).

May, C.A., M.R. Dusi, J.S. Fritzen, D.K. Hadad, M.G. Maximovich, K.G. Thrasher, and A. Wereta, ACS Symp. Ser., 227, 1 (1983).

McCullough, R.L., Comp. Sci. Tech., 22, 3 (1985).

McCrum, N.G., B.E. Read, and G. Williams, Anelastic and Dielectric Effects in Polymeric Solids, Wiley and Sons, London, 1967.

McLane, R.M., Proc. Ann. Tech. Conf., Am. Soc. Comp., 3, 23 (1988).

Meissonnier, J. and J.C. Seferis, J. Makromol. Chemie, in press.

Mijovic, J., J.G. Williams, and T. Donnellan, J. Appl. Polym. Sci., 30, 2351 (1985).

Mikols, W.J., J.C. Seferis, A. Apicella, L. Nicolais, Polym. Comp., 3, 118 (1982).

Mikols, W.J. and J.C. Seferis, ACS Symp. Series, 227, 95 (1983).

Morgan, L.J. and E.T. Mones, Polym. Prepr., 21, 921 (1980).

Munns, T.E. and J.C. Seferis, J. Appl. Polym. Sci., 28, 2227 (1983).

Munns, T.E. and J.C. Seferis, Analytical Calorimetry, Vol. 5, J.F. Johnson and P.S. Gill, Eds., Plenum, New York, 1984.

Nielsen, L.E., Polymer Rheology, Marcel Dekker, New York, 1977.

Persson, S., Polym. Test., 6, 47 (1986).

Polym. Comp., 28, (1988).

Prime, R.B. and E. Sacher, Polymer, 13, 455 (1972).

Prime, R.B., Thermal Characterization of Polymeric Materials, E. Turi, Ed., Academic Press, New York, 1981.

Provder, T., R.M. Holsworth, and T.H. Grentzer, Adv. Chem. Ser., 203, 77 (1983).

Reid, J.D., W.H. Lawrence, and R.P. Buck, J. Appl. Polym. Sci, 31, 1771 (1986).

Reid, J.D. and R.P. Buck, J. Appl. Polym. Sci, 33, 2293 (1987).

Richardson, M.J., Polymer Testing, 4, 101 (1984).

Roller, M.B., Polym. Eng. Sci., 15, 406 (1975).

Roller, M.B., Polym. Eng. Sci., 26, 432 (1986).

Romanchuk, W.A., J.E. Sohan, and J.F. Geibel, ACS Symp. Ser., 227, 85 (1983).

Sanford, W.M. and R.L. McCullough, Proc. Ann. Tech. Conf., Am. Soc. Comp., 2, 21 (1987).

Sanjana, Z.N., Polym. Eng. Sci., 26, 373 (1986).

Scarlata, S.F. and J.A. Ors, Polym. Comm., 27, 41 (1986).

Schwab, S.D. and R.L. Levy, Polym. Matl. Sci. Eng., 59, 591 (1988).

Seferis, J.C. and P.S. Theocaris, Eds., Interrelationships Between Processing, Structure, and Properties of Polymeric Materials, Elsevier, Amsterdam, 1983.

Seferis, J.C., Polym. Comp., 7, 158 (1986).

Seferis, J.C., SAMPE J., 24, 6 (1988).

Senturia, S.D., N.F. Sheppard, Jr., H.L. Lee, and S.B. Marshall, SAMPE J., 19, 22 (1983).

Sheppard, N.F., Jr., M.C.W. Coln, and S.D. Senturia, Proc. Ann. Conf., Soc. Adv. Matl. Proc. Eng., 29, 1243 (1984).

Sheppard, N.F. and S.D. Senturia, Polym. Eng. Sci., 26, 354 (1986).

Shimbo, M., M. Ochi, and H. Iesako, J. Polym. Sci.: Polym. Phys. Ed., 22, 1461 (1984).

Shmorhun, M., A.M. Jamieson, and R. Simha, Polymer, 29, 1960 (1988).

Sichina, W.J., DuPont Instruments Thermal Analysis Applications Brief, TA-93.

Sofer, G.A. and E.A. Hauser, J. Polym. Sci., 8, 611 (1952).

Souroor, S. and M.R. Kamal, Thermochimica Acta, 14, 41 (1976).

Stark, E.B., J.C. Seferis, A. Apicella, and L. Nicolais, Thermochimica Acta, 77, 19 (1984).

Stark, E.B., A.M. Ibrahim, and J.C. Seferis, Interrelationships Between Processing, Structure, and Properties of Polymeric Materials, J.C. Seferis and P.S. Theocaris, Eds., Elsevier, Amsterdam, 1984.

Stark, E.B., A.M. Ibrahim, T.E. Munns, and J.C. Seferis, J. Appl. Polym. Sci., 30, 1717 (1985).

Stark, E.B., Doctoral Dissertation, University of Washington, 1985.

Sung, C.S.P., I-J. Chen, and W-C. Yu, Macromol., 18, 1510 (1985).

Tajima, Y.A., Polym. Comp., 3, 162 (1982).

Tajima, Y.A. and D.G. Crozier, Polym. Eng. Sci., 26, 427 (1986).

Tajima, Y.A. and D.G. Crozier, Polym. Eng. Sci., 28, 491 (1988).

Torres-Filho, A., C.F. Perondi, and L.C. Miranda, J. Appl. Polym. Sci., 35, 103 (1988).

Turi, E., Ed., Thermal Characterization of Polymeric Materials, Academic Press, New York, 1981.

Uutratu, J.A., J. Polym. Sci., Polym. Chem. Ed., 27, 1609 (1986).

Walkup, C., R.J. Morgan, and T.H. Hoheisel, Polym. Prepr., 25, 187 (1984).

Wang, F.W., A.J. Bur, R.E. Lowry, and B.N. Fanconi, Polym. Matl. Sci. Eng., 59, 600 (1988).

Ward, I.M., Mechanical Properties of Solid Polymers, 2nd Ed., Wiley-Interscience, New York, 1983.

Warfield, R.W. and M.C. Petree, J. Polym. Sci., 37, 305 (1959).

Warfield, R.W. and M.C. Petree, Macromol. Chem., 58, 139 (1962).

Warfield, R.W., Testing of Polymers, Vol. 1, J.V. Schmitz, Ed., Interscience, New York, (1965).

Warner, A.J., ASTM Bull., 153, 60 (1948).

Wendlandt, W.W. and P.K. Gallagher, Thermal Characterization of Polymeric Materials, E. Turi, Ed., Academic Press, New York, 1981.

Wigotsky, V., Plast. Eng., 14, 25 (1988).

Williams, M.L., R.F. Landel, and J.D. Ferry, J. Am. Chem. Soc., 77, 370 (1955).

Woo, E.M. and J.C. Seferis, J. Comp. Matl., 21, 262 (1987).

Woo, E.M., L.B. Chen, and J.C. Seferis, J. Mat. Sci., 22, 3665 (1987).

Woo, E.M., J.C. Seferis, and L.D. Bravenec, Proc. Ann. Tech. Conf., Am. Soc. Comp., 2, 569 (1987).

Yalof, S.A. and W.J. Wrasidlo, J. Appl. Polym. Sci., 16, 2159 (1972).

Yalof, S., Adhesives Age, 18, 23 (1975).

Yokota, M.J., Proc. Ann. Conf., Soc. Adv. Matl. Proc. Eng., 22, 416 (1977).

Zhu, Y. and D.G. Watts, Polymer, 29, 325 (1988).

Zitomer, F., Anal. Chem., 40, 1091 (1983).

Zukas, W.X. and S.E. Wentworth, Proc. Ann. Tech. Conf., Soc. Plast. Eng., 32, 336 (1986).

Zukas, W.X. and S.E. Wentworth, Polym. Comp., 8, 232 (1987).

APPENDIX A

DERIVATION OF ACTIVATION ENERGY EXPRESSION FOR ε'' RATIO METHOD

The relationship between the activation energy and the ratios of isofrequency ε'' values to the maximum value during dielectric transition was derived for polymers exhibiting Havriliak-Negami dispersion behavior [1]. The complex dielectric constant, ε^*, was related to the mean dipolar relaxation time, τ, and applied frequency, w, by:

$$\varepsilon^* = \varepsilon_\infty + \frac{(\varepsilon_o - \varepsilon_\infty)}{(1 + (iw\tau)^{1-\alpha})^\beta} \qquad (A.1)$$

ε_o and ε_∞ are the values of the real component of ε^*, ε', at zero and infinite frequency. The dispersion parameters α and β may have values between 0 and 1 and are, in principle, related to the distribution of relaxation times about the mean value.

The imaginary, or loss, component of ε^*, ε'', was expressed as a function of $w\tau$ by applying DeMoivre's Theorem to Equation A.1:

$$\varepsilon'' = \frac{(\varepsilon_o - \varepsilon_\infty)\ \sin(\beta\varphi)}{[1+2(w\tau)^{(1-\alpha)}\cos((1-\alpha)\pi/2)+(w\tau)^{2(1-\alpha)}]^{\beta/2}} \quad (A.2)$$

The parameter φ is a collection of terms:

$$\varphi = \tan^{-1}\left[\frac{(w\tau)^{(1-\alpha)}\sin((1-\alpha)\pi/2)}{1 + (w\tau)^{(1-\alpha)}\cos((1-\alpha)\pi/2)}\right] \quad (A.3)$$

The maximum value of ε'' during the transition, ε''_m, is described by Equation A.2 as:

$$\varepsilon''_m = \frac{(\varepsilon_o - \varepsilon_\infty)\ \sin(\beta\varphi_m)}{[1+2(w\tau_m)^{(1-\alpha)}\cos((1-\alpha)\pi/2)+(w\tau_m)^{2(1-\alpha)}]^{\beta/2}} \quad (A.4)$$

The values of the relaxation time and φ at ε''_m were denoted as τ_m and φ_m. Dividing Equation A.2 by Equation A.4 and rearranging provided the relationship between ε'' and ε''_m:

$$\frac{\varepsilon''}{\varepsilon''_m} = \frac{1}{A}\ \frac{\sin(\beta\varphi)}{[1+2(w\tau)^{(1-\alpha)}\cos((1-\alpha)\pi/2)+(w\tau)^{2(1-\alpha)}]^{\beta/2}} \quad (A.5)$$

where:

$$A = \frac{\sin(\beta\varphi_m)}{[1+2(w\tau_m)^{(1-\alpha)}\cos((1-\alpha)\pi/2)+(w\tau_m)^{2(1-\alpha)}]^{\beta/2}} \quad (A.6)$$

and is simply a function of frequency. Therefore, A may be considered constant in isofrequency dielectric transition data, under the assumption that α and β are independent of temperature.

Equation A.5 may be simplified by assuming that at temperatures above the ε''_m temperature:

$$(w\tau)^{(1-\alpha)} << 1 \quad (A.7)$$

and therefore:

$$\frac{(w\tau)^{(1-\alpha)}\sin((1-\alpha)\pi/2)}{1 + (w\tau)^{(1-\alpha)}\cos((1-\alpha)\pi/2)} << 1 \quad (A.8)$$

In addition, for $x^2 < 1$:

$$\tan^{-1}(x) \approx x \quad (A.9)$$

The value of φ above the peak transition temperature then simplifies to:

$$\varphi \approx \frac{(w\tau)^{(1-\alpha)}\sin((1-\alpha)\pi/2)}{1 + (w\tau)^{(1-\alpha)}\cos((1-\alpha)\pi/2)} << 1 \qquad (A.10)$$

Since $\beta < 1$ and $\varphi < 1$, $\beta\varphi < 1$, and the numerator in Equation A.5 simplifies to:

$$\sin(\beta\varphi) \approx \beta\varphi \approx \frac{\beta(w\tau)^{(1-\alpha)}\sin((1-\alpha)\pi/2)}{1 + (w\tau)^{(1-\alpha)}\cos((1-\alpha)\pi/2)} \qquad (A.11)$$

This equation may be simplified further by recognizing that for α and $w\tau$ less than 1:

$$(w\tau)^{(1-\alpha)}\cos((1-\alpha)\pi/2) << 1 \qquad (A.12)$$

and therefore:

$$\sin(\beta\varphi) \approx \beta\varphi \approx \beta(w\tau)^{(1-\alpha)}\sin((1-\alpha)\pi/2) \qquad (A.13)$$

The denominator in Equation A.5 is also simplified for α and $w\tau$ less than 1:

$$2(w\tau)^{(1-\alpha)}\cos((1-\alpha)\pi/2)+(w\tau)^{2(1-\alpha)} << 1 \qquad (A.14)$$

Substituting Equations A.13 and A.14 into Equation A.5 yields an expression for the ratio of ε'' values above the transition temperature to the peak value:

$$\frac{\varepsilon''}{\varepsilon''_m} = \frac{\beta(w\tau)^{(1-\alpha)}\sin((1-\alpha)\pi/2)}{A} \qquad (A.15)$$

Taking the logarithm of both sides produces:

$$\ln\frac{\varepsilon''}{\varepsilon''_m} = \ln\frac{\beta\sin((1-\alpha)\pi/2)}{A} + (1-\alpha)\ln(w\tau) \qquad (A.16)$$

The temperature dependence of the relaxation time is incorporated into Equation A.16 by using an Arrhenius expression [2]:

$$\tau = \tau' \exp(E_\tau/RT) \qquad (A.17)$$

The final activation energy equation is then:

$$\ln\frac{\varepsilon''}{\varepsilon''_m} = \ln\frac{\beta\sin((1-\alpha)\pi/2)}{A} + (1-\alpha)\ln(w\tau') + \frac{(1-\alpha)E_\tau}{RT} \qquad (A.18)$$

Equation A.16 predicts that Arrhenius plots of post transition values of $\varepsilon''/\varepsilon''_m$ are linear. The activation energy is calculated from:

$$E_\tau \approx \frac{R}{(1-\alpha)} \frac{d[\ln(\varepsilon''/\varepsilon''_m)]}{d[1/T]} \qquad (A.19)$$

Notes to Appendix A

1. S. Havriliak and S. Negami, J. Polym. Sci.: Pt. C, 14, 99 (1966).

2. N.G. McCrum, B.E. Read, and G. Williams, Anelastic and Dielectric Effects in Polymeric Solids, Wiley and Sons, London, 1967.

APPENDIX B

DERIVATION OF RELATIONSHIP BETWEEN THE ENTANGLEMENT PARAMETER AND THE WLF EQUATION PARAMETERS

The kinetic viscoelastic equation, Equation 4.28, relates viscosity to the extent of reaction, α, using an entanglement parameter, Φ [1]:

$$\frac{1}{\eta} = \frac{1}{\eta_\infty} + \left[\frac{1}{\eta_o} - \frac{1}{\eta_\infty}\right](1-\alpha)^{\Phi} \qquad (B.1)$$

η_o represents the viscosity of uncured resin, while η_∞ is the viscosity of fully cured resin. Although essentially infinite for thermosetting resins, the value of η_∞ is assumed to finite, but very large.

After taking the logarithm of both sides and rearranging, Equation B.1 becomes:

$$\ln \eta = \ln \eta_\infty - \ln [1 + (\eta_\infty/\eta_o)(1-\alpha)^{\Phi}] \qquad (B.2)$$

At the beginning of cure when α is small,

$$(\eta_\infty/\eta_o)(1-\alpha)^{\Phi} >> 1 \qquad (B.3)$$

Equation B.2 then simplifies to a generalized form of the Dusi-May-Seferis equation [2]:

$$\ln \eta = \ln \eta_o - \Phi \ln (1-\alpha) \tag{B.4}$$

The ln (1-α) term in Equation B.4 was expressed as a power series in α since, for $x^2 < 1$:

$$\ln (1-x) = - \left[x + \frac{x^2}{2} + \frac{x^3}{3} + \cdots \right] \tag{B.5}$$

Equation B.4 was then restated as:

$$\ln \eta = \ln \eta_o + \Phi \left[\alpha + \frac{\alpha^2}{2} + \frac{\alpha^3}{3} + \cdots \right] \tag{B.6}$$

Therefore, for sufficiently small values of α,

$$\ln \eta \approx \ln \eta_o + \Phi\alpha \tag{B.7}$$

The WLF parameters and Φ were linked using the WLF-type viscosity model developed by Meissonnier and Seferis [3]. When expressed directly in terms of α, their equation became:

$$\ln \eta(\alpha,T) = \ln \eta_o(T) - \frac{C_1 T_{g\infty}(T-T_{go}) - C_1 T(T_{g\infty}-T_{go})\alpha}{T_{g\infty}(C_2+T-T_{go}) - (C_2+T)(T_{g\infty}-T_{go})\alpha} \qquad (B.8)$$

This equation was converted to a power series in α by explicitly evaluating the right hand term and gathering like powers of α:

$$\ln \eta(\alpha,T) = \ln \eta_o(T) + C_1 C_2 \frac{T_{go}}{T_{g\infty}} \frac{(T_{g\infty}-T_{go})}{(C_2+T-T_g)^2} \alpha + \cdots \qquad (B.9)$$

The final expression for Φ in terms of the WLF parameters was obtained by comparing Equations B.7 and B.9:

$$\Phi = C_1 C_2 \, (T_{gc}/T_{g\infty}) \frac{(T_{g\infty} - T_{go})}{(C_2 + T - T_{go})^2} \qquad (B.10)$$

Notes to Appendix B

1. S.H. Dillman and J.C. Seferis, J. Macromol. Sci., in press.

2. M.R. Dusi, C.A. May, and J.C. Seferis, ACS Symp. Ser., 227, 302 (1983).

3. J. Meissonnier and J.C. Seferis, J. Makromol. Chemie, in press.

VITA

Kirk A. Nass was born in Aurora, Illinois on January 23, 1960 to Susan C. and David E. Nass. After graduating as valedictorian from West Aurora High School in Aurora, Illinois in June, 1978, he attended the University of Illinois in Urbana, Illinois. While an undergraduate student, he participated in the School of Chemical Sciences Cooperative Education Program through employment with the Borg-Warner Corporation at the Roy C. Ingersoll Research Center in Des Plaines, Illinois. He received an Undergraduate General Chemistry Teaching Assistantship, and received several Excellent Teaching Assistant citations. In May, 1983, he received a Bachelor of Science degree in Chemical Engineering, and graduated with High Departmental Distinction. In September, 1984, he entered the University of Washington and joined the Polymeric Composites Laboratory to study dielectric cure monitoring techniques. As part of his studies, he spent a Summer Internship at the Owens-Corning Fiberglas Technical Center in Granville, Ohio in 1985. After receiving a Doctor of Philosophy degree in Chemical Engineering from the University of Washington in March, 1989, he began an industrial research career as a Research Engineer with Chevron Research Company in Richmond, California.